Thermodynamic Characterization of Hypertrophic Cardiomyopathy Associated Troponin C Mutations

by

Kaveh Rayani

B.Sc., Simon Fraser University, 2012

Thesis Submitted in Partial Fulfillment of the
Requirements for the Degree of
Doctor of Philosophy

in the
Department of Biomedical Physiology and Kinesiology
Faculty of Science

SIMON FRASER UNIVERSITY
Summer 2019

Approval

Name:	**Kaveh Rayani**
Degree:	**Doctor of Philosophy**
Title:	**Thermodynamic Characterization of Hypertrophic Cardiomyopathy Associated Troponin C Mutations**
Examining Committee:	**Chair:** William Cupples Professor
	Glen Tibbits Senior Supervisor Professor
	Thomas Claydon Supervisor Associate Professor
	Damon Poburko Supervisor Assistant Professor
	Edgar Young Internal Examiner Associate Professor Molecular Biology and Biochemistry
	Edwin Moore External Examiner Professor Cellular and Physiological Sciences University of British Columbia
Date Defended/Approved:	July 15, 2019

Abstract

Hypertrophic Cardiomyopathy (HCM) is the leading cause of sudden cardiac death in young adults under the age of 35; a devastating disease that is not yet well understood. To date, greater than 1000 HCM-associated mutations have been found in genes that encode mostly sarcomeric proteins. Familial Hypertrophic Cardiomyopathy (FHC) is the heritable form of HCM. The overlying phenotype of FHC is thought to be derived from an increase in calcium (Ca^{2+}) sensitivity of contraction and impaired relaxation of the myocardium. Dilated Cardiomyopathy (DCM) associated mutations are thought to have the opposite functional effect. This study focuses on cardiac troponin C (cTnC) a component of the cardiac troponin complex, where binding of Ca^{2+} acts as the regulatory switch, leading to a series of conformational changes that culminate in muscle contraction. This project explores Ca^{2+} binding by focusing on the proximal-most unit of the contractile apparatus. The interaction of Ca^{2+} with the regulatory domain of cTnC is studied through isothermal titration calorimetry in conjunction with Molecular Dynamics simulations to understand structural and functional changes in the N-terminal region of cTnC. Initially, we established a workflow by exploring the functional consequences of sequence variations in coordinating Ca^{2+} binding and the genetic control of paralog expression in response to environmental temperature change in zebrafish. We then focused on a series of FHC-associated mutations (A8V, L29Q, A31S, and C84Y), as well as an engineered Ca^{2+} sensitizing mutation (L48Q), and a DCM-associated mutation (Q50R). The effects of temperature in modulating the Ca^{2+}-cTnC interaction was also studied in these mutants. We further explored the role of cellularly abundant magnesium (Mg^{2+}) which also interacts with cTnC and may modulate the Ca^{2+} coordinating capabilities of this contractile protein. Lastly, the role of Mg^{2+} binding to the mutants of interest, under normal cellular condition and in energy depleted states was explored to better understand the etiology of FHC and provide biomedical and physiological insight into potential treatments for this disease.

Keywords: TnC; ITC; HCM; FHC; MD simulations; contractility

Acknowledgements

It would not be amiss to suggest that my role in the completion of this project is less than the sum of contributions by numerous others, and as such, only with their help has this project been achievable. While words will prove insufficient in doing justice to the role the many people listed here have played in my life over the last years, I will, nonetheless attempt to acknowledge each individual.

The time I have spent in graduate school has been the most significantly transformative period in my life and this has been due in large part to my supervisor and mentor Dr. Glen Tibbits. Glen has provided me with numerous opportunities; he has opened the door to establishing collaborations, presenting at conferences, contributing to publications, and the general freedom to pick my own scientific path. Glen's nourishment of scientific curiosity and encouragement of experimentation enabled me to explore numerous fields, much of which is not reflected in this thesis but all of which has enriched my scientific training. Glen's dedication to his chosen vocation and his committment to self established standards of excellence, which, while far beyond my own standards will exits in my mind as a benchmark for comparison. Beyond this, his door has always been open and he has always made time to discuss issues that I have faced over the years. In listening, Glen has consistently shown great patience and provided wise guidance on a range of topics whenever I was in need, and this was often!

I have also had the privilege to share my scientific journey with numerous collagues. My friend Dr. Bairam Lotfalisalmasi played a key role in my introduction to the lab. I worked under the guidance of Cindy Li, Dr. Charles Stevens, Bo Liang, Dr. Alison Li, Dr. Cynthia Gershome, Dr. Danielle Wilson, and Dr. Omid Haji-Ghassemi. Dr. Eric Lin spent time on many occasions to provide reassurances when I most needed them; without his help and counsel I would have struggled even more. Many others also have enriched the time I have spent in graduate school. I had the pleasure of working alongside Dr. Christine Genge, Dr. Laura Dewar, Dr. Sanam Shafaattalab, Lilian Lee, Dr. Helen Sheng, Elham Afshinmanesh, Valentine Sergeev, Marvin Gunawan, Sabi Sangha and more recently Drake Comber, Kevin Ye, Lisa Lin, Tiffany Barszczewski, and Renato Molina. Haruyo Kashihara has always provided indispensible services to the lab environment, as have Dr. Neil Dobson, and Deidre de Jong-Wong.

From adjacent labs I have enjoyed the comraderie of Saba Mojarad, Barun Kim, Dr. Samrat Thouta, Dr. Patrick Shi, Danielle Jeong, Dr. Christina Hull, Jake Kemp, Mandy Angus, Dr. Colin Peters, Dr. Mena Abdelsayed, Reza Ghovanloo, and Ravichandra Venkateshappa.

Over the years, numerous collaborators have provided invaluable expertise and guidance. These include Dr. Edgar Young, Dr. Filip Van Petegem, Dr. Jonathan Davis, Dr. Peter Tieleman, Dr. Steffen Lindert, Dr. Pieter de Tombe, Dr. Neil Branda, Dr. Gurpreet Singh, Justin Seffernick, Dr. John Solaro, and Dr. Anne Spuches. As part of my committee, Dr. Thomas Claydon and Dr. Damon Poburko have always been available and have asked thought provoking questions to challenge me throughout the duration of my studies. Dr. Edwin Moore has been most gracious in acting as a member of my examining committee, his thoughtful study of and insights into the nuances of my projects are greatly appreciated. Dr. Zachary Laksman has always been willing to take time from his schedule to provide advice in a wide variety of avenues. Dr. William Cupples and Dr. Peter Ruben have always been supportive, in whatever capacity was needed, of my endeavours both within academia and beyond.

Being a teaching assistant has been an enjoyable aspect of my graduate studies and this has been in large part due to the instructors who I have worked for: Craig Asmundson, Ryan Dill, Dr. Mike Walsh, and Dr. Jim Carter have all been excellent role models. The students I have had the pleasure of interacting with have made teaching worthwhile and have taught me much more than I was able to teach them.

The steadfast, unwavering support of my loved ones has enabled me to continue this graduate project to completion, to them I am eternally grateful.

Table of Contents

List of Tables

List of Figures

List of Acronyms

AF	Atrial fibrillation
AKTA FPLC	Fast protein liquid chromatography
AMP	Adenosine monophosphate
AMPK	AMP-activated protein kinase
ANG II	Angiotensin II
AP	Action potential
ATP	Adenosine triphosphate
AVN	Atrio-ventricular node
BME	β-mercaptoethanol
Ca^{2+}	Calcium
CaM	Calmodulin
CaMKII	Calcium/Calmodulin dependent protein kinase II
CASQ	Calsequestrin
CaV	Voltage-dependent calcium channel
CDF	Calcium dependent facilitation
CDI	Calcium dependent inhibition
CICR	Calcium-induced calcium release
CO	Cardiac output
CPVT	Cathecholamergic polymorphic ventricular tachycardia
cTnC	Cardiac troponin C
cTnI	Cardiac troponin I
cTnT	Cardiac troponin T
DAD	Delayed after depolarization
DCM	Dilated cardiomyopathy
DD	Diastolic dysfunction
DEAE FF	Diethylaminoethyl cellulose fast flow
DHPR	Dihydropyridine receptor
DNA	Deoxyribonucleic acid
DTT	Dithiothreitol
EAD	Early-after depolarization
ECG	Electrocardiogram
EDTA	Ethylenediaminetetraacetic acid

EDV	End diastolic volume
EGTA	Egtazic acid
ERK	Extracellular signal regulated kinase
FHC	Familial hypertrophic cardiomyopathy
FKBP 12.6	FK-506 binding protein
GPCR	G-protein coupled receptor
GSK3	Glycogen synthase kinase 3
HCM	Hypertrophic cardiomyopathy
hERG	Human ether-a-go-go related gene
HR	Heart rate
h-sasa	Hydrophobic solvent-accessible surface areas
I_{Ca}	Calcium current
$I_{Ca,L}$	L-type channel calcium current
I_{K1}	Inward rectifier potassium current
I_{Kr}	Rapid-delayed rectifier potassium current
I_{Ks}	Slow-delayed rectifier potassium current
I_{Kur}	Ultra-rapid delayed rectifier potassium current
I_{Na}	Sodium current
IP3R	Inositol 3 phosphate receptor
ITC	Isothermal titration calorimetry
I_{to}	Transient outward potassium current
JNK	c-Jun N-terminal kinase
jSR	Junctional sarcoplasmic reticulum
K^+	Potassium
K_A	Association constant
K_d	Dissociation constant
k_{off}	Off-rate constant
LB	Lysogeny broth
LDA	Length-dependent activation
LTCC	L-type calcium channel
LV	Left ventricle
LVH	Left ventricular hypertrophy
LVOTO	Left ventricular outflow tract obstruction
MAPK	Mitogen activated protein kinase

MD	Molecular dynamics
MLC	Myosin light chain
mTOR	Mammalian target of rapamycin
n	Binding stoichiometry or sample size
Na^+	Sodium
NaV	Voltage dependent sodium channel
NCX	Sodium/calcium exchanger
NFAT	Nuclear activator of T-cells
Pak1	p21 activated kinase 1
PCr	Phosphocreatine
pI	Isoelectric point
PI3K	Phosphoinositide 3 kinase
PKA	Protein kinase A
PLB	Phospholamban
PMF	Potential of mean force
PMSF	Phenylmethylsulfonyl fluoride
PNS	Parasympathetic nervous system
RMSF	Root mean squared fluctuation
ROS	Reactive oxygen species
RyR	Ryanodine receptor
SAN	Sinoatrial node
SCD	Suddent cardiac death
SDS-PAGE	Sodium dodecyl sulfate–polyacrylamide gel electrophoresis
SERCA	Sarcoplasmic/endoplasmic reticulum calcium ATPAse
SL	Sarcomere length
SNS	Sympathetic nervous system
SR	Sarcoplasmic reticulum
ssTnC	Slow skeletal troponin C
SV	Stroke volume
TCEP	Carboxyethylphosphine hydrochloride
TF	Thin filament
Tm	Tropomyosin
T_m	Melting point

Tn	Troponin
TnC	Troponin C
TnC1a	Cardiac troponin C
TnC1b	Slow Skelal troponin C
TnI	Troponin I
TnI_{SW}	Troponin I switch peptide
TnT	Troponin T
TTCC	T-type calcium channel
WHAM	Weighted histogram analysis method
ΔG	Change in Gibbs free energy
ΔH	Change in enthalpy
ΔS	Change in entropy

Chapter 1.

Introduction

1.1. Study justification

The heart continuously pumps blood through a closed circuit, delivering essential nutrients to and removing waste products from the tissues. The electrical activity which controls contractile function is inherent to the heart itself but can also be modified by input from the central nervous system. Electrical signals initiated in the nodal regions and conducted to the boundary of each cardiomyocytes causes for calcium (Ca^{2+}) to be released into the cytosol. Fluctuation of cytosolic Ca^{2+} throughout the heart cycle, and its subsequent binding to the contractile apparatus allows for contraction and force production to occur. The goal of this thesis is to explore the structural and functional implications of single amino acid changes in troponin C (cTnC); the protein responsible for sensing cytosolic Ca^{2+}-concentration. To this end, a review of the literature will be provided as it pertains to the contractile apparatus and how mutations that alter Ca^{2+} sensing can lead to cardiac dysfunction.

1.2. Electrical activity of the heart

The sino-atrial node undergoes rhythmic depolarizations which gives rise to action potentials (APs) that set heart rate (HR). The depolarizing wave first reaches atrial cells. As blood flows into the ventricles the atria contract, closing preceding valves and propelling blood through the atrial-ventricular valves. The atrio-ventricular node then temporarily slows the electrical signal before it is conducted through the bundle of His, left and right bundle branches, and Purkinje fibers. The right and left ventricles contract to send blood towards the lungs and the systemic circulation, respectively.

The physical and electrical coupling of adjacent cardiomyocytes throughout the heart allows for electrical excitation and subsequently, mechanical contraction to occur in a concerted manner (Cobb 1974). Intercalated discs and adhesion junctions create a physical coupling between adjacent cells (Bers 2002). The connexin proteins which compose gap junctions are critical for electrical coupling between cardiomyocytes which

are linked to form a functional syncytium (Essner, Laing et al. 1996). Electrical excitation and physical contraction (EC coupling) are linked through processes that will be further explored in the following sections.

1.3. Action potential

Channels and transporters allow for flux of sodium (Na^+), potassium (K^+), and Ca^{2+} ions across the sarcolemma to occur in a highly coordinated manner that determines AP morphology. In ventricular myocytes, voltage-gated Na^+ channels (Na_V) allow for inward flow of current to depolarize the cell membrane. Inward flow of Ca^{2+} through voltage-gated channels (Ca_V) prolongs the plateau phase of the AP. Finally, the efflux of K^+ from the cell through delayed rectifier channels (K_V) repolarizes the cell membrane back towards its resting membrane potential.

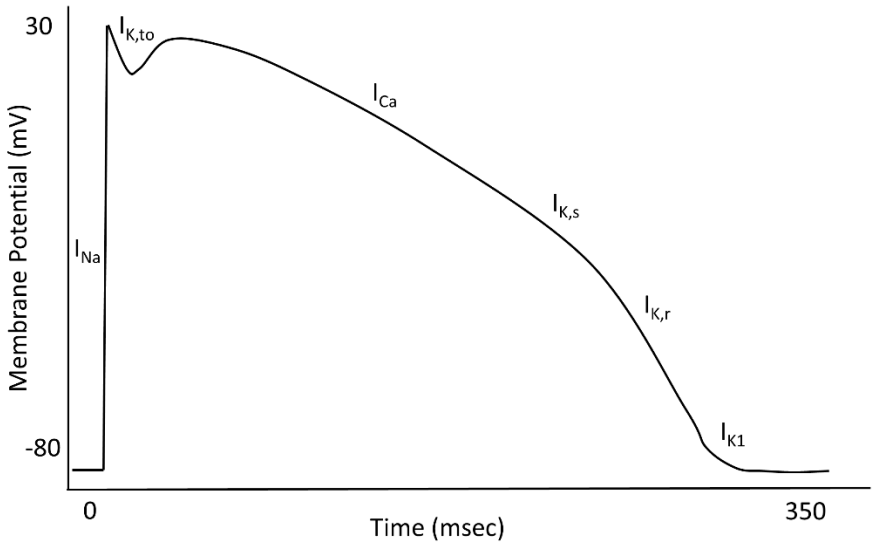

Figure 1-1 Schematic Depiction of the Ventricular AP
Illustration of the AP showing the relative time points for peak current of the most prominent Na^+, K^+, and Ca^{2+} currents in the human ventricular AP. The membrane potentials, time course, and shape are an approximation.

1.3.1. Phase 4 - resting membrane potential (inward rectifier current)

The *KCNJ2*, *KCNJ12*, and *KCNJ4* genes encode $K_{ir}2.1$, $K_{ir}2.2$, and $K_{ir}2.3$ channels, respectively. These channels pass the inward rectifier current (I_{K1}) which is largely responsible for maintaining a resting membrane potential (of approximately - 85

mV) close to E_{K+}. Outward flow of current through the inward rectifiers is modulated by cytosolic Mg^{2+}/polyamine molecules (Ficker, Taglialatela et al. 1994).

Inward rectifier K^+ channels are tetramers each containing two domains, with the loop between these domains forming the pore. In addition to the core domain, these channels co-assemble with numerous accessory subunits that modulate their function (Perozo, Cortes et al. 1999).

1.3.2. Phase 0 – rapid depolarization (sodium current)

The primary voltage-gated Na^+ channel in the heart is $Na_V1.5$ (encoded by the *SCN5A* gene) which opens with membrane depolarization to drive the membrane potential to E_{Na} (or approximately +60 mV). Initial inward flow of I_{Na} activates additional channels in a feedforward manner and helps further depolarize the cell membrane to approximately +35-50 mV (Asimaki, Kleber et al. 2015).

At the end of phase 0, $Na_V1.5$ channels inactivate reducing I_{Na} (Goldin 2003). These channels undergo both fast (milliseconds) and slow (seconds) inactivation. Intracellular particles occlude the pore to allow for fast inactivation. Slow inactivation is likely mediated through voltage sensor relaxation and pore collapse; this process has significant physiological consequences when channels are repeatedly depolarized (Richmond, Featherstone et al. 1998, Silva and Goldstein 2013).

Normally, cell membrane repolarization is required for the Na^+ channel recovery to allow for re-firing in response to another AP. Failure to inactivate gives rise to persistent or late I_{Na}. Gain of function mutations in Na^+ channels may lead to diseases such as Long QT (LQT3) (Wang, Shen et al. 1995) and loss of function may lead to Brugada Syndrome Type 1 (Chen, Kirsch et al. 1998).

$Na_V1.5$ is a single ~2,000 amino acid protein that is made up of 4 covalently linked domains (D_I-D_{IV}), each composed of 6 transmembrane sections (S1-S6); the domains assemble to form an ion-conducting central pore (Long, Campbell et al. 2005). In the voltage sensing domain (S4), positively charged lysine and arginine residues are spaced approximately 3 amino acids apart. These charged residues allow S4 to move in response to membrane potential and thus to control channel gating. S5 and S6 form the channel pore (Catterall, Perez-Reyes et al. 2005, Yarov-Yarovoy, DeCaen et al. 2012).

Numerous accessory β-subunits also associate with the channel to modulate its function (Tan, Kupershmidt et al. 2002, Calhoun and Isom 2014, Wang, Chung et al. 2014).

1.3.3. Phase 1 - early repolarization phase (transient outward current)

Expression of the *KCNA4* gene produces $K_V1.4$, *KCND2* encodes $K_V4.2$, and *KCND3* encodes $K_V4.3$ channels. Together, these molecular correlates conduct the transient outward current (I_{to}). The slow inactivating component of this current is conducted by $K_V1.4$ and the fast inactivating component is conducted by $K_V4.2$/$K_V4.3$ channels (Nerbonne, Nichols et al. 2001).

The majority of voltage-gated K^+ channels activate and deactivate in several hundred milliseconds. These channels also undergo inactivation (potentially through an N-terminal “ball and chain”) and subsequent recovery upon return to repolarized membrane potentials, albeit in a much shorter time frame (Sanguinetti, Jiang et al. 1995).

Greater density of I_{to} in the epicardium is thought to contribute in part to shorter AP duration and dispersion in AP morphology across the ventricular wall. This dispersion is essential for prevention of re-entry arrhythmias (Amin, Tan et al. 2010).

1.3.4. Phase 2 – plateau phase (calcium current)

The plateau phase results from the inward movement of Ca^{2+} and reduced extrusion of K^+ (London 2001, Sidi, Busch-Nentwich et al. 2004). The *CACNA1C* gene encodes the α_{1C} subunit of the $Ca_V1.2$ channel which conducts I_{Ca}.

$Ca_V1.2$ channels are also known as dihydropyridine receptors (DHPR) or L-Type Ca^{2+} channels (LTCCs) (Takahashi and Momiyama 1993, Rottbauer, Baker et al. 2001, Nerbonne and Kass 2005). The α_1-subunit is ~250 KDa and includes regions which function as the: pore, voltage sensor, and gate. Like the Na_V channel alpha, this subunit is composed of 4 identical domains (I-IV) each formed by 6 transmembrane segments (S1-S6) (Hell, Westenbroek et al. 1993). Among these, the S4 is the voltage sensor and the loop between S5 and S6 forms the channel pore (Catterall, Perez-Reyes et al. 2005). In addition to the α_1-subunit, numerous regulatory subunits play key modulatory roles in channel function, for example the $\alpha_2\delta$ -subunit contributes to control of channel

trafficking (Zhou, Saint-Amant et al. 2006, Zhou, Horstick et al. 2008). The β_2 subunit alters channel kinetics and drug sensitivities (Chien, Carr et al. 1996).

1.3.5. Phase 3 – late repolarization phase (delayed rectifier currents)

The repolarization phase is dominated by activity of the delayed rectifier currents which regulate K^+ efflux and repolarize the cell membrane potential back towards E_K. In the mammalian heart, the slow delayed rectifier K^+ current (I_{Ks}) provides a repolarization reserve. The molecular correlate of this channel is $K_V7.1$ (encoded by *KCNQ1*) in addition to the multiple accessory subunits including Min K (encoded by *KCNE1*). This channel activates slowly but does not appreciably inactivate, such that the current passed contributes to repolarization and is particularly important at times of elevated HR (Vandenberg, Perry et al. 2012). Mutations in this channel may give rise to Long QT Type 1. Some have postulated that low expression of this channel in the midmyocardium contributes to its longer AP duration compared to the endocardium and epicardium (Liu and Antzelevitch 1995).

The $K_V11.1$ channel is a product of the *KCNH2* gene, also known as the human ether-a-go-go related gene (hERG). This channel regulates the rapid delayed rectifier K^+ current (I_{Kr}) that plays a key role in late repolarization of the AP (Curran, Splawski et al. 1995, Sanguinetti and Tristani-Firouzi 2006, Leong, Skinner et al. 2010). hERG channels are characterized by slow activation and deactivation and very fast inactivation and recovery from inactivation. Functionally, hERG channels rapidly recover from inactivation to contribute to the late repolarization phase of the AP. The very slow movement of the voltage sensor in hERG is central to its function and allows it to play an essential role in AP termination (Sanguinetti and Tristani-Firouzi 2006, Vandenberg, Perry et al. 2012).

Interestingly, hERG is also thought to remain open at depolarized membrane potentials when it passes current in response to premature depolarization, instilling a protective property that is thought to suppress ectopic beats (Lu, Mahaut-Smith et al. 2001). The variable expression of repolarizing channels and thus the direction of repolarization across the transmural gradient of the ventricular wall is protective against arrhythmogenesis but this is diminished at more rapid HRs/shorter AP durations (Brunet, Aimond et al. 2004).

Loss of function in this channel can be associated with prolongation of the AP and long QT syndrome Type 2 (Chen, Zou et al. 1999). The unique structure (Thouta, Sokolov et al. 2014, Wang and MacKinnon 2017) and inactivation kinetics (Ficker, Jarolimek et al. 1998) of this channel predispose it to blockage by numerous drugs such as Dofetilide, Cisapride, and Terfenadine giving rise to acquired LQT; this fact necessitates careful screening prior to approval of all drugs by the Food and Drug Administration (Mitcheson, Chen et al. 2000).

KCNA5 which encodes $K_V1.5$ and passes the ultra rapid delayed rectifier current (I_{Kur}) is expressed minimally in the ventricles and to a much greater extent in atrial tissue (Boyle and Nerbonne 1991).

The majority of K^+ channels are made up of 4 separate subunits, each with 6 α-helical transmembrane domains. These subunits are expressed separately, not covalently linked, and assemble to form a tetrameric unit. Within each subunit of the channel, S4 is the voltage sensor and S5-S6 form the pore domain (Catterall 1988, Yu and Catterall 2004). Charged residues within the voltage sensor move in response to membrane depolarization to allow for pore opening and ion conduction down the electrochemical gradient (Tiwari-Woodruff, Schulteis et al. 1997).

1.4. Calcium release

Adult mammalian cardiomyocytes are typically rod-like in shape, measuring ~120 x 20 µm in dimension (Li, Stevens et al. 2013). Ca^{2+}-induced Ca^{2+}-release (CICR) is the process whereby Ca^{2+} entry through $Ca_V1.2$ causes release of intracellular Ca^{2+} stored in the sarcoplasmic reticulum (SR). CICR is the link between electrical activity and the contractile events which proceed it (Fabiato 1985, Meissner 2010). CICR requires proximity of $Ca_V1.2$ and RyR2, therefore mature mammalian cells develop an extensive transverse and axial tubule (T-tubule) network (Chugun, Taniguchi et al. 2003, Birkedal, Christopher et al. 2009). These networks carry the wave of depolarization initiated by the nodal cells to deep within the cell where voltage-dependent LTCCs open at about -35 mV to pass $I_{Ca,L}$.

T-type Ca^{2+} channels (TTCC), also known as $Ca_V3.1$ and encoded by the *CACNA1G* gene play a similar but smaller role in adult ventricular myocyte Ca^{2+} release

and are still not well defined. These channels are more prevalent in immature mammalian cells, conducting system of the heart, and pacemaker regions (Sidi, Busch-Nentwich et al. 2004, Bers 2008, Mesirca, Torrente et al. 2014). TTCCs are not specifically localized to couplons, they are activated at more negative membrane potentials than LTCCs, and they inactivate in a more rapid, Ca^{2+}-independent manner (Zhou and January 1998, Chen, Wilson et al. 2007).

The locus at which CICR occurs is termed a couplon; this is a region at the junction of T-tubules and the SR where approximately 10-25 LTCCs and 100-200 RyRs are co-localized (Franzini-Armstrong, Protasi et al. 1999). The channels in a couplon are activated in an all-or-none manner by the entry of Ca^{2+} through the LTCCs. The close proximity of DHPRs and RyR2 (~15-20 nm) allows for the latter to achieve peak release in 2-3 ms (Puglisi, Yuan et al. 1999). It is thought that each release event elevates junctional [Ca^{2+}] within the dyadic space up to 400 μM in 1 ms. Unitary release of Ca^{2+} from RyRs in a couplon is termed a Ca^{2+} spark (Bers 2002).

Adjacent couplons are approximately 1 μm apart and there are ~20,000 couplons in a cardiomyocyte. Activation of adjacent couplons is dependent on spark amplitude and distance of separation; sparks that diffuse to and activate multiple couplons lead to the propagation of a Ca^{2+}-wave across the cardiomyocyte (Lopez-Lopez, Shacklock et al. 1995). Diastolic levels of Ca^{2+} cytosolic (~100 nM) are thus increased by CICR to increase the cytosolic concentration of this ion up to 500-1200 nM (~600 nM Ca^{2+} gives a half maximal contraction) (Bers 2000). The elevation of cytosolic Ca^{2+} in the cardiomyocyte occurs rapidly (~100 ms) (Yue 1987). This elevation precedes interaction of ~50% of the released Ca^{2+} with troponin (~75 μM in the cell) which sets up a series of conformational changes that terminate in contraction (Schober, Huke et al. 2012).

Seminal work by Michael Stern explores the local control theory (Stern 1992). The Ca^{2+} trigger which enters through LTCCs preceeds the elevation of global Ca^{2+} in the cell. If a rise in global Ca^{2+} initiated RyR opening, further opening would be induced, and CICR would be all-or-none. In reality, such a response is inconsistent with the graded release that is characteristic of CICR in the cardiomyocyte. The theory of local control seeks to explain this by positing that local nanodomains in the vicinity of LTCCs control the release of Ca^{2+} through RyR. The activation of couplons is thus all-or-none. However, as a result of “self-termination” of SR Ca^{2+} release events the Ca^{2+} transient is

graded. The gradation in global Ca^{2+} signal needed to modulate function at elevated contractile states for example is thought to result from activation of variable numbers of couplons (Stern, Song et al. 1999).

Ca^{2+}-dependent inactivation (CDI) limits the amount of Ca^{2+} that enters the cell through LTCCs during every release event (Stern, Song et al. 1999). In diastole, calmodulin (CaM) associates with an IQ motif in the C-terminal domain of LTCCs to mediate CDI (Yuan, Ginsburg et al. 1996, Peterson, DeMaria et al. 1999, Pitt, Zühlke et al. 2001). Elevated Ca^{2+} binds the C-terminal sites of CaM during systole, helping to strengthen the interaction with the IQ motif thus accelerating inactivation (Sipido, Callewaert et al. 1995, Erickson, Alseikhan et al. 2001). LTCCs recover in ~100-200 ms prior to the next wave of depolarization (Bers 2008).

Ca^{2+}-dependent facilitation (CDF) is a Ca^{2+}/CaM dependent protein kinase II (CaMKII)-mediated process that only occurs at elevated HRs. CDF is induced by phosphorylation of key residues in the α_{1C}-subunit of the LTCC, increasing $I_{Ca,L}$ amplitude and slowing channel inactivation (Hudmon, Schulman et al. 2005).

1.4.1. Sarcoplasmic reticulum

The SR is a specialized endoplasmic reticulum, it is thought to make up ~10% of the mammalian cell volume and to have a free internal [Ca^{2+}] of ~1 mM (Bers 2001). Ca^{2+} release from the SR is the main player in activating contraction through the process of CICR, contributing about 60-70% of cytosolic Ca^{2+} during systole in human ventricular tissues (Bassani, Yuan et al. 1995, Bers 2001). The SR is almost never more than 60% depleted *in vivo* (Shannon, Guo et al. 2003).

Within the SR, calsequestrin (CASQ2), the buffer for luminal Ca^{2+}, is docked by and interacts closely with triadin, junctin, and RyR2 (Gyorke, Hester et al. 2004). Mutations in CASQ2 can cause increased delayed after depolarization (DAD) events (Liu, Colombi et al. 2006, George, Jundi et al. 2007). In general, increased SR Ca^{2+} load is the most likely substrate for aberrant events such as DADs. Elevated Ca^{2+} in the SR interacts with and increases the sensitivity of the RyR to cytosolic Ca^{2+}, thus increasing channel open probability (Sitsapesan and Williams 1994, Shannon, Ginsburg et al.

2000). Aberrant Ca^{2+} leak from the SR gives rise to Ca^{2+} sparks; subsequent extrusion of Ca^{2+} through NCX can lead to afterdepolarizations (Cheng, Lederer et al. 1993).

1.4.2. Ryanodine receptor

RyR2 is a ~2.2 MDa homotetramer that acts as a scaffold for multiple interrelated proteins that will be mentioned briefly (Sutko and Airey 1996). CaM allows for Ca^{2+}-dependent modulation of the RyR (Fruen, Bardy et al. 2000). Triadin, junctin, and CASQ2 buffer SR Ca^{2+} content and regulate release indirectly (Zhang, Kelley et al. 1997). FK-506 binding protein (FKBP 12.6) stabilizes RyR gating and allows for coupling of adjacent channels (Marx, Reiken et al. 2000). Protein Kinase A (PKA) localizes to the RyR and is thought to increase RyR opening (Valdivia, Kaplan et al. 1995, Marx, Reiken et al. 2000). The effects of PKA alone seem to be relatively mild compared to those induced by CaMKII which in fact enhances the effects of PKA (Haji-Ghassemi, Yuchi et al. 2019). Phosphatases 1 and 2A also interact with RyR2 and counter-regulate the effects of these kinases (Li, Kranias et al. 2002, Huke and Bers 2007).

Inositol triphosphate (IP_3) receptors co-localize with the RyR, especially in atrial cells (Mackenzie, Bootman et al. 2002). In response to G-protein coupled receptor (GPCR) dependent activation, IP_3 receptors can help cause local Ca^{2+} release from the SR leading to DADs (Zima, Copello et al. 2004).

1.5. Calcium removal

Ca^{2+} removal from the cytosol allows for relaxation. At steady state, this removal matches entry and occurs through the same route. The relative contribution of each component which participates in this removal is species and physiological state dependent. The human ventricular system is similar to mammals such as rabbits, dogs, and guinea pigs, in which the sarco/endoplasmic reticulum Ca^{2+}-ATPase (SERCA) removes ~70%, NCX ~28%, and sarcolemmal/mitochondrial Ca^{2+} ATPases ~1% (Bassani, Bassani et al. 1994). In mouse and rat cardiomyocytes, the contribution of SERCA is more pronounced (~92%) with NCX removing ~7% of the cytosolic Ca^{2+}. A small amount of Ca^{2+} is also taken up into the mitochondria where it elevates ATP production in response to increased energetic demand (Boyman, Chikando et al. 2014).

1.5.1. Sarco/endoplasmic reticulum Ca^{2+}-ATPase

The cardiac paralog of SERCA (SERCA2a) plays a key role in relaxation of the cardiac myocyte by pumping Ca^{2+} back into the SR lumen between each heartbeat. SERCA2a activity is highly regulated by phospholamban (PLB) whose dephosphorylated form strongly inhibits the pump. β-adrenergic stimulation leads to phosphorylation of PLB by PKA (Ser 16) or by CAMKII (Thr 17). Reduced inhibition and increased affinity of SERCA2a for Ca^{2+} by 2-3 fold in response to phosphorylation allows for more rapid uptake of Ca^{2+} into the SR (Bassani, Mattiazzi et al. 1995, Mattiazzi and Kranias 2014). This catecholamine-induced response is one of the main mechanisms governing acceleration of cardiac relaxation (Talosi, Edes et al. 1993). Catecholamines lead to changes in the competition between SERCA and NCX, shifting the balance to preferentially load the SR, and leading to an increase in SR Ca^{2+} content (Brittsan and Kranias 2000).

1.5.2. Na^+/Ca^{2+} exchanger

NCX is a reversible electrogenic anti-porter which moves 1 Ca^{2+} for every 3 Na^+ moved in the opposing direction. In cardiac tissue and under normal conditions, the majority of NCX1 function centers around removal of Ca^{2+}, which contributes to the slow decay of the Ca^{2+} transient at baseline (~400 ms) (Yue 1987, Bridge and Spitzer 1990, Nicoll, Longoni et al. 1990). Elevated cytosolic Ca^{2+} allosterically enhances NCX function to facilitate removal at above diastolic concentrations (Fujioka, Komeda et al. 2000, Philipson and Nicoll 2000).

NCX, for the most part does not localize to the couplon, therefore its contribution to elevation of the Ca^{2+} transient is thought to be negligible (Lipp, Egger et al. 2002). Ca^{2+} extrusion by NCX has to match sarcolemmal Ca^{2+} entry (LTCC and reverse mode NCX) in order to maintain Ca^{2+} homeostasis at steady-state. NCX removes an average of ~30% of cytosolic Ca^{2+}, ensuring that there is no net change in SR Ca^{2+} concentration on a beat-to-beat basis. Na^+ entry accompanies Ca^{2+} removal, thus the Na^+/K^+ ATPase must play a key role in resetting ionic gradients across the cellular membrane.

The reversal potential of NCX is dependent on Na^+ and Ca^{2+} ($E_{NXC} = 3E_{Na} – 2E_{Ca}$) and is approximately – 50 mV at baseline. Thus, as the membrane potential approaches

E_{NCX}, the exchanger is more likely to function in reverse mode. Depolarized membrane potentials, reduced DHPR function, and elevated Na^+ favor reverse-mode NCX function, whereby Ca^{2+} is brought into the cell (Dipla, Mattiello et al. 1999, Bers 2002). Ca^{2+} entry through NCX during the plateau phase is thought to contribute to AP prolongation (Weber, Piacentino et al. 2003). Prolongation of the AP is though to provide the substrate for DADs (Sipido, Callewaert et al. 1995). The mechanism for this is thought to be through removal of Ca^{2+} by, and aberrant entry of Na^+ through, NCX which depolarizes the membrane and may cause DADs (Pogwizd, Schlotthauer et al. 2001). DAD occurrence in multiple cells that are in close proximity may cause impulse propagation through the heart tissue and potentially fatal arrhythmias.

1.6. Contraction

The sarcomere is the smallest unit of the contractile apparatus (le Guennec, Mosca et al. 2008). Cardiomyocytes contain parallel myofibrils made up of repeating sarcomeric units, that are in turn comprised of interacting thick and thin myofilaments; this results in the characteristic striated appearance. These layers change in size as the cell contracts. Contraction is best understood through three main theories. These are the: 3-state model of contraction (Maytum, Lehrer et al. 1999), the 4-state model of contraction (Lehrer 2011), and the fly-casting model (Hoffman, Blumenschein et al. 2006).

1.6.1. The 3-state model of contraction

The 3-state model of contraction, is a simplification, put forth to help conceptualize the events that accompany Ca^{2+} fluctuations in the cardiomyocyte. The events which occur are not discreet but have been divided as such for ease of explanation. Perhaps appropriately, and to allow for better visualization these events are depicted in three distinct phases in **Figure 1-2** below.

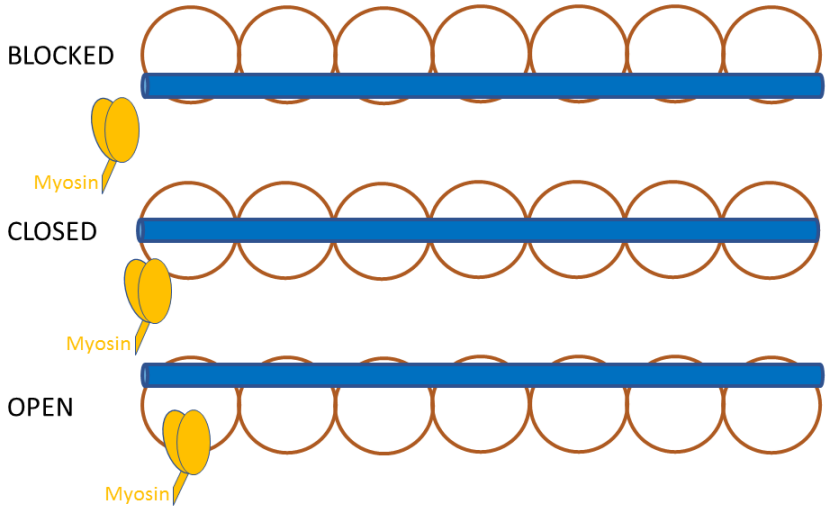

Figure 1-2 Schematic depiction of the 3-state model of contraction
This figure, is a simplified version of those presented in earlier publications (Maytum, Lehrer et al. 1999, McKillop and Geeves 1993). The circles indicate repeating actin units, the blue bars are representative of tropomyosin, and S1 mysoin heads are shown in yellow. The blocked-state accompanies diastolic concentrations of Ca^{2+}; in this state no myosin head binding occurs. Elevated Ca^{2+} during systole interacts with site II within TnC to cause conformational changes in the thin filament. These changes allow for the closed- and open-states to occur. In the closed-state, actin binding sites are exposed to some extent and some binding can occur. In the open-state, binding sites are more fully exposed and interaction of actin and myosin is more likely. In the 4-state model, the additional state is one where strong interaction between actin and myosin occurs at diastolic concentrations of free Ca^{2+}. The cytosolic free Ca^{2+} is continuously sensed by cTnC to re-orientate the thin filament. The conformational changes that accompany Ca^{2+} binding to cTnC determine the predominance of each state and amount of force production. The states in both models are not distinct, but rather exist on a continuum. These models are simplified to help visualize the occurance of events in the cell.

The components of the troponin complex (cTn) interact closely during the various phases of contraction. Cardiac troponin T (cTnT) connects the cTn complex to the thin filament and plays a role in actomyosin activation when Ca^{2+} is present. Troponin I (TnI) binds actin, TnT, and TnC; inhibiting contraction. The Blocked state (**B-state**) occurs during diastole when Ca^{2+} is not bound to site II of cardiac troponin C (cTnC) and its N-terminus is detached from the C-terminus of cardiac troponin I (cTnI). Cross-bridge activity is prevented as tropomyosin (Tm) blocks the myosin binding sites of actin (Pearlstone and Smillie 1983). The Closed state (**C-state**) occurs during systole and following CICR with Ca^{2+} binding to the regulatory domain of cTnC, but the low concentration means that weak cross-bridge activity is seen. Binding of the TnI regulatory domain to TnC, further opens the N-terminal domain of TnC; helices B and C move away from N, A, and D to expose a hydrophobic binding pocket (**Figure 4-1**) (Lindert, Kekenes-Huskey et al. 2012). This N-terminal pocket in cTnC is bound by the

cTnI switch peptide (TnI_{SW}) whose inhibitory function is weakened as the inhibitory peptide dissociates from the binding sites on actin (Li, Wang et al. 2005). Tm moves away from its inhibitory position on actin. By this process, the troponin-Tm complex moves into the actin binding-groove of the helix (Gordon, Regnier et al. 2001). The open/**M**yosin binding state (**M-state**) follows when greater amounts of Ca^{2+} to bind to site II; cooperatively exposing more binding sites on actin (Gordon, Homsher et al. 2000). As the conformational change is propagated through the cTn complex and the rest of the thin filament, contraction occurs through formation of actomyosin cross-bridges in an energy dependent step (Pinto, Parvatiyar et al. 2009, Tardiff 2011). The M-state is repeated while the cytosolic free concentration of Ca^{2+} is sufficiently high and the C-state is reverted to as the concentration drops. Once Ca^{2+} concentration is reduced to diastolic levels, with cTnC being the sensor, these processes are reversed, actin binding sites are no longer exposed, and force production can no longer occur (Gordon, Homsher et al. 2000). The thin filament is rarely ever fully off or on, instead it is often in a state of flux. In the presence of systolic levels of Ca^{2+}, the percentage occupancy (blocked/closed/open) is ~5, 80, and 25, respectively; and during diastole, these numbers are ~76, 22, and 1%, respectively (McKillop and Geeves 1993, Cordina, Liew et al. 2013).

1.6.2. The 4-state model of contraction

This model expands on the ideas set forth in the 3-state model. The 4 states are the: blocked Mg^{2+}-state (similar to the B-state), closed Ca^{2+}-state (equivalent to the C-state), open Mg^{2+}-S1 state, and open Ca^{2+}-S1 state (similar to the M-state). The open Mg^{2+}-S1-state, distinguishes the 4-state model from the 3-state model. In this state, S1-myosin interacts with actin in the absence of Ca^{2+}, relocates Tm on actin, and causes disconnection of the TnI mobile-domain from actin. As a result, the regulatory domain interacts with cTnC to increase its affinity for Ca^{2+} (Lehrer 2011).

The 4-state model also differs from the 3-state model, in that it incorporates a two-step relaxation process. In the first step, Ca^{2+} dissociates from site II of cTnC, then the mobile domain of cTnI dissociates from cTnC and subsequently associates with actin in a rapid initial step. The second step is slower and rate limiting, it involves interaction of the TnI inhibitory domain with actin which occurs simultaneously with continued interaction between myosin and actin to maintain cTnC in the open conformation and cause delayed relaxation (Xing, Jayasundar et al. 2009, Lehrer 2011).

1.6.3. The fly-casting model

The fly-casting model is formulated on the regulatory contribution of the cTnI mobile domain that is now well established (Li, Spyracopoulos et al. 1999). The regulatory domain fluctuates between actin and N-terminal cTnC binding sites. In contrast, at low Ca^{2+} concentration, the mobile domain forms stable interactions with actin. Elevated Ca^{2+} induces regulatory domain binding to N-terminal cTnC while the mobile domain becomes unbound from actin and enters a disordered state. The inhibitory domain of cTnI also dissociates from actin and binds the DE linker within cTnC. A drop in Ca^{2+} reverses these changes causing relaxation (Hoffman, Blumenschein et al. 2006).

Given the inherent similarities between the 3 models, it is feasible that each contains some aspects of the true mechanism. In general, cTnC and the cTn complex play key roles in regulating muscle contraction by sensing fluctuations in cytosolic Ca^{2+} levels. The conformational changes within the cTn complex are highly dependent on tertiary structure, which is in turn dependent on the amino acid sequence of the proteins. Mutations throughout the cTn complex may affect changes in the normal function of the complex leading to impaired force production capabilities of the heart, either by directly interfering with Ca^{2+} handling or by disrupting interactions between cTn complex proteins (Pinto, Parvatiyar et al. 2009).

1.6.4. Cross-bridge cycling

Muscle contraction in cardiac tissue results from the sliding of actin along myosin; this process has been somewhat arbitrarily divided into 8 steps. In the nucleotide-free rigour state, ATP binding to the S1 myosin head (**step 1**) causes detachment of S1 from actin (**step 2**). ATP is hydrolyzed (producing ADP and Pi) but remains attached to myosin which has high affinity for these products (**step 3**). This hydrolysis allows myosin to weakly bind the thin filament if Ca^{2+} is bound to cTnC (**step 4**). Actin availability allows for the formation of stronger interactions (**step 5**) and stronger cross-bridges needed for force generation. Release of Pi is coupled to the power stroke whereby the neck of myosin swings relative to the actin bound S1, producing force in an anti-parallel direction (**step 6**). Isomerization occurs in the S1 head

(**step 7**). Finally, ADP is released from myosin allowing ATP to bind and the thin and thick filaments to dissociate (**step 8**) (Gordon, Regnier et al. 2001).

1.7. Troponin complex

Ca^{2+} binding to cTnC within the cTn is the fundamental molecular switch which initiates a series of conformational changes that culminate in force production within cardiac tissue. Inhibitory cTnI and Tm binding cardiac troponin T (cTnT) are also components of the Tn complex, which along with Tm and actin forms the thin filament. The placement of the troponin complex occurs at regular intervals (~38 nm) along the actin filament and in the ratio of 1:1:7 of Tn:Tm:actin (Ebashi and Endo 1968, Yang, Barbu-Tudoran et al. 2014). In the heart, α-Tm forms a coiled-coil structure that associated with filamentous actin to comprise a helical structure that repeats every 7 globular actin units (Gordon, Homsher et al. 2000). The hexagonal array of the thin filament interacts with the thick filament of the contractile apparatus, which is composed primarily of: α and β myosin heavy chains, myosin light chains, myosin binding protein C (MyBP-C), and titin (Jaquet and Mügge 2012). In addition to the thin and thick filaments, many accessory proteins such as: obscurin, myomesin, nebulette, actinin, desmin, microtubules, and vimentin help arrange the filaments and play key signaling roles (Gautel and Djinovic-Carugo 2016).

The molecules of globular actin polymerize to form filamentous actin which has a double stranded helix-like appearance (Oda, Iwasa et al. 2009). Tm also polymerizes to form a continuous strand of dimers that lie in each actin groove, covering 7 actin monomers (Ebashi 1976, Zot and Potter 1987). The Tn complex interacts with Tm mainly though interactions with cTnT.

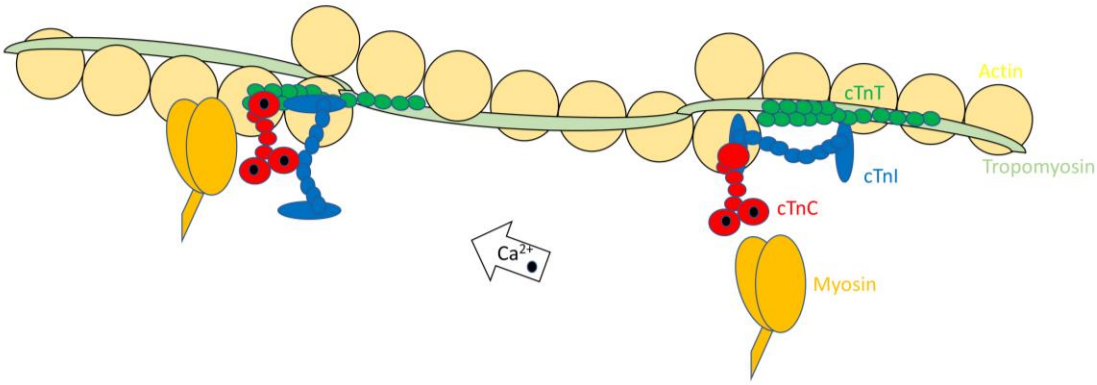

Figure 1-3 A schematic depiction of the simplified contractile apparatus showing the interacting thick and thin filament

In the apo-state C-terminal sites in cTnC (red) are occupied by diastolic concentrations of Ca^{2+}/Mg^{2+} (black spheres). Interaction is inhibited through the actions of cTnI (blue) and the Tn complex is located on the thin filament by cTnT (green). Presence of systolic concentrations of Ca^{2+} proceeds CICR, causes this cation to bind to the N-terminal site II of cTnC, and results in a series of conformational changes whereby the interaction with cTnI is strengthened and cTnT transmits the signal. Tm (light green) shifts to expose the binding sites on actin (beige), that are then bound by myosin (orange). Cross bridge formation is followed by ATP breakdown and energy dependent sliding of the filaments to cause muscle shortening and force production in the heart tissue. The rate of cross bridge turnover and ATP utilization is dependent in part on the isoform of myosin. α-MHC has higher cycling rate than β-MHC which is more highly expressed in adult humans compared to infants.

Light and heavy meromyosin wrap to form the double helix of the myosin heavy chain, the former is elongated while the later is more globular. Heavy meromyosin includes the S1 heads which contain the catalytic activity and the S2 arms which along with the light meromyosin compose the so-called tail. The myosin light chains (MLC1/MLC2) bind the S1 head to provide structure and allow for regulation. S1 myosin heads are oriented towards the z-lines at the ends of the sarcomere, leaving a central region on either side of the M-line (H-zone) that contains only tails.

1.7.1. Structure of the cTn complex

Tn is by necessity a highly flexible complex (Takeda, Yamashita et al. 2003). Therefore, adjustments were needed prior to structural determination; truncation of cTnI and cTnT was needed to facilitate crystallization as flexibility in the cTnT-Tm binding site was disruptive to global stability (Flicker, Phillips et al. 1982, White, Cohen et al. 1987). The core domain of the Ca^{2+}-saturated state of human cTn complex was solved by x-ray crystallography; this structure includes residues 1-161 in cTnC, 31-163 in cTnI (missing

part of N-terminal extension and C-terminal domain), and 183-288 in TnT (missing the Tm binding region) (**Figures 1-4 and 1-5**) (Takeda, Yamashita et al. 2003).

There are two key domains within the cTn complex. The first of these is the IT arm which anchors each component of the cTn to the actin-Tm filament (**Figures 1-4 and 1-5**). The IT arm includes helices 1 and 2 of TnI and TnT as well as the C-terminal domain of cTnC. H1 of TnI interacts with the hydrophobic cleft within the C-terminal domain of cTnC. H2 of TnI and TnT also interact to form a stabilizing, parallel coiled-coil α-helical structure (Stefancsik, Jha et al. 1998).

The second domain is the regulatory head, which is composed of helices 3 and 4 in TnI, as well as the C-terminal cTnI, and N-terminal cTnC (**Figures 1-4 and 1-5**). The sequence of cTnI includes the inhibitory region, followed by H3 and H4 sequentially. The inhibitory region of cTnI binds and blocks the actin binding sites in the Ca^{2+}-absent state. In the presence of Ca^{2+}, H3 of TnI binds the hydrophobic pocket located in N-TnC (Vassylyev, Takeda et al. 1998, Li, Spyracopoulos et al. 1999). The inhibitory region of TnI is removed from the actin-Tm complex. As a result, the inhibitory region of cTnI, H4 of TnI, as well as C-terminal TnI are also moved (Lehman, Hatch et al. 2000).

Binding of two Ca^{2+} ions offers sufficient stabilization to allow for N-TnC to be "open" in the absence of the TnI_{SW} (residues 147-163) (Gagne, Tsuda et al. 1995). However, given that cTnC only has one binding site for Ca^{2+}, this interaction alone is insufficient to maintain the molecule in the open state (Sia, Li et al. 1997). In the Ca^{2+}-bound state, cTnC may "sample" a semi-open state (Lindert, Kekenes-Huskey et al. 2012).

These proteins form a highly interrelated complex whose interactions and functions will be further discussed below.

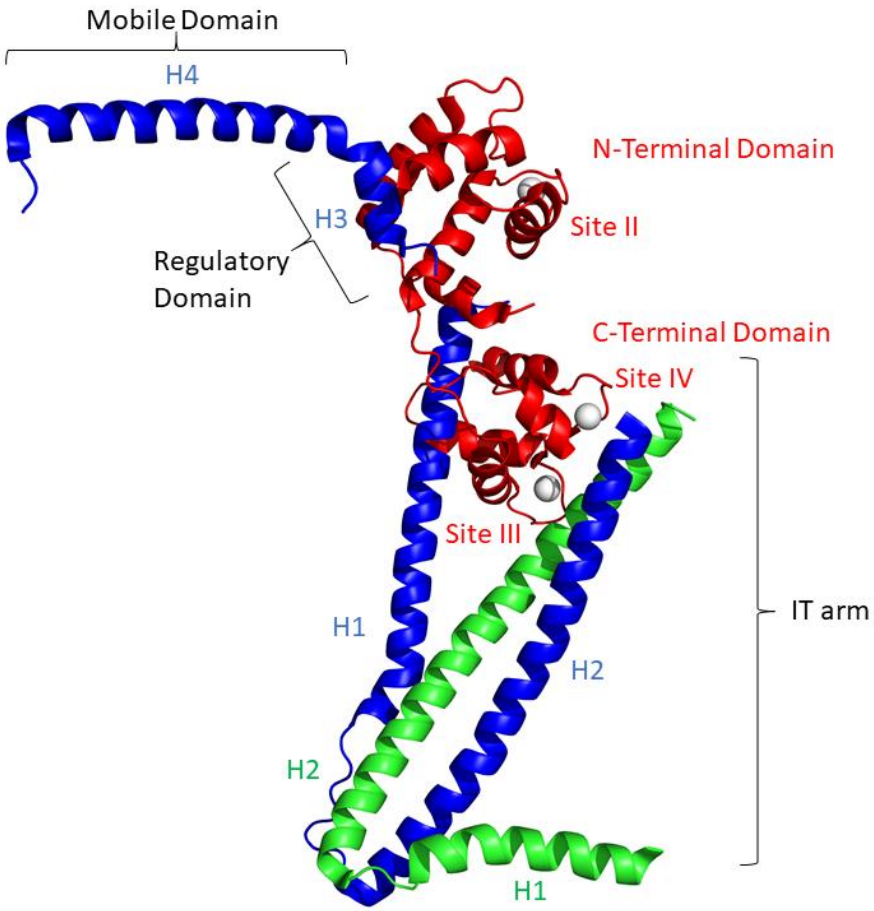

Figure 1-4 Structure of the Core domain of the cardiac Tn complex adapted from PDB:1J1E

The truncated cTnI (blue) and cTnT (green), as well as full length cTnC (red) were crystallized in the Ca^{2+}-bound state (Takeda, Yamashita et al. 2003). Ca^{2+} molecules are shown in white spheres. Helices H1 and H2 in TnT and H1, H2, H3, H4 in cTnI are shown. Within the cTn complex, the IT-arm consists of C-TnC (residues 93-161), H1 and H2 of cTnI (residues 42-136), and H1 and H2 of cTnT (residues 203-271). The regulatory domain consists of N-cTnC (residues 3-84) and cTnI (residues 150-159). The inhibitory region of cTnI, C-terminal domain of cTnI and N/C-terminal cTnT are characterized by ill-defined electron density maps. cTnI is composed of the: N-terminal domain (residues 2-32), IT hand (residues 32-136), inhibitory domain (residues 137-148), regulatory domain (residues 149-160), and mobile domain (residues 163-210). cTnT is composed of the: N-terminal variable domain (residues 2-67), central domain (residues 68-182), linker (residues 183-200), and C-terminal domain (residues 201-288). cTnC is composed of the: N-terminal domain (residues 1-87) and C-terminal domain (residues 92-161).

cTnC

MDDIYKAAVE QLTEEQKNEF KAAFDIFVLG AEDGCISTKE LGKVMRMLGQ NPTPEELQEM
IDEVDEDGSG TVDFDEFLVM MVRCMKDDSK GKSEEELSDL FRMFDKNADG YIDLDELKIM
LQATGETITE DDIEELMKDG DKNNDGRIDY DEFLEFMKGV E

cTnI

MADGSSDAAR EPRPAPAPIR R**RSSNYRAYA TEPHAKKKSK ISASRKLQLK TLLLQIAKQE**
LEREAEERRG EKGRALSTRC QPLELAGLGF AELQDLCRQL HARVDKVDEE RYDIEAKVTK
NITEIADLTQ KIFDLRGKFK RPTLRRVRIS ADAMMQALLG ARAKESLDLR AHLKQVKKED
TEKENREVGD WRKNIDALSG MEGRKKKFES

cTnT

MSDIEEVVEE YEEEEQEEAA VEEEEDWRED EDEQEEAAEE DAEAEAETEE TRAEEDEEEE
EAKEAEDGPM EESKPKPRSF MPNLVPPKIP DGERVDFDDI HRKRMEKDLN ELQALIEAHF
ENRKKEEEEL VSLKDRIERR RAERAEQQRI RNEREKERQN RLAEERARRE EEE**NRRKAED**
EARKKKALSN MMHFGGYIQK QAQTERKSGK RQTEREKKKK ILAERRKVLA IDHLNEDQLR
EKAKELWQSI YNLEAEKFDL QEKFKQQKYE INVLRNRIND NQKVSKTRGK AKVTGRWK

Figure 1-5 The sequence of cTnC, cTnI, and cTnT
The section of each protein which was included in the PDB:1J1E crystal structure (Takeda, Yamashita et al. 2003) is highlighted in bold font. The sequence for cTnC is shown in red, the sequence of cTnI is shown in blue, and the sequence of cTnT is shown in green.

Troponin I

TnI is the molecular key of the troponin complex and its main function is to inhibit contraction (Katrukha 2013). The slow skeletal variant of TnI (~21 KDa) is expressed in the heart during embryonic development but, is completely replaced by the lower affinity inducing cardiac variant (cTnI) (~24 KDa) within 9 months of birth (Sasse, Brand et al. 1993). cTnI is a 209 amino acid helical protein encoded by the *TNNI3* gene on the 19th chromosome. A fast skeletal TnI is also expressed in skeletal muscle of vertebrate species (Li, Wang et al. 2004).

cTnI contains regions that interact with actin, Tm, cTnC, and cTnT. Five key regions within the protein are: N-terminal domain, IT-arm, inhibitory domain, regulatory domain, and C-terminal mobile domain.

The *N-terminal domain* (residues 2-31) is specific to the cardiac isoform of TnI. This domain interacts with C-terminal cTnC (Ferrieres, Pugniere et al. 2000, Ward, Brewer et al. 2003). β-adrenergic stimulation and resultant phosphorylation of serines 23 and 24 by PKA disrupts the interaction between the N-terminal domain of TnI and C-terminus of cTnC ; N-terminal cTnI and the inhibitory domain interact instead (Kentish, McCloskey et al. 2001, Cheng, Lindert et al. 2014). Contractility is thus modulated and

the affinity of the thin filament for Ca^{2+} is reduced to allow for more rapid relaxation in times of stress/physical activity (Howarth, Meller et al. 2007, Solaro, Henze et al. 2013). It should be noted that other PKA mediated effects in the cell, such as increased I_{Ca} and reduced inhibition of SERCA2a may offset in part, or completely the resultant reduction in myofilament Ca^{2+} sensitivity (Bers 2002).

The *IT-arm* (residues 42-136) is an inflexible region of the protein that is composed of two α-helices connected by a linker; this region plays a structural role, it connects cTnI to cTnT and cTnC, and orients the molecule relative to the rest of the cTn complex (Takeda, Yamashita et al. 2003). The first helix (residues 42-79) connects the protein to the C-terminal domain of cTnC and the second helix (residues 90-136) links it to helix 2 (residues 226-271) within cTnT (Takeda, Yamashita et al. 2003).

The *inhibitory domain* has been variably defined by groups to span from residues 137-148 (Takeda, Yamashita et al. 2003, Kobayashi, Patrick et al. 2009) or 129-148 (Lindhout and Sykes 2003). This region binds actin during diastole, moving Tm to an obstructive position on the actin filament. During systole, this domain interacts with either the C-terminal domain (Lindhout and Sykes 2003) or the linker region of cTnC (Dong, Robinson et al. 2003) causing a disconnect of the TnI inhibitory domain from actin and movement of Tm (Li, Spyracopoulos et al. 1999, Wang, Li et al. 2002).

The *regulatory domain* (residues 149-163) contains helix 3 (H3) (residues 150-159). In the presence of high Ca^{2+}, H3 binds the hydrophobic patch within the N-terminal domain of cTnC and causes the inhibitory domain of TnI to shift away from Tm, exposing the actin binding sites (Li, Spyracopoulos et al. 1999).

The *mobile domain* (residues 163-210) is composed of H4 (residues 164-188) and the C-terminal section (residues 190-210). This region is not well characterized due to high structural flexibility (Takeda, Yamashita et al. 2003, Blumenschein, Stone et al. 2006, Julien, Mercier et al. 2011). The mobile domain is believed to play a role in positioning the cTn on the TF. *In vitro* study of recombinant proteins was used to show that the mobile domain interacts with Tm and actin at low Ca^{2+} concentration (Galinska-Rakoczy, Engel et al. 2008, Galinska, Hatch et al. 2010).

Troponin T

Three paralogs of TnT exist in the human genome. The slow skeletal paralog is encoded by *TNNT1*, the fast skeletal paralog is expressed by *TNNT3*, and the cardiac paralog is expressed by the *TNNT2* gene on chromosome 1 (Townsend, Farza et al. 1994, Mesnard, Logeart et al. 1995). cTnT is a 287 amino acid protein (~26 KDa) that is expressed in both heart tissue and skeletal muscle during gestation. By the 9th month of postnatal development, the exon 5 spliced-form of cTnT exists exclusively in the heart (Farza, Townsend et al. 1998).

The main role of cTnT is structural, whereby it anchors the cTn to the actin-Tm filament (Katrukha 2013). It does so through the following regions: N-terminal variable domain, conserved central domain, and C-terminal domain.

The *N-terminal region* (residues 2-68) has 32 unique amino acids that are not expressed in the skeletal isoforms of TnT. This region contains a number of glutamate residues and is therefore highly charged. There are conflicting reports regarding contact between this region and Tm/other cTn complex proteins (Verin and Gusev 1988, Pearlstone, Borgford et al. 1992). Regardless, there is an abundance of evidence which points to the role of this section of cTnT in orienting the cTn and thus regulating function of the contractile apparatus (Biesiadecki, Chong et al. 2007, Gollapudi and Chandra 2012).

The N-terminal segment of the *central domain* (residues 69-200) has high α-helical content. Within this domain, T1 (residues 98-136) connects to a binding site within adjacent dimer-forming Tm molecules. This interaction is independent of local Ca^{2+} concentration (Pearlstone and Smillie 1983). The C-terminal-most region of the central domain (residues 183-200) is more flexible and links to the C-terminus of cTnT (Manning, Tardiff et al. 2011).

The *C-terminal domain* of cTnT (residues 201-288) contains helices 1 (residues 204-220) and 2 (residues 226-271). T2 includes residues 197-239 according to some (Jin and Chong 2010) or residues 272-288 (Tanokura, Tawada et al. 1982, Morris and Lehrer 1984) and interacts with the IT-arm of cTnI, the C-terminal domain of cTnC, and Tm (Takeda, Yamashita et al. 2003). The interaction between cTnT and Tm is thought to

be strengthened during diastole thus stabilizing the Tn complex (Pearlstone and Smillie 1983, Franklin, Baxley et al. 2012).

Troponin C

The *TNNC1* gene is located on chromosome 3 and expresses the 161 amino acid (~18 KDa) cardiac/slow skeletal isoform of TnC, this variant is expressed in fetal skeletal and adult cardiac tissue (Parmacek and Leiden 1991). *TNNC2* is located on chromosome 20 and encodes fast skeletal TnC that is expressed exclusively in fast skeletal muscle and has 65% sequence similarity to cTnC (Townsend, Yacoub et al. 1997). The initiator methionine is removed from adult cTnT and cTnI. In contrast, the adult cTnC contains the initial methionine residue (van Eerd and Takahashi 1975).

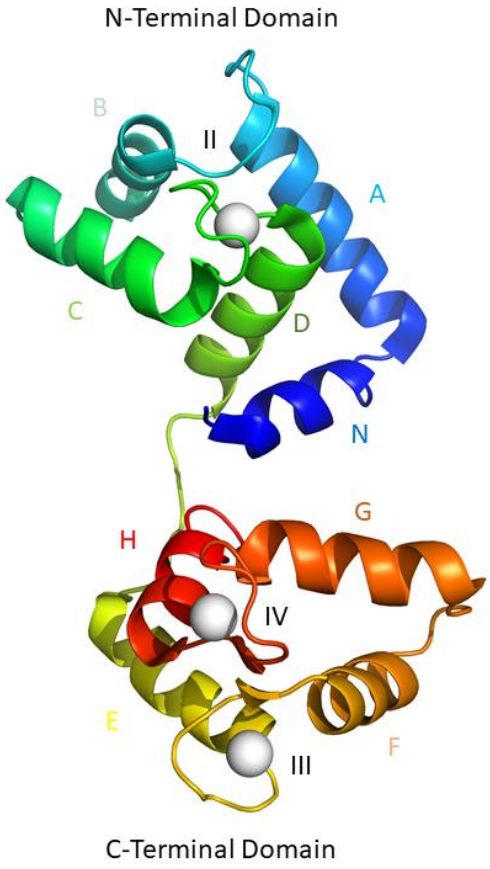

Figure 1-6 Image of Ca^{2+}-bound full length cTnC
The image of cTnC was generated in PyMol (L DeLano 2002) from the PDB:1J1E crystal structure (Takeda, Yamashita et al. 2003). α-helices formed by residues are shown in ribbon structure with the N-terminal most helix (N) in blue and the C-terminal most helix (H) in red. The EF hand binding site are labelled and contain Ca^{2+}/Mg^{2+} (depicted as white spheres).

cTnC is a dumbbell shaped protein containing two globular domains connected by a flexible linker; these are formed by a series of α-helices named N, A, B, C, D, E, F, G, and H (**Figure 1-6**) (Potter and Gergely 1975, Zot and Potter 1982). The N-terminal domain contains helices N (residues 1-13) through D (residues 74-81) and is connected by the flexible D-E linker to the C-terminal domain which contains helices E through H. The N-domain (residues 1-87) contains Ca^{2+}-binding EF hand motifs in sites I and II. The C-domain (residues 92-161) contains EF hand domains in sites III and IV (Takeda, Yamashita et al. 2003). Each EF-hand consists of a helix-loop-helix structure with 12 amino acid residues forming the loop (Kretsinger and Nockolds 1973). Residues 1(x), 3(y), 5(z), 7(-y), 9(-x), and 12(-z) form an octahedral coordination site for the Ca^{2+}/Mg^{2+} molecule and are often amino acids with acidic side chains containing oxygen atoms (Strynadka and James 1989). 7 residues located at the vertices of the pentagonal bipyramid coordinate Ca^{2+} and 6 are thought to be needed to coordinate Mg^{2+} (Lewit-Bentley and Rety 2000).

Table 1-1 cTnC structures used as the basis of computational work in this thesis

Structure	PDB ID	Technique	Species and Construct	Condition	Conformation and Interacting Partners	Section Used
1	PDB:1J1E	X-ray	Human cTnC	Ca^{2+} present	→Open-state →Certain domains of cTnI and cTnT present	→Tn structure (**Fig. 1-4**) →cTnC structure (**Fig. 1-5**) →N-cTnC bound to TnI_{SW} with FHC associated mutations (**Fig. 4-1**) →N-cTnC WT and D67A/D73A mutant structure (**Fig. 5-5**) →Tn, cTnC, and N-cTnC structures with FHC mutations (**Fig. 6-1**)
2	PDB:1AP4	NMR	Human N-cTnC	Ca^{2+} present	→Open-state	→Comparison of open and closed structure of N-cTnC (**Fig. 1-6**) →Starting parameters methods/results (**Chapter 3**) →Starting parameters procedures (**Chapter 4**) →WT structure for comparison with equilibrated FHC mutants (**Fig. 4-3**) →Starting parameters Thermodynamic Integration (**Chapter 5**)
3	PDB:1SPY	NMR	Human N-cTnC	Ca^{2+} free	→Closed-state	→Comparison of open and closed structure of N-cTnC (**Fig. 1-6**) →Starting parameters methods/results (**Chapter 3**) →AB interhelical angle (**Fig. 3-3**)
4	PDB:1MXL	NMR	Human N-cTnC	Ca^{2+} present	→Open-state →TnI_{SW} peptide present	→AB interhelical angle (**Fig. 3-3**) →Starting parameters procedures (**Chapter 4**)

The N-terminal domain of cTnC is the key region of interest for our studies. The N-terminal region contains α-helix N (residues 3-11). EF hand motif I contains: helix A (residues 14-28), EF hand I (residues 28-40), and helix B (residues 38-47). Residues 48-53 link the two EF hands. EF hand motif II contains helix C (residues 54-64), EF hand II (residues 65-73), and helix D (residues 74-81). The movement of helices NAD away from BC is the critical change which alleviates the strucural strain induced by Ca^{2+} binding to site II and causes the hydrophobic pocket within N-cTnC to be exposed for $cTnI_{SW}$ binding (Herzberg and James 1985). Residues 149 – 159 of the $cTnI_{SW}$ form an α-helical structure that inserts I148 and M153 that stabilize the exposed pocket (Li, Spyracopoulos et al. 1999).

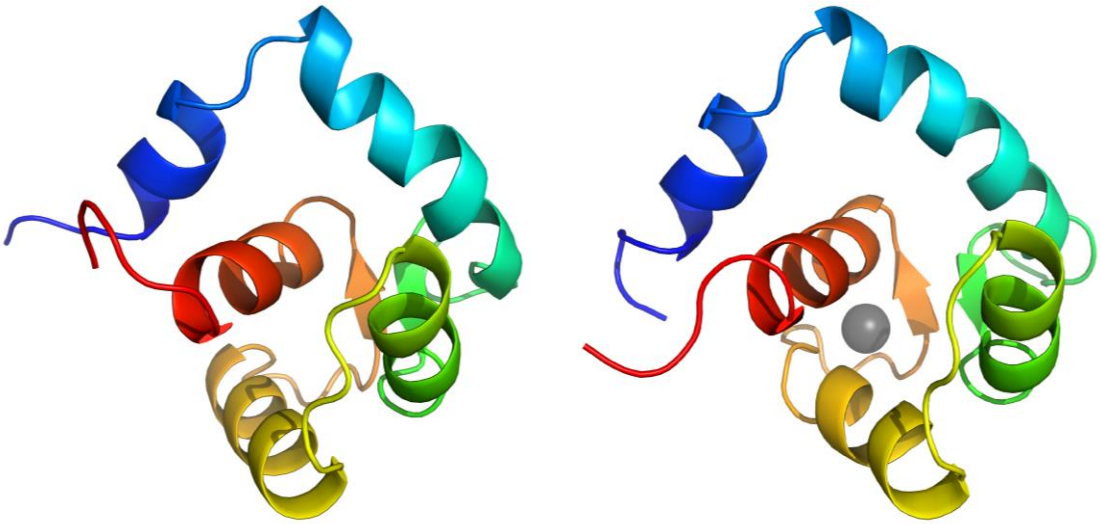

Figure 1-7 Structure of closed (apo-state) and open (holo-state) N-cTnC
The closed (no Ca^{2+}-bound) (left) and open (Ca^{2+}-bound) (right) structures were generated from the PDB:1SPY and PDB:1AP4 NMR structures, respectively. Ca^{2+} is depicted as a grey sphere. Unlike skeletal TnC, in cTnC the holo-state is much more closed, with the AB interhelical angle largely resembling that seen in the apo-state of cTnC (Spyracopoulos, Li et al. 1997).

Turkey and chicken skeletal TnC were the first to be crystalized. These structures suggested that binding of Ca^{2+} to site II causes helices B and C to move and tilt away from helices N, A, and D; exposing a hydrophobic cleft (Herzberg and James 1985, Sundaralingam, Bergstrom et al. 1985, Herzberg, Moult et al. 1986, Lindert, Kekenes-Huskey et al. 2012). This key conformational change is central to regulation of muscle contraction. Introduction of a disulfide bond or salt bridge structure that prevent helices BC moving away from helices NAD significantly reduces Ca^{2+} sensitivity and actomyosin ATPase activity (Fujimori, Sorenson et al. 1990, Grabarek, Tan et al. 1990).

Binding of Ca^{2+} to cTnC does not induce a large conformational change. In fact NMR-derived structures indicate that the holo-state of cTnC resembles the openness of apo-state skeletal TnC (**Figure 1-7**) (Houdusse, Love et al. 1997, Sia, Li et al. 1997, Spyracopoulos, Li et al. 1997). It is common to measure the AB interhelical angle to look at the openness of the N-domain of TnC. Previous works have used NMR derived structures to define AB interhelical angles less than 90º as open (Lindert, Kekenes-Huskey et al. 2012) and angles more than 135º as closed (Spyracopoulos, Li et al. 1997).

Sites III and IV are separated by 5 amino acids, these structural sites have high affinity for Ca^{2+} ($K_A = 10^7\ M^{-1}$) and Mg^{2+} ($K_A = 10^4\ M^{-1}$) and are thus completely occupied

at physiological free concentrations of each ion (0.1-1 µM and ~ 1 mM, respectively) (Potter and Gergely 1975, Johnson, Charlton et al. 1979, Rosenfeld and Taylor 1985, Johnson, Nakkula et al. 1994, Bers 2000). Binding of these cations exposes a hydrophobic patch to anchor the C-terminus of cTnC to the N-terminus of cTnI and prevents cTnC from drifting out of the cTn complex (Cheung, Tillotson et al. 1989). The openness of the C-terminal domain under physiological conditions is central to the structural role it plays in anchoring cTnC to the rest of the Tn complex (Zot and Potter 1987).

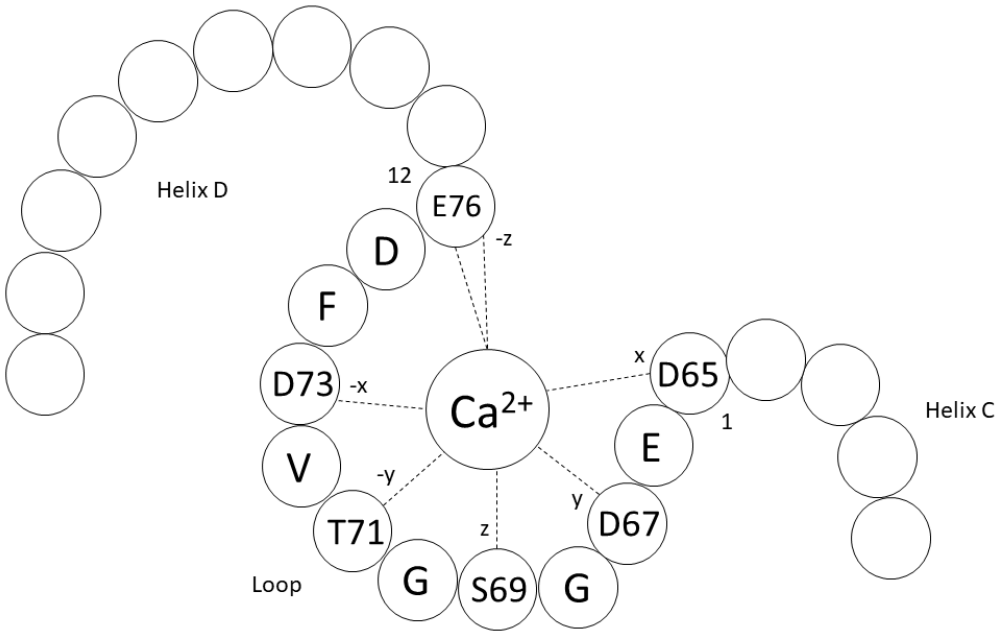

Figure 1-8 The Ca^{2+}-bound site II is shown with the coordinating residues labelled

The first 5 coordinating residues contain either carboxyl or hydroxyl oxygens to coordinate Ca^{2+}. The glutamine at position 12 contains 2 oxygen molecules. In total the pentagonal bipyramid which forms is able to offer 6 or 7 coordinating residues for divalent cation binding.

In the N-terminal domain of cTnC, two polar aspartic acid residues (30 and 32) in skeletal TnC are replaced by non-polar leucine and alanine at residues 29 and 31 of cTnC, respectively. A valine is also inserted at residue 28 of cTnC. The lack of a Ca^{2+}-coordinating oxygen molecule in the side chain of these amino acids has rendered site I of cTnC non-functional (van Eerd and Takahashi 1975, Johnson and Potter 1978). Despite this, site I activity is not needed to trigger the conformational change which accompanies Ca^{2+} binding to cTnC (Sweeney, Brito et al. 1990, Gulati 1992).

The "Ca^{2+}-specific" regulatory site II binds Ca^{2+} with low affinity ($K_A = 10^{-5}$ M) such that this site is unbound at diastolic concentrations (~0.1 µM) (Cheung, Tillotson et al. 1989) and bound at systolic concentrations (~ 1 µM) of the ion (**Figure 1-8**) (Rosenfeld and Taylor 1985, Kirschenlohr, Grace et al. 2000, Tikunova and Davis 2004). Binding of Ca^{2+} to cTnC occurs on the time-scale of ~1 msec (Robertson, Johnson et al. 1981) and results in a series of conformational changes that remove TnI inhibition from actin causing movement of Tm and exposure of the myosin binding sites on actin. Cytosolic Ca^{2+} buffering is complex, but thought to be due mainly to TnC, SERCA2a, and CaM with a Kd of ~ 1-2 µM. Importantly, TnC is a key Ca^{2+} buffer, where sites III/IV bind about 80% of the 100-200 µM $[Ca^{2+}]_{in}$ at resting concentrations of free Ca^{2+} (~100 nM) (Bers 2000). Altered Ca^{2+} binding to cTnC is thought to lead to arrhythmogenesis in the heart (Holroyde, Robertson et al. 1980, Bers 2001).

1.7.2. Length-dependent activation

Frank Starling mechanism

In response to stressful situations in the environment, the heart's pumping activity is intensified. Cardiac output (CO) is modulated through numerous mechanisms that cause an increased frequency of beating (HR) and strength of contraction (stroke volume (SV)). Length-dependent activation (LDA) is a property, inherent to the heart itself, whereby increased sarcomere length (SL) causes an increase in myofilament Ca^{2+} sensitivity, independent of end diastolic volume (EDV).

Higher CO corresponds to greater venous return and stretching of the heart tissue which must be coupled to altered pumping function. The absolutely critical Frank-Starling relationship of the heart explains this length dependent phenomenon, whereby an increase in EDV gives rise to greater SV (de Tombe, Mateja et al. 2010). This process is well documented in all species studied to date (Allen and Kurihara 1982, Janssen and de Tombe 1997, Dweck, Hus et al. 2008).

The spring-like, giant protein titin plays a critical role in the generation of passive tension and thus also contributes to LDA (Granzier and Labeit 2002, Moss and Fitzsimons 2002) in a manner that is dependent on: isoform (Seeley, Huang et al. 2007, Zou, Tran et al. 2015), phosphorylation (Driever, Solnica-Krezel et al. 1996), and species (Fukuda and Granzier 2005).

At the molecular level, sarcomere length of ~2 μm is normally seen at baseline and allows for optimal overlap between the actin and myosin filaments. Increase in length of the sarcomere beyond this causes elevated Ca^{2+} sensitivity of the cardiac TF (Kentish, ter Keurs et al. 1986). However, the mechanisms for LDA are disputed. The theory of lattice spacing, posits that at longer sarcomere lengths, the probability of actomyosin crossbridge formation increases due to proximity. Early studies assumed a fixed cell volume and thus correlated an increase in length to a decrease in width and closer proximity of the negatively charged myofilaments to the Ca^{2+} substrate. Skinned myofibril studies were carried out with results that support this theory (Fuchs and Wang 1996, Fukuda, Sasaki et al. 2001).

However, x-ray diffraction of the myocytes at different sarcomere lengths does not support this theory (Konhilas, Irving et al. 2002). Also, compression of the myocyte independent of length does not result in the same increase in affinity (Farman, Walker et al. 2006). Thus, these groups suggest that lattice spacing plays a smaller role with stiffness of Tm, effect of Ca^{2+} binding to adjacent cTn complexes, and myosin head orientation being key contributors to LDA (Konhilas, Irving et al. 2003, Farman, Allen et al. 2010, Farman, Gore et al. 2011, Kumar, Govindan et al. 2015). The consensus now is that lattice spacing is too simplistic an explanation for LDA. Instead, some have more recently suggested radial force as a key player (Williams, Regnier et al. 2010).

1.8. Cardiac muscle relaxation

The diastolic phase of the heart cycle is just as essential as the systole, proof in point are diseased states where diastolic dysfunction (the inability to relax adequately) causes significant impairment of heart function. During the relaxation phase, the chambers of the heart are filled through multiple mechanisms, some like intrathoracic pressure and the closed loop of the circulatory system allow for passive filling of the atrial chambers. Other mechanisms are active and include contraction of the atria and closing of the atrioventricular valves to prevent backflow of blood.

At the molecular level, dissociation of Ca^{2+} from the cTnC within the contractile apparatus allows for termination of contraction and distension of the heart chambers to allow for filling to happen in a synchronous manner.

The rate of Ca^{2+} dissociation from isolated cTnC is two orders of magnitude faster than myocardial relaxation (Hazard, Kohout et al. 1998). However, the incorporation of cTnC into the thin filament slows this rate by an order of magnitude and the binding of myosin-S1 to the thin filament slows the rate of dissociation by an additional order of magnitude (Davis, Norman et al. 2007). We have shown here (Chapter 2) and in the past studies (Gillis, Marshall et al. 2000, Gillis, Blumenschein et al. 2003) that the rate of Ca^{2+} dissociation from cTnC is minimally affected by temperature. However cross-bridge cycling is highly temperature dependent (Siemankowski, Wiseman et al. 1985). Others have found that while the rate of cross-bridge detachment and Ca^{2+} dissociation from the thin filament both play a role in muscle relaxation, under various ATP/temperature conditions, the effects may vary. Dissociation of Ca^{2+} from site II of cTnC is thought to be a rate-limiting step in muscle relaxation (Little, Biesiadecki et al. 2012).

1.9. Hypertrophic Cardiomyopathy

Familial Hypertrophic Cardiomyopathy (FHC) is the inherited, normally autosomal dominant subset of Hypertrophic Cardiomyopathy (HCM). With an incidence between 1 in 200 (Semsarian, Ingles et al. 2015) and 1 in 500 (Maron, Maron et al. 2012), HCM is the most common genetic cardiovascular disease and is noted as the main cause of sudden cardiac death (SCD) in young adults under the age of 35 (Huke 2017). Since the discovery of the first HCM-causing mutation in the gene for β-myosin heavy chain (*MYH7*) (Jarcho, McKenna et al. 1989), over 1400 mutations in 20 different genes that encode mostly sarcomeric proteins have been discovered (Fung, Yu et al. 1999, Willott, Gomes et al. 2010). HCM has also been associated with over 100 mutations in the cTn complex (Maron, Shirani et al. 1996, Ashrafian and Watkins 2007, Pinto, Parvatiyar et al. 2009, Maron and Maron 2013). Given that the genes for these proteins are often not routinely screened, most of these mutations have been identified following symptomatic presentation. FHC is genetically heterogeneous as associated mutations have been found in more than 10 predominantly contractile proteins. These include myosin heavy chain (Geisterfer-Lowrance, Kass et al. 1990), myosin light chains (Poetter, Jiang et al. 1996), myosin binding protein C (Bonne, Carrier et al. 1995), titin (Satoh, Takahashi et al. 1999), actin (Mogensen, Klausen et al. 1999), Tm (Thierfelder, Watkins et al. 1994), cTnT (Moolman-Smook, De Lange et al. 1999, Ho, Lever et al. 2000), cTnI (Mogensen,

Klausen et al. 1999), and cTnC (Landstrom, Parvatiyar et al. 2008, Pinto, Parvatiyar et al. 2009, Willott, Gomes et al. 2010). Of note to this project is the sequence of cTnC which is 97 – 99 % conserved in more than 60 variants and across more than 40 species studied to date (Gillis, Marshall et al. 2000).

The penetrance of HCM is not clear due to the vagaries of clinical diagnostic criteria. Manifestation of the disease has been shown to be age dependent; left ventricular hypertrophy (LVH) increases with age in younger patients but remains stable in the elderly (Maron, Spirito et al. 1986). Most are heterozygous for the mutant protein but the penetrance is variable, such that the disease manifests between the ages of 20-50. However, some homozygotes do exist, in which case there is noteworthy early manifestation of the disease in childhood (Maron, Maron et al. 2012). The disease manifestation varies from asymptomatic to extreme cases of hypertrophy (Prinz, Farr et al. 2011).

Interpretation of the data is suspect however, as cross-sectional and longitudinal studies are rarely performed. Phenotypic heterogeneity in HCM cannot be explained by genetic defects alone; gender, environmental factors, and additional diseases are likely modifiers. To further complicate matters, it is not uncommon for a single mutation to manifest in numerous ways, even in a given family (Menon, Michels et al. 2008). Cases of HCM have been reported in more than 50 countries across 5 continents, afflicting a wide variety of ethnic groups and demographics (Maron, Gardin et al. 1995, Kitaoka, Doi et al. 2003, Maron, Chaitman et al. 2004, Maron, Olivotto et al. 2006). The devastating nature of this disease is rooted in the frequent absence of overt symptoms combined with the age of initial outward manifestation. The first symptom is often SCD, which is normally attributed to ventricular tachycardia and/or fibrillation following premature ventricular contractions. Although mortality is similar across genders, the disease is thought to be under-diagnosed in females (Olivotto, Maron et al. 2005). HCM induced SCD is more common among men. SCD often occurs in athletic settings which are, even now frequented to a greater extent by men in most parts of the world (Maron, Carney et al. 2003). Moreover, HCM is rarely seen in children with the onset of symptoms in 65% of people by the age of 30 and 95% of people by the age of 60; this is highly mutation-depedent (Charron and Komajda 2006, Morita, Rehm et al. 2008).

1.9.1. Phenotypic manifestation

HCM causes only ~1% annual mortality in affected patients. Often resulting from physical activity, SCD accounts for 50% of these deaths. HCM is the most frequent cause of SCD in children and young adults, underlying the devastating nature of this disease where the first overt symptom is often death (Liberthson 1996). SCD is especially prevalent in young athletes, likely triggered by bouts of intense physical activity (Maron, Shirani et al. 1996). While the prevalence of HCM is consistent across genders, males are afflicted with a higher risk of SCD, likely due to lifestyle differences (Maron, Carney et al. 2003). The use of an Implantable Cardioverter Defibrillators (ICDs) offers an effective means of reducing the risk of SCD. However, as discussed above, identification of appropriate candidates for implantation is far from simple.

Increased left or right ventricular thickness, and declining cardiac output resulting from reduced diastolic volume and relaxation rate is seen in HCM patients (Maisch, Noutsias et al. 2012). Histopathology of the disease is characterized by cardiac and myocyte hypertrophy, hyperplasia of the coronary arteries, disarray of myocytes affecting up to 20% of the ventricles, fibrosis, septal hypertrophy, and abnormal diastolic function (Maron 2002, Elliott and McKenna 2004). Symptoms such as dyspnea (shortness of breath), chest pain, syncope, or presyncope (often upon exertion) have also been seen in patients. HCM is often accompanied by left ventricular (LV) wall thickness greater than 15 mm causing decreased chamber size and LV outflow tract obstruction (LVOTO) often managed through myectomy (Ashrafian and Watkins 2007). This disease is associated with no dilation in the LV with unaltered or improved systolic function of the heart as determined through electro/echo-cardiography (Elliott, Andersson et al. 2007). LVOTO is caused by anterior motion of the anterior leaflet of the mitral valve during systole with about 40% of patients showing this feature at rest and a further 50% developing it in a state of increased contractility (Maron, Olivotto et al. 2006). HCM has been shown to affect not only the systolic but also the diastolic phase of the heart cycle with increased LV stiffness and prolongation of relaxation being features of the disease. Despite these well-characterized features in cases of clear disease manifestation, there is a great deal of diversity in the clinical presentation of HCM cases with some individuals experiencing minimal symptoms (and presenting with little hypertrophy) and others showing: dyspnea during exercise/at rest, angina pectoris, palpitations, atrial fibrillation (AF), dizziness, presyncope/syncope, fatigue, or end stage

heart failure requiring cardiac transplantation. Similarly, electrocardiogram (ECG) based identification of the disease is made difficult through inconsistent observations in various patients and includes: left axis deviation, conduction abnormalities, ST-depression/abnormalities, and negative/giant T-waves. These abnormalities have been shown to occur in the absence of morphological hypertrophy in more than 50% of patients (Konno, Chang et al. 2010).

1.9.2. Molecular changes

Observable anatomical changes are not a prerequisite for the generally accepted theory of increased Ca^{2+} sensitivity of the thin filament in HCM (Baudenbacher, Schober et al. 2008, Brouwer, van Dijk et al. 2011). However, cTnC mutations account for less than 1% of FHC cases and are not yet well characterized. In general, HCM associated mutations have been fairly consistent in causing an increased Ca^{2+} sensitivity of force development (Chandra, Rundell et al. 2001, Hernandez, Szczesna-Cordary et al. 2005, Baudenbacher, Schober et al. 2008).

cTnC sensitizers such as CK-2017357 slow the rate of Ca^{2+} dissociation from cTnC in a system containing proteins of the thin filament but not in isolated cTnC. Increased affinity attributed to FHC-mutant cTnC likely results from tighter binding, however it may require at least the other cTn complex proteins to be observed (Russell, Hartman et al. 2012). Increased affinity is theorized to cause tighter binding and result in slower Ca^{2+} dissociation from cTnC, likely keeping the heart in a state of systole for longer periods and perhaps resulting in thickening of the ventricles, ventricular arrhythmias, diastolic dysfunction (DD), and decreased ventricular filling (Pinto, Parvatiyar et al. 2009). The Ca^{2+} sensitization that is though to lead to HCM also presents as a candidate for causing ventricular arrythmias (Knollmann, Kirchhof et al. 2003, Baudenbacher, Schober et al. 2008, Parvatiyar, Landstrom et al. 2012, Schober, Huke et al. 2012).

Mutations throughout the cTn complex change force production capability of the heart through altered Ca^{2+} handling or disrupted cTn complex protein interactions (Pinto, Parvatiyar et al. 2009, Kalyva, Parthenakis et al. 2014, Stevens, Rayani et al. 2017). Such changes can lead to phenotypic manifestations as severe as DD, arrhythmias, and

SCD. Implicated in HCM, DD is an increase in the resistance to filling of the ventricles due to structural abnormalities or impaired relaxation.

1.10. Dilated Cardiomyopathy

Dilated Cardiomyopathy (DCM) is associated with characteristic enlarged ventricles and impaired contractility observed as reduced ejection fraction and cardiac output (Maisch, Noutsias et al. 2012, McNally, Golbus et al. 2013). DCM is less prevalent than HCM and is seen in ~1 in 3000 individuals (Codd, Sugrue et al. 1989). Others have reported that DCM is 10 times less prevalent than HCM (Willott, Gomes et al. 2010). DCM is associated with LV enlargement with arrhythmias and systolic dysfunction causing ejection fraction less than 45% in the absence of hypertrophy and coronary artery disease (Redwood, Moolman-Smook et al. 1999, van Spaendonck-Zwarts, van Tintelen et al. 2010). Compensatory changes are thought to become maladaptive over time, eventually resulting in heart failure and SCD (Pinto, Siegfried et al. 2011). Approximately 50% of DCM patients survive for more than 5 years following the age of initial diagnosis (Seidman and Seidman 2001). In contrast to HCM, DCM mutants were generally believed to cause decreased Ca^{2+} sensitivity of force development (Venkatraman, Harada et al. 2003, Chang and Potter 2005, Venkatraman, Gomes et al. 2005, Robinson, Griffiths et al. 2007). However, more recently, it has been suggested that DCM associated mutations can increase or decrease the Ca^{2+} sensitivity of the thin filament (Marston 2011).

In general, DCM is a less prevalent and less well characterized disease whose genetic basis is less inclusive than HCM. DCM-associated mutations have been found in a handful of sarcomeric proteins: actin (Olson, Michels et al. 1998), β-myosin heavy chain (Kamisago, Sharma et al. 2000), MBP-C (Shimizu, Ino et al. 2005), Tm (Olson, Kishimoto et al. 2001), titin (Gerull, Gramlich et al. 2002), cTnT (Mogensen, Murphy et al. 2004), and cTnC (van Spaendonck-Zwarts, van Tintelen et al. 2010).

An integrated tension index has recently been developed as a predictive tool to model the HCM to DCM continuum through the type (concentric/eccentric) and extent/severity of hypertrophy. This index allows for monitoring of force production in isolated fibers to generate a curve over time, with the integral of the area under the curve being used to predict HCM/DCM severity (Davis, Davis et al. 2016). Mouse

models of HCM/DCM mutations were used to make in vivo measurements of tension. Mechanical relaxation and Ca^{2+} decay kinetics are factors that were found to predict heart tissue thickness. The area under the tension/shortening curve as a function of time was normalized to the WT and was predictive of ventricular mass with positive values corresponding to HCM and negative values corresponding to DCM. Myocyte growth seemed to be largely determined by duration and magnitude of mechanical tension (Davis, Davis et al. 2016).

Mutations in cTnC have been implicated in altered cardiac contraction and relaxation and predispose carriers to cardiomyopathies. It is theorized that changes in Ca^{2+} sensitivity of the contractile machinery observed in the majority of FHC-associated mutations in cTnC may lead to altered relaxed state of the tissue that may result in thickening of the ventricles causing DD (Maron, Carney et al. 2003). Currently, no study has comprehensively studied the thermodynamic landscape that governs the favourability of the interaction between Ca^{2+} and site II of cTnC containing FHC and DCM associated mutations.

The final section of this introduction will lay out the sections that are to come. With this in mind, the primary hypotheses formed and the corresponding aims of this thesis are listed below.

1.10.1. Hypotheses

Hypothesis 1: We hypothesize that different affinity for Ca^{2+} underlies variable expression of two TnC paralogs in the zebrafish heart, upon temperature acclimation.

Hypothesis 2: We hypothesize that the Ca^{2+} binding affinity of cTnC is elevated by HCM-associated mutations and decreased by DCM-associated mutations.

Hypothesis 3: We hypothesize that Mg^{2+} competes with Ca^{2+} for binding to the regulatory site II of cTnC, binding this site with physiologically relevant affinity.

Hypothesis 4: We hypothesize that the Mg^{2+} binding affinity of HCM-mutant cTnC is variable and affects Ca^{2+} binding to different degrees.

1.10.2. Aims

Aim 1: To establish a protocol for carrying out isothermal titration calorimetry (ITC) experiments on the N-terminal domain of cTnC. To explore the effect of temperature on the thermodynamic landscape of the interaction between site II and Ca^{2+} under various experimental protocols. (Chapters 2 and 3)

Aim 2: To establish a complement of techniques involving Molecular Dynamics (MD) Simulations, ITC, and melting point analysis to study the N-terminal domain of TnC using *in silico* methodology and recombinant protein-based *in vitro* experiments. Having done so we aim to explore the functional implications of variable expression pattern of TnC paralogs in the zebrafish system. (Chapter 3)

Aim 3: To study the effect of a series of N-terminal mutations in cTnC that are associated with FHC, DCM, and increased Ca^{2+} affinity using the previously developed workflow involving MD Simulations, ITC, and melting point analysis. (Chapter 4)

Aim 4: to explore the binding of Ca^{2+} to site II in N-cTnC and full length cTnC and explore the effects of baseline and elevated Mg^{2+} on this fundamental interaction. (Chapter 5)

Aim 5: to probe, as a culmination of the previous work, the effect of Mg^{2+} on the Ca^{2+} binding properties of the same series of mutations in N-cTnC using ITC and Themodynamic Integration (TI) Simulations. (Chapter 6)

Having outlined these aims and hypotheses, the next section will summarize the overall objectives of this thesis and complete the introduction to this project.

1.10.3. Objectives

The objective of our study was to better understand the structural and functional impact of a series of N-terminal mutations in cTnC. We have explored the mechanisms by which these single amino acid changes may cause disease. The focus of this study is a host of FHC-associated mutations (A8V, L29Q, A31S, C84Y), one engineered Ca^{2+} sensitizing mutation (L48Q), and one DCM-associated mutation (Q50R) in the N-terminus of cTnC. This is a major subset of the 7 HCM and 7 DCM mutations identified

to date in cTnC (Kalyva, Parthenakis et al. 2014). We have studed the effects of the above stated mutations using recombinant human cTnC.

There are a large number of HCM-associated mutations in a wide variety of sarcomeric proteins. The most established paradigm states that mutations in sarcomeric proteins which increase myofilament Ca^{2+} sensitivity cause HCM and those that reduce Ca^{2+} sensitivity result in DCM (Dweck, Hus et al. 2008). Therefore, these mutations feedback on cTn to cause a characteristic change in Ca^{2+} sensitivity of force development and cTnC is the gatekeeper.

We have utilized reductionist science to explore complex physiological phenomena by studying only the proximal most element in the Ca^{2+} binding complex of the contractile apparatus. While this approach is not without limitations, we hope to avoid confounding variables in studying this interaction.

Higher Ca^{2+} binding affinities (lower K_d) result in lower concentrations of free Ca^{2+} in the cytosol for a given amount of total Ca^{2+}. Assuming these alterations affect both “on” and “off” rates, slower Ca^{2+} dissociation rate (k_{off}) from the myofilament is a consequence. Increasing concentration of free Ca^{2+} at the end of diastole increases the load of the SR. Aberrant release of Ca^{2+} from the SR, AP prolongation, and EADs may trigger arrhythmias (Schober, Huke et al. 2012).

Within this framework, we have also explored the Mg^{2+}-binding properties of cTnC. The binding of this cation is thought to play a structural role within the contractile apparatus, however despite the prevalence, it is not thought to regulate contraction directly. As the culmination of this work, we have questioned this notion based on findings by other groups (Ogawa 1985, Yumoto, Nara et al. 2001, Davis, Rall et al. 2002) and explored the possible role of Mg^{2+} in contractile regulation in the normal heart and the diseased state.

1.11. References

Allen, D. and S. Kurihara (1982). "The effects of muscle length on intracellular calcium transients in mammalian cardiac muscle." The Journal of physiology 327(1): 79-94.

Amin, A. S., H. L. Tan and A. A. Wilde (2010). "Cardiac ion channels in health and disease." Heart Rhythm 7(1): 117-126.

Ashrafian, H. and H. Watkins (2007). "Reviews of translational medicine and genomics in cardiovascular disease: new disease taxonomy and therapeutic implications: Cardiomyopathies: Therapeutics based on molecular phenotype." Journal of the American College of Cardiology 49(12): 1251-1264.

Asimaki, A., A. G. Kleber and J. E. Saffitz (2015). "Pathogenesis of Arrhythmogenic Cardiomyopathy." The Canadian journal of cardiology 31(11): 1313-1324.

Bassani, J., R. A. Bassani and D. M. Bers (1994). "Relaxation in rabbit and rat cardiac cells: species-dependent differences in cellular mechanisms." The Journal of Physiology 476(2): 279.

Bassani, J. W., W. Yuan and D. M. Bers (1995). "Fractional SR Ca release is regulated by trigger Ca and SR Ca content in cardiac myocytes." Am J Physiol 268(5 Pt 1): C1313-1319.

Bassani, R. A., A. Mattiazzi and D. M. Bers (1995). "CaMKII is responsible for activity-dependent acceleration of relaxation in rat ventricular myocytes." Am J Physiol 268(2 Pt 2): H703-712.

Baudenbacher, F., T. Schober, J. R. Pinto, V. Y. Sidorov, F. Hilliard, R. J. Solaro, J. D. Potter and B. C. Knollmann (2008). "Myofilament Ca2+ sensitization causes susceptibility to cardiac arrhythmia in mice." J Clin Invest 118(12): 3893-3903.

Bers, D. (2001). Excitation-contraction coupling and cardiac contractile force, Springer Science & Business Media.

Bers, D. M. (2000). "Calcium Fluxes Involved in Control of Cardiac Myocyte Contraction." Circulation Research 87(4): 275-281.

Bers, D. M. (2001). Sources and sinks of activator calcium. Excitation-Contraction Coupling and Cardiac Contractile Force, Springer: 39-62.

Bers, D. M. (2002). "Cardiac excitation–contraction coupling." Nature 415(6868): 198-205.

Bers, D. M. (2008). "Calcium cycling and signaling in cardiac myocytes." Annu. Rev. Physiol. 70: 23-49.

Biesiadecki, B. J., S. M. Chong, T. M. Nosek and J. P. Jin (2007). "Troponin T core structure and the regulatory NH2-terminal variable region." Biochemistry **46**(5): 1368-1379.

Birkedal, R., J. Christopher, A. Thistlethwaite and H. A. Shiels (2009). "Temperature acclimation has no effect on ryanodine receptor expression or subcellular localization in rainbow trout heart." Journal of Comparative Physiology B **179**(8): 961.

Blumenschein, T. M., D. B. Stone, R. J. Fletterick, R. A. Mendelson and B. D. Sykes (2006). "Dynamics of the C-terminal region of TnI in the troponin complex in solution." Biophys J **90**(7): 2436-2444.

Bonne, G., L. Carrier, J. Bercovici, C. Cruaud, P. Richard, B. Hainque, M. Gautel, S. Labeit, M. James, J. Beckmann, J. Weissenbach, H.-P. Vosberg, M. Fiszman, M. Komajda and K. Schwartz (1995). "Cardiac myosin binding protein–C gene splice acceptor site mutation is associated with familial hypertrophic cardiomyopathy." Nature Genetics **11**(4): 438-440.

Boyle, W. A. and J. M. Nerbonne (1991). "A novel type of depolarization-activated K+ current in isolated adult rat atrial myocytes." Am J Physiol **260**(4 Pt 2): H1236-1247.

Boyman, L., A. C. Chikando, G. S. Williams, R. J. Khairallah, S. Kettlewell, C. W. Ward, G. L. Smith, J. P. Kao and W. J. Lederer (2014). "Calcium movement in cardiac mitochondria." Biophys J **107**(6): 1289-1301.

Bridge, J. and K. W. Spitzer (1990). "The relationship between charge movements associated with ICa and INa-Ca in cardiac myocytes." Science **248**(4953): 376-378.

Brittsan, A. G. and E. G. Kranias (2000). "Phospholamban and cardiac contractile function." J Mol Cell Cardiol **32**(12): 2131-2139.

Brouwer, W. P., S. J. van Dijk, G. J. M. Stienen, A. C. van Rossum, J. van der Velden and T. Germans (2011). "The development of familial hypertrophic cardiomyopathy: from mutation to bedside." European Journal of Clinical Investigation **41**(5): 568-578.

Brunet, S., F. Aimond, H. Li, W. Guo, J. Eldstrom, D. Fedida, K. A. Yamada and J. M. Nerbonne (2004). "Heterogeneous expression of repolarizing, voltage-gated K+ currents in adult mouse ventricles." The Journal of physiology **559**(1): 103-120.

Calhoun, J. D. and L. L. Isom (2014). "The role of non-pore-forming beta subunits in physiology and pathophysiology of voltage-gated sodium channels." Handb Exp Pharmacol **221**: 51-89.

Catterall, W. A. (1988). "Structure and function of voltage-sensitive ion channels." Science **242**(4875): 50-61.

Catterall, W. A., E. Perez-Reyes, T. P. Snutch and J. Striessnig (2005). "International Union of Pharmacology. XLVIII. Nomenclature and structure-function relationships of voltage-gated calcium channels." Pharmacological reviews **57**(4): 411-425.

Chandra, M., V. L. Rundell, J. C. Tardiff, L. A. Leinwand, P. P. De Tombe and R. J. Solaro (2001). "Ca2+ activation of myofilaments from transgenic mouse hearts expressing R92Q mutant cardiac troponin T." American Journal of Physiology-Heart and Circulatory Physiology **280**(2): H705-H713.

Chang, A. N. and J. D. Potter (2005). "Sarcomeric protein mutations in dilated cardiomyopathy." Heart failure reviews **10**(3): 225-235.

Charron, P. and M. Komajda (2006). "Molecular genetics in hypertrophic cardiomyopathy: towards individualized management of the disease." Expert Review of Molecular Diagnostics **6**(1): 65-78.

Chen, J., A. Zou, I. Splawski, M. T. Keating and M. C. Sanguinetti (1999). "Long QT syndrome-associated mutations in the Per-Arnt-Sim (PAS) domain of HERG potassium channels accelerate channel deactivation." J Biol Chem **274**(15): 10113-10118.

Chen, Q., G. E. Kirsch, D. Zhang, R. Brugada, J. Brugada, P. Brugada, D. Potenza, A. Moya, M. Borggrefe, G. Breithardt, R. Ortiz-Lopez, Z. Wang, C. Antzelevitch, R. E. O'Brien, E. Schulze-Bahr, M. T. Keating, J. A. Towbin and Q. Wang (1998). "Genetic basis and molecular mechanism for idiopathic ventricular fibrillation." Nature **392**(6673): 293-296.

Chen, X., R. M. Wilson, H. Kubo, R. M. Berretta, D. M. Harris, X. Zhang, N. Jaleel, S. M. MacDonnell, C. Bearzi, J. Tillmanns, I. Trofimova, T. Hosoda, F. Mosna, L. Cribbs, A. Leri, J. Kajstura, P. Anversa and S. R. Houser (2007). "Adolescent Feline Heart Contains a Population of Small, Proliferative Ventricular Myocytes With Immature Physiological Properties." Circulation Research **100**(4): 536-544.

Cheng, H., W. Lederer and M. B. Cannell (1993). "Calcium sparks: elementary events underlying excitation-contraction coupling in heart muscle." Science: 740-744.

Cheng, Y., S. Lindert, P. Kekenes-Huskey, V. S. Rao, R. J. Solaro, P. R. Rosevear, R. Amaro, A. D. McCulloch, J. A. McCammon and M. Regnier (2014). "Computational studies of the effect of the S23D/S24D troponin I mutation on cardiac troponin structural dynamics." Biophys J **107**(7): 1675-1685.

Cheung, J. Y., D. L. Tillotson, R. Yelamarty and R. Scaduto (1989). "Cytosolic free calcium concentration in individual cardiac myocytes in primary culture." American Journal of Physiology-Cell Physiology **256**(6): C1120-C1130.

Chien, A. J., K. M. Carr, R. E. Shirokov, E. Rios and M. M. Hosey (1996). "Identification of palmitoylation sites within the L-type calcium channel beta2a subunit and effects on channel function." J Biol Chem **271**(43): 26465-26468.

Chugun, A., K. Taniguchi, T. Murayama, T. Uchide, Y. Hara, K. Temma, Y. Ogawa and T. Akera (2003). "Subcellular distribution of ryanodine receptors in the cardiac muscle of carp (Cyprinus carpio)." American Journal of Physiology-Regulatory, Integrative and Comparative Physiology **285**(3): R601-R609.

Cobb, J. L. (1974). "Gap junctions in the heart of teleost fish." Cell and tissue research **154**(1): 131-134.

Codd, M. B., D. D. Sugrue, B. J. Gersh and L. J. Melton, 3rd (1989). "Epidemiology of idiopathic dilated and hypertrophic cardiomyopathy. A population-based study in Olmsted County, Minnesota, 1975-1984." Circulation **80**(3): 564-572.

Cordina, N. M., C. K. Liew, D. A. Gell, P. G. Fajer, J. P. Mackay and L. J. Brown (2013). "Effects of Calcium Binding and the Hypertrophic Cardiomyopathy A8V Mutation on the Dynamic Equilibrium between Closed and Open Conformations of the Regulatory N-Domain of Isolated Cardiac Troponin C." Biochemistry **52**(11): 1950-1962.

Curran, M. E., I. Splawski, K. W. Timothy, G. M. Vincent, E. D. Green and M. T. Keating (1995). "A molecular basis for cardiac arrhythmia: HERG mutations cause long QT syndrome." Cell **80**(5): 795-803.

Davis, J., L. C. Davis, R. N. Correll, C. A. Makarewich, J. A. Schwanekamp, F. Moussavi-Harami, D. Wang, A. J. York, H. Wu and S. R. Houser (2016). "A tension-based model distinguishes hypertrophic versus dilated cardiomyopathy." Cell **165**(5): 1147-1159.

Davis, J. P., C. Norman, T. Kobayashi, R. J. Solaro, D. R. Swartz and S. B. Tikunova (2007). "Effects of thin and thick filament proteins on calcium binding and exchange with cardiac troponin C." Biophysical journal **92**(9): 3195-3206.

Davis, J. P., J. A. Rall, P. J. Reiser, L. B. Smillie and S. B. Tikunova (2002). "Engineering competitive magnesium binding into the first EF-hand of skeletal troponin C." J Biol Chem **277**(51): 49716-49726.

de Tombe, P. P., R. D. Mateja, K. Tachampa, Y. A. Mou, G. P. Farman and T. C. Irving (2010). "Myofilament length dependent activation." Journal of molecular and cellular cardiology **48**(5): 851-858.

Dipla, K., J. A. Mattiello, K. B. Margulies, V. Jeevanandam and S. R. Houser (1999). "The sarcoplasmic reticulum and the Na+/Ca2+ exchanger both contribute to the Ca2+ transient of failing human ventricular myocytes." Circ Res **84**(4): 435-444.

Dong, W.-J., J. M. Robinson, S. Stagg, J. Xing and H. C. Cheung (2003). "Ca2+-induced conformational transition in the inhibitory and regulatory regions of cardiac troponin I." Journal of Biological Chemistry **278**(10): 8686-8692.

Driever, W., L. Solnica-Krezel, A. Schier, S. Neuhauss, J. Malicki, D. Stemple, D. Stainier, F. Zwartkruis, S. Abdelilah and Z. Rangini (1996). "A genetic screen for mutations affecting embryogenesis in zebrafish." Development **123**(1): 37-46.

Dweck, D., N. Hus and J. D. Potter (2008). "Challenging current paradigms related to cardiomyopathies Are changes in the Ca2+ sensitivity of myofilaments containing cardiac troponin C mutations (G159D and L29Q) good predictors of the phenotypic outcomes?" Journal of Biological Chemistry **283**(48): 33119-33128.

Ebashi, S. (1976). "Proceedings: Regulation of the myosin-actin interaction by the Ca2+-troponin-tropomyosin system." Journal of biochemistry **79**(4): 48P.

Ebashi, S. and M. Endo (1968). "Calcium ion and muscle contraction." Prog Biophys Mol Biol **18**: 123-183.

Elliott, P., B. Andersson, E. Arbustini, Z. Bilinska, F. Cecchi, P. Charron, O. Dubourg, U. Kühl, B. Maisch and W. J. McKenna (2007). "Classification of the cardiomyopathies: a position statement from the European Society Of Cardiology Working Group on Myocardial and Pericardial Diseases." European heart journal **29**(2): 270-276.

Elliott, P. and W. J. McKenna (2004). "Hypertrophic cardiomyopathy." Lancet **363**(9424): 1881-1891.

Erickson, M. G., B. A. Alseikhan, B. Z. Peterson and D. T. Yue (2001). "Preassociation of calmodulin with voltage-gated Ca(2+) channels revealed by FRET in single living cells." Neuron **31**(6): 973-985.

Essner, J., J. Laing, E. Beyer, R. Johnson and P. Hackett Jr (1996). "Expression of Zebrafishconnexin43. 4in the Notochord and Tail Bud of Wild-Type and Mutantno tailEmbryos." Developmental biology **177**(2): 449-462.

Fabiato, A. (1985). "Time and calcium dependence of activation and inactivation of calcium-induced release of calcium from the sarcoplasmic reticulum of a skinned canine cardiac Purkinje cell." The Journal of general physiology **85**(2): 247-289.

Farman, G. P., E. J. Allen, K. Q. Schoenfelt, P. H. Backx and P. P. De Tombe (2010). "The role of thin filament cooperativity in cardiac length-dependent calcium activation." Biophysical journal **99**(9): 2978-2986.

Farman, G. P., D. Gore, E. Allen, K. Schoenfelt, T. C. Irving and P. P. de Tombe (2011). "Myosin head orientation: a structural determinant for the Frank-Starling relationship." American Journal of Physiology-Heart and Circulatory Physiology **300**(6): H2155-H2160.

Farman, G. P., J. S. Walker, P. P. de Tombe and T. C. Irving (2006). "Impact of osmotic compression on sarcomere structure and myofilament calcium sensitivity of isolated rat myocardium." Am J Physiol Heart Circ Physiol **291**(4): H1847-1855.

Farza, H., P. J. Townsend, L. Carrier, P. J. Barton, L. Mesnard, E. Bährend, J.-F. Forissier, M. Fiszman, M. H. Yacoub and K. Schwartz (1998). "Genomic Organisation, Alternative Splicing and Polymorphisms of the Human Cardiac Troponin T Gene." Journal of Molecular and Cellular Cardiology **30**(6): 1247-1253.

Ferrieres, G., M. Pugniere, J. C. Mani, S. Villard, M. Laprade, P. Doutre, B. Pau and C. Granier (2000). "Systematic mapping of regions of human cardiac troponin I involved in binding to cardiac troponin C: N- and C-terminal low affinity contributing regions." FEBS Lett **479**(3): 99-105.

Ficker, E., W. Jarolimek, J. Kiehn, A. Baumann and A. M. Brown (1998). "Molecular determinants of dofetilide block of HERG K+ channels." Circ Res **82**(3): 386-395.

Ficker, E., M. Taglialatela, B. A. Wible, C. M. Henley and A. M. Brown (1994). "Spermine and spermidine as gating molecules for inward rectifier K+ channels." Science **266**(5187): 1068-1072.

Flicker, P. F., G. N. Phillips, Jr. and C. Cohen (1982). "Troponin and its interactions with tropomyosin. An electron microscope study." J Mol Biol **162**(2): 495-501.

Franklin, Andrew J., T. Baxley, T. Kobayashi and Joseph M. Chalovich (2012). "The C-Terminus of Troponin T Is Essential for Maintaining the Inactive State of Regulated Actin." Biophysical Journal **102**(11): 2536-2544.

Franzini-Armstrong, C., F. Protasi and V. Ramesh (1999). "Shape, size, and distribution of Ca(2+) release units and couplons in skeletal and cardiac muscles." Biophys J **77**(3): 1528-1539.

Fruen, B. R., J. M. Bardy, T. M. Byrem, G. M. Strasburg and C. F. Louis (2000). "Differential Ca(2+) sensitivity of skeletal and cardiac muscle ryanodine receptors in the presence of calmodulin." Am J Physiol Cell Physiol **279**(3): C724-733.

Fuchs, F. and Y.-P. Wang (1996). "Sarcomere Length Versus Interfilament Spacing as Determinants of Cardiac Myofilament Ca2+Sensitivity and Ca2+Binding." Journal of Molecular and Cellular Cardiology **28**(7): 1375-1383.

Fujimori, K., M. Sorenson, O. Herzberg, J. Moult and F. Reinach (1990). "Probing the calcium-induced conformational transition of troponin C with site-directed mutants."

Fujioka, Y., M. Komeda and S. Matsuoka (2000). "Stoichiometry of Na+-Ca2+ exchange in inside-out patches excised from guinea-pig ventricular myocytes." J Physiol **523 Pt 2**: 339-351.

Fukuda, N. and H. L. Granzier (2005). "Titin/connectin-based modulation of the Frank-Starling mechanism of the heart." Journal of Muscle Research & Cell Motility **26**(6-8): 319-323.

Fukuda, N., D. Sasaki, S. Ishiwata and S. Kurihara (2001). "Length dependence of tension generation in rat skinned cardiac muscle: role of titin in the Frank-Starling mechanism of the heart." Circulation **104**(14): 1639-1645.

Fung, D. C., B. Yu, T. Littlejohn and R. J. Trent (1999). "An online locus-specific mutation database for familial hypertrophic cardiomyopathy." Human mutation **14**(4): 326.

Gagne, S. M., S. Tsuda, M. X. Li, L. B. Smillie and B. D. Sykes (1995). "Structures of the troponin C regulatory domains in the apo and calcium-saturated states." Nat Struct Biol **2**(9): 784-789.

Galinska-Rakoczy, A., P. Engel, C. Xu, H. Jung, R. Craig, L. S. Tobacman and W. Lehman (2008). "Structural basis for the regulation of muscle contraction by troponin and tropomyosin." J Mol Biol **379**(5): 929-935.

Galinska, A., V. Hatch, R. Craig, A. M. Murphy, J. E. Van Eyk, C. L. Wang, W. Lehman and D. B. Foster (2010). "The C terminus of cardiac troponin I stabilizes the Ca2+-activated state of tropomyosin on actin filaments." Circ Res **106**(4): 705-711.

Gautel, M. and K. Djinovic-Carugo (2016). "The sarcomeric cytoskeleton: from molecules to motion." J Exp Biol **219**(Pt 2): 135-145.

Geisterfer-Lowrance, A. A., S. Kass, G. Tanigawa, H. P. Vosberg, W. McKenna, C. E. Seidman and J. G. Seidman (1990). "A molecular basis for familial hypertrophic cardiomyopathy: a beta cardiac myosin heavy chain gene missense mutation." Cell **62**(5): 999-1006.

George, C. H., H. Jundi, N. L. Thomas, D. L. Fry and F. A. Lai (2007). "Ryanodine receptors and ventricular arrhythmias: emerging trends in mutations, mechanisms and therapies." J Mol Cell Cardiol **42**(1): 34-50.

Gerull, B., M. Gramlich, J. Atherton, M. McNabb, K. Trombitás, S. Sasse-Klaassen, J. G. Seidman, C. Seidman, H. Granzier, S. Labeit, M. Frenneaux and L. Thierfelder (2002). "Mutations of TTN, encoding the giant muscle filament titin, cause familial dilated cardiomyopathy." Nature Genetics **30**(2): 201-204.

Gillis, T. E., T. M. Blumenschein, B. D. Sykes and G. F. Tibbits (2003). "Effect of temperature and the F27W mutation on the Ca2+ activated structural transition of trout cardiac troponin C." Biochemistry **42**(21): 6418-6426.

Gillis, T. E., C. R. Marshall, X.-H. Xue, T. J. Borgford and G. F. Tibbits (2000). "Ca2+ binding to cardiac troponin C: effects of temperature and pH on mammalian and salmonid isoforms." American Journal of Physiology-Regulatory, Integrative and Comparative Physiology **279**(5): R1707-R1715.

Goldin, A. L. (2003). "Mechanisms of sodium channel inactivation." Curr Opin Neurobiol **13**(3): 284-290.

Gollapudi, S. K. and M. Chandra (2012). "Cardiomyopathy-Related Mutations in Cardiac Troponin C, L29Q and G159D, Have Divergent Effects on Rat Cardiac Myofiber Contractile Dynamics." Biochemistry research international **2012**: 824068-824068.

Gordon, A., E. Homsher and M. Regnier (2000). "Regulation of contraction in striated muscle." Physiological reviews **80**(2): 853-924.

Gordon, A. M., M. Regnier and E. Homsher (2001). "Skeletal and Cardiac Muscle Contractile Activation: Tropomyosin “Rocks and Rolls”." Physiology **16**(2): 49-55.

Grabarek, Z., R.-Y. Tan, J. Wang, T. Tao and J. Gergely (1990). "Inhibition of mutant troponin C activity by an intra-domain disulphide bond." Nature **345**(6271): 132-135.

Granzier, H. and S. Labeit (2002). "Cardiac titin: an adjustable multi-functional spring." The Journal of physiology **541**(2): 335-342.

Granzier, H. L. and T. C. Irving (1995). "Passive tension in cardiac muscle: contribution of collagen, titin, microtubules, and intermediate filaments." Biophysical journal **68**(3): 1027-1044.

Gulati, J. (1992). "Length-sensing function of troponin C and Starling's law of the heart." Circulation **85**(5): 1954-1955.

Gyorke, I., N. Hester, L. R. Jones and S. Gyorke (2004). "The role of calsequestrin, triadin, and junctin in conferring cardiac ryanodine receptor responsiveness to luminal calcium." Biophys J **86**(4): 2121-2128.

Haji-Ghassemi, O., Z. Yuchi and F. Van Petegem (2019). "The Cardiac Ryanodine Receptor Phosphorylation Hotspot Embraces PKA in a Phosphorylation-Dependent Manner." Molecular Cell.

Hazard, A. L., S. C. Kohout, N. L. Stricker, J. A. Putkey and J. J. Falke (1998). "The kinetic cycle of cardiac troponin C: calcium binding and dissociation at site II trigger slow conformational rearrangements." Protein Science **7**(11): 2451-2459.

Hell, J. W., R. E. Westenbroek, C. Warner, M. K. Ahlijanian, W. Prystay, M. M. Gilbert, T. P. Snutch and W. A. Catterall (1993). "Identification and differential subcellular localization of the neuronal class C and class D L-type calcium channel alpha 1 subunits." The Journal of cell biology **123**(4): 949-962.

Hernandez, O. M., D. Szczesna-Cordary, B. C. Knollmann, T. Miller, M. Bell, J. Zhao, S. G. Sirenko, Z. Diaz, G. Guzman and Y. Xu (2005). "F110I and R278C troponin T mutations that cause familial hypertrophic cardiomyopathy affect muscle contraction in transgenic mice and reconstituted human cardiac fibers." Journal of Biological Chemistry **280**(44): 37183-37194.

Herzberg, O. and M. N. James (1985). "Structure of the calcium regulatory muscle protein troponin-C at 2.8 Å resolution."

Herzberg, O., J. Moult and M. N. James (1986). "A model for the Ca2+-induced conformational transition of troponin C. A trigger for muscle contraction." J Biol Chem **261**(6): 2638-2644.

Ho, C. Y., H. M. Lever, R. DeSanctis, C. F. Farver, J. G. Seidman and C. E. Seidman (2000). "Homozygous mutation in cardiac troponin T: implications for hypertrophic cardiomyopathy." Circulation **102**(16): 1950-1955.

Hoffman, R. M., T. M. Blumenschein and B. D. Sykes (2006). "An interplay between protein disorder and structure confers the Ca2+ regulation of striated muscle." J Mol Biol **361**(4): 625-633.

Holroyde, M., S. Robertson, J. Johnson, R. Solaro and J. Potter (1980). "The calcium and magnesium binding sites on cardiac troponin and their role in the regulation of myofibrillar adenosine triphosphatase." Journal of Biological Chemistry **255**(24): 11688-11693.

Houdusse, A., M. L. Love, R. Dominguez, Z. Grabarek and C. Cohen (1997). "Structures of four Ca2+-bound troponin C at 2.0 A resolution: further insights into the Ca2+-switch in the calmodulin superfamily." Structure **5**(12): 1695-1711.

Howarth, J. W., J. Meller, R. J. Solaro, J. Trewhella and P. R. Rosevear (2007). "Phosphorylation-dependent conformational transition of the cardiac specific N-extension of troponin I in cardiac troponin." Journal of molecular biology **373**(3): 706-722.

Hudmon, A., H. Schulman, J. Kim, J. M. Maltez, R. W. Tsien and G. S. Pitt (2005). "CaMKII tethers to L-type Ca2+ channels, establishing a local and dedicated integrator of Ca2+ signals for facilitation." J Cell Biol **171**(3): 537-547.

Huke, S. (2017). "Linking myofilaments to sudden cardiac death: recent advances." J Physiol **595**(12): 3939-3947.

Huke, S. and D. M. Bers (2007). "Temporal dissociation of frequency-dependent acceleration of relaxation and protein phosphorylation by CaMKII." Journal of Molecular and Cellular Cardiology **42**(3): 590-599.

Janssen, P. and P. P. de Tombe (1997). "Uncontrolled sarcomere shortening increases intracellular Ca2+ transient in rat cardiac trabeculae." American Journal of Physiology-Heart and Circulatory Physiology **272**(4): H1892-H1897.

Jaquet, K. and A. Mügge (2012). Consequences of Mutations in Genes Encoding Cardiac Troponin C, T and I-Molecular Insights, INTECH Open Access Publisher.

Jarcho, J. A., W. McKenna, J. P. Pare, S. D. Solomon, R. F. Holcombe, S. Dickie, T. Levi, H. Donis-Keller, J. Seidman and C. E. Seidman (1989). "Mapping a gene for familial hypertrophic cardiomyopathy to chromosome 14q1." New England Journal of Medicine **321**(20): 1372-1378.

Jin, J. P. and S. M. Chong (2010). "Localization of the two tropomyosin-binding sites of troponin T." Arch Biochem Biophys **500**(2): 144-150.

Johnson, J. D., S. C. Charlton and J. D. Potter (1979). "A fluorescence stopped flow analysis of Ca2+ exchange with troponin C." J Biol Chem **254**(9): 3497-3502.

Johnson, J. D., R. J. Nakkula, C. Vasulka and L. B. Smillie (1994). "Modulation of Ca2+ exchange with the Ca(2+)-specific regulatory sites of troponin C." J Biol Chem **269**(12): 8919-8923.

Johnson, J. D. and J. Potter (1978). "Detection of two classes of Ca2+ binding sites in troponin C with circular dichroism and tyrosine fluorescence." Journal of Biological Chemistry **253**(11): 3775-3777.

Julien, O., P. Mercier, C. N. Allen, O. Fisette, C. H. Ramos, P. Lague, T. M. Blumenschein and B. D. Sykes (2011). "Is there nascent structure in the intrinsically disordered region of troponin I?" Proteins **79**(4): 1240-1250.

Kalyva, A., F. I. Parthenakis, M. E. Marketou, J. E. Kontaraki and P. E. Vardas (2014). "Biochemical characterisation of Troponin C mutations causing hypertrophic and dilated cardiomyopathies." Journal of muscle research and cell motility **35**(2): 161-178.

Kamisago, M., S. D. Sharma, S. R. DePalma, S. Solomon, P. Sharma, B. McDonough, L. Smoot, M. P. Mullen, P. K. Woolf, E. D. Wigle, J. G. Seidman, J. Jarcho, L. R. Shapiro and C. E. Seidman (2000). "Mutations in Sarcomere Protein Genes as a Cause of Dilated Cardiomyopathy." New England Journal of Medicine **343**(23): 1688-1696.

Katrukha, I. (2013). "Human cardiac troponin complex. Structure and functions." Biochemistry (Moscow) **78**(13): 1447-1465.

Kentish, J. C., D. T. McCloskey, J. Layland, S. Palmer, J. M. Leiden, A. F. Martin and R. J. Solaro (2001). "Phosphorylation of troponin I by protein kinase A accelerates relaxation and crossbridge cycle kinetics in mouse ventricular muscle." Circ Res **88**(10): 1059-1065.

Kentish, J. C., H. E. ter Keurs, L. Ricciardi, J. J. Bucx and M. I. Noble (1986). "Comparison between the sarcomere length-force relations of intact and skinned trabeculae from rat right ventricle. Influence of calcium concentrations on these relations." Circulation research **58**(6): 755-768.

Kirschenlohr, H. L., A. A. Grace, J. I. Vandenberg, J. C. Metcalfe and G. A. Smith (2000). "Estimation of systolic and diastolic free intracellular Ca2+ by titration of Ca2+ buffering in the ferret heart." Biochem J **346 Pt 2**: 385-391.

Kitaoka, H., Y. Doi, S. A. Casey, N. Hitomi, T. Furuno and B. J. Maron (2003). "Comparison of prevalence of apical hypertrophic cardiomyopathy in Japan and the United States." The American Journal of Cardiology **92**(10): 1183-1186.

Knollmann, B. C., P. Kirchhof, S. G. Sirenko, H. Degen, A. E. Greene, T. Schober, J. C. Mackow, L. Fabritz, J. D. Potter and M. Morad (2003). "Familial hypertrophic cardiomyopathy-linked mutant troponin T causes stress-induced ventricular tachycardia and Ca2+-dependent action potential remodeling." Circ Res **92**(4): 428-436.

Kobayashi, T., S. E. Patrick and M. Kobayashi (2009). "Ala scanning of the inhibitory region of cardiac troponin I." J Biol Chem **284**(30): 20052-20060.

Konhilas, J. P., T. C. Irving and P. P. de Tombe (2002). "Myofilament calcium sensitivity in skinned rat cardiac trabeculae: role of interfilament spacing." Circ Res **90**(1): 59-65.

Konhilas, J. P., T. C. Irving, B. M. Wolska, E. E. Jweied, A. F. Martin, R. J. Solaro and P. P. d. Tombe (2003). "Troponin I in the murine myocardium: influence on length-dependent activation and interfilament spacing." The Journal of physiology **547**(3): 951-961.

Konno, T., S. Chang, J. G. Seidman and C. E. Seidman (2010). "Genetics of hypertrophic cardiomyopathy." Current opinion in cardiology **25**(3): 205-209.

Kretsinger, R. H. and C. E. Nockolds (1973). "Carp muscle calcium-binding protein. II. Structure determination and general description." J Biol Chem **248**(9): 3313-3326.

Kumar, M., S. Govindan, M. Zhang, R. J. Khairallah, J. L. Martin, S. Sadayappan and P. P. de Tombe (2015). "Cardiac myosin-binding protein C and Troponin-I phosphorylation independently modulate myofilament length-dependent activation." Journal of Biological Chemistry **290**(49): 29241-29249.

L DeLano, W. (2002). The PyMOL Molecular Graphics System (2002) DeLano Scientific, Palo Alto, CA, USA. http://www.pymol.org.

Landstrom, A. P., M. S. Parvatiyar, J. R. Pinto, M. L. Marquardt, J. M. Bos, D. J. Tester, S. R. Ommen, J. D. Potter and M. J. Ackerman (2008). "Molecular and functional characterization of novel hypertrophic cardiomyopathy susceptibility mutations in TNNC1-encoded troponin C." Journal of molecular and cellular cardiology **45**(2): 281-288.

le Guennec, J.-Y., E. Mosca, P. P. de Tombe and O. Cazorla (2008). "Differential contribution of cardiac sarcomeric proteins in the myofibrillar force response to stretch." Pflügers Archiv-European Journal of Physiology **457**(1): 25-36.

Lehman, W., V. Hatch, V. Korman, M. Rosol, L. Thomas, R. Maytum, M. A. Geeves, J. E. Van Eyk, L. S. Tobacman and R. Craig (2000). "Tropomyosin and actin isoforms modulate the localization of tropomyosin strands on actin filaments11Edited by W. Baumeister." Journal of Molecular Biology **302**(3): 593-606.

Lehrer, S. S. (2011). "The 3-state model of muscle regulation revisited: is a fourth state involved?" J Muscle Res Cell Motil **32**(3): 203-208.

Leong, I., J. Skinner, A. Shelling and D. Love (2010). "Zebrafish as a model for long QT syndrome: the evidence and the means of manipulating zebrafish gene expression." Acta physiologica **199**(3): 257-276.

Lewit-Bentley, A. and S. Rety (2000). "EF-hand calcium-binding proteins." Curr Opin Struct Biol **10**(6): 637-643.

Li, A. Y., C. M. Stevens, B. Liang, K. Rayani, S. Little, J. Davis and G. F. Tibbits (2013). "Familial hypertrophic cardiomyopathy related cardiac troponin C L29Q mutation alters length-dependent activation and functional effects of phosphomimetic troponin I*."

Li, M. X., L. Spyracopoulos and B. D. Sykes (1999). "Binding of Cardiac Troponin-I147-163 Induces a Structural Opening in Human Cardiac Troponin-C." Biochemistry **38**(26): 8289-8298.

Li, M. X., X. Wang and B. D. Sykes (2004). "Structural based insights into the role of troponin in cardiac muscle pathophysiology." J Muscle Res Cell Motil **25**(7): 559-579.

Li, M. X., X. Wang and B. D. Sykes (2005). "Structural based insights into the role of troponin in cardiac muscle pathophysiology." Journal of Muscle Research & Cell Motility **25**(7): 559-579.

Li, Y., E. G. Kranias, G. A. Mignery and D. M. Bers (2002). "Protein kinase A phosphorylation of the ryanodine receptor does not affect calcium sparks in mouse ventricular myocytes." Circ Res **90**(3): 309-316.

Liberthson, R. R. (1996). "Sudden Death from Cardiac Causes in Children and Young Adults." New England Journal of Medicine **334**(16): 1039-1044.

Lindert, S., P. M. Kekenes-Huskey, G. Huber, L. Pierce and J. A. McCammon (2012). "Dynamics and calcium association to the N-terminal regulatory domain of human cardiac troponin C: a multiscale computational study." The Journal of Physical Chemistry B **116**(29): 8449-8459.

Lindhout, D. A. and B. D. Sykes (2003). "Structure and dynamics of the C-domain of human cardiac troponin C in complex with the inhibitory region of human cardiac troponin I." J Biol Chem **278**(29): 27024-27034.

Lipp, P., M. Egger and E. Niggli (2002). "Spatial characteristics of sarcoplasmic reticulum Ca2+ release events triggered by L-type Ca2+ current and Na+ current in guinea-pig cardiac myocytes." The Journal of physiology **542**(Pt 2): 383-393.

Little, S. C., B. J. Biesiadecki, A. Kilic, R. S. Higgins, P. M. Janssen and J. P. Davis (2012). "The rates of Ca2+ dissociation and cross-bridge detachment from ventricular myofibrils as reported by a fluorescent cardiac troponin C." Journal of Biological Chemistry **287**(33): 27930-27940.

Liu, D. W. and C. Antzelevitch (1995). "Characteristics of the delayed rectifier current (IKr and IKs) in canine ventricular epicardial, midmyocardial, and endocardial myocytes. A weaker IKs contributes to the longer action potential of the M cell." Circ Res **76**(3): 351-365.

Liu, N., B. Colombi, M. Memmi, S. Zissimopoulos, N. Rizzi, S. Negri, M. Imbriani, C. Napolitano, F. A. Lai and S. G. Priori (2006). "Arrhythmogenesis in catecholaminergic polymorphic ventricular tachycardia: insights from a RyR2 R4496C knock-in mouse model." Circ Res **99**(3): 292-298.

London, B. (2001). "Cardiac arrhythmias: from (transgenic) mice to men." Journal of cardiovascular electrophysiology **12**(9): 1089-1091.

Long, S. B., E. B. Campbell and R. Mackinnon (2005). "Voltage sensor of Kv1.2: structural basis of electromechanical coupling." Science **309**(5736): 903-908.

Lopez-Lopez, P. Shacklock, C. Balke and W. Wier (1995). "Local calcium transients triggered by single L-type calcium channel currents in cardiac cells." Science **268**(5213): 1042-1045.

Lu, Y., M. P. Mahaut-Smith, A. Varghese, C. L. Huang, P. R. Kemp and J. I. Vandenberg (2001). "Effects of premature stimulation on HERG K(+) channels." The Journal of physiology **537**(Pt 3): 843-851.

Mackenzie, L., M. D. Bootman, M. Laine, M. J. Berridge, J. Thuring, A. Holmes, W. H. Li and P. Lipp (2002). "The role of inositol 1,4,5-trisphosphate receptors in Ca(2+) signalling and the generation of arrhythmias in rat atrial myocytes." J Physiol **541**(Pt 2): 395-409.

Maisch, B., M. Noutsias, V. Ruppert, A. Richter and S. Pankuweit (2012). "Cardiomyopathies: classification, diagnosis, and treatment." Heart failure clinics **8**(1): 53-78.

Manning, E. P., J. C. Tardiff and S. D. Schwartz (2011). "A model of calcium activation of the cardiac thin filament." Biochemistry **50**(34): 7405-7413.

Maron, B. J. (2002). "Hypertrophic cardiomyopathy: a systematic review." Jama **287**(10): 1308-1320.

Maron, B. J., K. P. Carney, H. M. Lever, J. F. Lewis, I. Barac, S. A. Casey and M. V. Sherrid (2003). "Relationship of race to sudden cardiac death in competitive athletes with hypertrophic cardiomyopathy." Journal of the American College of Cardiology **41**(6): 974-980.

Maron, B. J., B. R. Chaitman, M. J. Ackerman, A. B. d. Luna, D. Corrado, J. E. Crosson, B. J. Deal, D. J. Driscoll, N. A. M. Estes, C. G. S. Araújo, D. H. Liang, M. J. Mitten, R. J. Myerburg, A. Pelliccia, P. D. Thompson, J. A. Towbin and S. P. V. Camp (2004). "Recommendations for Physical Activity and Recreational Sports Participation for Young Patients With Genetic Cardiovascular Diseases." Circulation **109**(22): 2807-2816.

Maron, B. J., J. M. Gardin, J. M. Flack, S. S. Gidding, T. T. Kurosaki and D. E. Bild (1995). "Prevalence of hypertrophic cardiomyopathy in a general population of young adults Echocardiographic analysis of 4111 subjects in the CARDIA Study." Circulation **92**(4): 785-789.

Maron, B. J. and M. S. Maron (2013). "Hypertrophic cardiomyopathy." Lancet **381**(9862): 242-255.

Maron, B. J., M. S. Maron and C. Semsarian (2012). "Double or compound sarcomere mutations in hypertrophic cardiomyopathy: a potential link to sudden death in the absence of conventional risk factors." Heart Rhythm **9**(1): 57-63.

Maron, B. J., J. Shirani, L. C. Poliac, R. Mathenge, W. C. Roberts and F. O. Mueller (1996). "Sudden death in young competitive athletes: clinical, demographic, and pathological profiles." JAMA **276**(3): 199-204.

Maron, B. J., P. Spirito, Y. Wesley and J. Arce (1986). "Development and Progression of Left Ventricular Hypertrophy in Children with Hypertrophic Cardiomyopathy." New England Journal of Medicine **315**(10): 610-614.

Maron, M. S., I. Olivotto, A. G. Zenovich, M. S. Link, N. G. Pandian, J. T. Kuvin, S. Nistri, F. Cecchi, J. E. Udelson and B. J. Maron (2006). "Hypertrophic Cardiomyopathy Is Predominantly a Disease of Left Ventricular Outflow Tract Obstruction." Circulation **114**(21): 2232-2239.

Marston, S. B. (2011). "How do mutations in contractile proteins cause the primary familial cardiomyopathies?" Journal of cardiovascular translational research **4**(3): 245-255.

Marx, S. O., S. Reiken, Y. Hisamatsu, T. Jayaraman, D. Burkhoff, N. Rosemblit and A. R. Marks (2000). "PKA phosphorylation dissociates FKBP12. 6 from the calcium release channel (ryanodine receptor): defective regulation in failing hearts." Cell **101**(4): 365-376.

Mattiazzi, A. and E. Kranias (2014). "The role of CaMKII regulation of phospholamban activity in heart disease." Frontiers in pharmacology **5**: 5.

Maytum, R., S. S. Lehrer and M. A. Geeves (1999). "Cooperativity and switching within the three-state model of muscle regulation." Biochemistry **38**(3): 1102-1110.

McKillop, D. and M. A. Geeves (1993). "Regulation of the interaction between actin and myosin subfragment 1: evidence for three states of the thin filament." Biophysical journal **65**(2): 693.

McNally, E. M., J. R. Golbus and M. J. Puckelwartz (2013). "Genetic mutations and mechanisms in dilated cardiomyopathy." The Journal of Clinical Investigation **123**(1): 19-26.

Meissner, G. (2010). "Regulation of ryanodine receptor ion channels through posttranslational modifications." Current topics in membranes **66**: 91-113.

Menon, S. C., V. V. Michels, P. A. Pellikka, J. D. Ballew, M. L. Karst, K. J. Herron, S. M. Nelson, R. J. Rodeheffer and T. M. Olson (2008). "Cardiac troponin T mutation in familial cardiomyopathy with variable remodeling and restrictive physiology." Clinical genetics **74**(5): 445-454.

Mesirca, P., A. G. Torrente and M. E. Mangoni (2014). "T-type channels in the sino-atrial and atrioventricular pacemaker mechanism." Pflügers Archiv-European Journal of Physiology **466**(4): 791-799.

Mesnard, L., D. Logeart, S. Taviaux, S. Diriong, J. J. Mercadier and F. Samson (1995). "Human cardiac troponin T: cloning and expression of new isoforms in the normal and failing heart." Circ Res **76**(4): 687-692.

Mitcheson, J. S., J. Chen, M. Lin, C. Culberson and M. C. Sanguinetti (2000). "A structural basis for drug-induced long QT syndrome." Proc Natl Acad Sci U S A **97**(22): 12329-12333.

Mogensen, J., I. C. Klausen, A. K. Pedersen, H. Egeblad, P. Bross, T. A. Kruse, N. Gregersen, P. S. Hansen, U. Baandrup and A. D. Børglum (1999). "α-cardiac actin is a novel disease gene in familial hypertrophic cardiomyopathy." The Journal of Clinical Investigation **103**(10): R39-R43.

Mogensen, J., R. T. Murphy, T. Shaw, A. Bahl, C. Redwood, H. Watkins, M. Burke, P. M. Elliott and W. J. McKenna (2004). "Severe disease expression of cardiac troponin C and T mutations in patients with idiopathic dilated cardiomyopathy." Journal of the American College of Cardiology **44**(10): 2033-2040.

Moolman-Smook, J. C., W. J. De Lange, E. C. Bruwer, P. A. Brink and V. A. Corfield (1999). "The origins of hypertrophic cardiomyopathy-causing mutations in two South African subpopulations: a unique profile of both independent and founder events." American journal of human genetics **65**(5): 1308-1320.

Morita, H., H. L. Rehm, A. Menesses, B. McDonough, A. E. Roberts, R. Kucherlapati, J. A. Towbin, J. G. Seidman and C. E. Seidman (2008). "Shared Genetic Causes of Cardiac Hypertrophy in Children and Adults." New England Journal of Medicine **358**(18): 1899-1908.

Morris, E. P. and S. S. Lehrer (1984). "Troponin-tropomyosin interactions. Fluorescence studies of the binding of troponin, troponin T, and chymotryptic troponin T fragments to specifically labeled tropomyosin." Biochemistry **23**(10): 2214-2220.

Moss, R. L. and D. P. Fitzsimons (2002). Frank-starling relationship, Am Heart Assoc.

Nerbonne, J. M. and R. S. Kass (2005). "Molecular physiology of cardiac repolarization." Physiol Rev **85**(4): 1205-1253.

Nerbonne, J. M., C. G. Nichols, T. L. Schwarz and D. Escande (2001). "Genetic manipulation of cardiac K(+) channel function in mice: what have we learned, and where do we go from here?" Circ Res **89**(11): 944-956.

Nicoll, D. A., S. Longoni and K. D. Philipson (1990). "Molecular cloning and functional expression of the cardiac sarcolemmal Na (+)-Ca2+ exchanger." Science **250**(4980): 562-565.

Oda, T., M. Iwasa, T. Aihara, Y. Maéda and A. Narita (2009). "The nature of the globular- to fibrous-actin transition." Nature **457**: 441.

Ogawa, Y. (1985). "Calcium binding to troponin C and troponin: effects of Mg2+, ionic strength and pH." The Journal of Biochemistry **97**(4): 1011-1023.

Olivotto, I., M. S. Maron, A. S. Adabag, S. A. Casey, D. Vargiu, M. S. Link, J. E. Udelson, F. Cecchi and B. J. Maron (2005). "Gender-Related Differences in the Clinical Presentation and Outcome of Hypertrophic Cardiomyopathy." Journal of the American College of Cardiology **46**(3): 480-487.

Olson, T. M., N. Y. Kishimoto, F. G. Whitby and V. V. Michels (2001). "Mutations that Alter the Surface Charge of Alpha-tropomyosin are Associated with Dilated Cardiomyopathy." Journal of Molecular and Cellular Cardiology **33**(4): 723-732.

Olson, T. M., V. V. Michels, S. N. Thibodeau, Y.-S. Tai and M. T. Keating (1998). "Actin mutations in dilated cardiomyopathy, a heritable form of heart failure." Science **280**(5364): 750-752.

Parmacek, M. S. and J. M. Leiden (1991). "Structure, function, and regulation of troponin C." Circulation **84**(3): 991-1003.

Parvatiyar, M. S., A. P. Landstrom, C. Figueiredo-Freitas, J. D. Potter, M. J. Ackerman and J. R. Pinto (2012). "A mutation in TNNC1-encoded cardiac troponin C, TNNC1-A31S, predisposes to hypertrophic cardiomyopathy and ventricular fibrillation." Journal of Biological Chemistry **287**(38): 31845-31855.

Pearlstone, J. R., T. Borgford, M. Chandra, K. Oikawa, C. M. Kay, O. Herzberg, J. Moult, A. Herklotz, F. C. Reinach and L. B. Smillie (1992). "Construction and characterization of a spectral probe mutant of troponin C: application to analyses of mutants with increased calcium affinity." Biochemistry **31**(28): 6545-6553.

Pearlstone, J. R. and L. B. Smillie (1983). "Effects of troponin-I plus-C on the binding of troponin-T and its fragments to alpha-tropomyosin. Ca2+ sensitivity and cooperativity." J Biol Chem **258**(4): 2534-2542.

Perozo, E., D. M. Cortes and L. G. Cuello (1999). "Structural rearrangements underlying K+-channel activation gating." Science **285**(5424): 73-78.

Peterson, B. Z., C. D. DeMaria, J. P. Adelman and D. T. Yue (1999). "Calmodulin is the Ca2+ sensor for Ca2+ -dependent inactivation of L-type calcium channels." Neuron **22**(3): 549-558.

Philipson, K. D. and D. A. Nicoll (2000). "Sodium-calcium exchange: a molecular perspective." Annu Rev Physiol **62**: 111-133.

Pinto, J. R., M. S. Parvatiyar, M. A. Jones, J. Liang, M. J. Ackerman and J. D. Potter (2009). "A functional and structural study of troponin C mutations related to hypertrophic cardiomyopathy." J Biol Chem **284**(28): 19090-19100.

Pinto, J. R., J. D. Siegfried, M. S. Parvatiyar, D. Li, N. Norton, M. A. Jones, J. Liang, J. D. Potter and R. E. Hershberger (2011). "Functional characterization of TNNC1 rare variants identified in dilated cardiomyopathy." J Biol Chem **286**(39): 34404-34412.

Pitt, G. S., R. D. Zühlke, A. Hudmon, H. Schulman, H. Reuter and R. W. Tsien (2001). "Molecular Basis of Calmodulin Tethering and Ca2+-dependent Inactivation of L-type Ca2+ Channels." Journal of Biological Chemistry **276**(33): 30794-30802.

Poetter, K., H. Jiang, S. Hassanzadeh, S. R. Master, A. Chang, M. C. Dalakas, I. Rayment, J. R. Sellers, L. Fananapazir and N. D. Epstein (1996). "Mutations in either the essential or regulatory light chains of myosin are associated with a rare myopathy in human heart and skeletal muscle." Nat Genet **13**(1): 63-69.

Pogwizd, S. M., K. Schlotthauer, L. Li, W. Yuan and D. M. Bers (2001). "Arrhythmogenesis and contractile dysfunction in heart failure: Roles of sodium-calcium exchange, inward rectifier potassium current, and residual beta-adrenergic responsiveness." Circ Res **88**(11): 1159-1167.

Potter, J. D. and J. Gergely (1975). "The calcium and magnesium binding sites on troponin and their role in the regulation of myofibrillar adenosine triphosphatase." Journal of Biological Chemistry **250**(12): 4628-4633.

Prinz, C., M. Farr, D. Hering, D. Horstkotte and L. Faber (2011). "The diagnosis and treatment of hypertrophic cardiomyopathy." Dtsch Arztebl Int **108**(13): 209-215.

Puglisi, J. L., W. Yuan, J. W. Bassani and D. M. Bers (1999). "Ca2+ influx through Ca2+ channels in rabbit ventricular myocytes during action potential clamp." Circulation Research **85**(6): e7-e16.

Redwood, C. S., J. C. Moolman-Smook and H. Watkins (1999). "Properties of mutant contractile proteins that cause hypertrophic cardiomyopathy." Cardiovascular Research **44**(1): 20-36.

Richmond, J. E., D. E. Featherstone, H. A. Hartmann and P. C. Ruben (1998). "Slow inactivation in human cardiac sodium channels." Biophys J **74**(6): 2945-2952.

Robertson, S., J. D. Johnson and J. Potter (1981). "The time-course of Ca2+ exchange with calmodulin, troponin, parvalbumin, and myosin in response to transient increases in Ca2+." Biophysical journal **34**(3): 559.

Robinson, P., P. J. Griffiths, H. Watkins and C. S. Redwood (2007). "Dilated and hypertrophic cardiomyopathy mutations in troponin and α-tropomyosin have opposing effects on the calcium affinity of cardiac thin filaments." Circulation research **101**(12): 1266-1273.

Rosenfeld, S. and E. Taylor (1985). "Kinetic studies of calcium and magnesium binding to troponin C." Journal of Biological Chemistry **260**(1): 242-251.

Rottbauer, W., K. Baker, Z. G. Wo, M.-A. P. Mohideen, H. F. Cantiello and M. C. Fishman (2001). "Growth and function of the embryonic heart depend upon the cardiac-specific L-type calcium channel α1 subunit." Developmental cell **1**(2): 265-275.

Russell, A. J., J. J. Hartman, A. C. Hinken, A. R. Muci, R. Kawas, L. Driscoll, G. Godinez, K. H. Lee, D. Marquez and W. F. Browne IV (2012). "Activation of fast skeletal muscle troponin as a potential therapeutic approach for treating neuromuscular diseases." Nature medicine **18**(3): 452-455.

Sanguinetti, M. C., C. Jiang, M. E. Curran and M. T. Keating (1995). "A mechanistic link between an inherited and an acquired cardiac arrhythmia: HERG encodes the IKr potassium channel." Cell **81**(2): 299-307.

Sanguinetti, M. C. and M. Tristani-Firouzi (2006). "hERG potassium channels and cardiac arrhythmia." Nature **440**(7083): 463-469.

Sasse, S., N. J. Brand, P. Kyprianou, G. K. Dhoot, R. Wade, M. Arai, M. Periasamy, M. H. Yacoub and P. J. Barton (1993). "Troponin I gene expression during human cardiac development and in end-stage heart failure." Circ Res **72**(5): 932-938.

Satoh, M., M. Takahashi, T. Sakamoto, M. Hiroe, F. Marumo and A. Kimura (1999). "Structural Analysis of the Titin Gene in Hypertrophic Cardiomyopathy: Identification of a Novel Disease Gene." Biochemical and Biophysical Research Communications **262**(2): 411-417.

Schober, T., S. Huke, R. Venkataraman, O. Gryshchenko, D. Kryshtal, H. S. Hwang, F. J. Baudenbacher and B. C. Knollmann (2012). "Myofilament Ca sensitization increases cytosolic Ca binding affinity, alters intracellular Ca homeostasis, and causes pause-dependent Ca-triggered arrhythmia." Circulation research **111**(2): 170-179.

Seeley, M., W. Huang, Z. Chen, W. O. Wolff, X. Lin and X. Xu (2007). "Depletion of zebrafish titin reduces cardiac contractility by disrupting the assembly of Z-discs and A-bands." Circulation research **100**(2): 238-245.

Seidman, J. and C. Seidman (2001). "The genetic basis for cardiomyopathy: from mutation identification to mechanistic paradigms." Cell **104**(4): 557-567.

Semsarian, C., J. Ingles, M. S. Maron and B. J. Maron (2015). "New perspectives on the prevalence of hypertrophic cardiomyopathy." Journal of the American College of Cardiology **65**(12): 1249-1254.

Shannon, T. R., K. S. Ginsburg and D. M. Bers (2000). "Potentiation of fractional sarcoplasmic reticulum calcium release by total and free intra-sarcoplasmic reticulum calcium concentration." Biophys J **78**(1): 334-343.

Shannon, T. R., T. Guo and D. M. Bers (2003). "Ca2+ scraps: local depletions of free [Ca2+] in cardiac sarcoplasmic reticulum during contractions leave substantial Ca2+ reserve." Circ Res **93**(1): 40-45.

Shimizu, M., H. Ino, T. Yasuda, N. Fujino, K. Uchiyama, T. Mabuchi, T. Konno, T. Kaneda, T. Fujita, E. Masuta, M. Katoh, A. Funada and H. Mabuchi (2005). "Gene Mutations in Adult Japanese Patients With Dilated Cardiomyopathy." Circulation Journal **69**(2): 150-153.

Sia, S. K., M. X. Li, L. Spyracopoulos, S. M. Gagné, W. Liu, J. A. Putkey and B. D. Sykes (1997). "Structure of cardiac muscle troponin C unexpectedly reveals a closed regulatory domain." Journal of Biological Chemistry **272**(29): 18216-18221.

Sidi, S., E. Busch-Nentwich, R. Friedrich, U. Schoenberger and T. Nicolson (2004). "gemini encodes a zebrafish L-type calcium channel that localizes at sensory hair cell ribbon synapses." Journal of Neuroscience **24**(17): 4213-4223.

Siemankowski, R. F., M. O. Wiseman and H. D. White (1985). "ADP dissociation from actomyosin subfragment 1 is sufficiently slow to limit the unloaded shortening velocity in vertebrate muscle." Proceedings of the National Academy of Sciences of the United States of America **82**(3): 658-662.

Silva, J. R. and S. A. Goldstein (2013). "Voltage-sensor movements describe slow inactivation of voltage-gated sodium channels I: wild-type skeletal muscle Na(V)1.4." J Gen Physiol **141**(3): 309-321.

Sipido, K. R., G. Callewaert and E. Carmeliet (1995). "Inhibition and rapid recovery of Ca2+ current during Ca2+ release from sarcoplasmic reticulum in guinea pig ventricular myocytes." Circ Res **76**(1): 102-109.

Sitsapesan, R. and A. J. Williams (1994). "Regulation of the gating of the sheep cardiac sarcoplasmic reticulum Ca(2+)-release channel by luminal Ca2+." J Membr Biol **137**(3): 215-226.

Solaro, R. J., M. Henze and T. Kobayashi (2013). "Integration of Troponin I Phosphorylation With Cardiac Regulatory Networks." Circulation Research **112**(2): 355-366.

Spyracopoulos, L., M. X. Li, S. K. Sia, S. M. Gagne, M. Chandra, R. J. Solaro and B. D. Sykes (1997). "Calcium-induced structural transition in the regulatory domain of human cardiac troponin C." Biochemistry **36**(40): 12138-12146.

Stefancsik, R., P. K. Jha and S. Sarkar (1998). "Identification and mutagenesis of a highly conserved domain in troponin T responsible for troponin I binding: Potential role for coiled coil interaction." Proceedings of the National Academy of Sciences **95**(3): 957-962.

Stern, M. D. (1992). "Theory of excitation-contraction coupling in cardiac muscle." Biophysical journal **63**(2): 497-517.

Stern, M. D., L.-S. Song, H. Cheng, J. S. Sham, H. T. Yang, K. R. Boheler and E. Ríos (1999). "Local control models of cardiac excitation–contraction coupling: a possible role for allosteric interactions between ryanodine receptors." The Journal of general physiology **113**(3): 469-489.

Strynadka, N. C. and M. N. James (1989). "Crystal structures of the helix-loop-helix calcium-binding proteins." Annu Rev Biochem **58**: 951-998.

Sundaralingam, M., R. Bergstrom, G. Strasburg, S. T. Rao, P. Roychowdhury, M. Greaser and B. C. Wang (1985). "Molecular structure of troponin C from chicken skeletal muscle at 3-angstrom resolution." Science **227**(4689): 945-948.

Sutko, J. L. and J. A. Airey (1996). "Ryanodine receptor Ca2+ release channels: does diversity in form equal diversity in function?" Physiological Reviews **76**(4): 1027-1071.

Sweeney, H. L., R. M. Brito, P. R. Rosevear and J. A. Putkey (1990). "The low-affinity Ca2(+)-binding sites in cardiac/slow skeletal muscle troponin C perform distinct functions: site I alone cannot trigger contraction." Proceedings of the National Academy of Sciences **87**(24): 9538-9542.

Takahashi, T. and A. Momiyama (1993). "Different types of calcium channels mediate central synaptic transmission." Nature **366**(6451): 156.

Takeda, S., A. Yamashita, K. Maeda and Y. Maéda (2003). "Structure of the core domain of human cardiac troponin in the Ca2+-saturated form." Nature **424**(6944): 35-41.

Talosi, L., I. Edes and E. G. Kranias (1993). "Intracellular mechanisms mediating reversal of beta-adrenergic stimulation in intact beating hearts." Am J Physiol **264**(3 Pt 2): H791-797.

Tan, H. L., S. Kupershmidt, R. Zhang, S. Stepanovic, D. M. Roden, A. A. Wilde, M. E. Anderson and J. R. Balser (2002). "A calcium sensor in the sodium channel modulates cardiac excitability." Nature **415**(6870): 442-447.

Tanokura, M., Y. Tawada and I. Ohtsuki (1982). "Chymotryptic subfragments of troponin T from rabbit skeletal muscle. I. Determination of the primary structure." J Biochem **91**(4): 1257-1265.

Tardiff, J. C. (2011). "Thin filament mutations developing an integrative approach to a complex disorder." Circulation Research **108**(6): 765-782.

Thierfelder, L., H. Watkins, C. MacRae, R. Lamas, W. McKenna, H.-P. Vosberg, J. G. Seldman and C. E. Seidman (1994). "α-tropomyosin and cardiac troponin T mutations cause familial hypertrophic cardiomyopathy: A disease of the sarcomere." Cell **77**(5): 701-712.

Thouta, S., S. Sokolov, Y. Abe, S. J. Clark, Y. M. Cheng and T. W. Claydon (2014). "Proline scan of the HERG channel S6 helix reveals the location of the intracellular pore gate." Biophys J **106**(5): 1057-1069.

Tikunova, S. B. and J. P. Davis (2004). "Designing calcium-sensitizing mutations in the regulatory domain of cardiac troponin C." Journal of Biological Chemistry **279**(34): 35341-35352.

Tiwari-Woodruff, S. K., C. T. Schulteis, A. F. Mock and D. M. Papazian (1997). "Electrostatic interactions between transmembrane segments mediate folding of Shaker K+ channel subunits." Biophys J **72**(4): 1489-1500.

Townsend, P. J., H. Farza, C. Macgeoch, N. K. Spurr, R. Wade, R. Gahlmann, M. H. Yacoub and P. J. R. Barton (1994). "Human Cardiac Troponin T: Identification of Fetal Isoforms and Assignment of the TNNT2 Locus to Chromosome 1q." Genomics **21**(2): 311-316.

Townsend, P. J., M. H. Yacoub and P. J. Barton (1997). "Assignment of the human fast skeletal muscle troponin C gene (TNNC2) between D20S721 and GCT10F11 on chromosome 20 by somatic cell hybrid analysis." Ann Hum Genet **61**(Pt 5): 457-459.

Valdivia, H. H., J. H. Kaplan, G. C. Ellis-Davies and W. J. Lederer (1995). "Rapid adaptation of cardiac ryanodine receptors: modulation by Mg2+ and phosphorylation." Science **267**(5206): 1997-2000.

van Eerd, J.-P. and K. Takahashi (1975). "The amino acid sequence of bovine cardiac troponin-C. Comparison with rabbit skeletal troponin-C." Biochemical and Biophysical Research Communications **64**(1): 122-127.

van Spaendonck-Zwarts, K. Y., J. P. van Tintelen, D. J. van Veldhuisen, R. van der Werf, J. D. Jongbloed, W. J. Paulus, D. Dooijes and M. P. van den Berg (2010). "Peripartum cardiomyopathy as a part of familial dilated cardiomyopathy." Circulation **121**(20): 2169-2175.

Vandenberg, J. I., M. D. Perry, M. J. Perrin, S. A. Mann, Y. Ke and A. P. Hill (2012). "hERG K+ channels: structure, function, and clinical significance." Physiological reviews **92**(3): 1393-1478.

Vassylyev, D. G., S. Takeda, S. Wakatsuki, K. Maeda and Y. Maeda (1998). "Crystal structure of troponin C in complex with troponin I fragment at 2.3-A resolution." Proc Natl Acad Sci U S A **95**(9): 4847-4852.

Venkatraman, G., A. V. Gomes, W. G. L. Kerrick and J. D. Potter (2005). "Characterization of troponin T dilated cardiomyopathy mutations in the fetal troponin isoform." Journal of Biological Chemistry **280**(18): 17584-17592.

Venkatraman, G., K. Harada, A. V. Gomes, W. G. L. Kerrick and J. D. Potter (2003). "Different functional properties of troponin T mutants that cause dilated cardiomyopathy." Journal of Biological Chemistry **278**(43): 41670-41676.

Verin, A. D. and N. B. Gusev (1988). "Ca2+-induced conformational changes in cardiac troponin C as measured by N-(1-pyrene)maleimide fluorescence." Biochim Biophys Acta **956**(2): 197-208.

Wang, C., B. C. Chung, H. Yan, H. G. Wang, S. Y. Lee and G. S. Pitt (2014). "Structural analyses of Ca(2)(+)/CaM interaction with NaV channel C-termini reveal mechanisms of calcium-dependent regulation." Nat Commun **5**: 4896.

Wang, Q., J. Shen, I. Splawski, D. Atkinson, Z. Li, J. L. Robinson, A. J. Moss, J. A. Towbin and M. T. Keating (1995). "SCN5A mutations associated with an inherited cardiac arrhythmia, long QT syndrome." Cell **80**(5): 805-811.

Wang, W. and R. MacKinnon (2017). "Cryo-EM Structure of the Open Human Ether-a-go-go-Related K(+) Channel hERG." Cell **169**(3): 422-430.e410.

Wang, X., M. X. Li and B. D. Sykes (2002). "Structure of the regulatory N-domain of human cardiac troponin C in complex with human cardiac troponin I147-163 and bepridil." J Biol Chem **277**(34): 31124-31133.

Ward, D. G., S. M. Brewer, M. P. Cornes and I. P. Trayer (2003). "A Cross-Linking Study of the N-Terminal Extension of Human Cardiac Troponin I†." Biochemistry **42**(34): 10324-10332.

Weber, C. R., V. Piacentino, 3rd, S. R. Houser and D. M. Bers (2003). "Dynamic regulation of sodium/calcium exchange function in human heart failure." Circulation **108**(18): 2224-2229.

White, S. P., C. Cohen and G. N. Phillips Jr (1987). "Structure of co-crystals of tropomyosin and troponin." Nature **325**(6107): 826-828.

Williams, C. D., M. Regnier and T. L. Daniel (2010). "Axial and radial forces of cross-bridges depend on lattice spacing." PLoS Comput Biol **6**(12): e1001018.

Willott, R. H., A. V. Gomes, A. N. Chang, M. S. Parvatiyar, J. R. Pinto and J. D. Potter (2010). "Mutations in Troponin that cause HCM, DCM AND RCM: what can we learn about thin filament function?" Journal of molecular and cellular cardiology **48**(5): 882-892.

Xing, J., J. J. Jayasundar, Y. Ouyang and W. J. Dong (2009). "Forster resonance energy transfer structural kinetic studies of cardiac thin filament deactivation." J Biol Chem **284**(24): 16432-16441.

Yang, S., L. Barbu-Tudoran, M. Orzechowski, R. Craig, J. Trinick, H. White and W. Lehman (2014). "Three-dimensional organization of troponin on cardiac muscle thin filaments in the relaxed state." Biophys J **106**(4): 855-864.

Yarov-Yarovoy, V., P. G. DeCaen, R. E. Westenbroek, C. Y. Pan, T. Scheuer, D. Baker and W. A. Catterall (2012). "Structural basis for gating charge movement in the voltage sensor of a sodium channel." Proc Natl Acad Sci U S A **109**(2): E93-102.

Yu, F. H. and W. A. Catterall (2004). "The VGL-chanome: a protein superfamily specialized for electrical signaling and ionic homeostasis." Sci STKE **2004**(253): re15.

Yuan, W., K. S. Ginsburg and D. M. Bers (1996). "Comparison of sarcolemmal calcium channel current in rabbit and rat ventricular myocytes." The Journal of Physiology **493**(3): 733-746.

Yue, D. T. (1987). "Intracellular [Ca2+] related to rate of force development in twitch contraction of heart." American Journal of Physiology-Heart and Circulatory Physiology **252**(4): H760-H770.

Yumoto, F., M. Nara, H. Kagi, W. Iwasaki, T. Ojima, K. Nishita, K. Nagata and M. Tanokura (2001). "Coordination structures of Ca2+ and Mg2+ in Akazara scallop troponin C in solution. FTIR spectroscopy of side-chain COO- groups." Eur J Biochem **268**(23): 6284-6290.

Zhang, L., J. Kelley, G. Schmeisser, Y. M. Kobayashi and L. R. Jones (1997). "Complex formation between junctin, triadin, calsequestrin, and the ryanodine receptor. Proteins of the cardiac junctional sarcoplasmic reticulum membrane." J Biol Chem **272**(37): 23389-23397.

Zhou, W., E. J. Horstick, H. Hirata and J. Y. Kuwada (2008). "Identification and expression of voltage-gated calcium channel β subunits in Zebrafish." Developmental dynamics **237**(12): 3842-3852.

Zhou, W., L. Saint-Amant, H. Hirata, W. W. Cui, S. M. Sprague and J. Y. Kuwada (2006). "Non-sense mutations in the dihydropyridine receptor β1 gene, CACNB1, paralyze zebrafish relaxed mutants." Cell calcium **39**(3): 227-236.

Zhou, Z. and C. T. January (1998). "Both T- and L-Type Ca2+ Channels Can Contribute to Excitation-Contraction Coupling in Cardiac Purkinje Cells." Biophysical Journal **74**(4): 1830-1839.

Zima, A. V., J. A. Copello and L. A. Blatter (2004). "Effects of cytosolic NADH/NAD(+) levels on sarcoplasmic reticulum Ca(2+) release in permeabilized rat ventricular myocytes." J Physiol **555**(Pt 3): 727-741.

Zot, A. S. and J. D. Potter (1987). "Structural aspects of troponin-tropomyosin regulation of skeletal muscle contraction." Annual review of biophysics and biophysical chemistry **16**(1): 535-559.

Zot, H. G. and J. D. Potter (1982). "A structural role for the Ca2+-Mg2+ sites on troponin C in the regulation of muscle contraction. Preparation and properties of troponin C depleted myofibrils." J Biol Chem **257**(13): 7678-7683.

Zou, J., D. Tran, M. Baalbaki, L. F. Tang, A. Poon, A. Pelonero, E. W. Titus, C. Yuan, C. Shi and S. Patchava (2015). "An internal promoter underlies the difference in disease severity between N-and C-terminal truncation mutations of Titin in zebrafish." Elife **4**.

Chapter 2.

Isothermal Titration Calorimetry (ITC) Methodology

Isothermal titration calorimetry (ITC) is a technique used to measure the heat absorbed by or evolved from an interaction between two compounds; often a macromolecule ligand and a small molecule titrant. The ligand is known as the titrand/titrate and is often a protein or nucleic acid with a specific number of sites that the injected titrant (ex. drug, metal ion, etc.) binds non-covalently.

Heat exchange which accompanies almost every molecular interaction allows calorimetry-based quantification to be used in the absence of reporters (Ladbury and Doyle 2004). The lack of a tag needed by spectroscopic methods to monitor the progress of a reaction precludes steric interactions/functional effects that said tag might alter.

ITC has the unique capability to quantify multiple thermodynamic parameters associated with a given reaction. In systems at constant pressure (isobaric), heat evolved/absorbed is equal to the change in enthalpy (ΔH). Reactions that also occur under constant temperature (isothermal) conditions can be used to determine the affinity of the interaction through measurement of the binding constant (K_A), as well as the stoichiometry associated with the interaction (n), the change in entropy (ΔS), and the change in Gibbs free energy of the system (ΔG).

Modern ITC instruments have improved on the initial MicroCal instruments (Wiseman, Williston et al. 1989) and now have a lower heat detection limit of 0.1 µcal and upper limit on K_A of 10^9 M^{-1} (Freire, Mayorga et al. 1990). These capabilities allow for routine, rapid characterization of interactions between biological substrates. One of the main applications of ITC is in high affinity drug/ligand design (Brown, Mensah et al. 2000, Todd, Luque et al. 2000, Zhang, Yao et al. 2000, Velazquez-Campoy, Kiso et al. 2001).

2.1. Instrumentation

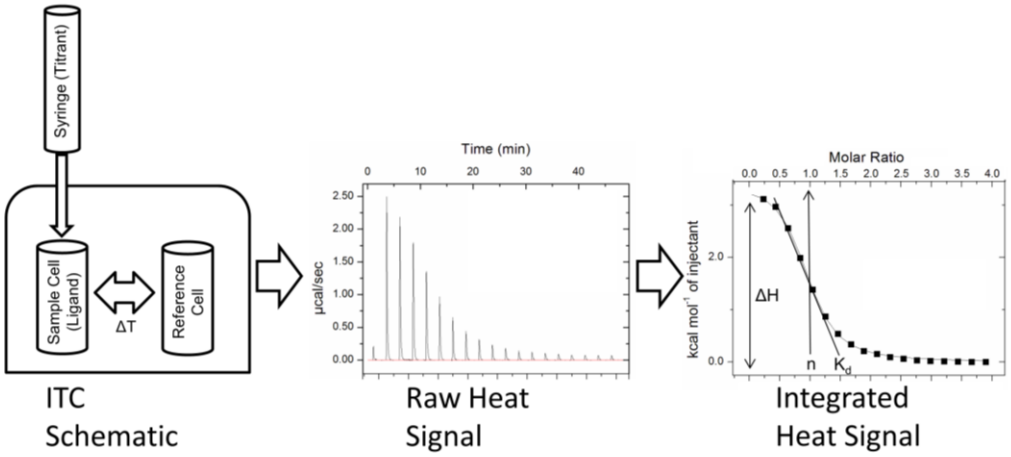

Figure 2-1 Schematic depiction of an ITC apparatus and data visualization. The water-containing reference cell and the ligand-containing sample cell into which the titrant is injected are shown (left). The two cells are surrounded by an adiabatic shield. Power compensation allows for rapid adjustment of the sample cell temperature to the baseline level following each injection. The power supplied to adjust the temperature is measured to generate the raw signal (middle). In the depicted isotherm, positive heat signal deflections indicate an endothermic interaction. This is, in turn, integrated to measure the heat per unit time (right). In this case, a single binding site model was used to fit the data and obtain thermodynamic parameters.

An ITC instrument is composed of a reaction cell which houses the ligand. A water-containing reference cell is also located within the adiabatic chamber of the instrument and comparisons between these two chambers' temperature is used to allow for feedback-based adjustment of the experimental chamber's temperature. The power compensation methods used by instruments such as the MicroCal ITC_{200} gives a raw signal in the units of power (µcal/sec) that is applied to return the sample cell's temperature back to baseline following each injection. Integrating the heater power over the time that it takes to return to baseline gives the heat change (Freyer and Lewis 2008). For example, an exothermic interaction is visualized as a downward deflection in the isotherm. In this situation, the power supplied to the control heater is reduced and constant cooling supplied to the sample cell. Cooling reduces the reaction cell temperature back to baseline (Freyer and Lewis 2008). In addition to injecting the titrant, the pedal-shaped syringe acts as a stirrer allowing for mixing of the reaction components at a pre-set rate.

2.2. Thermodynamics Parameters

$$\text{Ligand} + \text{Titrant} \leftrightarrow \text{Ligand-Titrant}$$

[1] $$K_A = \frac{[Ligand-Titrant]}{[Ligand][Titrant]}$$

[2] $$K_A = e^{-\Delta G/RT}$$

[3] $$\Delta G = -R*T*\ln(K_A)$$

[4] $$\Delta G = \Delta H - T*\Delta S$$

Figure 2-2 Relevant equations for a generic reaction

ΔG denotes the spontaneity of a reaction; those characterized by a negative ΔG (exergonic) do not require work by the surroundings to proceed. Endergonic reactions (ΔG>0) in contrast do not occur spontaneously without external work. The K_A associated with an interaction is related to the ΔG by equation [3] that is derived from the fundamental equation [2]. K_A>1 results from favourable reactions, conversely K_A<1 corresponds to unfavourable reactions.

There are infinitely many combinations for the ΔH and ΔS (which is further modified by the reaction temperature), that can lead to a spontaneous interaction. Given equation [4], a reaction that is enthalpically favourably (ΔH<0) can overcome entropical hinderances (relatively small ΔS). In contrast, unfavourable enthalpic conditions (ΔH>0) or a slightly exothermic interaction can be overcome through favourable ΔS (with the right temperature conditions), giving rise to an exergonic interaction.

Affinity is determined by the enthalpic and the entropic changes associated with an interaction as these terms dictate the ΔG of the system through equation [4] (Rekharsky and Inoue 1998). Heat requiring reactions are termed endothermic and characterized by a positive ΔH, by convention; these are visualized as an upward deflection in an ITC isotherm. For such an interaction to be exergonic, a favourable change in the entropy of the system is required. Exothermic interactions are characterized by negative ΔH values.

ΔH reflects the strength of hydrogen bonds, van der Waals interactions, and electrostatic forces between the titrant and the target ligand. Optimal placement of hydrogen bond donors and acceptors balances de-solvation of polar groups to contribute to the enthalpy change. Transient Van der Waals forces are distance dependent, with molecules too close or too far having repulsive and a lack of attractive forces between them, respectively. Ionic interactions between charged molecules give rise to electrostatic/dipole-dipole forces that are also transient in nature (Ward and Holdgate 2001).

The entropic change reflects solvation and conformational changes resulting from the interaction. Entropy can be thought of as the randomness of the system or the number of available micro-states that every molecule can occupy at any time (i.e. the degrees of freedom) (Lambert 2002). This is a complex parameter but one which nonetheless plays a role in determining reaction spontaneity as dictated by equation [4]. Entropic changes are a trade-off between the increase in entropy resulting from removal of ordered solvent molecules from the binding site upon binding and the increase in orderliness of the titrant-bound ligand (Cabani, Gianni et al. 1981).

As binding results in the release of water molecules and a gain in solvent entropy, this is particularly important for interactions involving hydrophobic residues. Binding also reduces the conformational freedom of the ligand and thus the conformational entropy (Leavitt and Freire 2001). Stabilization of the disordered binding site following the binding interaction is characteristic of low molecular weight proteins (Luque and Freire 2000).

2.3. ITC experiments

It is recommended to set a small volume first injection in a protocol; the signal associated with this “dummy” injection is due to diffusion during the equilibration period and should be excluded from the analysis. Subsequent incremental injections should be sufficiently small to allow for elucidation of the reaction coordinates and to provide multiple data points at the steepest portion of the curve. At least 5 data points are required to define the titration in the curved region which surrounds the equivalence point (Hansen, Fellingham et al. 2011).The ligand concentration, titrant concentration, and titrant injection volume should be adjusted based on the affinity associated with the

interaction to achieve the appropriate number of data points in this critical region. The temptation to decrease the volume of injections should also be avoided as smaller heats will increase the error associated with each measured signal. Initially, there are many unpopulated binding sites, this number falls with each subsequent injection and the raw heat signal becomes smaller as the ligand is saturated (Lewis and Murphy 2005). These heat signals are integrated and then fit with a model appropriate to the interaction.

Concentration determination is dependent on the characteristics of the reactants and should be guided by previous published experiments or through pilot studies which inform regarding reactant affinity. A rule of thumb is to have a concentration in the cell of 50– 500*K_d, with an optimal value of about 100*K_d (usually ~10-50 μM). As a reasonable first estimation in cases where K_d is unknown, K_d can be thought to approximately equal 10*EC_{50}. The syringe concentration should be in the range of 20x – 10x the cell concentration with higher ratios corresponding to lower affinities (Wiseman, Williston et al. 1989).

2.4. Recombinant Protein Preparation

High quality, pure protein is essential to successfully carrying out ITC experiments. In steps that are often overlooked, the selection of appropriate bacterial strains, expression, and purification can significantly alter the quality of ITC experiments. Details will be provided regarding the purification of each construct used in this project in subsequent chapters with a general guide laid out here.

The purification protocols used in our studies have been modified from previous work (Li, Stevens et al. 2013, Stevens, Rayani et al. 2016, Stevens, Rayani et al. 2017) and optimized to avoid prolongation of the time during which the protein may break down. Previous studies utilized extensive dialysis steps during the purification, however these have been minimized and in the case of N-cTnC purification, deemed altogether unnecessary.

Fungi, yeasts, algae and bacteria each have advantages and disadvantages associated with their use in over-expression of proteins *in vitro* (Adrio and Demain 2010). *E. coli* systems while lacking the post translational modification capabilities of eukaryotes, have fast growth kinetics whereby populations double every ~20 mins

(Sezonov, Joseleau-Petit et al. 2007, Sahdev, Khattar et al. 2008). They allow for rapid DNA transformation (Pope and Kent 1996) and can grow in inexpensive media to achieve high cell density (Shiloach and Fass 2005).

Selection of the appropriate expression vector is an important consideration given that the copy number should be maximized (Del Solar and Espinosa 2000), while avoiding a reduction in bacterial growth (Birnbaum and Bailey 1991). pET vectors contain 15-60 plasmids per cell (Bolivar, Rodriguez et al. 1977) allowing for efficient gene expression (Graumann and Premstaller 2006). The gene is cloned behind a T7 promoter and under control of the lac-UV5 promoter that allows for regulation of gene transcription by lactose or other analogs such as isopropyl β-D-1- thiogalactopyranoside (IPTG) (Moffatt and Studier 1987).

2.4.1. Mutagenesis

Our gene of interest was originally purchased from a vendor and contained the 161 amino acid full-length human cTnC gene within the pET21(+) vector (Novagen). The various mutant constructs were generated through site-directed mutagenesis using the Phusion protocol (Thermo) that employs overlapping forward and reverse primers. Though we have had success with the Quickchange kit (Agilent) as well. To generate the N-terminal construct, we performed a site-directed mutagenesis to insert a stop codon at residue 90 in the protein, thus generating a construct that includes only the 89 most N-terminal amino acids of the full-length protein. Following each mutagenesis reactions, the linear DNA was ligated into a circular plasmid and transformed into cloning strain *E. coli* cells (DH5α) to allow for sequencing and long-term storage as glycerol stocks.

BL21(DE3) competent cells, also purchased commercially initially and later produced in house were transformed, stored as stocked aliquots, and used for over-expression of each protein construct.

```
cTnC           MDDIYKAAVEQLTEEQKNEFKAAFDIFVLGAEDGCISTKELGKVMRMLGQNPTPEELQEM  60
N-cTnC         MDDIYKAAVEQLTEEQKNEFKAAFDIFVLGAEDGCISTKELGKVMRMLGQNPTPEELQEM  60
A8V N-cTnC     MDDIYKAVVEQLTEEQKNEFKAAFDIFVLGAEDGCISTKELGKVMRMLGQNPTPEELQEM  60
L29Q N-cTnC    MDDIYKAAVEQLTEEQKNEFKAAFDIFVQGAEDGCISTKELGKVMRMLGQNPTPEELQEM  60
A31S N-cTnC    MDDIYKAAVEQLTEEQKNEFKAAFDIFVLGSEDGCISTKELGKVMRMLGQNPTPEELQEM  60
L48Q N-cTnC    MDDIYKAAVEQLTEEQKNEFKAAFDIFVLGAEDGCISTKELGKVMRMQGQNPTPEELQEM  60
Q50R N-cTnC    MDDIYKAAVEQLTEEQKNEFKAAFDIFVLGAEDGCISTKELGKVMRMLGRNPTPEELQEM  60
C84Y N-cTnC    MDDIYKAAVEQLTEEQKNEFKAAFDIFVLGAEDGCISTKELGKVMRMLGQNPTPEELQEM  60
               ******* ******************* * *************** * **********

cTnC           IDEVDEDGSGTVDFDEFLVMMVRCMKDDSKGKSEEELSDLFRMFDKNADGYIDLDELKIM  120
N-cTnC         IDEVDEDGSGTVDFDEFLVMMVRCMKDDS------------------------------  89
A8V N-cTnC     IDEVDEDGSGTVDFDEFLVMMVRCMKDDS------------------------------  89
L29Q N-cTnC    IDEVDEDGSGTVDFDEFLVMMVRCMKDDS------------------------------  89
A31S N-cTnC    IDEVDEDGSGTVDFDEFLVMMVRCMKDDS------------------------------  89
L48Q N-cTnC    IDEVDEDGSGTVDFDEFLVMMVRCMKDDS------------------------------  89
Q50R N-cTnC    IDEVDEDGSGTVDFDEFLVMMVRCMKDDS------------------------------  89
C84Y N-cTnC    IDEVDEDGSGTVDFDEFLVMMVRYMKDDS------------------------------  89
               ********************** *****

cTnC           LQATGETITEDDIEELMKDGDKNNDGRIDYDEFLEFMKGVE 161
N-cTnC         ------------------------------------------ 89
A8V N-cTnC     ------------------------------------------ 89
L29Q N-cTnC    ------------------------------------------ 89
A31S N-cTnC    ------------------------------------------ 89
L48Q N-cTnC    ------------------------------------------ 89
Q50R N-cTnC    ------------------------------------------ 89
C84Y N-cTnC    ------------------------------------------ 89
```

Figure 2-3 The aligned sequence of wild-type full-length and WT/mutant N-terminal cTnC

Constructs are shown along with the 6 studied N-terminal mutants bolded: A8V, L29Q, A31S, L48Q, Q50R, and C84Y. In Chapter 4 the effect of these single amino acid changes on the Ca^{2+} binding affinity of N-cTnC is explored and discussed.

```
Human cTnC     MDDIYKAAVEQLTEEQKNEFKAAFDIFVLGAEDGCISTKELGKVMRMLGQNPTPEELQEM 60
ZF ssTnC (1b)  MDDVYKAAVENLTEEQKNEFRAAFDIFVQDAEDGCISTKELGKVMRMLGQNPTQEELQEM 60
ZF cTnC (1a)   MNDIYKAAAEQLTDEQKNEFRAAFDIFVQDAEDGCISTKELGKVMRMLGQNPTPEELQEM 60
               *:*:****.*:**:******:******* .********************** ******

Human cTnC     IDEVDEDGSGTVDFDEFLVMMVRCMKDDS 89
ZF ssTnC (1b)  VDEVDEDGSGTVDFDEFLVMMVRCMKEES 89
ZF cTnC (1a)   IDEVDEDGSGTVDFEEFLVMMVRCMKDDS 89
               :*************:***********::*
```

Figure 2-4 The aligned sequences for WT human N-cTnC and zebrafish TnC constructs (1a/1b)

In Chapter 3 the effects of temperature and sequence variations arising from functional divergent evolution of the TnC gene which has given rise to differentially expressed paralogs in zebrafish is explored.

2.4.2. Protein Expression

For all constructs, a stab was supplied into 100 mL of Lysogeny Broth (LB) supplemented with 100 µg/mL of ampicillin and allowed to grow overnight (16-20 hrs) with 225-250 rpm shaking and under 37°C conditions. In the morning, preheated 1 L

batches (6 L total) of autoclaved and sterile LB media also supplemented with ampicillin were induced with 1-5% overnight culture and allowed to grow until reasonably cloudy and having an OD_{600} of 0.8-1.0; this took 3-4 hrs and was done under the same conditions previously listed. The cells were then supplemented with 1 mM IPTG from a 1 M stock and allowed to grow for a further 3 hours after which they were pelleted by centrifugation and the supernatant discarded. The cells were re-suspended in the first column buffer and frozen at -80 °C until use.

2.4.3. Protein purification

Column Chromatography

Ion exchange chromatography (Fekete, Beck et al. 2015) and size exclusion chromatography are classic molecular biology techniques that allow for protein separation by charge and size, respectively, and are often used in series to purify proteins of interest. Positively charged (amino group-containing) beads are used in anion exchange chromatography to retain proteins with negative charges on their surface. These proteins can then be eluted through application of a salt gradient of increasing concentration, proteins with the weakest ionic interactions elute first (Ståhlberg 1999, Bruch, Graalfs et al. 2009, Schmidt, Hafner et al. 2014).

The pH of the mobile phase should be set between the pK_A of the charged beads and the isoelectric point (pI) of the protein (Shan and Anderson 2002). The pI of the protein is determined by the number of surface exposed negative (aspartate and glutamate) and positive (arginine, histidine, and lysine) groups (Heinisch and Rocca 2009).

Size exclusion chromatography is rapid, reproducible, and relies on the differential elution speed of molecules from a stationary phase containing beads with pores, often dextrans linked with epichlorohydrins (Sephadex) (Tantipolphan, Romeijn et al. 2010). The elution speed is inversely proportional to the size of the molecule in its folded state. A secondary consideration is the presence of ionic interactions between the proteins and the beads, these interactions can be minimized using salt of varying concentrations (Arakawa, Ejima et al. 2010).

N-terminal cTnC

50 mM Tris-Cl, 100 mM NaCl, 1 mM DTT (diothiothreitol) at pH 8.0 (Buffer A) was used to re-suspend the cell pellet. The solution was sonicated 4-5 times for 30 seconds each at 80% amplitude with cooling on ice in the intervals. The solution was spun down at 30,000 xg for 15 mins, two times, with the pellet discarded and the supernatant applied to a diethylamino ethane fast-flow (DEAE FF) anion exchanger column (Amersham) at room temperature using an AKTA FPLC (GE healthcare) to switch solutions. A Q Sepharose FF anion exchanger can also be used in place of the DEAE FF. The solution used to elute the protein was Buffer A + 0.5 M NaCl (Buffer B) and was applied with a ramp protocol over a 180 mL gradient. The protein eluted at approximately 40%-60% of the salt gradient; these fractions were run on an SDS-PAGE gel and stained with Page Blue or Acquastain (Bulldog Bio) stain to visualize the bands.

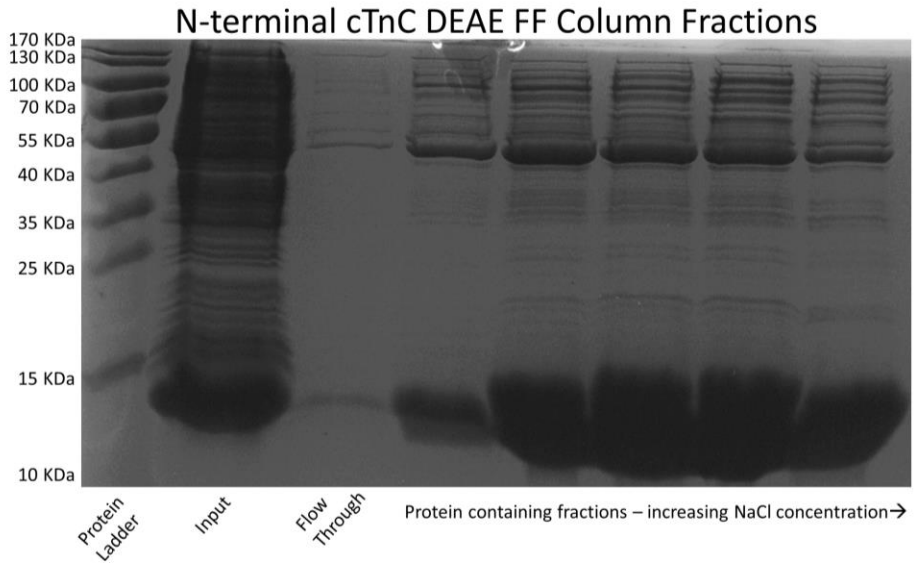

Figure 2-5 SDS-PAGE gel depicting the DEAE FF column fractions in the purification of human N-cTnC

The fractions containing the protein (aligning with a molecular marker at about 10 KDa) were pooled and concentrated with an Amicon tube with a 3 KDa molecular weight cut-off (Millipore). The sample, now less than 5 mL was pushed through a 0.45 µm filter to remove aggregates prior to being applied to the HiPrep 26/60 Sephracryl S-100 column (GE Healthcare) using the AKTA FPLC. The protein eluted at around the 180 - 200 mL mark. This column also acted as a buffer exchanger, with the Size Exclusion

buffer being: 50 mM Tris-Cl, 150 mM NaCl, and 1 mM DTT pH 8.0. The fractions were again run on an SDS-PAGE gel and stained to visualize.

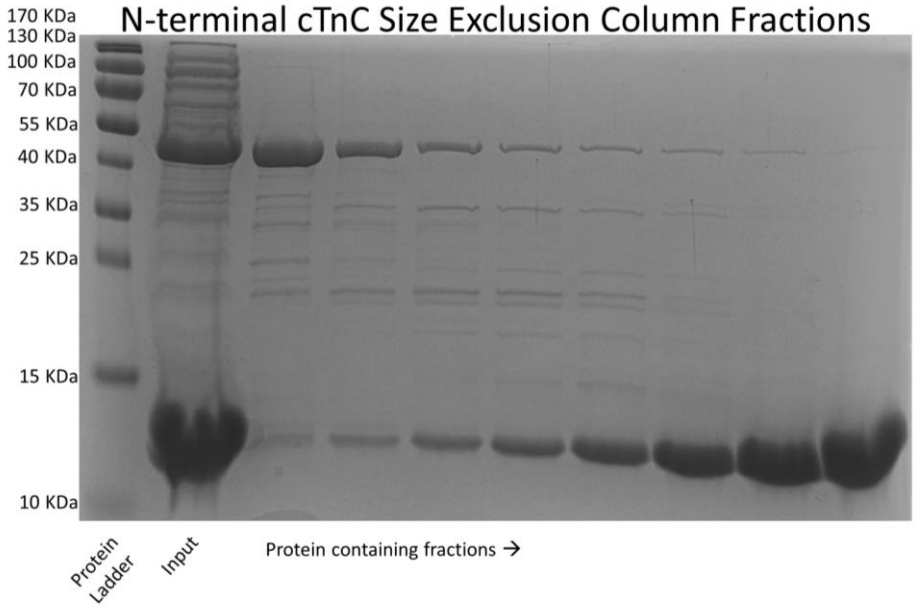

Figure 2-6 SDS-PAGE gel depicting the size exclusion column fractions in the purification of human N-cTnC.

Fractions containing the pure protein were pooled and concentrated by the same method as previously described, then stored at -80 °C. To avoid protein breakdown the two columns and steps between were completed in a 12-hour period with no overnight storage.

Full Length cTnC

The protein pellet was re-suspended in Buffer A and sonicated as previously with the pellet being removed. An ammonium sulfate cut equal to 30% of the supernatant volume by weight was used for 30 mins with spinning and on ice. Following this, the supernatant was again spun down and the pellet removed. The solution (less than 50 mL) was buffer exchanged into 4 L of Buffer A to remove the salt overnight (16-20 hrs). In the morning the solution was filtered and applied as before to a DEAE FF column with all subsequent steps being the same as for the purification of the N-terminal construct.

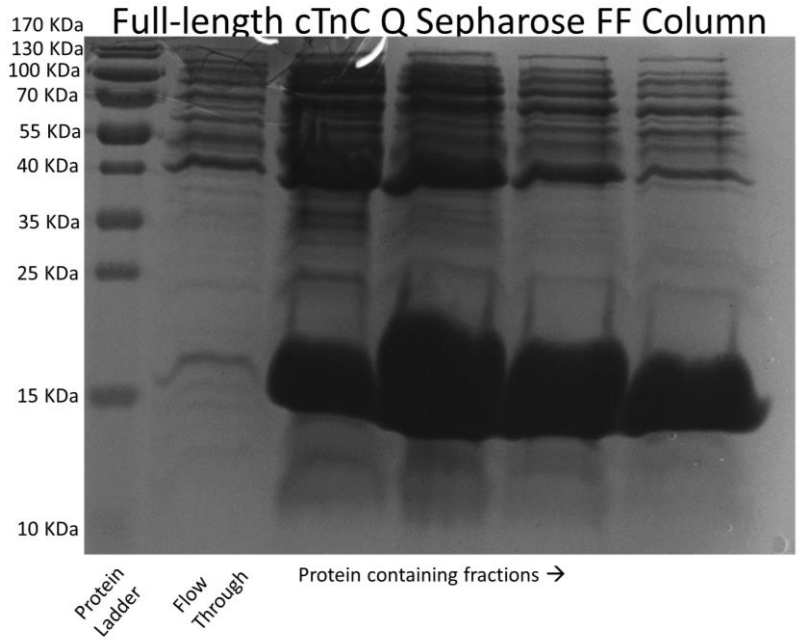

Figure 2-7 Q-Sepharose FF column fractions containing full-length human cTnC visualized on an SDS-PAGE gel

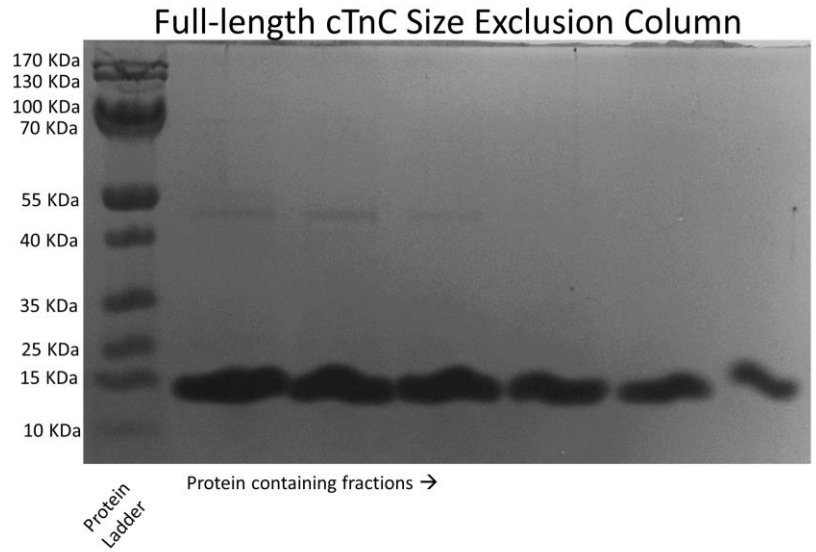

Figure 2-8 Size-exclusion column fractions containing purified full-length human cTnC

2.4.4. Measurement of Protein Concentration

Low stoichiometry can be indicative of lower than expected ligand concentration or higher than expected titrant concentration. ITC itself is a powerful method for determining the concentration of folded and active protein. Though aggregated protein of interest, degradation of the protein, and contaminants in the preparation would all lead to erroneous estimation of the effective protein concentration.

An accurate estimate of protein concentration is necessary to begin experiments and we have used 4 methods for determining protein concentration with varying levels of success. Initially, UV-vis spectroscopy was used to measure protein concentration at 280 nm using a NanoDrop 2000C spectrophotometer (Thermo). In this system we used a molar absorptivity of 1490 $cm^{-1}M^{-1}$ for zebrafish and 1289 $cm^{-1}M^{-1}$ for human N-cTnC and a MW of 10.1 KDa calculated from the protein sequence using the Expasy Protparam tool (Stevens, Rayani et al. 2016, Stevens, Rayani et al. 2017). We found that this number often under-estimated the concentration of the functional, folded protein as indicated by the stoichiometry measured in the ITC experiments that was less than 1 ($0<n<1$). In contrast, adding much greater than estimated concentrations of protein would lead to an $n>1$. Therefore, while we similarly estimated the concentrations of full length H-cTnC using a molar absorptivity of 4595 $cm^{-1}M^{-1}$ and a molecular weight of 18.4 KDa (Skowronsky, Schroeter et al. 2013), we sought alternative methods.

Initially we used the Bradford assay whereby a curve was constructed from standards at known concentrations and the absorbance of the diluted sample was used in conjunction with the line of best fit to determine the concentration of the protein (Bradford 1976, Zor and Selinger 1996). We then utilized the Edelhoch method (Edelhoch 1967) and absorbance spectroscopy by reliance on the Beer Lambert Law:

Absorbance (A) = Extinction Coefficient (ε) * Path Length (l) * Concentration (c)

The contribution of amino acid side chains was used to estimate the ε at 280 nm by summing:

Extinction Coefficient (ε) = #Tryptophan*5500 + #Tyrosine*1490 + Cysteine*125

The protein was linearized with 6 M guanidine hydrochloride prior to measurement (Grimsley and Pace 2003). While the combination of spectrophotometry and ITC experiments was sufficient as an initial estimate to determine the active concentration of protein in an N-TnC sample, we used the Edelhoch method to do so with greater accuracy for samples of full-length cTnC.

2.5. ITC Experimental Protocol

Purified protein was dialyzed against 3 buffer exchanges of 2 L each for at least 8 hrs at 4°C with stirring. The first buffer contained 50 mM HEPES, 150 mM KCl, 2 mM Ethylene diamine tetraacetic acid (EDTA), and 15 mM β–mercaptoethanol (BME) at pH 7.2 to remove divalent cations and generate the apo-state cTnC. EDTA has finite binding capacity and may not completely removal all of the Ca^{2+} in the solution, however at the given concentrations used, remaining Ca^{2+} is expected to be in the nM range. This concentration of Ca^{2+} may still bind sites III/IV of full length cTnC; however, to work around this issue, we compared between different conditions to gain relative measures of changes in affinity and binding. The second buffer had the same contents but lacked EDTA. The third buffer contained 50 mM HEPES, 150 mM KCl, and 2 mM BME at pH 7.2. Through SDS-PAGE gel analysis, we found that storage, dialysis, and filtration removed a majority of the small amount of impurities present in the sample following the size exclusion step.

The concentrations utilized in the experiments were altered slightly to accommodate varying amounts of protein. Initially, for 4 mM Ca^{2+} we used 1 dummy injection of 0.8 µL and 18 subsequent injections of 2 µL each into 200 µM sample of N-TnC (Rayani, Stevens et al. 2016, Stevens, Rayani et al. 2017). We also found that 100 µM N-TnC injected with the same protocol but 2 mM Ca^{2+} was a sufficient concentration at which to carry out these experiments (data presented in chapter 6). However, as expected the error-to-signal (noise) ratio increased with lesser protein concentrations. We used 20 mM Mg^{2+} to titrate 100 µM N-TnC using the same number and volume of injections. For full-length cTnC, we used 100 µM samples of protein, titrated with either 6 mM Ca^{2+} or 40 mM Mg^{2+} (data presented in Chapter 5).

For all experiments, we loaded the cell with 200 µL of protein, spaced the titrations 120 seconds apart, and set the stirring speed to 1,000 rpm.

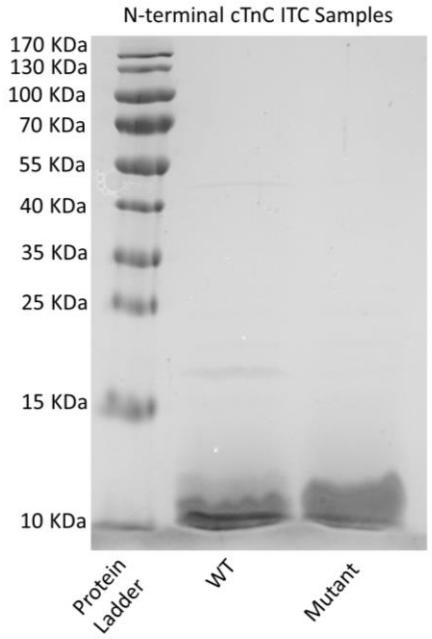

Figure 2-9 cTnC fractions following dialysis against ITC buffer and prior to experiments.

The pooled, dialyzed, and filtered protein samples often appeared purer than the fractions collected from the final column.

2.5.1. Background titration

To reduce noise, the buffer should be identical for both the titrant and titrate, through extensive dialysis steps. To avoid heat of dilution signals, the pH, salt concentration, and all other factors should be identical between the solutions. If the titrant is a solid, it should be dissolved in the dialysate to avoid buffer mismatch. To avoid noise and altering the structure of the protein, reducing agents such as DTT, BME, or Tri-2-carboxyehtylphosphine hydrochloride (TCEP) should be minimized as they may bind to the divalent cations. Details of the protocols employed in each study presented in this thesis are in keeping with these recommendations. We avoided using reducing reagents with the exception of BME which was minimized.

Background experiments are used to differentiate the heat of interaction with the ligand and the heat of dilution. The injection volumes and other conditions should be identical in the blank titrations and the experimental trial. Buffer-into-buffer, buffer-into-ligand, and titrant-into-buffer can be subtracted from the isotherm. An instrument blank of buffer into buffer is at times employed, which allows for measurement of the often-

negligible effects of macromolecule dilution. Most commonly, a titrant into buffer condition titration is carried out and subtracted from the titrant into ligand trial. We found that these methods were not ideal given that the collection of a large sample size necessitated that experiments be carried out over the course of multiple days. Given the drift in the instrument, to get applicable blank trials would have required such trials be performed every 3 – 4 experiments. Therefore, we sought an internal control, whereby each experiment could be compared to a baseline.

The mean value that corresponds to the last 2-3 heat signals when the ligand has been saturated is indicative of titrant-buffer interactions and nonspecific interactions between the titrant and the ligand. We subtracted this value from our titrations to account for background as an internal control and to help improve curve fitting.

A further consideration is the appearance of erroneous heat signals upon introduction of air bubbles into the reaction solution. To avoid this issue, bubbles should be absent in both the sample cell and the titrant solutions prior to initiation of the protocol.

2.6. Analysis of Experimental Results

Raw data from the ITC experiments were analyzed using OriginLab 7 software provided with the MicroCal ITC_{200}. Curve fitting in the software can be utilized for reactions with one, two, or three binding sites. Given the understanding we have of our experimental system, we hypothesized that the use of less complex fits would be most appropriate for each set of experiments. Details of these fits are provided in each chapter to which they correspond.

The integrated heat data were fit with a single binding site model for N-cTnC and two binding sites for full length cTnC. Non-linear regression was used to determine the best fit parameters through iterative least squares error minimization as the Chi-squared value was minimized.

Given the iterative nature employed in modeling the data collected in ITC, the initial estimates of the parameters (K_A, ΔH, and n) are used to fit a curve to the data. At times, it may be necessary to provide a starting point for the algorithm to approach the minimum in error. When fitting using built in functions, the deviation of the curve from the

data points (i.e. the sum of the squared error values) is minimized with every subsequent iterative change in the above listed parameters through application of a simplex algorithm. This is continued until the changes no longer cause significant changes in the error. We have found that the initial parameters that may be estimates from the steepness of the graph, the heat change seen, and the inflexion point are essential in fitting data sets that are more complex than a single binding site. Moreover, varying one or two of the parameters at a time and keeping the others fixed, for example when fitting 2 binding sites, varying 2 and keeping 4 fixed, then varying 3 and keeping 3 fixed etc. can allow the sum of the error to more successfully converge on a global minimum.

As shown in **Figure 2-1**, the inflection point of the titration curve can be used to find the n, with the slope of the graph at this point indicative of the dissociation constant (K_d). The K_d is the reciprocal of K_A. Manipulation of equation [1] in **Figure 2-2** above and replacement of K_A by K_d (through $K_A=1/K_d$) can be used to derive a basic relationship. Simplification of equation [1] allows one to see that K_d is the concentration of the ligand at which the binding site is half-saturated. A higher K_d indicates a lower affinity interaction and thus a higher concentration of ligand being required to half-saturate the binding site.

The ΔG can be calculated from equation [2] above with R being the universal gas constant, T the temperature in Kelvin, and K_A the equilibrium constant (equal to $1/K_d$). Equation [3] can then be used to calculate the ΔS associated with the interaction. With the exception of the ΔG, these values were computed upon fitting of the reaction data and reported per unit mole (Leavitt and Freire 2001).

The stoichiometry, n is indicative of the moles of titrant and the moles of functional binding sites. When the affinity of the ligand for titrant was low, the n was fixed to the appropriate value (1.0) to avoid errors in ΔH; this is common when the stoichiometry of the interaction and the concentration of the reactants is known, as is the case with such a well studied protein.

2.7. Additional considerations

2.7.1. Day-to-day variability

In the initial stages of our study, the question of random variability in the ITC experiments came to the fore. It became clear that the associated error was a product of the fitting. However, the approach of compounding the error to give a sum in errors associated with each mean was explored and resulted in inflated and unrealistic numbers. We wanted to study possible fluctuations in the values collected throughout the day on one day and multiple different days for each WT/mutant construct.

We compared the means for the measurements all done on one day and those randomized, i.e. 3 measurements on 3 different days. One inherent issue was that the sample size associated with the latter was much smaller. Another confounding effect was the inter-batch variability, as the measurements were carried out on different batches of separately purified protein. It was not standardized when the same batch was used for each protocol and when other batches were required; this would in itself cause some variability. Lastly, the smaller standard error of the mean (SEM) associated with the great majority of thermodynamic parameters derived from the same-day measurements compared to the multiple-day protocols is of interest. It is difficult to be certain regarding protocol selection and which gives a more physiologically correct value, if they are different at all (**Figure 2-10**). It is clear that there are advantages to each of the one-day and multi-day protocols.

With the exception of C84Y at 37 °C which resulted in unstable readings and was hard to measure with certainty, K_A values were not significantly different between the two measurement protocols. The other thermodynamic parameters were also highly consistent in spite of the protocol used.

Table 2-1 Comparison of the thermodynamic parameters of the WT and 6 N-cTnC constructs.

N-cTnC	Protocol	n	N ± SEM	K_A*10^3 (M^{-1}) ± SEM	K_d (uM) ± SEM	ΔH (kcal/mol) ± SEM	T*ΔS (kcal/mol) ± SEM	ΔG (kcal/mol) ± SEM
WT	Same day	7	0.91 ± 0.01	68.47 ± 1.10	14.63 ± 0.23	3.46 ± 0.01	10.06 ± 0.16	-6.59 ± 0.03
	Multiple days	3	1.05 ± 0.01	67.27 ± 2.91	14.93 ± 0.66	3.42 ± 0.14	10.01 ± 0.15	-6.59 ± 0.02
A8V	Same day	8	0.91 ± 0.01	72.09 ± 5.09	14.28 ± 0.85	3.53 ± 0.06	10.14 ± 0.13	-6.61 ± 0.04
	Multiple days	3	1.01 ± 0.02	65.70 ± 3.88	15.32 ± 0.87	3.51 ± 0.09	10.09 ± 0.13	-6.58 ± 0.04
L29Q	Same day	8	1.02 ± 0.01	101.54 ± 1.45	9.86 ± 0.15	3.69 ± 0.03	10.52 ± 0.09	-6.83 ± 0.09
	Multiple days	3	0.99 ± 0.01	70.47 ± 1.89	14.21 ± 0.38	3.72 ± 0.09	10.34 ± 0.08	-6.61 ± 0.01
A31S	Same day	7	0.96 ± 0.01	128.86 ± 2.08	7.77 ± 0.12	2.25 ± 0.01	9.23 ± 0.12	-6.97 ± 0.10
	Multiple days	3	0.88 ± 0.03	85.97 ± 7.01	11.8 ± 1.05	2.15 ± 0.06	8.87 ± 0.11	-6.73 ± 0.06
L48Q	Same day	9	1.08± 0.01	705.78 ± 45.20	1.45 ± 0.07	-3.84 ± 0.02	4.13 ± 0.04	-7.94 ± 0.02
	Multiple days	3	1.02 ± 0.03	676.00 ± 23.59	1.48 ± 0.05	-4.39 ± 0.05	3.57 ± 0.04	-7.95 ± 0.02
Q50R	Same day	8	1.03 ± 0.01	181.00 ± 9.51	5.64 ± 0.31	1.42 ± 0.02	8.59 ± 0.04	-7.17 ± 0.03
	Multiple days	3	1.05 ± 0.01	171.00 ± 3.79	5.85 ± 0.13	1.47 ± 0.03	8.61 ± 0.04	-7.14 ± 0.02
C84Y	Same day	6	0.97 ± 0.01	211.67 ± 15.63	4.88 ± 0.43	0.90 ± 0.01	8.15 ± 0.10	-7.25 ± 0.05
	Multiple days	3	0.96 ± 0.02	262.33 ± 56.29	4.19 ± 0.90	0.75 ± 0.03	8.12 ± 0.10	-7.37 ± 0.13

Experiments were run at 25 °C using both the same day and multiple day protocols. The multiple day condition data has been published (Stevens, Rayani et al. 2017).

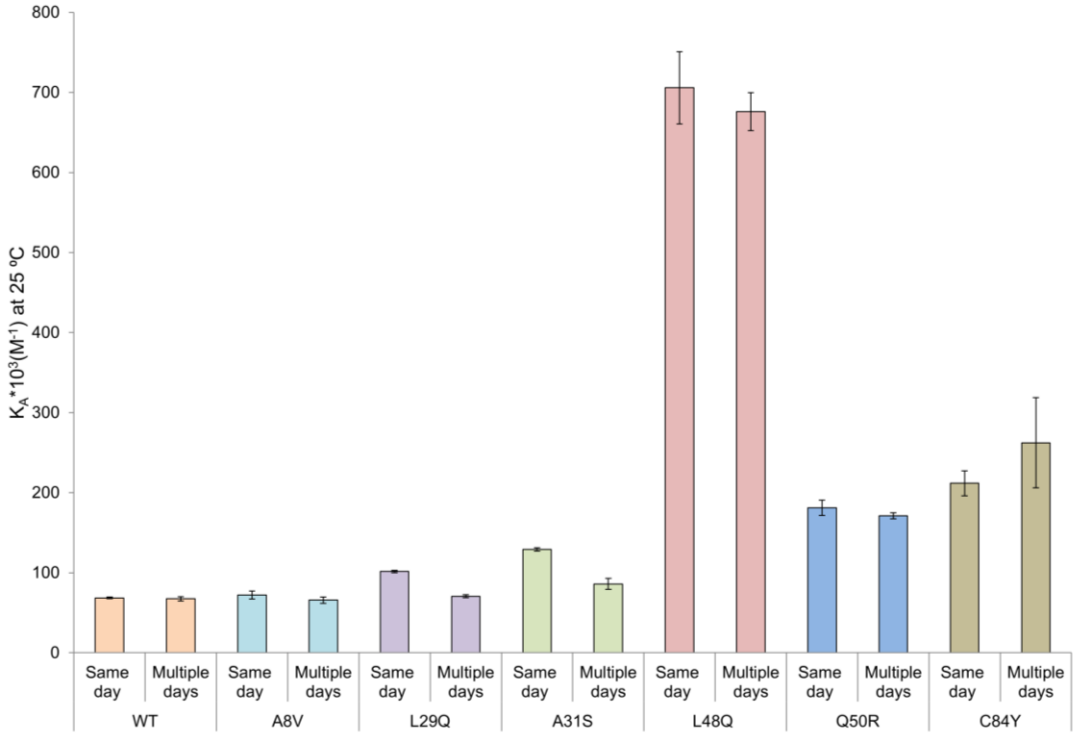

Figure 2-10 Comparing N-cTnC construct affinity between same day and multiple day protocols at 25 °C

For the majority of the trials the same day protocol showed a smaller amount of variability, as depicted by the SEM error bars. The overlap of the error bars in many of the cases is indicative of

a negligible effect of recording on one day vs. on multiple days. Statistical analysis of results was not carried out as biologically significant difference was not observed between same day and multiple day protocols.

Table 2-2 Comparison of thermodynamic parameters between the same day and multiple day protocols at 37 °C

N-cTnC	Protocol	n	N ± SEM	K_A*10^3 (M^{-1}) ± SEM	K_d (uM) ± SEM	ΔH (kcal/mol) ± SEM	T*ΔS (kcal/mol) ± SEM	ΔG(kcal/mol) ± SEM
WT	Same day	7	0.91 ± 0.01	68.00 ± 1.70	14.76 ± 0.34	3.68 ± 0.02	10.54 ± 0.03	-6.85 ± 0.01
	Multiple days	3	1.06 ± 0.01	71.73 ± 1.09	13.95 ± 0.22	3.49 ± 0.14	10.37 ± 0.08	-6.88 ± 0.01
A8V	Same day	7	0.88 ± 0.01	73.47 ± 5.84	14.02 ± 0.86	3.56 ± 0.05	10.46 ± 0.02	-6.86 ± 0.02
	Multiple days	3	1.04 ± 0.03	73.10 ± 2.75	13.72 ± 0.50	3.42 ± 0.12	10.32 ± 0.06	-6.90 ± 0.02
L29Q	Same day	8	0.95± 0.01	117.30 ± 3.74	8.59 ± 0.28	3.86 ± 0.06	11.05 ± 0.07	-7.19 ± 0.02
	Multiple days	3	0.98± 0.04	90.77 ± 13.29	11.45 ± 1.49	3.53 ± 0.11	10.55 ± 0.02	-7.02 ± 0.09
A31S	Same day	7	0.95 ± 0.01	118.69 ± 7.17	8.66 ± 0.65	2.34 ± 0.03	9.53 ± 0.03	-7.23 ± 0.02
	Multiple days	3	0.90 ± 0.04	76.53 ± 9.55	13.54 ± 1.91	2.32 ± 0.02	9.24 ± 0.05	-6.93 ± 0.09
L48Q	Same day	9	1.08 ± 0.01	618.11 ± 18.11	1.63 ± 0.05	-7.32 ± 0.03	0.89 ± 0.04	-8.22 ± 0.02
	Multiple days	3	1.02 ± 0.04	681.67 ± 36.67	1.47 ± 0.08	-8.19 ± 0.13	0.08 ± 0.004	-8.28 ± 0.03
Q50R	Same day	8	0.95 ± 0.02	140.13 ± 6.35	7.24 ± 0.34	1.38 ± 0.01	8.67 ± 0.02	-7.30 ± 0.03
	Multiple days	3	1.00 ± 0.04	148.00 ± 14.93	6.89 ± 0.67	1.36 ± 0.04	8.68 ± 0.05	-7.32 ± 0.07
C84Y	Same day	11	0.97 ± 0.02	157.73 ± 12.38	6.74 ± 0.53	0.48 ± 0.01	7.84 ± 0.04	-7.36 ± 0.05
	Multiple days	3	0.99 ± 0.04	92.17 ± 14.93	11.37 ± 1.59	0.56 ± 0.03	7.56 ± 0.03	-7.03 ± 0.10

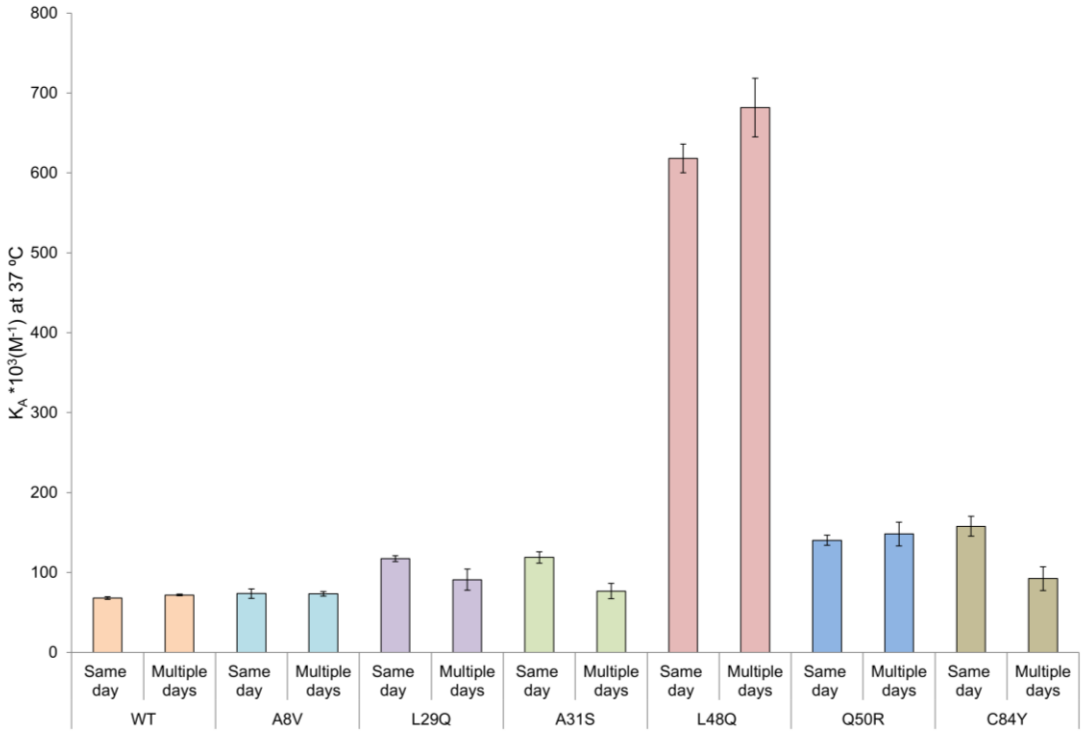

Figure 2-11 Comparison of N-cTnC construct affinity between the same day and multiple day protocols at 37 °C

For the majority of the trials the same day protocol shows a smaller amount of variability, as depicted by the SEM error bars. The overlap of the error bars in many of the cases is indicative of a negligible effect of recording on one day vs. on multiple days. Statistical analysis of results was not carried out as biologically significant difference was not observed between same day and multiple day protocols.

2.7.2. Effect of Temperature

The effects of temperature can also be explored with the data presented above, to this end, the same day trials that present lesser variability are presented in Table 2.3. Protein structure at the secondary (α-helices and β-sheets), tertiary (folding), and quaternary (subunit assembly) level is affected by multiple forces: Van der Waals interactions, hydrogen bonds, electrostatic interactions, and hydrophobic interactions. All these forces are affected by temperature. With the exception of hydrophobic interactions, an increase in temperature would be expected to reduce the negative enthalpy change that accompanies the formation of these bonds. In addition, the aqueous environment is temperature sensitive, whereby an increase in temperature should increase the ionization number of water and thus $[H^+]$ while pH remains unaltered. We sought to explore the potential effect of changing temperature from 25 °C

to 37 °C on the Ca^{2+} binding properties of WT and mutant N-cTnC. 37 °C is of interest as it would indicate a physiological human body temperature. 25 °C is closer to room temperature and as we found out, corresponded to higher signal quality, likely due to greater protein stability at lower temperatures.

Table 2-3 Comparison of thermodynamic parameters between isotherms collected at 25 °C and 37 °C using the same-day protocols

N-cTnC	Protocol	n	N ± SEM	K_A*10^3 (M^{-1}) ± SEM	K_d (uM) ± SEM	ΔH (kcal/mol) ± SEM	T*ΔS (kcal/mol) ± SEM	ΔG(kcal/mol) ± SEM
WT	25 ºC	7	0.91 ± 0.01	68.47 ± 1.10	14.63 ± 0.23	3.46 ± 0.01*	10.06 ± 0.16*	-6.59 ± 0.03*
	37 ºC	7	0.91 ± 0.01	68.00 ± 1.70	14.76 ± 0.34	3.68 ± 0.02*	10.54 ± 0.03*	-6.85 ± 0.01*
A8V	25 ºC	8	0.91 ± 0.01	72.09 ± 5.09	14.28 ± 0.85	3.53 ± 0.06	10.14 ± 0.13*	-6.61 ± 0.04*
	37 ºC	7	0.88 ± 0.01	73.47 ± 5.84	14.02 ± 0.86	3.56 ± 0.05	10.46 ± 0.02*	-6.86 ± 0.02*
L29Q	25 ºC	8	1.02 ± 0.01	101.54 ± 1.45	9.86 ± 0.15	3.69 ± 0.03*	10.52 ± 0.09*	-6.83 ± 0.09*
	37 ºC	8	0.95± 0.01	117.30 ± 3.74	8.59 ± 0.28	3.86 ± 0.06*	11.05 ± 0.07*	-7.19 ± 0.02*
A31S	25 ºC	7	0.96 ± 0.01	128.86 ± 2.08	7.77 ± 0.12	2.25 ± 0.01	9.23 ± 0.12*	-6.97 ± 0.10*
	37 ºC	7	0.95 ± 0.01	118.69 ± 7.17	8.66 ± 0.65	2.34 ± 0.03	9.53 ± 0.03*	-7.23 ± 0.02*
L48Q	25 ºC	9	1.08± 0.01	705.78 ± 45.20*	1.45 ± 0.07*	-3.84 ± 0.02*	4.13 ± 0.04*	-7.94 ± 0.02*
	37 ºC	9	1.08 ± 0.01	618.11 ± 18.11*	1.63 ± 0.05*	-7.32 ± 0.03*	0.89 ± 0.04*	-8.22 ± 0.02*
Q50R	25 ºC	8	1.03 ± 0.01	181.00 ± 9.51	5.64 ± 0.31	1.42 ± 0.02	8.59 ± 0.04	-7.17 ± 0.03
	37 ºC	8	0.95 ± 0.02	140.13 ± 6.35	7.24 ± 0.34	1.38 ± 0.01	8.67 ± 0.02	-7.30 ± 0.03
C84Y	25 ºC	6	0.97 ± 0.01	211.67 ± 15.63*	4.88 ± 0.43*	0.90 ± 0.01*	8.15 ± 0.10*	-7.25 ± 0.05
	37 ºC	11	0.97 ± 0.02	157.73 ± 12.38*	6.74 ± 0.53*	0.48 ± 0.01*	7.84 ± 0.04*	-7.36 ± 0.05

ANOVA was initially performed, followed by Tukey's post-hoc test. Each parameter marked with an "*" is significantly different between temperature conditions $p<0.05$.

Pair-wise comparison of temperature conditions for each mutant construct showed few differences as depicted above. Even those that are different are likely to be biologically negligible, with the exception of the L48Q construct where the effect of temperature was relatively significant. While shedding some insight on protein thermal stability, these studies did not provide sufficiently novel findings. The thermal stability of N-cTnC was instead explored using other techniques and presented in Chapters 3 and 4.

In this chapter, we have established an understanding of the basic principles underlying ITC, the means by which thermodynamic parameters are derived from experiments, and discussed experimental protocols. We also established that there is not significant variability in thermodynamic parameters when measurements are carried

out using a same day or multi-day experimental protocols. Due to the ease of performance, being the standard practice in the field, and other reasons outlined above, multi-day protocols were employed for all subsequent studies presented in this thesis.

2.8. References

Adrio, J.-L. and A. L. Demain (2010). "Recombinant organisms for production of industrial products." Bioengineered bugs **1**(2): 116-131.

Arakawa, T., D. Ejima, T. Li and J. S. Philo (2010). "The critical role of mobile phase composition in size exclusion chromatography of protein pharmaceuticals." Journal of Pharmaceutical Sciences **99**(4): 1674-1692.

Birnbaum, S. and J. Bailey (1991). "Plasmid presence changes the relative levels of many host cell proteins and ribosome components in recombinant Escherichia coli." Biotechnology and bioengineering **37**(8): 736-745.

Bolivar, F., R. L. Rodriguez, P. J. Greene, M. C. Betlach, H. L. Heyneker, H. W. Boyer, J. H. Crosa and S. Falkow (1977). "Construction and characterization of new cloning vehicle. II. A multipurpose cloning system." Gene **2**(2): 95-113.

Bradford, M. M. (1976). "A rapid and sensitive method for the quantitation of microgram quantities of protein utilizing the principle of protein-dye binding." Analytical Biochemistry **72**(1): 248-254.

Brown, M. J., L. M. Mensah, M. L. Doyle, N. J. Broom, N. Osbourne, A. K. Forrest, C. M. Richardson, P. J. O'Hanlon and A. J. Pope (2000). "Rational design of femtomolar inhibitors of isoleucyl tRNA synthetase from a binding model for pseudomonic acid-A." Biochemistry **39**(20): 6003-6011.

Bruch, T., H. Graalfs, L. Jacob and C. Frech (2009). "Influence of surface modification on protein retention in ion-exchange chromatography: Evaluation using different retention models." Journal of Chromatography A **1216**(6): 919-926.

Cabani, S., P. Gianni, V. Mollica and L. Lepori (1981). "Group contributions to the thermodynamic properties of non-ionic organic solutes in dilute aqueous solution." Journal of Solution Chemistry **10**(8): 563-595.

Del Solar, G. and M. Espinosa (2000). "Plasmid copy number control: an ever-growing story." Molecular microbiology **37**(3): 492-500.

Fekete, S., A. Beck, J.-L. Veuthey and D. Guillarme (2015). "Ion-exchange chromatography for the characterization of biopharmaceuticals." Journal of pharmaceutical and biomedical analysis **113**: 43-55.

Freire, E., O. L. Mayorga and M. Straume (1990). "Isothermal titration calorimetry." Analytical chemistry **62**(18): 950A-959A.

Freyer, M. W. and E. A. Lewis (2008). "Isothermal titration calorimetry: experimental design, data analysis, and probing macromolecule/ligand binding and kinetic interactions." Methods in cell biology **84**: 79-113.

Graumann, K. and A. Premstaller (2006). "Manufacturing of recombinant therapeutic proteins in microbial systems." Biotechnology Journal: Healthcare Nutrition Technology **1**(2): 164-186.

Grimsley, G. R. and C. N. Pace (2003). "Spectrophotometric Determination of Protein Concentration." Current Protocols in Protein Science **33**(1): 3.1.1-3.1.9.

Hansen, L. D., G. W. Fellingham and D. J. Russell (2011). "Simultaneous determination of equilibrium constants and enthalpy changes by titration calorimetry: Methods, instruments, and uncertainties." Analytical biochemistry **409**(2): 220-229.

Heinisch, S. and J.-L. Rocca (2009). "Sense and nonsense of high-temperature liquid chromatography." Journal of Chromatography A **1216**(4): 642-658.

Ladbury, J. E. and M. L. Doyle (2004). Biocalorimetry 2: applications of calorimetry in the biological sciences, John Wiley & Sons.

Lambert, F. L. (2002). "Entropy is simple, qualitatively." Journal of Chemical Education **79**(10): 1241.

Leavitt, S. and E. Freire (2001). "Direct measurement of protein binding energetics by isothermal titration calorimetry." Current opinion in structural biology **11**(5): 560-566.

Lewis, E. A. and K. P. Murphy (2005). Isothermal titration calorimetry. Protein-Ligand Interactions, Springer**:** 1-15.

Li, A. Y., C. M. Stevens, B. Liang, K. Rayani, S. Little, J. Davis and G. F. Tibbits (2013). "Familial hypertrophic cardiomyopathy related cardiac troponin C L29Q mutation alters length-dependent activation and functional effects of phosphomimetic troponin I*."

Luque, I. and E. Freire (2000). "Structural stability of binding sites: consequences for binding affinity and allosteric effects." Proteins: Structure, Function, and Bioinformatics **41**(S4): 63-71.

Moffatt, B. A. and F. W. Studier (1987). "T7 lysozyme inhibits transcription by T7 RNA polymerase." Cell **49**(2): 221-227.

Pope, B. and H. M. Kent (1996). "High efficiency 5 min transformation of Escherichia coli." Nucleic acids research **24**(3): 536-537.

Rekharsky, M. V. and Y. Inoue (1998). "Complexation thermodynamics of cyclodextrins." Chemical reviews **98**(5): 1875-1918.

Sahdev, S., S. K. Khattar and K. S. Saini (2008). "Production of active eukaryotic proteins through bacterial expression systems: a review of the existing biotechnology strategies." Molecular and cellular biochemistry **307**(1-2): 249-264.

Schmidt, M., M. Hafner and C. Frech (2014). "Modeling of salt and pH gradient elution in ion-exchange chromatography." Journal of separation science **37**(1-2): 5-13.

Sezonov, G., D. Joseleau-Petit and R. D'Ari (2007). "Escherichia coli physiology in Luria-Bertani broth." Journal of bacteriology **189**(23): 8746-8749.

Shan, L. and D. J. Anderson (2002). "Gradient Chromatofocusing. Versatile pH Gradient Separation of Proteins in Ion-Exchange HPLC: Characterization Studies." Analytical Chemistry **74**(21): 5641-5649.

Shiloach, J. and R. Fass (2005). "Growing E. coli to high cell density—a historical perspective on method development." Biotechnology advances **23**(5): 345-357.

Skowronsky, R. A., M. Schroeter, T. Baxley, Y. Li, J. M. Chalovich and A. M. Spuches (2013). "Thermodynamics and molecular dynamics simulations of calcium binding to the regulatory site of human cardiac troponin C: evidence for communication with the structural calcium binding sites." JBIC Journal of Biological Inorganic Chemistry **18**(1): 49-58.

Ståhlberg, J. (1999). "Retention models for ions in chromatography." Journal of Chromatography A **855**(1): 3-55.

Stevens, C. M., K. Rayani, C. E. Genge, G. Singh, B. Liang, J. M. Roller, C. Li, A. Y. Li, D. P. Tieleman and F. van Petegem (2016). "Characterization of Zebrafish Cardiac and Slow Skeletal Troponin C Paralogs by MD Simulation and ITC." Biophysical Journal **111**(1): 38-49.

Stevens, C. M., K. Rayani, G. Singh, B. Lotfalisalmasi, D. P. Tieleman and G. F. Tibbits (2017). "Changes in the dynamics of the cardiac troponin C molecule explain the effects of Ca2+-sensitizing mutations." Journal of Biological Chemistry **292**(28): 11915-11926.

Tantipolphan, R., S. Romeijn, J. d. Engelsman, R. Torosantucci, T. Rasmussen and W. Jiskoot (2010). "Elution behavior of insulin on high-performance size exclusion chromatography at neutral pH." Journal of Pharmaceutical and Biomedical Analysis **52**(2): 195-202.

Todd, M. J., I. Luque, A. Velázquez-Campoy and E. Freire (2000). "Thermodynamic basis of resistance to HIV-1 protease inhibition: calorimetric analysis of the V82F/I84V active site resistant mutant." Biochemistry **39**(39): 11876-11883.

Velazquez-Campoy, A., Y. Kiso and E. Freire (2001). "The binding energetics of first-and second-generation HIV-1 protease inhibitors: implications for drug design." Archives of Biochemistry and Biophysics **390**(2): 169-175.

Ward, W. H. and G. A. Holdgate (2001). 7 Isothermal Titration Calorimetry in Drug Discovery. Progress in medicinal chemistry, Elsevier. **38:** 309-376.

Wiseman, T., S. Williston, J. F. Brandts and L.-N. Lin (1989). "Rapid measurement of binding constants and heats of binding using a new titration calorimeter." Analytical biochemistry **179**(1): 131-137.

Zhang, Y.-L., Z.-J. Yao, M. Sarmiento, L. Wu, T. R. Burke and Z.-Y. Zhang (2000). "Thermodynamic study of ligand binding to protein-tyrosine phosphatase 1B and its substrate-trapping mutants." Journal of Biological Chemistry **275**(44): 34205-34212.

Zor, T. and Z. Selinger (1996). "Linearization of the Bradford Protein Assay Increases Its Sensitivity: Theoretical and Experimental Studies." Analytical Biochemistry **236**(2): 302-308.

Chapter 3.

Comparison of the Effects of Species-Specific Expression Patterns and Acute Temperature on Troponin C Calcium Binding

This chapter entails the work entitled “Characterization of Zebrafish Cardiac and Slow Skeletal Troponin C Paralogs by MD Simulation and ITC” published in the Biophysical Journal in 2016. Minor modifications have been made to ensure the contents of this chapter are in keeping with the prescribed format of this thesis.

My contributions to this publication were in designing, carrying out, and analysing the ITC experiments. I also helped to carry out and analyze the results of the melting point experiments. I contributed to manuscript preparation and subsequent review. Dr. Charles Stevens carried out the MD Simulations in collaboration with Dr. Gurpreet Singh, he also analyzed the MD results, and prepared the manuscript. Dr. Christine Genge carried out the melting point experiments and assisted with manuscript preparation.

3.1. Abstract

Zebrafish, as a model for teleost fish, have two paralogous troponin C (TnC) genes that are expressed in the heart differentially in response to temperature acclimation. Upon Ca^{2+} binding, TnC changes conformation and exposes a hydrophobic patch that interacts with troponin I and initiates cardiac muscle contraction. Teleost-specific TnC paralogs have not yet been functionally characterized. In this study we have modeled the structures of the paralogs using molecular dynamics simulations at 18°C and 28°C and calculated the different Ca^{2+}-binding properties between the teleost cardiac (cTnC or TnC1a) and slow-skeletal (ssTnC or TnC1b) paralogs through potential-of-mean-force calculations. These values are compared with thermodynamic binding properties obtained through isothermal titration calorimetry (ITC). The modeled structures of each of the paralogs are similar at each temperature, with the exception of helix C, which flanks the Ca^{2+} binding site; this region is also home to paralog-specific sequence substitutions that we predict have an influence on protein function. The short

timescale of the potential-of-mean-force calculation precludes the inclusion of the conformational change on the ΔG of Ca^{2+} interaction, whereas the ITC analysis includes the Ca^{2+} binding and conformational change of the TnC molecule. ITC analysis has revealed that ssTnC has higher Ca^{2+} affinity than cTnC for Ca^{2+} overall, whereas each of the paralogs has increased affinity at 28°C compared to 18°C. Microsecond-timescale simulations have calculated that the cTnC paralog transitions from the closed to the open state more readily than the ssTnC paralog, an unfavorable transition that would decrease the ITC-derived Ca^{2+} affinity while simultaneously increasing the Ca^{2+} sensitivity of the myofilament. We propose that the preferential expression of cTnC at lower temperatures increases myofilament Ca^{2+} sensitivity by this mechanism, despite the lower Ca^{2+} affinity that we have measured by ITC.

3.2. Introduction

Ectothermic species tolerate a range of acute and seasonal temperatures through plasticity in protein function and changes in gene expression (Somero and Hochachka 1969, Genge, Davidson et al. 2013). Central to this tolerance is the maintenance of cardiac function across a range of temperatures. The optimal temperature for ectothermic zebrafish (*Danio rerio*) lies between 25°C and 28°C (Spence, Gerlach et al. 2008); however, *D. rerio* cardiac function must be maintained through daily, seasonal, and geographic temperature fluctuations between 6°C and 38°C (Spence, Gerlach et al. 2008). Many species of fish, including *D. rerio*, increase their heart rate up to two-fold per 10°C increase in temperature in response to acute temperature fluctuations (Churcott, Moyes et al. 1994, Tiitu and Vornanen 2002, Gollock, Currie et al. 2006, Clark, Sandblom et al. 2008, Mendonça and Gamperl 2010, Lin, Ribeiro et al. 2014, Little and Seebacher 2014, Lee, Genge et al. 2016). The adaptation to acute temperature changes occurs more quickly than transcriptional changes can account for. Long-term temperature acclimation confers greater tolerance through altered composition of the cardiomyocyte transcriptome, that includes critical proteins of the contractile apparatus such as members of the troponin complex (Alderman, Klaiman et al. 2012, Genge, Davidson et al. 2013).

The cardiac troponin (cTn) complex contains three proteins: cardiac troponin C (cTnC), a Ca^{2+} sensor protein; cardiac troponin I (cTnI), an inhibitory protein; and cardiac troponin T (cTnT), that tethers the complex to the remainder of the thin filament by

interacting with tropomyosin (Parmacek and Solaro 2004). cTnC is a two-domain protein with four EF-hand motifs designated as sites I through IV. Site I does not bind Ca^{2+}, site II is responsible for the Ca^{2+}-sensing function of cTnC, and sites III and IV have a structural role and always bind Ca^{2+} or Mg^{2+} under physiological conditions (Potter and Gergely 1975). The bulk-phase cytosolic Ca^{2+} concentration increases from ~100 nM during diastole to a maximum of 1 μM in systole (Bers 2002). As the cytosolic Ca^{2+} concentration increases, the regulatory site II of cTnC is bound by Ca^{2+}, leading to conformational changes that expose a hydrophobic patch. This hydrophobic patch then interacts with cTnI and allows the cTnI inhibitory peptide to withdraw from the actin filament (Parmacek and Solaro 2004). The cTnC-Ca^{2+} binding interaction also interrupts the cTnT-tropomyosin interaction, permits actin/myosin cross-bridge formation, and initiates muscle contraction.

Several structures have been solved for the cTnC protein, including the N-terminal domain of human cTnC in the Ca^{2+}-bound (PDB:1AP4) and Ca^{2+}-free (PDB:1SPY) (Spyracopoulos, Li et al. 1997) forms, and in complex with the cTnI switch peptide (PDB:1MXL) (Li, Spyracopoulos et al. 1999), with TnI (PDB:1J1D), and with TnT (PDB:1J1E) (Takeda, Yamashita et al. 2003). The N-terminal domain of trout cTnC has also been solved at 7°C (PDB:1R6P) and 30°C (PDB:1R2U) (Gillis, Marshall et al. 2000). Under similar conditions, these structures differ minimally. The addition of Ca^{2+} causes a slight change in the cTnC structure, although the angle between helices A and B and the status of the hydrophobic patch are unchanged (Spyracopoulos, Li et al. 1997). The trout cTnC at 7°C closely resembles mammalian cTnC at 30°C, which suggests a common structure at their respective physiological temperatures (Gillis, Marshall et al. 2000).

The cardiac contractile element is less sensitive to Ca^{2+} at lower temperatures, an effect that is not observed in skeletal muscle (Harrison and Bers 1989, Harrison and Bers 1990). This desensitizing effect was rescued in mammalian cardiomyocytes by introducing four fish-TnC specific amino acid substitutions, Asn2, Ile28, Gln29, and Asp30 (NIQD) (Gillis, Moyes et al. 2003). The increased sensitivity was attributed to an allosteric effect on the ability of site II of cTnC to bind Ca^{2+} (Gillis, Marshall et al. 2000), that allows a lower cytosolic Ca^{2+} concentration to trigger cardiac contraction at lower temperatures. A structural explanation was elusive, as there were no obvious differences between the human cTnC structure and that with the NIQD substitutions

introduced (Zhang, Tibbits et al. 2013). Because these residues are in the N-helix and hydrophobic patch of cTnC, regions that interact with the other members of the cTn complex (Takeda, Yamashita et al. 2003), the NIQD substitutions may stabilize the Ca^{2+}-bound, open conformation of cTnC in the complex.

The fish contractile element adjusts to temperature change in part through the differential expression of a slow-skeletal TnC (ssTnC or TnC1b) variant (Sogah, Serluca et al. 2010, Genge, Davidson et al. 2013). The slow-skeletal paralog differs from the cardiac paralog (cTnC or TnC1a) at 18 out of 161 amino acid positions. Interestingly, the ssTnC paralog is missing one of the four NIQD residues, where asparagine 2 is replaced by aspartic acid, which is found at that position in mammals (Genge, Davidson et al. 2013). The ssTnC paralog in *D. rerio* is the result of a tandem gene duplication event. Although many redundant duplicate genes are lost, in some cases the ancestral gene function is divided between the duplicates. This process, referred to as subfunctionalization (Lynch and Katju 2004), results in the retention of functional paralogs in the genome (Force, Lynch et al. 1999).

The ability of ssTnC to rescue cardiac contraction in a cTnC knockout in *D. rerio* embryos indicates that the *D. rerio* TnC paralogs have some overlap in function (Sogah, Serluca et al. 2010). When *D. rerio* are acclimated to 18°C, cTnC is expressed preferentially in both chambers of the heart, whereas after 28°C acclimation, the ssTnC is upregulated and becomes the dominantly expressed form in the atrium. ssTnC expression in the ventricle is also increased after 28°C acclimation, but does not supersede cTnC expression (Genge, Davidson et al. 2013). The differential expression of TnC paralogs is consistent with a temperature-dependent functional difference.

In this study, we report the thermodynamic properties of the interaction between Ca^{2+} and *D. rerio* cTnC and that between Ca^{2+} and *D. rerio* ssTnC at 18°C and 28°C. The TnC-Ca^{2+} interaction was found to be endothermic and entropy driven, similar to the case for human cTnC (Skowronsky, Schroeter et al. 2013). The ssTnC-Ca^{2+} interaction, measured by isothermal titration calorimetry (ITC), is stronger at both temperatures, despite very limited structural deviation between the simulation-based structural models. Potential-of-mean-force (PMF) calculations, which do not sample the conformational change, yield similar ΔG values for the two paralogs at 28°C and a lower ΔG for ssTnC at 18°C. This discrepancy is resolved through the use of long (μs)-timescale simulations,

during which the cTnC protein more readily transitions from the closed to the open state, an unfavorable process that produces lower Ca^{2+} affinity as measured by ITC. We propose that the temperature-dependent change in myofilament Ca^{2+} sensitivity that is expected as a function of paralog selection is dictated by the favorability of the TnC conformational change, which transduces the Ca^{2+} binding signal to the myofilament, rather than the affinity of the regulatory domain of TnC for Ca^{2+}.

3.3. Materials and Methods

3.3.1. Homology modeling and equilibrium molecular dynamics simulations

The initial models for the TnC constructs were generated using the Swiss-model Workspace (Bordoli and Schwede 2012). These models used the NMR-derived Ca^{2+}-bound or Ca^{2+}-free N-terminal domain of the human cTnC structure (PDB:1AP4 or PDB:1SPY, respectively) as a template. Models were built for the N-terminal domain of the cardiac and slow-skeletal paralogs of TnC.

The resulting models were equilibrated with GROMACS 4.6.5 (Pronk, Pall et al. 2013), using the AMBER99-sb-ILDN (Lindorff-Larsen, Piana et al. 2010) force field. The simulation system was defined as a periodic “cubic” box and was prepared as described in Table S3-1 in the Supporting Material using the TIP3P water model (Jorgensen, Chandrasekhar et al. 1983). This was followed by steepest-descent energy minimization to a tolerance of 10 $kJ*mol^{-1}*nm^{-1}$ and conjugate gradient energy minimization for 10,000 steps. The minimized system was restrained with 1000 $kJ*mol^{-1}*nm^{-1}$ absolute position restraints on all of the nonsolvent atoms and equilibrated for 1 ns. The restrained simulations were held at 28°C or 18°C using V-rescale temperature coupling (Bussi, Donadio et al. 2007) and isotropic Berendsen pressure coupling (Berendsen, Postma et al. 1984) with a τ_T of 0.1 and τ_P of 1.0, respectively. Interactions were calculated using ME electrostatics (Cerutti, Duke et al. 2009) and the Verlet cut-off scheme (Páll and Hess 2013). Bond lengths were constrained using the LINCS algorithm (Hess, Bekker et al. 1997). Production simulations were done in five replicated 100 ns NPT simulations with no position restraints; other parameters were carried forward from the position-restrained simulations. Long-timescale simulations were identical, with the exception that the run

time was extended to 1 μs and snapshots were saved every 100 ps. Simulations of the open conformation of the TnC molecule were stabilized in the open conformation by the presence of the TnI_{SW} peptide, as described in Genge et al. (Genge, Stevens et al. 2016).

The final models were produced by clustering with the Daura algorithm (Daura, Gademann et al. 1999) over the backbone and C_β atoms of each structure across the five trajectory replicates of each paralog-temperature combination; the middle structure of each of the largest clusters from each mutant simulation was used for further analysis. Protein structure superimpositions were performed with VMD (Humphrey, Dalke et al. 1996), and structural quality assessments were carried out using RAMPAGE (Lovell, Davis et al. 2003), QMEAN (Benkert, Künzli et al. 2009), WHATCHECK (Hooft, Vriend et al. 1996), and MOLPROBITY (Chen, Arendall et al. 2010). Quality statistics may be found in Tables S3-1 to S3-4. Interhelical angles were measured using interhlx (Yap, Ames et al. 2002) over each replicated simulation. Similarly, the hydrophobic solvent-accessible surface areas (h-sasa) of the TnC molecules were calculated with g_sas over each simulation and averaged (Eisenhaber, Lijnzaad et al. 1995). The TnI_{SW} was excluded from the complex simulations for the h-sasa calculations of TnC in the open conformation. The number of hydrogen bonds in TnC was calculated with g_hbond, which uses a cutoff radius of 3.5 Å and a 30° angle to enumerate donor/acceptor pairs; these values were averaged over each simulation.

3.3.2. Free-energy calculations

The Ca^{2+}-bound TnC model was placed in a “cubic” box with dimensions 6 nm × 6 nm × 15 nm, solvated, and neutralized as in Table S3-1. This was followed by steepest-descent energy minimization to a tolerance of 10 $kJ*mol^{-1}*nm^{-1}$ and conjugate gradient energy minimization for 1000 steps. The minimized system was restrained with 1000 $kJ*mol^{-1}*nm^{-1}$ absolute position restraints on all of the nonsolvent atoms and equilibrated for 1 ns.

The initial conformations for umbrella sampling were generated as follows: protein *α*-helical C_α atoms were restrained in three dimensions with a potential with a force constant of 1000 $kJ*mol^{-1}*nm^{-1}$, and the site II Ca^{2+} were restrained only in the y and z dimensions to permit the movement of the ion. A constraint pulling force was

applied in the x dimension at 0.001 nm*ps^{-1}. Windows for umbrella sampling were extracted from the resulting trajectory at distance intervals of 0.5 Å between 0 and 1 nm, every 1 Å between 1 nm and 2 nm, and every 2 Å between 2 nm and 5 nm.

3.3.3. Umbrella sampling and the weighted-histogram analysis method

Umbrella simulations were run as above, with no restraining potentials aside from the umbrella potential between the Ca^{2+} ion and the center of mass of the α-carbons of the TnC molecule. These simulations used the same parameters as the pull simulations, with the pull rate set to 0, and were run for 30 ns. Analysis was performed using g_wham (Hub, de Groot et al. 2010) and the first 5 ns of each sampling window simulation were discarded; errors were estimated with 10,000 bootstraps of the weighted-histogram analysis method of calculation.

3.3.4. Protein expression and purification

Synthetic codon-optimized genes (GeneArt, Regensberg, Germany) encoding full-length *D. rerio* cTnC (gi 28822163) and ssTnC (gi 50344824) were cloned into the pET-21a(+) expression vector (Novagen, Madison, WI), and the codon corresponding to residue 90 was replaced with a stop codon using the Phusion site-directed mutagenesis protocol (Thermo Scientific, Waltham, MA) to generate N-TnC constructs. The resulting constructs were verified by DNA sequencing and transformed into the *Escherichia coli* BL21(DE3) expression host strain.

Overnight cultures were diluted 20-fold into lysogeny broth and incubated at 37°C with shaking at 250 rpm. Cultures were induced at OD_{600} = 0.8 with a final concentration of 1 mM isopropyl *β*-D-1-thiogalactopyranoside followed by 3 h of growth. Cells were harvested by centrifugation, resuspended in 20 mL of 50 mM Tris-HCl pH 8.0, 5 mM EDTA, 1 mM phenylmethylsulfonyl fluoride, and one “c0mplete” protease Inhibitor tablet (Roche, Basel, Switzerland). The cells were lysed by sonication on ice at 80% amplitude using ten 30 s pulses at 30 s intervals. Lysate was clarified by centrifugation at 30,000 × *g* for 30 min and the supernatant was applied to a fast-flow diethylaminoethyl cellulose column (GE Healthcare, Little Chalfont, UK) equilibrated with 50 mM Tris-HCl, pH 8.0, 5 mM EDTA, and 1 mM dithiothreitol and eluted with a 180 mL gradient between

the equilibration buffer and the high-salt buffer comprised of equilibration buffer and 0.55 M NaCl. Fractions containing the TnC protein were pooled and concentrated to 5 mL using an Amicon centrifugal concentrator with a MWCO of 3,000 Da (Millipore, Billerica, MA). The concentrated protein was applied to a HiPrep 26/60 Sephacryl S-100 column (GE Healthcare) equilibrated with 50 mM Tris-HCl pH 8.0, 100 mM NaCl, and 1 mM dithiothreitol. Fractions containing the TnC protein were pooled, concentrated, and stored at −80°C.

3.3.5. Melting-point determination

Protein solutions in the apo state were dialyzed four times against 2 L of MT buffer (150 mM KCl, 10 mM HEPES, pH 7.5, 3 mM $MgCl_2$, and 2 mM EGTA). Ca^{2+}-saturated TnC was dialyzed and diluted similarly with MT buffer supplemented with 3 mM of $CaCl_2$.

Each melting-temperature replicate contained 3 mg*mL^{-1} of TnC and 2.5 µL of 100× diluted sypro orange. Temperatures were increased from 4°C to 95°C at 5 s intervals on a CFX96 Touch Real-Time PCR System (BioRad, Hercules, CA). The melting temperature of the protein was determined at the minimum of the first derivative curve, which represents the midpoint of the unfolding transition.

3.3.6. Isothermal titration calorimetry

Protein solutions were dialyzed three times against 2 L of ITC buffer (50 mM HEPES, pH 7.2, and 150 mM KCl) and diluted to a final concentration of 200 µM. Buffers were supplemented with 15 mM, 15 mM, and 2 mM, respectively, of *β*-mercaptoethanol. Initial buffer contained 2 mM EDTA to generate TnC in the apo-state with two subsequent exchanges to remove the EDTA. Concentration was determined using an extinction coefficient of 1490 M^{-1}*cm^{-1} and a molecular mass of 10.1 kDa. The Ca^{2+} solution was prepared in the dialysis buffer from the final exchange to a final Ca^{2+} concentration of 4 mM. Ca^{2+} was titrated into the protein solution in a series of 19 injections of 2 µL (the first being a dummy injection of 0.4 µL), 2 min apart, with a stirring speed of 1000 rpm. These experiments were repeated at 18°C and 28°C. The heat of dilution of Ca^{2+} into buffer was estimated by averaging three data points after the protein was saturated with Ca^{2+}. The average of these three points was then

subtracted from the Ca^{2+}-protein titration curve. Data were analyzed with Origin 8.0 (OriginLab, Northampton, MA).

3.4. Results

3.4.1. Homology models

After 100 ns of simulation, each of the modeled systems had diverged from the starting coordinates (**Figures S3-1 to S3-4**). The middle structure of the largest cluster for each paralog at each temperature was selected as representative for further analysis. The quality indicators for the representative structures used in the PMF calculations may be found in Tables S3-2 to S3-5.

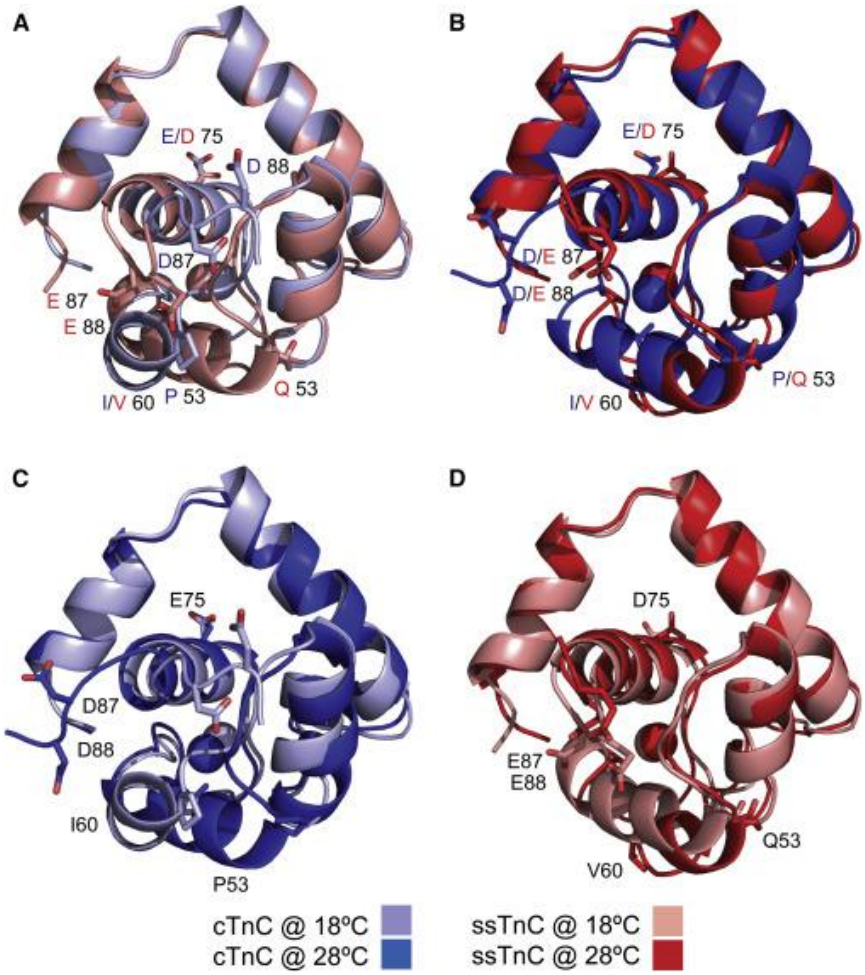

Figure 3-1 Superimposed Structures of the Equilibriated Representative cTnC and ssTnC

After Daura clustering using backbone and β-carbon atoms during 100 ns equilibration trajectories, residues that differ between paralogs are labeled. (A) cTnC (light blue) and ssTnC (salmon) at 18°C. (B) cTnC (blue) and ssTnC (red) at 28°C. (C) cTnC at 18°C (light blue) and 28°C (blue). (D) ssTnC at 18°C (salmon) and 28°C (red). The differences between these structures are minimal, but they are most pronounced in the orientation of helix C relative to the remainder of the protein.

The structures of the equilibrated homology models are very similar to each other, except in their length and orientation of helix C (**Figure 3-1**). Helix C immediately follows the Ca^{2+}-binding site II, and changes in this helix may affect the Ca^{2+} interaction. Helix C contains two sequence substitutions between the TnC paralogs: proline 54 in cTnC is replaced with a glutamine in ssTnC, and isoleucine 61 in cTnC is replaced with a valine in ssTnC. The secondary structure is variable between paralog temperature combinations, with helical lengths that vary by up to four residues in the case of helix C (**Figure 3-2**). The difference in orientation of helix C was the greatest between the paralog-temperature combinations. In cTnC at 18°C, helix C is nearly antiparallel to helix

D at 153°, whereas in the other representative structures, helices C and D are at angles of 128°, 123°, and 112° for ssTnC at 28°C, ssTnC at 18°C, and cTnC at 28°C, respectively.

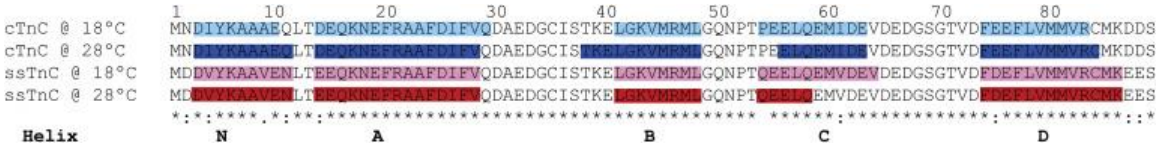

Figure 3-2 Sequence alignment of cTnC and ssTnC
Highlighting is used to visualize the changes in secondary structure after equilibration at each temperature and energy minimization. The most salient change is in helix C, and it is likely due to the temperature-dependent effect of the P55Q, I61V, and E75D substitutions on the stability of helix C and its interaction with helix D.

AB interhelical angles were monitored over the course of each simulation. None of the structures reached the open state, defined by an AB interhelical angle below 90° (**Figure 3-3**). During the five replicated 1 μs simulations, the TnC structures at 28°C each had several frames in an intermediate state: seven frames were below 105° in the Ca^{2+}-free simulations, whereas 359 frames were below 105° in the Ca^{2+}-bound simulations (**Figures 3-4 and 3-5**). There was a single frame that contained a structure of the ssTnC molecule with an AB interhelical angle below 105° (**Table S3-6**).

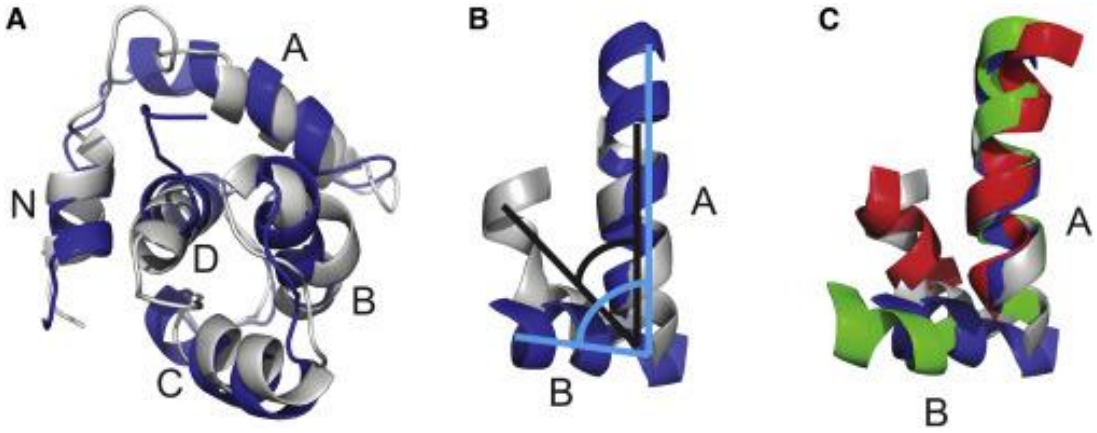

Figure 3-3 Interhelical angle determination
(A) Superimposition of snapshots from the 1 ms simulation of cTnC at 28°C, with helices labeled N, A, B, C, and D. The most open conformation from this simulation is shown in blue and the most closed conformation is shown in white. (B) Angles are drawn onto the superimposed and isolated A and B helices. (C) The helices are superimposed with equivalent structures from the NMR-derived human cTnC structures in the Ca^{2+}-free, closed form (PDB:1SPY), shown in red, and in the open conformation in complex with the TnI switch peptide (PDB:1MXL), shown in green.

When the h-sasa of each structure at each temperature was calculated, there were only slight differences as a function of temperature or sequence substitution; however when the h-sasa were calculated for either the cardiac or slow-skeletal TnC molecule isolated from the TnC/TnI complex and therefore in the open conformation, the average h-sasa of cTnC at 28°C increased by 4.9 nm^2, whereas the average h-sasa of ssTnC at 28°C increased by 4.1 nm^2 as a result of the closed-to-open transition. At 18°C, the closed-to-open transition increased the h-sasa by 4.2 nm^2 and 4.6 nm^2 for cTnC and ssTnC, respectively. This is in contrast to the effect of Ca^{2+} binding, which had little effect on the average h-sasa of either paralog at each temperature (**Table 3-1**).

Table 3-1 Average Hydrophobic Solvent-Accessible Surface Area over the Final 50 ns of Five Replicated 100 ns Simulations

	18°C (Ca^{2+} -Bound)	28°C (Ca^{2+} -Bound)	18°C (Ca^{2+} -free)	28°C (Ca^{2+} -free)	18°C (Open)	28°C (Open)
cTnC	22.3 ± 0.4	21.8 ± 0.5	22.6 ± 0.6	22.4 ± 0.7	26.5 ± 0.9	26.8 ± 0.5
ssTnC	21.0 ± 0.5	20.8 ± 0.7	20.8 ± 0.8	21.5 ± 0.5	25.6 ± 0.9	25.0 ± 0.8

Surface area (nm^2).

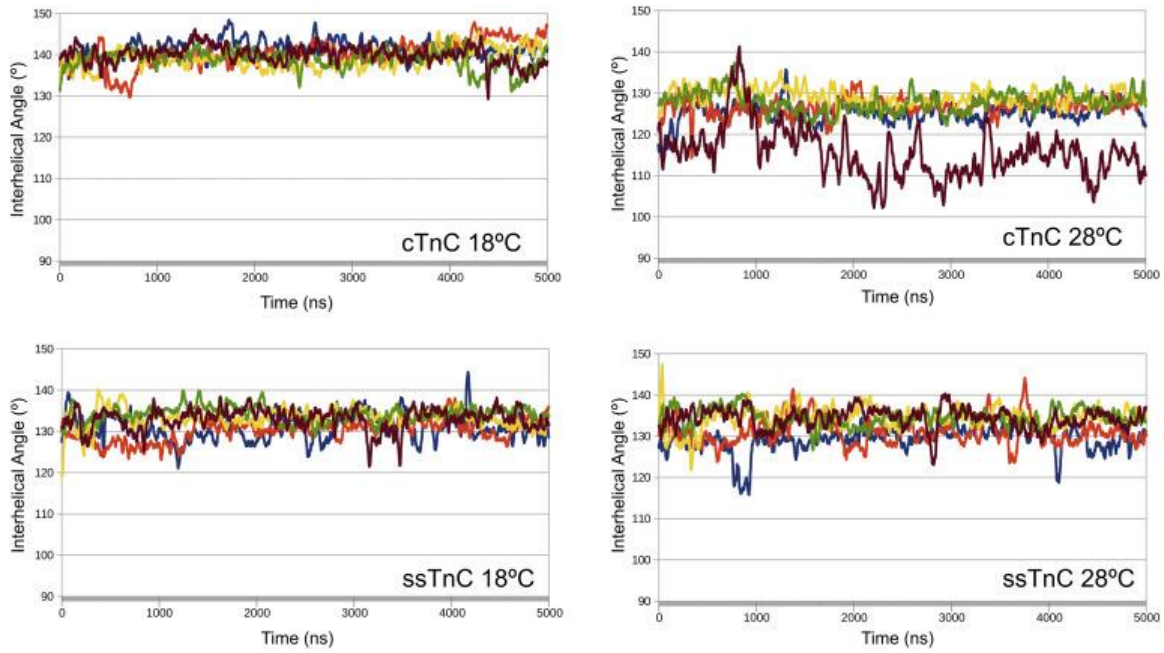

Figure 3-4 The AB interhelical angle over time for 1 ms simulations of TnC-Ca^{2+} at each temperature, plotted as a 25 ns rolling average.

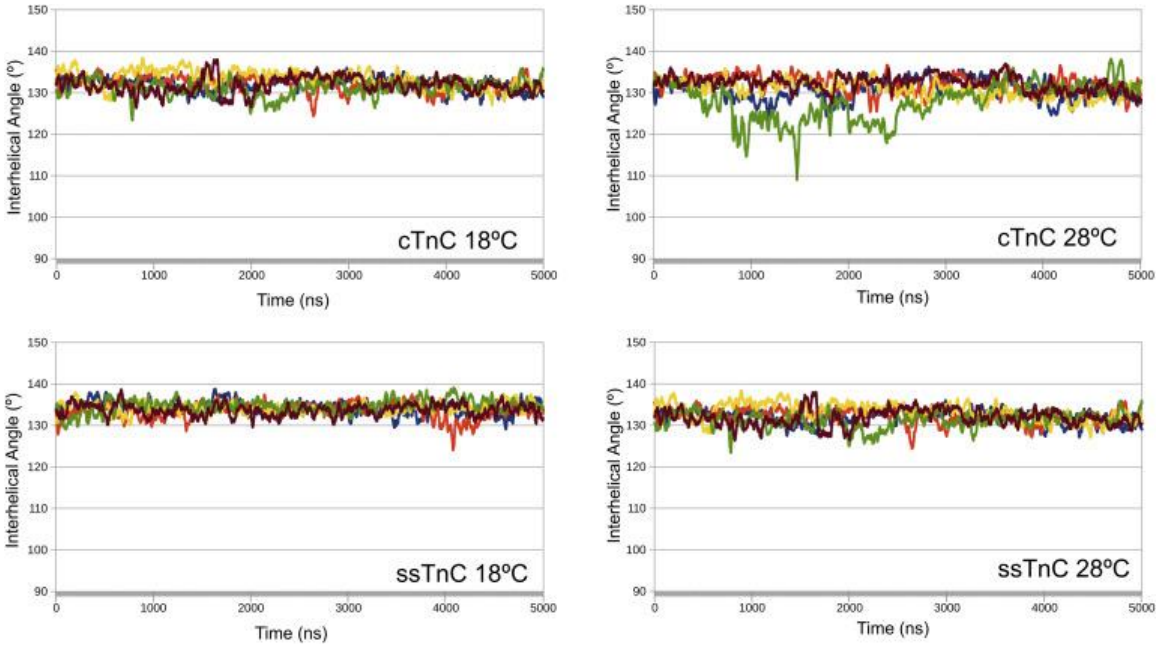

Figure 3-5 The AB interhelical angle over time for 1 ms apo-TnC simulations at each temperature, plotted as a 25 ns rolling average.

The flexibility of the paralog-temperature combinations is similar (**Figure 3-6**), as represented by the root mean-square fluctuation (RMSF) of each Cα atom sampled over the final 10 ns of each of the simulations and averaged over five replicated simulations. The numbers of hydrogen bonds are identical for the Ca^{2+}-free TnC molecules but are increased by ~1 hydrogen bond in each paralog-temperature combination in the Ca^{2+}-bound state (**Table 3-2**).

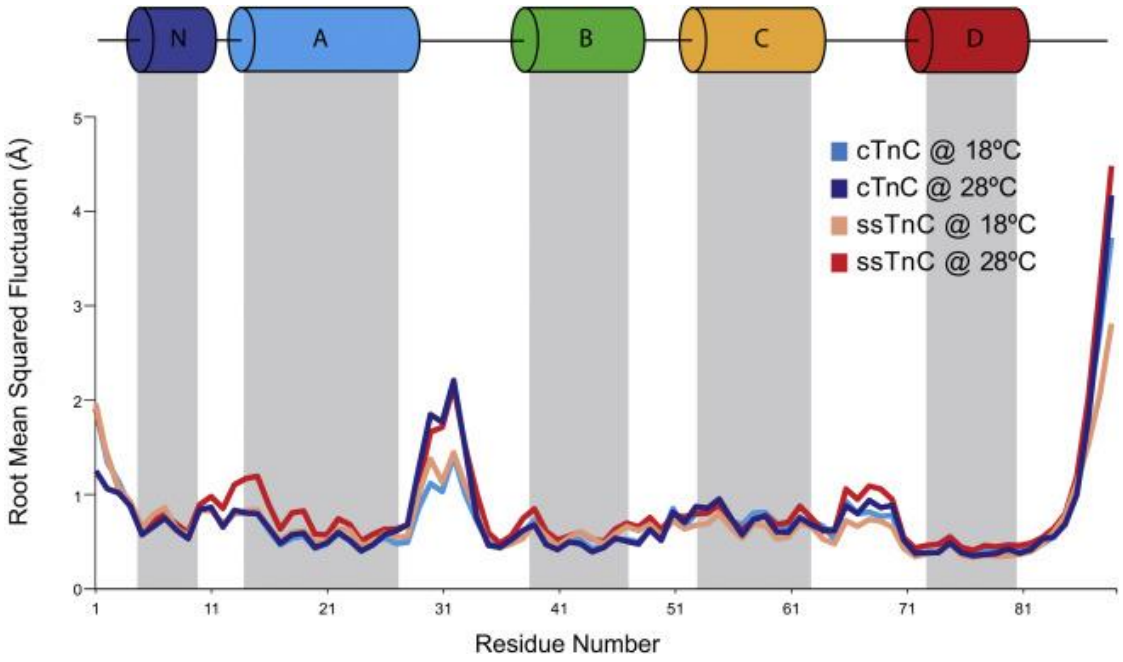

Figure 3-6 Average RMSFs per residue
Residues (n - 5) are plotted for the final 50 ns of each 100 ns simulations for the paralog-temperature combinations. The protein is most flexible at the termini and EF-hand loops. There is limited variability in RMSFs between paralog-temperature combinations, which suggests that the sequence differences do not greatly influence the protein flexibility. There is a slight effect of temperature on flexibility in the loop regions between helices A and B, as well as in the loop between helices C and D.

The coordination distances for the Ca^{2+} ions were measured for each of the side-chain ligand atoms, as well as any nearby potential substitutes (**Figure 3-7**). There was very little difference between paralog-temperature combinations, particularly in the distances between ligand atoms that are involved in coordination of the Ca^{2+} ion.

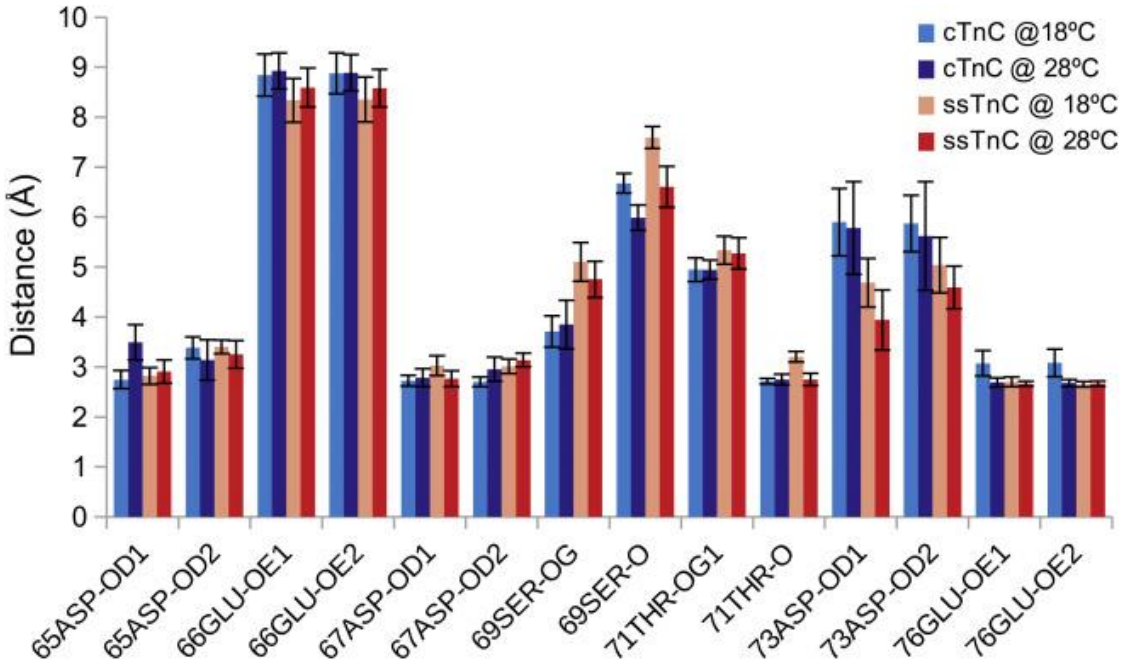

Figure 3-7 Ca^{2+} coordination distances for each paralog-temperature combination.

Residues that may offer substitute ligands are also included. The distances are similar for the two paralogs at both temperatures. Ser69-OG is slightly closer to the Ca^{2+} ion in the cTnC simulations, whereas Asp73-OD1 is slightly closer to the Ca^{2+} ion in the ssTnC simulations.

3.4.2. Free-energy calculations

The change in free energy for each of the paralog temperature combinations was determined using PMF calculations (**Figure 3-8**). The PMF profile is plotted in **Figure 3-9**. The free-energy differences indicate little variance between the paralogs at 28°C (-55.5 ± 4.1 kJ*mol^{-1} and -58.0 ± 2.7 kJ*mol^{-1} for cTnC and ssTnC, respectively), whereas at 18°C, cTnC has a higher ΔG of Ca^{2+} interaction than ssTnC (-51.4 ± 3.6 kJ*mol^{-1} vs. -45.5 ± 3.0 kJ*mol^{-1}).

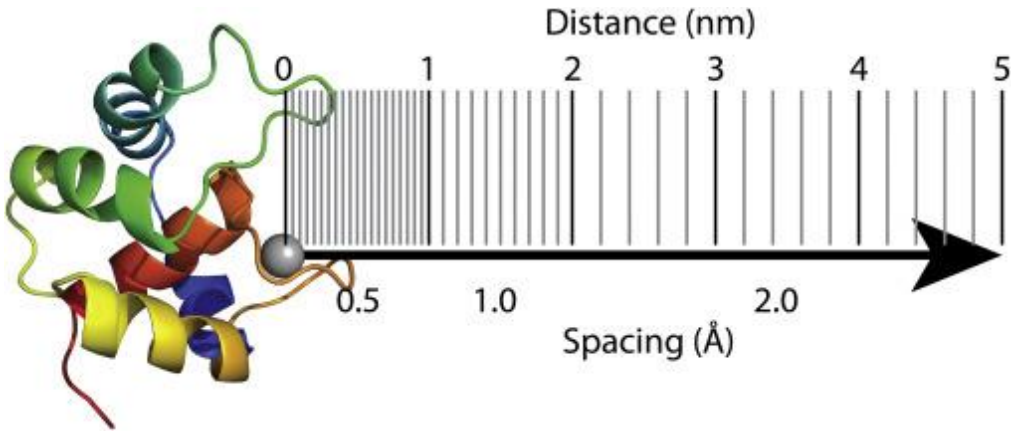

Figure 3-8 PMF reaction coordinate.
The Ca^{2+} ion is removed from the site II binding loop along the x-axis. Vertical lines indicate the frequency of PMF sampling windows over the reaction coordinate. Sampling windows were arranged at 0.5 Å below 1.0 nm distance, 1 Å between 1.0 and 2.0 nm, and 2 Å between 2.0 and 5.0 nm.

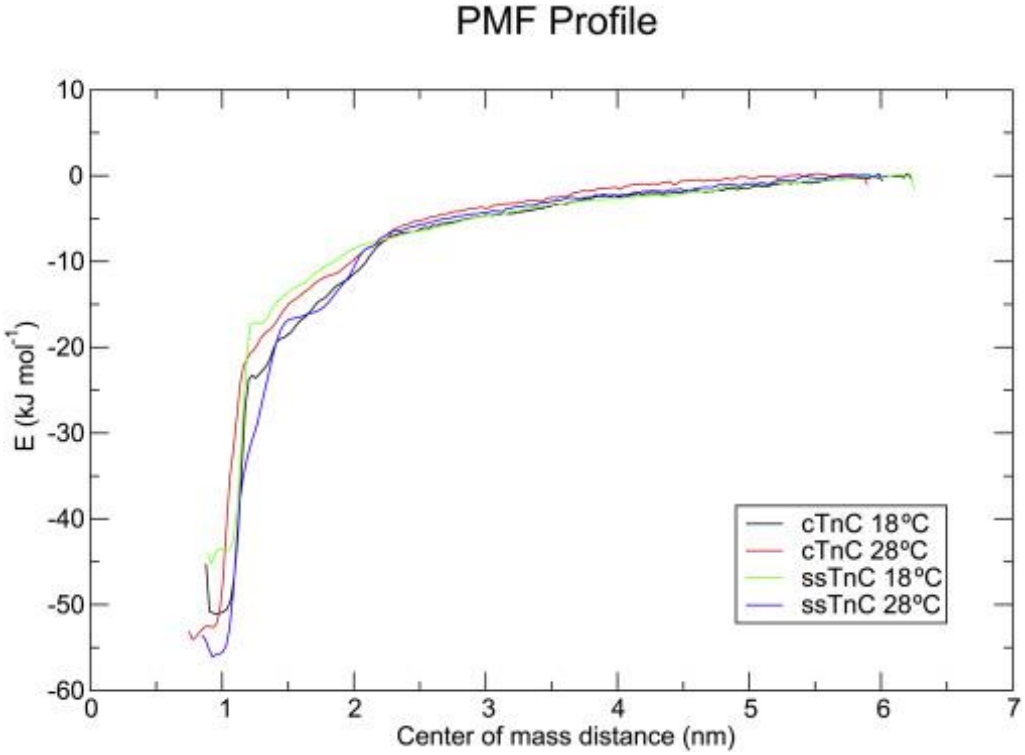

Figure 3-9 WHAM-derived umbrella potentials for each temperature-paralog combination.
The plots for the two paralogs appear to overlap at each temperature; however, the values at low center-of-mass distance reach minima at different points. At 28°C, the ΔG values of Ca^{2+} interaction for cTnC and ssTnC were -55.5 ± 4.1 kJ*mol^{-1} and -58.0 ± 2.7 kJ*mol^{-1}, respectively. At 18°C, the ΔG of Ca^{2+} interaction was -51.4 ± 3.6 kJ*mol^{-1} for cTnC and -45.5 ± 3.0 kJ*mol^{-1} for ssTnC.

3.4.3. Melting-point determination

The melting points (Tms) of the Apo-cTnC and Apo-ssTnC were 70.1°C and 65.9°C, respectively. The Tms of the Ca^{2+}-bound forms of the proteins were ~15°C higher in both cases at 84.9°C and 82.3°C for cTnC and ssTnC, respectively.

3.4.4. ITC

The interactions between TnC and Ca^{2+} were endothermic; in each case, the stoichiometric ratio of Ca^{2+} binding was ~1, indicating that the regulatory site II was exclusively titrated during these experiments. Representative isotherms are available in **Figure S3-5**. The change in entropy (ΔS) was higher for cTnC at 28°C than at 18°C, and both of these values were greater than the ΔS values for ssTnC, which did not differ significantly with temperature. The change in enthalpy (ΔH) values were greatest for the cTnC paralogs: Ca^{2+} binding to cTnC at 28°C yielded a greater ΔH in response to increased temperature, whereas the ΔH values reported for ssTnC did not differ significantly with temperature. The ΔG values were most favorable for ssTnC at 28°C, followed by ssTnC at 18°C and cTnC at 28°C, which did not differ significantly; the ΔG value for cTnC at 18°C was the least favorable.

The thermodynamic parameters are listed in **Table 3-3**. The dissociation constant (K_d) value was 2.4 μM higher at 18°C than at 28°C for cTnC, whereas the K_d value for ssTnC was 1.3 μM higher at 18°C than at 28°C (**Figure 3-10**).

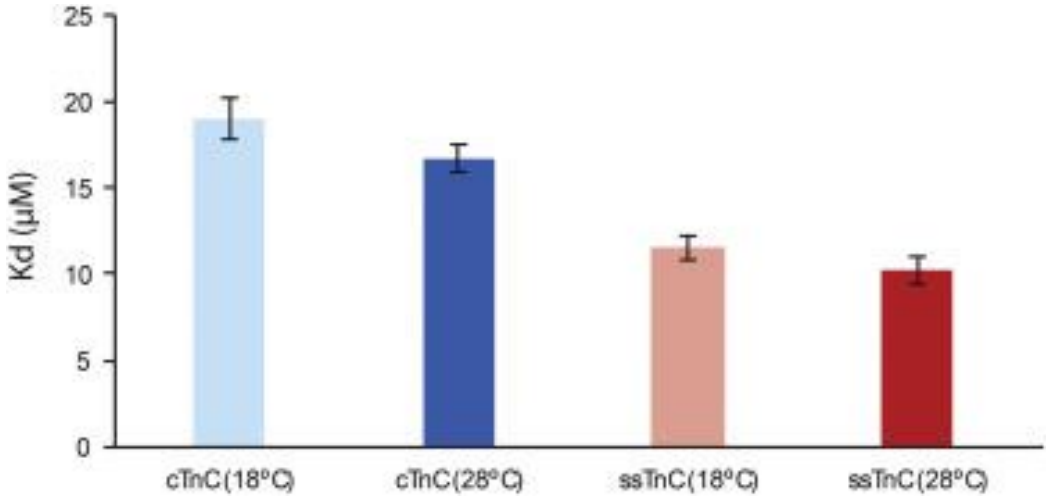

Figure 3-10 Plot of the mean K_d values
Mean is given ± SE. cTnC has a higher K_d than ssTnC at each temperature, and at each temperature, the K_d values for each paralog are comparable, though higher at 18°C than at 28°C for each paralog.

3.5. Discussion

Examination of the effect of sequence substitutions between TnC paralogs on Ca^{2+} interaction has yielded mechanistic insight into the function of TnC. When compared with wild-type human cTnC, the introduction of the fish-specific NIQD molecular phenotype to the human cTnC increases the Ca^{2+} sensitivity of myofilaments (Gillis, Moyes et al. 2003, Gillis, Liang et al. 2005). The explanation for the increase in sensitivity is that these sequence substitutions allosterically influence the affinity of site II for Ca^{2+}. MD-based PMF analysis has shown that the Ca^{2+}-binding properties are similar for the two paralogs at both temperatures, with the exception of ssTnC at 18°C, which has a lower ΔG (**Figure 3-9**). The absolute ΔG values from MD simulations are overestimated due to the parameterization of Ca^{2+} in the MD force field and the use of nonpolarizable water; however, the reported values are reasonable as a relative measure (Li, Ngo et al. 2015). ITC measurements indicate that ssTnC has higher affinity for Ca^{2+} at both temperatures, but cTnC is more sensitive to temperature (**Figure 3-10**).

Increased stability of the protein can be conferred by a stronger hydrophobic core or by antiparallel stacking of helices to mutually stabilize helical dipoles (Gifford, Walsh et al. 2007). The melting temperatures of cTnC and ssTnC indicate that the relative stability of the apo and Ca^{2+}-bound forms are similar, since the melting temperature for each was increased by 15°C as a function of Ca^{2+} interaction. Paradoxically, cTnC,

which is dominantly expressed at lower temperatures, has a higher melting point than ssTnC despite RMSF values that show that flexibilities of the paralogs are approximately equal (**Figure 3-6**). The MD simulations predict that there is one additional hydrogen bond on average in the Ca^{2+}-bound states compared to the Ca^{2+}-free state, but the total numbers of H-bonds were similar between paralogs at each temperature (**Table 3-2**). The h-sasa upon Ca^{2+} binding decreased for each paralog-temperature combination, with the exception of ssTnC at 18°C, which suggests that any stabilizing effect of Ca^{2+} binding was less pronounced in that condition.

Table 3-2 Average Number of Hydrogen Bonds in Each Structure over the Final 100 ns of Five Replicated 1 ms Simulations for Ca^{2+}- Bound and Ca^{2+}-free Models of cTnC and ssTnC

	18°C (Ca^{2+} -Bound)	28°C (Ca^{2+} -Bound)	18°C (Ca^{2+} -free)	28°C (Ca^{2+} -free)
cTnC	62.0 ± 1.6	61.0 ± 1.3	60.9 ± 0.6	60.6 ± 1.0
ssTnC	61.8 ± 0.8	61.3 ± 1.6	60.9 ± 1.4	60.6 ± 1.2

The process of Ca^{2+} binding to Ca^{2+}-sensing EF-hand proteins is a balance between conformational strain and conformational change (Gifford, Walsh et al. 2007). The strain induced by Ca^{2+} binding is released by the unfavorable exposure of the hydrophobic patch (Gifford, Walsh et al. 2007). A more stable closed conformation relative to the open conformation will increase the energetic cost of the closed-open conformational change and decrease the affinity for Ca^{2+}. Changes in secondary structure have been noted in response to Ca^{2+} binding of other TnC proteins through the use of CD spectroscopy; greater helical content in the Ca^{2+}-bound form conferred greater stability and increased the favorability of the Ca^{2+} interaction (Pinto, Parvatiyar et al. 2009, Parvatiyar, Landstrom et al. 2012). The structural differences between the temperature-paralog combinations are primarily found in the length and orientation of helix C, which is adjacent to site II and alters the C/D helical interface (**Figures 3-1 and 3-2**). This helix is shorter in the representative structure of ssTnC at 28°C than in the others, which suggests that the stability of this helix may be compromised at 28°C while under the conformational strain induced by Ca^{2+} binding. Helices C and D contain three sequence substitutions between cTnC and ssTnC. Residues 54, 61, and 75 are proline, isoleucine, and glutamic acid, respectively, in cTnC, which are replaced by glutamine, valine, and aspartic acid, respectively, in ssTnC. The proline-to-glutamine

substitution in particular may increase affinity by destabilizing the closed conformation in ssTnC, and relieve the conformational strain through shortening of helix C. In addition, there is evidence that the I61Q substitution in human cTnC can affect the stability of the helical packing at the B/C helical interface (Wang, Robertson et al. 2012).

Sequence substitutions that stabilize the open conformation of N-cTnC produce an increase in Ca^{2+} sensitivity without altered coordination of Ca^{2+} by site II. These substitutions increase the favorability of the conformational change through the release of the Ca^{2+}-induced conformational strain on the tertiary structure of the protein, and they minimize the energetic penalty of the conformational change (Tikunova, Rall et al. 2002, Gifford, Walsh et al. 2007, Li, Stevens et al. 2013). The TnI switch peptide (TnI_{SW}) binds to the hydrophobic cleft and stabilizes the open conformation of TnC while simultaneously occluding the hydrophobic residues (Li, Spyracopoulos et al. 1999). In the absence of TnI_{SW}, TnC opening and exposure of the hydrophobic patch results in the unfavorable formation of a clathrate water shell. In the cTnC-TnI_{SW} system, this shell is replaced by hydrophobic interactions between N-cTnC and TnI_{SW} and by interactions between water and the hydrophilic side chains of the solvent-exposed portion of the TnI_{SW}. Many fluorescence-based measurements have been used to measure TnC Ca^{2+} affinity in the presence of the other members of the Tn complex and thin filament (Li, Stevens et al. 2013). However, the use of fluorophores such as IAANS (Dong, Wang et al. 1997, Hazard, Kohout et al. 1998) or the fluorogenic F27W mutation (Gillis, Blumenschein et al. 2003) makes it possible to monitor Ca^{2+} binding by responding to the change in hydrophobicity precipitated by the conformational change, and different results are achieved with the addition of other Tn-complex and thin-filament proteins. The absence of the remainder of the Tn complex and its stabilizing effect on the open conformation of TnC thus constitutes a limitation to this work.

In a population of TnC molecules, Ca^{2+} binding leads to a shift in the equilibrium between the closed and open states, with the proportion shifting from 0% open in the apo-state to between 20% and 27% open in the Ca^{2+}-bound state (McKay, Saltibus et al. 2000, Cordina, Liew et al. 2013). The free-energy cost of this transition has been estimated, through the use of long timescale simulations, at 8 kcal*mol^{-1} (33.5 kJ*mol^{-1}) for Ca^{2+}-bound human wild-type cTnC (Lindert, Kekenes-Huskey et al. 2012), which is comparable to the energy of conformational changes in other proteins, such as

the ligand-binding domain of an ionotropic glutamate receptor (Lau and Roux 2007) and 38α kinase (Wang, Shao et al. 2014) at 29 kJ*mol^{-1} and 50 kJ*mol^{-1}, respectively. The conformational change can confound ITC measurements, as the energetics of the shift in equilibrium between the open and closed states cannot be decoupled experimentally from the Ca^{2+}-binding interaction.

The disparity between the Δ*G* values obtained from ITC and PMF calculations may be attributed to whether the conformational change is included in the measurement. Sequence modifications that affect the relative stability of the closed or open forms, including changes to the size or degree of hydrophobicity of the hydrophobic patch or the packing of the core of the TnC molecule, will influence the affinity of TnC for Ca^{2+}. MD-derived ΔG values report the affinity of site II as a function of structural differences due to sequence substitution and equilibration at each temperature, but they do not account for the thermodynamic consequences of the open-to-closed conformational change. ITC measurements of the equilibrium energy include the change in proportion of open and closed TnC molecules as a function of Ca^{2+} titration. The MD simulations presented here indicate that the ΔG of Ca^{2+} binding is similar for both paralogs at 28°C, and for cTnC at 18°C, whereas the ΔG of Ca^{2+} binding for ssTnC at 18°C is less favorable. The timescale of the PMF simulation is inadequate to sample the conformational change of the protein, and therefore, its energetic contribution cannot be included. The ΔG values collected by ITC are in the range −26.4 to −28.8 kJ*mol^{-1} (**Table 3-3**) and are similar to those reported for human cTnC, with comparable effects of temperature on binding. The free energy of the Ca^{2+}-human-cTnC measured at 10°C and 25°C had ΔG values of −26.6 and −30.5 kcal*mol^{-1}, respectively (Skowronsky, Schroeter et al. 2013). The *D. rerio* TnC paralogs are much less temperature sensitive than human cTnC, as demonstrated by a 0.3 kcal*mol^{-1} increase in the ΔG of cTnC for Ca^{2+} when temperature is increased from 18°C to 28°C, but this effect is not present in ssTnC due to lower values of ΔS. The lower ΔH values in ssTnC maintain Ca^{2+} binding at a similar ΔG, despite the reduced magnitude of ssTnC ΔS.

Table 3-3 Thermodynamic Parameters Derived from ITC for Each Paralog-Temperature Combination

	cTnC (18°C)	cTnC (28°C)	ssTnC (18°C)	ssTnC (28°C)
K_d (μM)	19.0 ± 1.2^{A}	16.7 ± 0.8^{B}	11.5 ± 0.7^{C}	10.2 ± 0.8^{D}
ΔS (J mol^{-1})	153.9 ± 2.1^{B}	158.6 ± 5.0^{A}	147.7 ± 2.9^{C}	148.1 ± 2.1^{C}
ΔH (kJ mol^{-1})	18.5 ± 0.5^{B}	20.2 ± 1.4^{A}	15.4 ± 0.8^{C}	15.9 ± 0.5^{C}
ΔG(kJ mol^{-1})	-26.4 ± 0.2^{A}	-27.6 ± 0.1^{B}	-27.5 ± 0.1^{B}	-28.8 ± 0.2^{C}

Analysis of variance was used to determine that a significant difference existed between mutant-temperature conditions for all four factors. Tukey's post-hoc test was carried out at the level of each factor and is indicated by superscript letters, where mutant-temperature conditions with unique letters are significantly different ($p < 0.05$), $n = 3$.

In most species, reduced temperature causes a decrease in cardiac myofilament Ca^{2+} sensitivity, an effect that is mediated by cTnC (Harrison and Bers 1990, Harrison and Bers 1990). In ectothermic species, cardiac function must be maintained through acute and seasonal temperature change. The differentially expressed ssTnC protein may play a role in this temperature tolerance. The *D. rerio* ssTnC has higher Ca^{2+} affinity at both temperatures, and its expression is increased in warm-acclimated *D. rerio* (Genge, Davidson et al. 2013). Our work suggests that the changes in TnC Ca^{2+} binding are dictated by three residue substitutions that alter the structure of helices C and D and together modify the energetic landscape of the TnC conformational change, which exposes the hydrophobic patch less frequently in ssTnC than in cTnC. Given that higher relative Ca^{2+} sensitivity is required for survival at lower temperatures (Churcott, Moyes et al. 1994), and that cTnC is dominantly expressed at low temperatures (Genge, Davidson et al. 2013), we expect that cTnC should have higher affinity for Ca^{2+}. That is not what was found in this study. Monitoring the AB interhelical angle over 1 μs simulations has shown that the Ca^{2+}-bound cTnC molecule is more amenable to conformational change than ssTnC. From this, we infer that cTnC has a less stable closed conformation than ssTnC, and is therefore less able to tolerate the conformational strain induced by Ca^{2+} binding. cTnC is more likely to transition between the closed and open states, which should create higher myofilament Ca^{2+} sensitivity while also accounting for the lower Ca^{2+} affinity we have observed by ITC. In this way, the molecular mechanism that produces higher affinity of the isolated ssTnC molecule for Ca^{2+} may contribute to the lower myofilament Ca^{2+} sensitivity needed for cardiac

function at high temperatures through less frequent exposure of the hydrophobic patch (Gillis, Moyes et al. 2003, Gillis, Liang et al. 2005, Genge, Davidson et al. 2013). Based on the ITC and MD-simulation evidence presented here, we propose that the temperature-dependent effect of TnC paralog substitution is influenced by differences in the favorability of the TnC conformational change, which transduces the Ca^{2+}-binding signal to the myofilament rather than being directly related to Ca^{2+} affinity of the TnC molecule.

3.6. Supplementary Appendix

Supplemental Table 3-1 Dimensions, Ions, and water molecules for each simulation system

		100 ns Ca^{2+}-bound	PMF	200 ns TnC+Ca^{2+}+TnI_{sw}	1 µs Ca^{2+}-free	1 µs Ca^{2+}-bound
cTnC 18°C	Box Dimensions (nm)	596 x 5.96 x 5.96	14.94 x 5.98 x 5.98	7.68 x 7.68 x 7.68	596 x 5.96 x 5.96	5.96 x 5.96 x 5.96
	K^+ Ions	14	14	11	15	14
	Cl^- Ions	1	1	1	0	1
	Ca^{2+} Ions	1	1	1	0	1
	Water Molecules	6612	17349	14555	6655	6612
cTnC 28°C	Box Dimensions (nm)	5.97 x 5.97 x 5.97	14.99 x 5.99 x 5.99	7.72 x 7.72 x 7.72	5.98 x 5.98 x 5.98	5.97 x 5.97 x 5.97
	K^+ Ions	14	13	11	15	14
	Cl^- Ions	1	0	1	0	1
	Ca^{2+} Ions	1	1	1	0	1
	Water Molecules	6612	17352	14555	6655	6612
ssTnC 18°C	Box Dimensions (nm)	5.95 x 5.95 x 5.95	14.95 x 5.98 x 5.98	7.68 x 7.68 x 7.68	5.97 x 5.97 x 5.97	5.96 x 5.96 x 5.96
	K^+ Ions	15	14	12	16	15
	Cl^- Ions	1	0	1	0	1
	Ca^{2+} Ions	1	1	1	0	1
	Water Molecules	6612	17343	14555	6657	6612
ssTnC 28°C	Box Dimensions (nm)	5.97 x 5.97 x 5.97	15.00 x 6.00 x 6.00	7.72 x 7.72 x 7.72	5.98 x 5.98 x 5.98	5.97 x 5.97 x 5.97
	K^+ Ions	15	14	12	16	15
	Cl^- Ions	1	0	1	0	1
	Ca^{2+} Ions	1	1	1	0	1
	Water Molecules	6612	17340	14555	6657	6612

Supplemental Table 3-2 Homology model quality indicators for representative structures from 100 ns TnC+Ca^{2+} simulations.

	cTnC (18°C)	cTnC (28°C)	ssTnC (18°C)	ssTnC (28°C)
RAMPAGE				
Favored	85 (98.84%)	83 (96.51%)	84 (97.67%)	86 (100.00%)
Allowed	1 (1.16%)	3 (3.49%)	2 (2.33%)	0 (0.00%)
Outlier	0 (0.00%)	0 (0.00%)	0 (0.00%)	0 (0.00%)
PROCHECK				
Bad Backbone Bonds	0.00%	0.00%	0.00%	0.00%
Bad Backbone Angles	4.60%	5.40%	4.10%	4.60%
Bad Contacts	0	0	0	0
Molprobity Score	1.62	1.69	1.54	1.70
QMEAN Score	0.627	0.669	0.767	0.69
Whatcheck Structure Z-Score				
1st Generation Packing	-1.836	-1.079	-1.237	-1.322
2n Generation Packing	-0.89	-1.245	-1.349	-1.079
χ_1/χ_2 Rotamer Normality	-1.45	-1.685	-2.472	-1.836
Backbone Conformation	0.672	0.93	1.177	0.662
Inside/Outside	0.955	0.966	0.926	0.999
Whatcheck RMS Z-Score				
Bond Lengths	0.644	0.635	0.642	0.662
Bond Angles	1.173	1.175	1.109	1.177
Omega Angle Restraints	1.471	1.235	1.422	1.369
Side Chain Planarity	1.886	1.732	1.488	1.789
Improper Dihedral Distribution	1.175	1.163	1.211	1.255

Supplemental Table 3-3 Homology model quality indicators for representative structures of TnC+Ca^{2+} in complex with TnI_{sw}.

	cTnC (18°C)	cTnC (28°C)	ssTnC (18°C)	ssTnC (28°C)
RAMPAGE				
Favored	99 (99.00%)	96 (96.00%)	94 (94.00%)	98 (98.00%)
Allowed	1 (1.00%)	4 (4.00%)	6 (6.00%)	2 (2.00%)
Outlier	0 (0.00%)	0 (0.00%)	0 (0.00%)	0 (0.00%)
PROCHECK				
Bad Backbone Bonds	0.00%	0.20%	0.00 %	0.00%
Bad Backbone Angles	4.30%	4.30%	5.00%	6.40%
Bad Contacts	0.00%	0.00%	0.00%	0.00%
Molprobity Score	1.22	1.59	1.93	2.25
QMEAN Score	0.563	0.512	0.515	0.463
Whatcheck Structure Z-Score				
1st Generation Packing	-1.027	-0.607	-1.175	-1.329
2n Generation Packing	0.614	0.548	-1.175	-0.09
χ_1/χ_2 Rotamer Normality	-1.924	1.122	-0.118	-2.428
Backbone Conformation	0.856	0.959	-1.724	1.234
Inside/Outside	0.988	0.959	0.928	1.077
Whatcheck RMS Z-Score				
Bond Lengths	0.505	0.600	0.485	0.547
Bond Angles	-1.027	1.157	1.216	1.223
Omega Angle Restraints	1.297	1.419	1.608	1.638
Side Chain Planarity	2.012	1.767	1.972	2.083
Improper Dihedral Distribution	1.305	1.19	1.447	1.281

Supplemental Table 3-4 Homology model quality indicators for representative structures of Ca^{2+}-free TnC from 1 μs simulations.

	cTnC (18°C)	cTnC (28°C)	ssTnC (18°C)	ssTnC (28°C)
RAMPAGE				
Favored	85 (98.80%)	83 (96.50%)	84 (97.70%)	84 (97.70%)
Allowed	1 (1.20%)	3 (3.50%)	2 (23.00%)	2 (23.00%)
Outlier	0 (0.00%)	0 (0.00%)	0 (0.00%)	0 (0.00%)
PROCHECK				
Bad Backbone Bonds	0.00%	0.00%	0.00%	0.00%
Bad Backbone Angles	5.60%	4.60%	4.30%	4.60%
Bad Contacts	0.00%	0.00%	0.00%	0.00%
Molprobity Score	0.83	0.82	0.57	1.37
QMEAN Score	0.842	0.605	0.794	0.72
Whatcheck Structure Z-Score				
1st Generation Packing	-0.916	-0.814	-0.855	-1.237
2n Generation Packing	-0.658	-0.518	-0.365	-1.074
χ_1/χ_2 Rotamer Normality	-2.497	-2.265	-1.093	-0.818
Backbone Conformation	1.771	1.23	1.23	0.934
Inside/Outside	0.961	0.984	0.982	0.955
Whatcheck RMS Z-Score				
Bond Lengths	0.513	0.553	0.551	0.501
Bond Angles	1.156	1.241	1.17	1.232
Omega Angle Restraints	1.428	1.377	1.512	1.38
Side Chain Planarity	1.524	1.69	1.774	1.496
Improper Dihedral Distribution	1.177	1.206	1.16	1.224

Supplemental Table 3-5 Homology model quality indicators for representative structures of TnC+Ca^{2+} from 1 µs simulations.

	cTnC (18°C)	cTnC (28°C)	ssTnC (18°C)	ssTnC (28°C)
RAMPAGE				
Favored	84 (97.70%)	85 (98.80%)	81 (94.20%)	85 (98.80%)
Allowed	2 (23.00%)	1 (1.20%)	5 (5.80%)	1 (1.20%)
Outlier	0 (0.00%)	0 (0.00%)	0 (0.00%)	0 (0.00%)
PROCHECK				
Bad Backbone Bonds	0.00%	0.00%	0.00%	0.00%
Bad Backbone Angles	7.10%	7.60%	6.10%	4.40%
Bad Contacts	0.00%	0.00%	0.00%	0.00%
Molprobity Score	1.2	0.57	1.08	0.81
QMEAN Score	0.664	0.584	0.718	0.684
Whatcheck Structure Z-Score				
1st Generation Packing	-0.875	-1.506	-2.138	-0.616
2n Generation Packing	-0.398	-1.155	-2.061	-0.606
χ_1/χ_2 Rotamer Normality	-3.038	-2.781	-3.188	-2.315
Backbone Conformation	1.06	1.013	0.356	0.948
Inside/Outside	1.019	0.985	0.993	0.95
Whatcheck RMS Z-Score				
Bond Lengths	0.488	0.525	0.542	0.495
Bond Angles	1.265	1.273	1.209	1.122
Omega Angle Restraints	1.73	1.554	1.57	1.786
Side Chain Planarity	2.332	1.775	1.686	1.797
Improper Dihedral Distribution	1.441	1.31	1.224	1.258

Supplemental Table 3-6 Cumulative interhelical angle frequencies combined over replicated long timescale simulations.

Paralog	cTnC	cTnC	cTnC	cTnC	ssTnC	ssTnC	ssTnC	ssTnC
Temperature	18ºC	28ºC	18ºC	28ºC	18ºC	28ºC	18ºC	28ºC
Ca^{2+}			+	+			+	+
<90	0	0	0	0	0	0	0	0
<95	0	0	0	10	0	0	0	0
<100	0	0	0	66	0	0	0	0
<105	0	7	0	283	0	0	0	1
<110	0	36	0	876	0	0	0	4
<115	2	121	0	1743	2	4	10	56
<120	25	447	1	2920	13	24	114	210
<125	205	2147	19	7330	109	540	1056	1189
<130	3123	9532	216	12210	2426	5932	5761	5745
>130	21666	15420	24744	5412	22456	18497	18142	18059

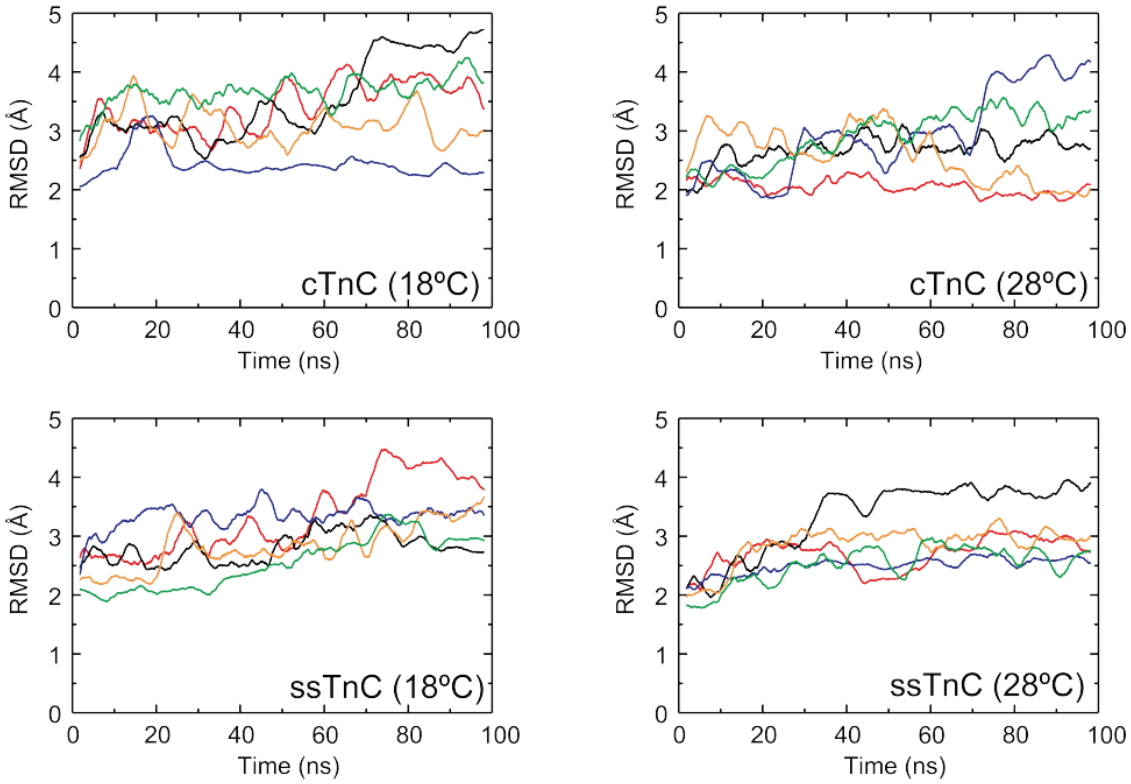

Supplemental Figure 3-1 RMSD as a function of time for 100 ns simulations of TnC+Ca^{2+} that preceded PMF calculations for each temperature paralog combination.

These indicate that each of the simulations has diverged substantially from the starting coordinates. Plots are a running average over 0.5% of the total number of data points.

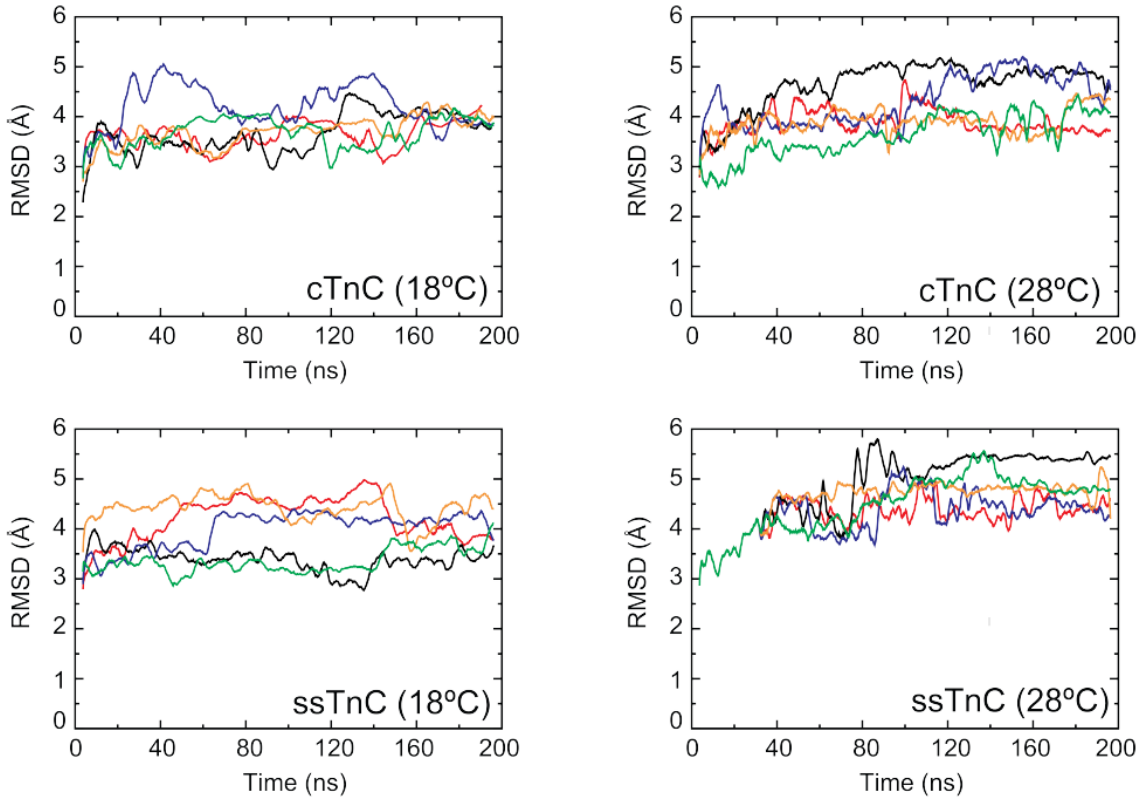

Supplemental Figure 3-2 RMSD as a function of time for 200 ns simulations of TnI_{sw}+TnC+Ca^{2+} for each temperature paralog combination.

These indicate that each of the simulations has diverged substantially from the starting coordinates. Plots are a running average over 0.5% of the total number of data points.

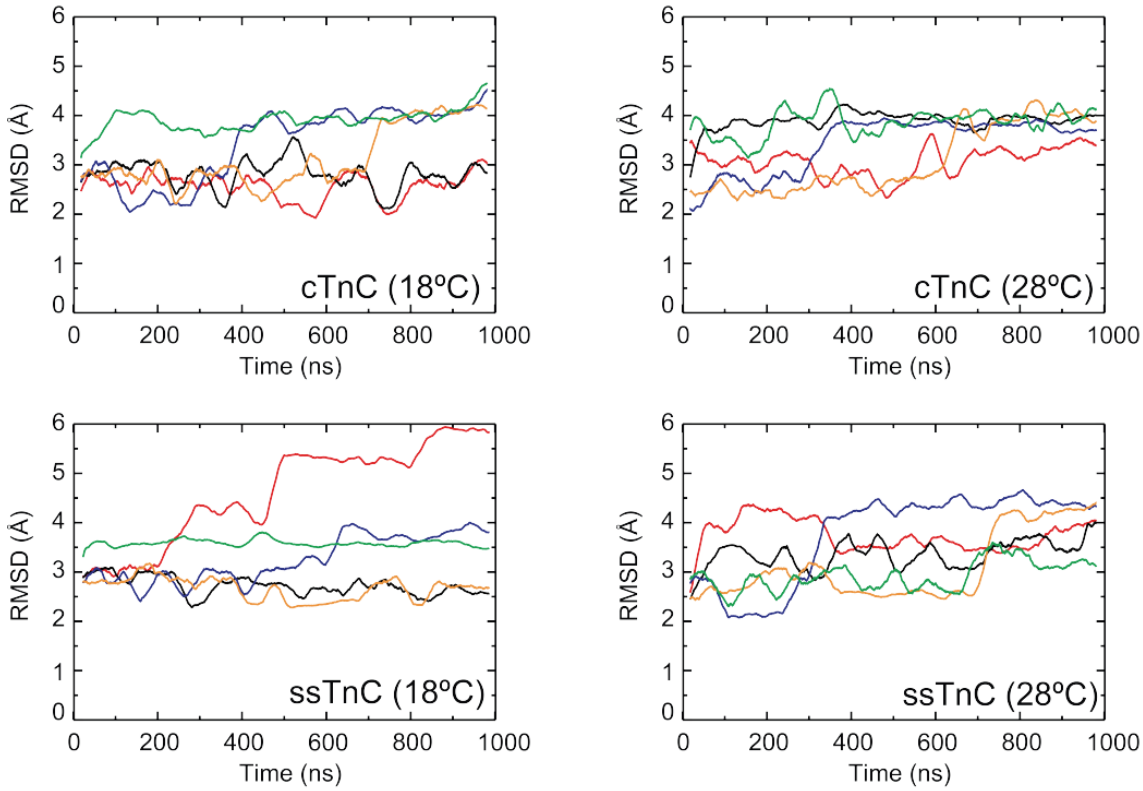

Supplemental Figure 3-3 RMSD as a function of time for 1 μs simulations of TnC+Ca^{2+} for each temperature paralog combination.

These indicate that each of the simulations has diverged substantially from the starting coordinates. Plots are a running average over 0.5% of the total number of data points.

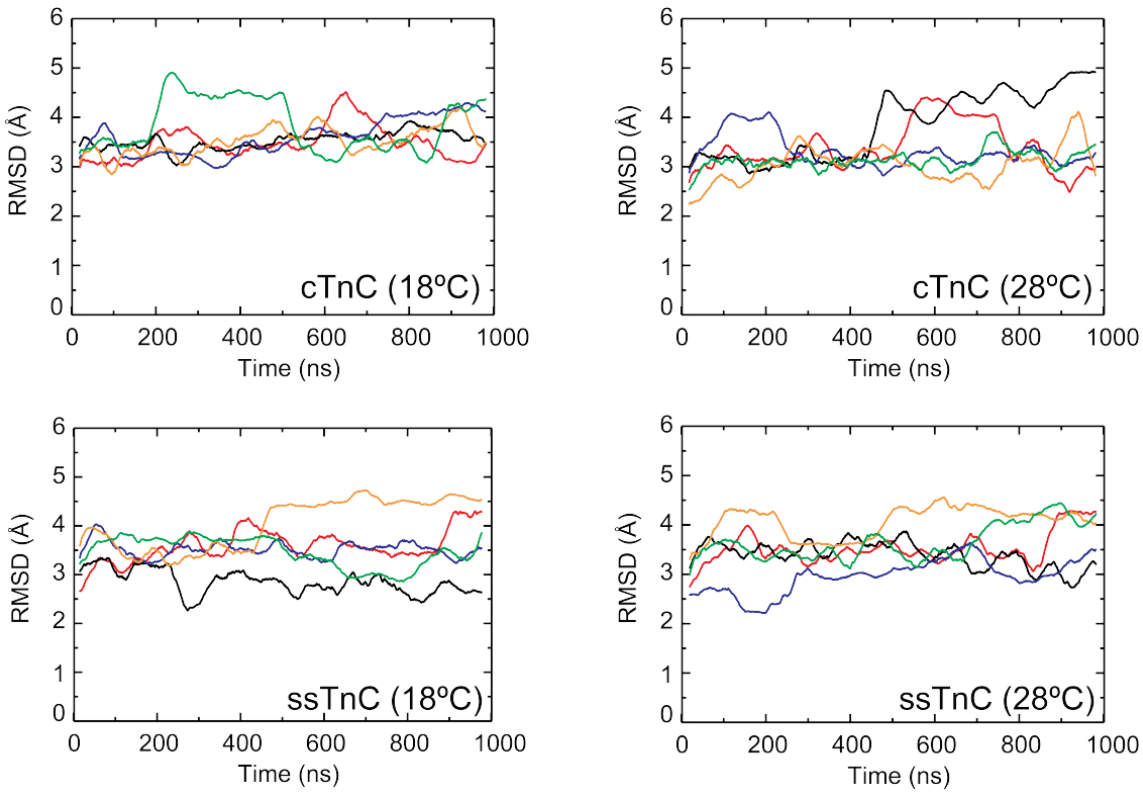

Supplemental Figure 3-4 RMSD as a function of time for 1 μs simulations of TnC in the absence of Ca^{2+} for each temperature paralog combination.
These indicate that each of the simulations has diverged substantially from the starting coordinates. Plots are a running average over 0.5% of the total number of data points.

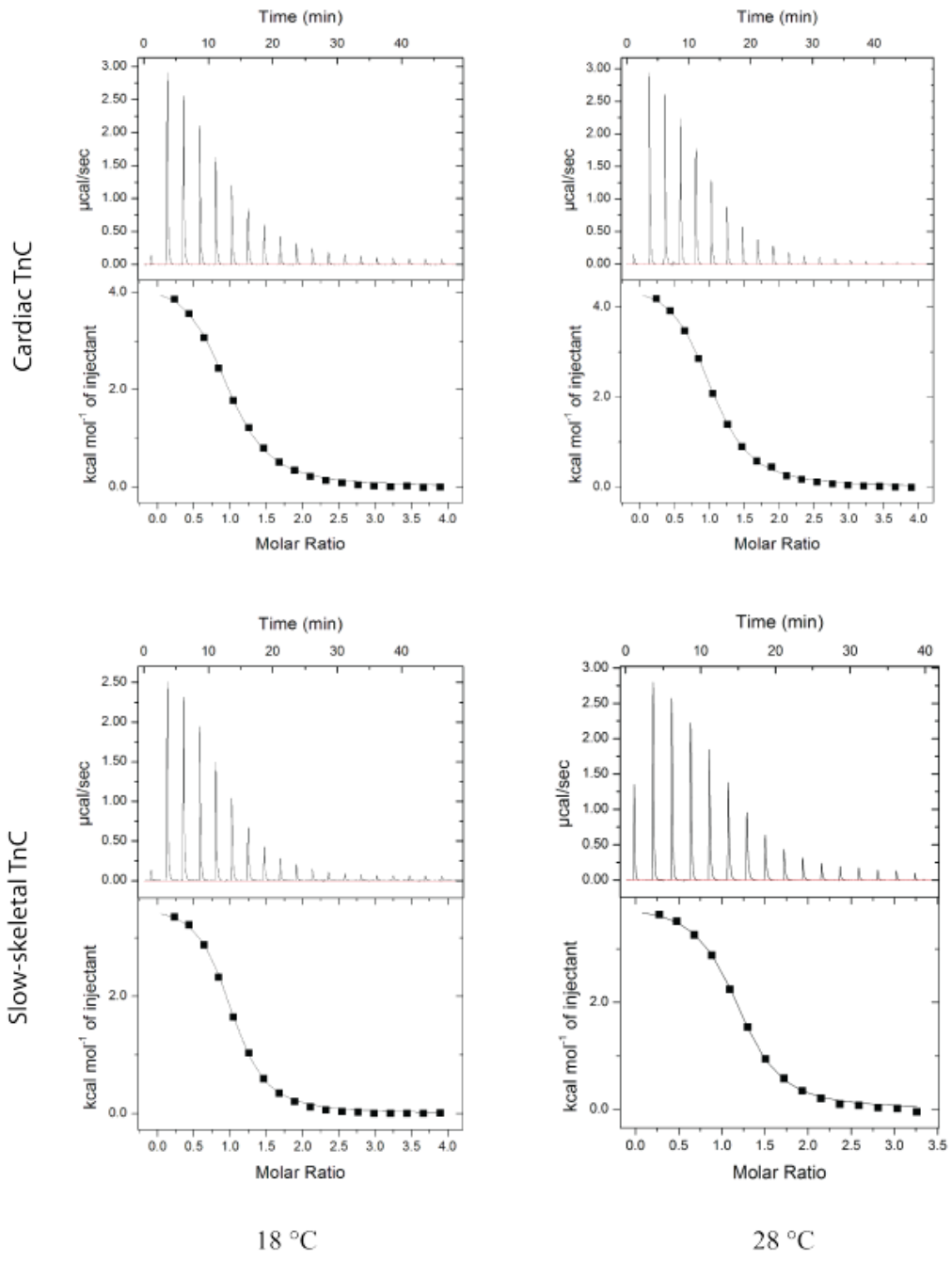

Supplemental Figure 3-5 Representative ITC binding isotherms show the interaction between N-nC and Ca^{2+} for each TnC paralog at each temperature.

Thermodynamic parameters and K_d values are listed in Table 4.

3.7. References

Alderman, S. L., J. M. Klaiman, C. A. Deck and T. E. Gillis (2012). "Effect of cold acclimation on troponin I isoform expression in striated muscle of rainbow trout." American Journal of Physiology-Regulatory, Integrative and Comparative Physiology **303**(2): R168-R176.

Benkert, P., M. Künzli and T. Schwede (2009). "QMEAN server for protein model quality estimation." Nucleic Acids Research **37**(suppl_2): W510-W514.

Berendsen, H. J. C., J. P. M. Postma, W. F. v. Gunsteren, A. DiNola and J. R. Haak (1984). "Molecular dynamics with coupling to an external bath." The Journal of Chemical Physics **81**(8): 3684-3690.

Bers, D. M. (2002). "Cardiac excitation–contraction coupling." Nature **415**(6868): 198-205.

Bordoli, L. and T. Schwede (2012). "Automated protein structure modeling with SWISS-MODEL Workspace and the Protein Model Portal." Methods Mol Biol **857**: 107-136.

Bussi, G., D. Donadio and M. Parrinello (2007). "Canonical sampling through velocity rescaling." J Chem Phys **126**(1): 014101.

Cerutti, D. S., R. E. Duke, T. A. Darden and T. P. Lybrand (2009). "Staggered Mesh Ewald: An extension of the Smooth Particle-Mesh Ewald method adding great versatility." J Chem Theory Comput **5**(9): 2322.

Chen, V. B., W. B. Arendall, III, J. J. Headd, D. A. Keedy, R. M. Immormino, G. J. Kapral, L. W. Murray, J. S. Richardson and D. C. Richardson (2010). "MolProbity: all-atom structure validation for macromolecular crystallography." Acta Crystallographica Section D **66**(1): 12-21.

Churcott, C., C. Moyes, B. Bressler, K. Baldwin and G. Tibbits (1994). "Temperature and pH effects on Ca2+ sensitivity of cardiac myofibrils: a comparison of trout with mammals." American Journal of Physiology-Regulatory, Integrative and Comparative Physiology **267**(1): R62-R70.

Clark, T. D., E. Sandblom, G. K. Cox, S. G. Hinch and A. P. Farrell (2008). "Circulatory limits to oxygen supply during an acute temperature increase in the Chinook salmon (Oncorhynchus tshawytscha)." American Journal of Physiology-Regulatory, Integrative and Comparative Physiology **295**(5): R1631-R1639.

Cordina, N. M., C. K. Liew, D. A. Gell, P. G. Fajer, J. P. Mackay and L. J. Brown (2013). "Effects of Calcium Binding and the Hypertrophic Cardiomyopathy A8V Mutation on the Dynamic Equilibrium between Closed and Open Conformations of the Regulatory N-Domain of Isolated Cardiac Troponin C." Biochemistry **52**(11): 1950-1962.

Daura, X., K. Gademann, B. Jaun, D. Seebach, W. F. van Gunsteren and A. E. Mark (1999). "Peptide Folding: When Simulation Meets Experiment." Angewandte Chemie International Edition **38**(1-2): 236-240.

Dong, W.-J., C.-K. Wang, A. M. Gordon and H. C. Cheung (1997). "Disparate Fluorescence Properties of 2-[4′-(Iodoacetamido)anilino]-Naphthalene-6-Sulfonic Acid Attached to Cys-84 and Cys-35 of Troponin C in Cardiac Muscle Troponin." Biophysical Journal **72**(2, Part 1): 850-857.

Eisenhaber, F., P. Lijnzaad, P. Argos, C. Sander and M. Scharf (1995). "The double cubic lattice method: Efficient approaches to numerical integration of surface area and volume and to dot surface contouring of molecular assemblies." Journal of Computational Chemistry **16**(3): 273-284.

Force, A., M. Lynch, F. B. Pickett, A. Amores, Y. L. Yan and J. Postlethwait (1999). "Preservation of duplicate genes by complementary, degenerative mutations." Genetics **151**(4): 1531-1545.

Genge, C. E., W. S. Davidson and G. F. Tibbits (2013). "Adult teleost heart expresses two distinct troponin C paralogs: cardiac TnC and a novel and teleost-specific ssTnC in a chamber-and temperature-dependent manner." Physiological genomics **45**(18): 866-875.

Genge, C. E., C. M. Stevens, W. S. Davidson, G. Singh, D. Peter Tieleman and G. F. Tibbits (2016). "Functional divergence in teleost cardiac troponin paralogs guides variation in the interaction of TnI switch region with TnC." Genome biology and evolution **8**(4): 994-1011.

Gifford, Jessica L., Michael P. Walsh and Hans J. Vogel (2007). "Structures and metal-ion-binding properties of the Ca²⁺-binding helix–loop–helix EF-hand motifs." Biochemical Journal **405**(2): 199-221.

Gillis, T. E., T. M. Blumenschein, B. D. Sykes and G. F. Tibbits (2003). "Effect of temperature and the F27W mutation on the Ca2+ activated structural transition of trout cardiac troponin C." Biochemistry **42**(21): 6418-6426.

Gillis, T. E., B. Liang, F. Chung and G. F. Tibbits (2005). "Increasing mammalian cardiomyocyte contractility with residues identified in trout troponin C." Physiological genomics **22**(1): 1-7.

Gillis, T. E., C. R. Marshall, X.-H. Xue, T. J. Borgford and G. F. Tibbits (2000). "Ca2+ binding to cardiac troponin C: effects of temperature and pH on mammalian and salmonid isoforms." American Journal of Physiology-Regulatory, Integrative and Comparative Physiology **279**(5): R1707-R1715.

Gillis, T. E., C. D. Moyes and G. F. Tibbits (2003). "Sequence mutations in teleost cardiac troponin C that are permissive of high Ca 2+ affinity of site II." American Journal of Physiology-Cell Physiology **284**(5): C1176-C1184.

Gollock, M., S. Currie, L. Petersen and A. Gamperl (2006). "Cardiovascular and haematological responses of Atlantic cod (Gadus morhua) to acute temperature increase." Journal of Experimental Biology **209**(15): 2961-2970.

Harrison, S. M. and D. M. Bers (1989). "Influence of temperature on the calcium sensitivity of the myofilaments of skinned ventricular muscle from the rabbit." The Journal of General Physiology **93**(3): 411-428.

Harrison, S. M. and D. M. Bers (1990). "Modification of temperature dependence of myofilament Ca sensitivity by troponin C replacement." American Journal of Physiology-Cell Physiology **258**(2): C282-C288.

Harrison, S. M. and D. M. Bers (1990). "Temperature dependence of myofilament Ca sensitivity of rat, guinea pig, and frog ventricular muscle." American Journal of Physiology-Cell Physiology **258**(2): C274-C281.

Hazard, A. L., S. C. Kohout, N. L. Stricker, J. A. Putkey and J. J. Falke (1998). "The kinetic cycle of cardiac troponin C: calcium binding and dissociation at site II trigger slow conformational rearrangements." Protein Science **7**(11): 2451-2459.

Hess, B., H. Bekker, H. J. C. Berendsen and J. G. E. M. Fraaije (1997). "LINCS: A linear constraint solver for molecular simulations." Journal of Computational Chemistry **18**(12): 1463-1472.

Hooft, R. W. W., G. Vriend, C. Sander and E. E. Abola (1996). "Errors in protein structures." Nature **381**(6580): 272-272.

Hub, J. S., B. L. de Groot and D. van der Spoel (2010). "g_wham—A Free Weighted Histogram Analysis Implementation Including Robust Error and Autocorrelation Estimates." Journal of Chemical Theory and Computation **6**(12): 3713-3720.

Humphrey, W., A. Dalke and K. Schulten (1996). "VMD: Visual molecular dynamics." Journal of Molecular Graphics **14**(1): 33-38.

Jorgensen, W. L., J. Chandrasekhar, J. D. Madura, R. W. Impey and M. L. Klein (1983). "Comparison of simple potential functions for simulating liquid water." The Journal of Chemical Physics **79**(2): 926-935.

Lau, A. Y. and B. Roux (2007). "The Free Energy Landscapes Governing Conformational Changes in a Glutamate Receptor Ligand-Binding Domain." Structure **15**(10): 1203-1214.

Lee, L., C. Genge, M. Cua, X. Sheng, K. Rayani, M. Beg, M. Sarunic and G. Tibbits (2016). "Functional Assessment of Cardiac Responses of Adult Zebrafish (Danio rerio) to Acute and Chronic Temperature Change Using High-Resolution Echocardiography." PloS one **11**(1): e0145163.

Li, A. Y., C. M. Stevens, B. Liang, K. Rayani, S. Little, J. Davis and G. F. Tibbits (2013). "Familial hypertrophic cardiomyopathy related cardiac troponin C L29Q mutation alters length-dependent activation and functional effects of phosphomimetic troponin I*."

Li, H., V. Ngo, M. C. Da Silva, D. R. Salahub, K. Callahan, B. Roux and S. Y. Noskov (2015). "Representation of Ion–Protein Interactions Using the Drude Polarizable Force-Field." The Journal of Physical Chemistry B **119**(29): 9401-9416.

Li, M. X., L. Spyracopoulos and B. D. Sykes (1999). "Binding of Cardiac Troponin-I147-163 Induces a Structural Opening in Human Cardiac Troponin-C." Biochemistry **38**(26): 8289-8298.

Lin, E., A. Ribeiro, W. Ding, L. Hove-Madsen, M. V. Sarunic, M. F. Beg and G. F. Tibbits (2014). "Optical mapping of the electrical activity of isolated adult zebrafish hearts: acute effects of temperature." American Journal of Physiology-Regulatory, Integrative and Comparative Physiology **306**(11): R823-R836.

Lindert, S., P. M. Kekenes-Huskey, G. Huber, L. Pierce and J. A. McCammon (2012). "Dynamics and calcium association to the N-terminal regulatory domain of human cardiac troponin C: a multiscale computational study." The Journal of Physical Chemistry B **116**(29): 8449-8459.

Lindorff-Larsen, K., S. Piana, K. Palmo, P. Maragakis, J. L. Klepeis, R. O. Dror and D. E. Shaw (2010). "Improved side-chain torsion potentials for the Amber ff99SB protein force field." Proteins **78**(8): 1950-1958.

Little, A. G. and F. Seebacher (2014). "Thyroid hormone regulates cardiac performance during cold acclimation in zebrafish (Danio rerio)." The Journal of experimental biology **217**(5): 718-725.

Lovell, S. C., I. W. Davis, W. B. Arendall III, P. I. W. de Bakker, J. M. Word, M. G. Prisant, J. S. Richardson and D. C. Richardson (2003). "Structure validation by Cα geometry: ϕ,ψ and Cβ deviation." Proteins: Structure, Function, and Bioinformatics **50**(3): 437-450.

Lynch, M. and V. Katju (2004). "The altered evolutionary trajectories of gene duplicates." Trends Genet **20**(11): 544-549.

McKay, R. T., L. F. Saltibus, M. X. Li and B. D. Sykes (2000). "Energetics of the Induced Structural Change in a Ca2+ Regulatory Protein: Ca2+ and Troponin I Peptide Binding to the E41A Mutant of the N-Domain of Skeletal Troponin C." Biochemistry **39**(41): 12731-12738.

Mendonça, P. C. and A. K. Gamperl (2010). "The effects of acute changes in temperature and oxygen availability on cardiac performance in winter flounder (Pseudopleuronectes americanus)." Comparative Biochemistry and Physiology Part A: Molecular & Integrative Physiology **155**(2): 245-252.

Páll, S. and B. Hess (2013). "A flexible algorithm for calculating pair interactions on SIMD architectures." Computer Physics Communications **184**(12): 2641-2650.

Parmacek, M. S. and R. J. Solaro (2004). "Biology of the troponin complex in cardiac myocytes." Prog Cardiovasc Dis **47**(3): 159-176.

Parvatiyar, M. S., A. P. Landstrom, C. Figueiredo-Freitas, J. D. Potter, M. J. Ackerman and J. R. Pinto (2012). "A mutation in TNNC1-encoded cardiac troponin C, TNNC1-A31S, predisposes to hypertrophic cardiomyopathy and ventricular fibrillation." Journal of Biological Chemistry **287**(38): 31845-31855.

Pinto, J. R., M. S. Parvatiyar, M. A. Jones, J. Liang, M. J. Ackerman and J. D. Potter (2009). "A functional and structural study of troponin C mutations related to hypertrophic cardiomyopathy." J Biol Chem **284**(28): 19090-19100.

Potter, J. D. and J. Gergely (1975). "The calcium and magnesium binding sites on troponin and their role in the regulation of myofibrillar adenosine triphosphatase." Journal of Biological Chemistry **250**(12): 4628-4633.

Pronk, S., S. Pall, R. Schulz, P. Larsson, P. Bjelkmar, R. Apostolov, M. R. Shirts, J. C. Smith, P. M. Kasson, D. van der Spoel, B. Hess and E. Lindahl (2013). "GROMACS 4.5: a high-throughput and highly parallel open source molecular simulation toolkit." Bioinformatics **29**(7): 845-854.

Skowronsky, R. A., M. Schroeter, T. Baxley, Y. Li, J. M. Chalovich and A. M. Spuches (2013). "Thermodynamics and molecular dynamics simulations of calcium binding to the regulatory site of human cardiac troponin C: evidence for communication with the structural calcium binding sites." JBIC Journal of Biological Inorganic Chemistry **18**(1): 49-58.

Sogah, V. M., F. C. Serluca, M. C. Fishman, D. L. Yelon, C. A. Macrae and J. D. Mably (2010). "Distinct troponin C isoform requirements in cardiac and skeletal muscle." Dev Dyn **239**(11): 3115-3123.

Somero, G. N. and P. W. Hochachka (1969). "Isoenzymes and short-term temperature compensation in poikilotherms: activation of lactate dehydrogenase isoenzymes by temperature decreases." Nature **223**(5202): 194-195.

Spence, R., G. Gerlach, C. Lawrence and C. Smith (2008). "The behaviour and ecology of the zebrafish, Danio rerio." Biological Reviews **83**(1): 13-34.

Spyracopoulos, L., M. X. Li, S. K. Sia, S. M. Gagné, M. Chandra, R. J. Solaro and B. D. Sykes (1997). "Calcium-induced structural transition in the regulatory domain of human cardiac troponin C." Biochemistry **36**(40): 12138-12146.

Takeda, S., A. Yamashita, K. Maeda and Y. Maéda (2003). "Structure of the core domain of human cardiac troponin in the Ca2+-saturated form." Nature **424**(6944): 35-41.

Tiitu, V. and M. Vornanen (2002). "Regulation of cardiac contractility in a cold stenothermal fish, the burbot Lota lota L." Journal of Experimental Biology **205**(11): 1597-1606.

Tikunova, S. B., J. A. Rall and J. P. Davis (2002). "Effect of hydrophobic residue substitutions with glutamine on Ca2+ binding and exchange with the N-domain of troponin C." Biochemistry **41**(21): 6697-6705.

Wang, D., I. M. Robertson, M. X. Li, M. E. McCully, M. L. Crane, Z. Luo, A.-Y. Tu, V. Daggett, B. D. Sykes and M. Regnier (2012). "Structural and functional consequences of the cardiac troponin C L48Q Ca2+-sensitizing mutation." Biochemistry **51**(22): 4473-4487.

Wang, J., Q. Shao, Z. Xu, Y. Liu, Z. Yang, B. P. Cossins, H. Jiang, K. Chen, J. Shi and W. Zhu (2014). "Exploring Transition Pathway and Free-Energy Profile of Large-Scale Protein Conformational Change by Combining Normal Mode Analysis and Umbrella Sampling Molecular Dynamics." The Journal of Physical Chemistry B **118**(1): 134-143.

Yap, K. L., J. B. Ames, M. B. Swindells and M. Ikura (2002). Vector Geometry Mapping. Calcium-Binding Protein Protocols: Volume 2: Methods and Techniques. H. J. Vogel. Totowa, NJ, Springer New York**:** 317-324.

Zhang, X. L., G. F. Tibbits and M. Paetzel (2013). "The structure of cardiac troponin C regulatory domain with bound Cd2+ reveals a closed conformation and unique ion coordination." Acta Crystallographica Section D: Biological Crystallography **69**(5): 722-734.

Chapter 4.

The Effect of Single Amino Acid Changes on Calcium Binding to Troponin C

This chapter contains the publication entitled: “Changes in the Dynamics of the Cardiac Troponin C Molecule Explain the Effects of Ca^{2+}-Sensitizing Mutations” published in the Journal of Biological Chemistry in 2017 with a small number of formatting and modifications to keep in line with the format of this thesis.

My contributions to this publication included design, implementation, and analysis of the ITC experiments. I also carried out the melting point experiments and analysis of the results, I contributed to manuscript preparation and subsequent revisions. Dr. Charles Stevens carried out the MD Simulations in collaboration with Dr. Gurpreet Singh, he also analyzed the MD results, and prepared the manuscript.

4.1. Abstract

Cardiac troponin C (cTnC) is the regulatory protein that initiates cardiac contraction in response to Ca^{2+}. TnC binding Ca^{2+} initiates a cascade of protein-protein interactions that begins with the opening of the N-terminal domain of cTnC (N-TnC), followed by cTnC binding the troponin I switch peptide (TnI_{SW}). We have evaluated, through isothermal titration calorimetry (ITC) and molecular dynamics (MD) simulation, the effect of several clinically relevant mutations (A8V, L29Q, A31S, L48Q, Q50R and C84Y) on the Ca^{2+} affinity, structural dynamics, and calculated interaction strengths between cTnC and each of Ca^{2+} and TnI_{SW}. Surprisingly the Ca^{2+} affinity measured by ITC was only significantly affected by half of these mutations including: L48Q, which had a 10-fold higher affinity than WT and the Q50R and C84Y mutants which each had affinities 3-fold higher than wild-type. This suggests that Ca^{2+} affinity of N-TnC in isolation is insufficient to explain the pathogenicity of these mutations. Molecular Dynamics (MD) simulation was used to evaluate the effects of these mutations on Ca^{2+} binding, structural dynamics, and TnI interaction independently. Many of the mutations had a pronounced effect on the balance between the open and closed conformations of the TnC molecule, which provides an indirect mechanism for their pathogenic properties.

Our data demonstrate that the structural dynamics of the cTnC molecule are key in determining myofilament Ca^{2+} sensitivity. Our data further suggest that modulation of the structural dynamics is the underlying molecular mechanism for many disease mutations that are far from the regulatory Ca^{2+} binding site of cTnC.

4.2. Background

Familial Hypertrophic Cardiomyopathy (FHC) is the inherited form of Hypertrophic Cardiomyopathy (HCM), the most common cause of sudden cardiac death in young athletes (Maron, Shirani et al. 1996), with a prevalence of 1 in 200 individuals (Semsarian, Ingles et al. 2015). There is a growing list of over 1000 mutations that have been associated with HCM, primarily in genes that code for sarcomeric proteins such as the cardiac troponin (cTn) complex (Harada and Morimoto 2004, Pinto, Parvatiyar et al. 2009, Seidman and Seidman 2011). FHC is difficult to diagnose as it can be clinically asymptomatic prior to sudden cardiac death. The cTn complex is composed of three proteins: cTnC, the Ca^{2+} sensing component; cTnI, the inhibitory subunit, and cTnT, that tethers the cTn complex to the cardiac thin filament (Parmacek and Solaro 2004). Mutations in cTnC have a pronounced functional effect as the sequence of cTnC is highly conserved throughout vertebrates (Gillis, Marshall et al. 2007).

In cardiac contraction, the cytosolic Ca^{2+} concentration fluctuates between 100 nM in diastole and 400 – 1000 nM during systole (Bers 2000, Kirschenlohr, Grace et al. 2000). When Ca^{2+} binds to the regulatory N-terminal domain of cTnC (N-cTnC), a conformational change exposes a hydrophobic region on the surface, which binds to the "switch" region of cTnI. The Ca^{2+} signal ultimately permits actomyosin cross-bridge formation and force production (Parmacek and Solaro 2004). Sequence substitutions in cTn components demonstrably affect the Ca^{2+} sensitivity of force production in myofibrils, skinned cardiomyocytes and trabeculae (Tikunova and Davis 2004, Landstrom, Parvatiyar et al. 2008, Liang, Chung et al. 2008, Tikunova, Liu et al. 2010, Parvatiyar, Landstrom et al. 2012, Feest, Steven Korte et al. 2014, Shettigar, Zhang et al. 2016). The N-cTnC-Ca^{2+} interaction has been measured with fluorescent probes such as anilino-napthalenesulfote iodoacetamide (IAANS) (Dong, Wang et al. 1997, Hazard, Kohout et al. 1998, Li, Stevens et al. 2013), in which a shift in the dynamic equilibrium between populations of open and closed cTnC is reported in response to the addition of Ca^{2+}. These experiments produced different results for the isolated N-TnC compared to

experiments that include the cTn complex and cardiac thin filament proteins actin and tropomyosin (Davis, Norman et al. 2007, Li, Stevens et al. 2013). By understanding the thermodynamic basis of the function of N-cTnC, we can explain this variation and explore the specific effects of disease-associated mutations.

The function of cTnC and other Ca^{2+}-sensing EF-hand proteins has been described as a balance between the opposing forces that push the cTnC molecule open, and those that keep it closed (Gifford, Walsh et al. 2007). When Ca^{2+} binds N-cTnC, it creates a strain on the molecule, which is alleviated when N-cTnC changes conformation to better accommodate the presence of the ion; however, the energetic cost of the unfavorable exposure of a hydrophobic cleft provides a thermodynamic incentive to keep the N-cTnC molecule closed (Gifford, Walsh et al. 2007). The balance between these forces can be disrupted by sequence substitutions that alter the ability of N-cTnC to tolerate the conformational strain imposed by Ca^{2+} binding, or substitutions that modify the hydrophobic cleft. The TnI switch peptide (TnI_{SW}) binds to TnC and stabilizes the open TnC conformation by occluding the hydrophobic cleft from the aqueous environment. The structural effects of Ca^{2+} binding have been examined through NMR and X-ray crystallographic data (Spyracopoulos, Li et al. 1997, Li, Spyracopoulos et al. 1999, Takeda, Yamashita et al. 2003, Zhang, Tibbits et al. 2013), including for the HCM-associated TnC mutant L29Q (Zhang, Tibbits et al. 2013, Robertson, Sevrieva et al. 2015). These structures and data from MD simulations have demonstrated minimal effects of sequence substitutions on the static structure, but a greater effect on the dynamics of the protein (Lindert, Kekenes-Huskey et al. 2012, Dewan, McCabe et al. 2016, Stevens, Rayani et al. 2016).

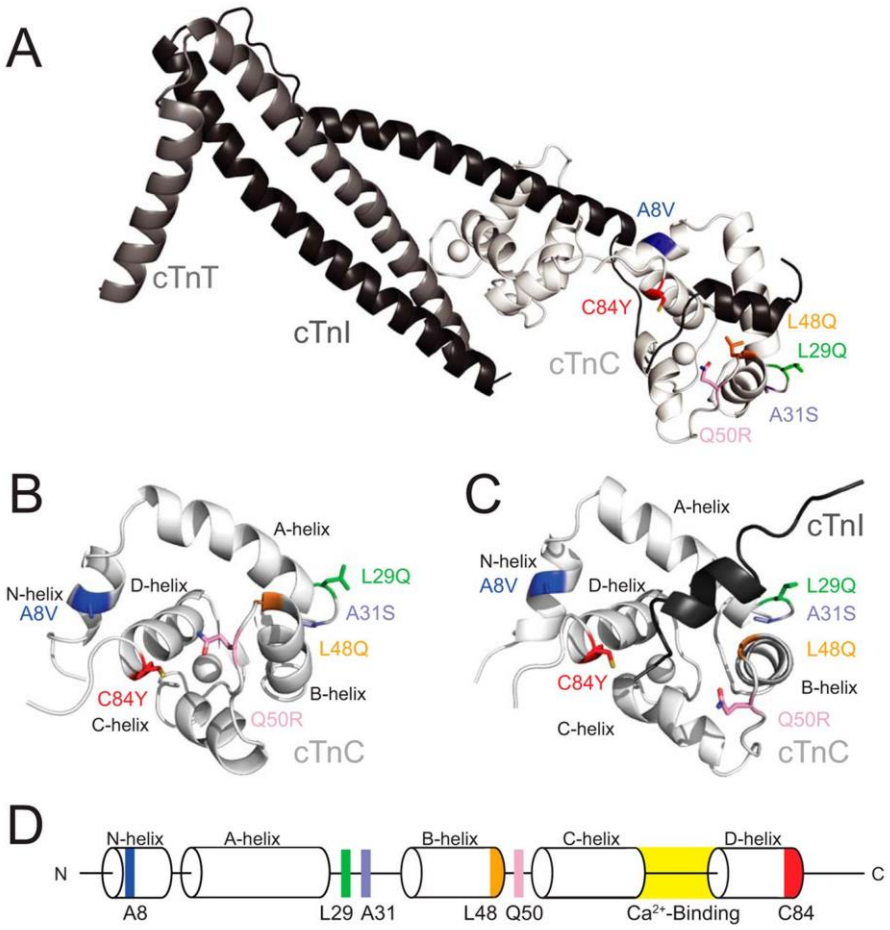

Figure 4-1 Structure of the core domain of the Tn complex.
A. Adapted from (PDB:1J1E) with each of the residues that were selected for this study highlighted. The troponin complex proteins are colored white (cTnC), grey (cTnT), and black (cTnI); B. The isolated N-cTnC domain bound to Ca^{2+} used in the PMF simulations. Helices and mutation sites are labeled; C. The N-cTnC domain bound to the TnI_{SW} and Ca^{2+} is the system used in the TnI_{SW} binding simulations; D. A schematic of the N-cTnC construct. The helices, Ca^{2+} binding loop and the residues being examined in this study are labeled.

In this study, we report the ITC-derived Ca^{2+} binding affinity of N-cTnC mutant constructs and their calculated effects on the dynamics, Ca^{2+} interaction and TnI_{SW} interaction strengths. The N-cTnC mutations selected for analysis in this work are the FHC-associated mutations A8V (Cordina, Liew et al. 2013, Martins, Parvatiyar et al. 2015, Zot, Hasbun et al. 2016), L29Q (Hoffmann, Schmidt-Traub et al. 2001, Schmidtmann, Lindow et al. 2005, Liang, Chung et al. 2008, Li, Stevens et al. 2013), A31S (Parvatiyar, Landstrom et al. 2012) and C84Y (Landstrom, Parvatiyar et al. 2008), the engineered Ca^{2+}-sensitizing mutation L48Q (Tikunova and Davis 2004, Tikunova, Liu et al. 2010, Kekenes-Huskey, Lindert et al. 2012, Davis, Davis et al. 2016, Shettigar, Zhang et al. 2016), and the Dilated Cardiomyopathy (DCM) associated mutation Q50R

(van Spaendonck-Zwarts, van Tintelen et al. 2010) (**Figure 4-1**). The C84Y and Q50R mutations each conferred Ca^{2+} affinities 3-fold higher than WT, while the L48Q Ca^{2+} affinity was 10-fold higher than wild-type. The combination of MD simulation techniques with ITC explains the molecular etiology of these mutations in terms of the energy landscape of the conformational change. The mutations that favor the open conformation of TnC indirectly increase the Ca^{2+} affinity of the isolated N-cTnC molecule (Tikunova, Rall et al. 2002, Li and Hwang 2015, Schlecht, Li et al. 2016). We propose, that mutations that increase the Ca^{2+} sensitivity of the myofilament destabilize the closed conformation of N-cTnC, stabilize the open conformation of N-cTnC and/or promote association with the TnI_{SW}. The results presented in this work demonstrate that many N-cTnC mutations affect myofilament Ca^{2+} sensitivity by affecting the molecular motions that govern the regulation of cardiac contraction.

4.3. Experimental Procedures

The codon-optimized gene sequence for human TNNC1 (Uniprot ID P63316) was cloned into the pET21a(+) vector (Novagen). A stop codon was introduced at position 90 by following the Phusion site-directed mutagenesis protocol (Thermo). Protein expression, purification, melting point determination, and ITC were carried out using protocols modified from previous work (Stevens, Rayani et al. 2016). Mutated constructs were sequenced and transformed into the BL21(DE3) host strain. Overnight cultures were grown in lysogeny broth supplemented with 50 µg/mL ampicillin at 37ºC overnight with shaking at 250 RPM, 1% subcultures were grown for 3 h followed by induction with 1 mM Isopropyl β-D-1-thiogalactopyranoside (IPTG) and a further 3 h of growth. Cells were harvested by centrifugation and resuspended in 50 mM Tris-HCl at pH 8.0, 1 mM phenylmethylsulfonyl fluoride (PMSF), 5 mM ethylenediamine-tetraacetic acid (EDTA), and a c0mplete protease inhibitor tablet (Roche). The cells were sonicated on ice at 80% amplitude with 30-second pulses separated by 30 seconds. The lysate was centrifuged at 30,000 x g for 30 mins, and the supernatant decanted. The protein was purified with a fast-flow DEAE column (GE Healthcare). The column was equilibrated with 50 mM Tris-HCl at pH 8.0, 1 mM dithiothreitol (DTT), 5 mM EDTA and the protein was eluted with a 180 mL NaCl gradient up to 0.55 M. Fractions containing the TnC protein were retained and concentrated to 5 mL with an Amicon centrifugal concentrator with a molecular weight cut off of 3 kDa (Millipore). The protein was further

purified with a HiPrep 26/60 Sephacryl S-100 column (GE Healthcare) equilibrated with 50 mM Tris-HCl pH 8.0, 100 mM NaCl and 1 mM DTT. The fractions that contain the pure N-cTnC protein were pooled, concentrated and stored at -80°C.

ITC buffer contained 50 mM HEPES at pH 7.2, and 150 mM KCl, protein samples were dialyzed 3 times against 2 L of ITC buffer and diluted to 200 µM. In successive dialysis steps, 15 mM β-mercaptoethanol (BME), 15 mM BME, and 2 mM of BME were added to the buffers. An extinction coefficient of 1490 M^{-1}*cm^{-1} and a MW of 10.1 kDa were used to measure protein concentration. The Ca^{2+} solution was diluted from a 1 M Ca^{2+} solution (Sigma) into the buffer from the final dialysis step to a final concentration of 4 mM. Ca^{2+} was titrated into the protein solution by a single 0.4 µl injection, followed by a series of 18, 2 µl injections at 2 min intervals while stirring at 1,000 rpm. The experiments were carried out at 25ºC. The heat of dilution of Ca^{2+} was accounted for by subtracting the average of the final three data points from the titration curve. Analysis was performed with Origin 8.0 (OriginLab, Northampton, MA).

To measure the melting point of the proteins, the samples were first dialyzed 4 times against 2 L of MT buffer (10 mM HEPES pH 7.5, 150 mM KCl, 3 mM $MgCl_2$, 2 mM EGTA) and combined with 2.5 µL of 100-fold diluted SYPRO orange (Thermo) to a final concentration of 3 mg/mL. The temperature was increased from 4ºC to 95ºC at 5 second intervals using a CFX96 Touch Real-Time PCR system (BioRad). The melting point was determined at the midpoint of the unfolding transition, which is indicated by the peak of the first derivative curve.

Equilibrium MD simulations of WT and mutant TnC were performed as previously described (Genge, Stevens et al. 2016, Stevens, Rayani et al. 2016) with the exception that all calculations in this study were performed at 300 K. Structural models of the mutant constructs were generated with the Swiss-model workspace (Bordoli and Schwede 2012), The N-cTnC+Ca^{2+} models used the NMR-derived structure of human N-TnC as a template (PDB:1AP4) (Spyracopoulos, Li et al. 1997) and the models of the human N-TnC in complex with TnI_{SW} were based on the WT NMR derived structure of N-cTnC in complex with Ca^{2+} and cTnI residues 147-163 (PDB:1MXL) (Li, Spyracopoulos et al. 1999).

The structural models were simulated using GROMACS 4.6.5 (Pronk, Pall et al. 2013), and the AMBER99sb-ILDN force field (Lindorff-Larsen, Piana et al. 2010), the models were placed in a periodic, cubic simulation system and solvated with the TIP3P water model (Mahoney and Jorgensen 2000), charges were neutralized with the addition of K^+ or Cl^- ions. The composition of each system is listed in Table S4-1. The systems were energy minimized using the steepest descent algorithm to a tolerance of 10 $kJ*mol^{-1}*nm^{-1}$ followed by conjugate gradient minimization for 10,000 steps. 100 $kJ*mol^{-1}*nm^{-1}$ restraints were placed on every protein and Ca^{2+} atom and the system was simulated for 1 ns to allow the water to equilibrate around the protein.

The WT and mutant N-cTnC+Ca^{2+} systems were then simulated for either 100 ns or 1 μs total time and the WT and mutant N-cTnC+$cTnI_{SW}$+Ca^{2+} constructs were simulated for 100 ns total (**Figure 4-1 B & C**). All of the simulations were performed with Berendsen pressure coupling (Berendsen, Postma et al. 1984) with a τ_T of 0.1. V-rescale temperature coupling (Bussi, Donadio et al. 2007) with a τ_P of 4.0, PME electrostatics (Cerutti, Duke et al. 2009) with a grid spacing of 0.12 nm and interpolation order of 6, the Verlet cut-off scheme was used with a 1.0 nm cut-off (Páll and Hess 2013). Bond lengths were constrained with the LINCS algorithm (Hess, Bekker et al. 1997).

Clustering was carried out over the backbone and C_β atoms of each construct using the Daura algorithm (Daura, Gademann et al. 1999). The degree of the open/closed N-cTnC conformational change and protein stability were assessed through measurements of the solvent accessible surface area, the interhelical angles and the number of hydrogen bonds, which were calculated using g_sas (Eisenhaber, Lijnzaad et al. 1995), Interhlx (Hub, de Groot et al. 2010), and g_hbond (Pronk, Pall et al. 2013), respectively. The g_hbond program used a cut-off radius of 3.5 Å, and 30º angle to define a given hydrogen bond.

Umbrella Sampling and Potential of Mean Force (PMF) calculations were performed as described previously (Stevens, Rayani et al. 2016).The Ca^{2+} was extracted from the N-cTnC molecule by restraining the α-helical Cα atoms with a force constant of 1000 $kJ*mol^{-1}*nm^{-1}$ and restraining the Ca^{2+} ion in the Y and Z dimensions with a force constant of 1000 kJ mol^{-1} nm^{-1}. A constraint pulling force in the X direction as applied at 0.01 Å per second until the Ca^{2+} ion was 5 nm from the N-cTnC molecule. The conformations for umbrella sampling were extracted from the resulting trajectory at

distance intervals of 0.5 Å between 0 and 1 nm, every 1 Å between 1 nm and 2 nm, and every 2 Å between 2 nm and 5 nm. Umbrella simulations were run with the same parameters as the pull simulations, with the “pull rate” parameter set to 0, and were unrestrained aside from a single restraining potential between the center of mass of the N-cTnC molecule and the center of mass of the Ca^{2+} ion. These simulations were run for 30 ns each and a potential of mean force was calculated with the weighted histogram analysis method (WHAM) through the use of g_wham (Hub, de Groot et al. 2010), and errors were estimated with 5,000 bootstraps of the WHAM calculation. To further explore the outlier A8V mutation, the process was repeated using the center structure of the most populous cluster from the 5 replicated 1 μs simulations.

Interaction energies between the TnC models and TnI_{SW} were calculated with g_mmpbsa (Kumari, Kumar et al. 2014) 100 ps apart over the last 10 ns of each equilibrium simulation of the TnI_{SW}/N-cTnC complex. The MM/PBSA calculations used the non-linear Poisson-Boltzmann equation and calculations were performed at 300 K, with a solvent dielectric constant of 80, and probe radius of 1.4 Å. Contact maps of the interacting surfaces between N-cTnC and the $cTnI_{SW}$ were calculated over the final 50 ns of each simulation and were based on measurements made with g_mindist (Pronk, Pall et al. 2013).

4.4. Results

4.4.1. ITC

The interaction between TnC and Ca^{2+} was endothermic for each of the TnC constructs except L48Q, which was exothermic. In each case the stoichiometric ratio (N) of Ca^{2+} binding to N-cTnC was 1:1, indicating that the regulatory site II was exclusively titrated during these experiments. Thermodynamic parameters are listed in **Table 4-1** and ITC isotherms are shown in **Figure 4-2**. At 25ºC each of the K_d values was within error from the WT, with the exceptions Q50R and C84Y, which each had K_d values approximately one third of WT, and L48Q, in which the K_d was one tenth of WT. The ΔS values were lower than WT for A31S, L48Q, Q50R and C84Y. The ΔH values were less favorable than WT for A31S, Q50R, and C84Y but more favorable than WT for the L48Q construct.

Table 4-1 Thermodynamic parameters derived from ITC

N-cTnC construct	N	K_d (μM)	ΔS ($J \cdot mol^{-1} \cdot deg^{-1}$)	ΔH ($J \cdot mol^{-1}$)	ΔG ($J \cdot mol^{-1}$)
WT	1.05 ± 1e-2	14.9 ± 0.7	140.5 ± 2	1.43e4 ± 6e2	-2.76e4 ±1e2
A8V	1.01 ± 2e-2	15.3 ± 0.9	141.6 ± 2	1.47e4 ± 4e2	-2.75e4 ± 2e2
L29Q	0.99 ± 1e-2	14.2 ± 0.4	145.0 ± 1	1.56e4 ± 4e2	-2.77e4 ± 5e1
A31S	0.88 ± 3e-2	11.8 ± 1.1	124.5 ± 2*	8.99e3 ± 3e2*	-2.81e4 ± 2e2
L48Q	1.02 ± 3e-2	1.48 ± 0.1*	50.1 ± 1*	-1.84e4 ± 2e2*	-3.33e4 ± 8e1*
Q50R	1.05 ± 1e-2	5.85 ± 0.1*	120.8 ± 1*	6.15e3 ± 1e2*	-2.99e4 ± 8e1*
C84Y	0.96 ± 2e-2	4.19 ± 0.9*	113.9 ± 2*	3.12e3 ± 1e2*	-3.09e4 ± 5e2*

For all mutants (n=3). For each parameter * indicates significant difference from WT ($p<0.05$).

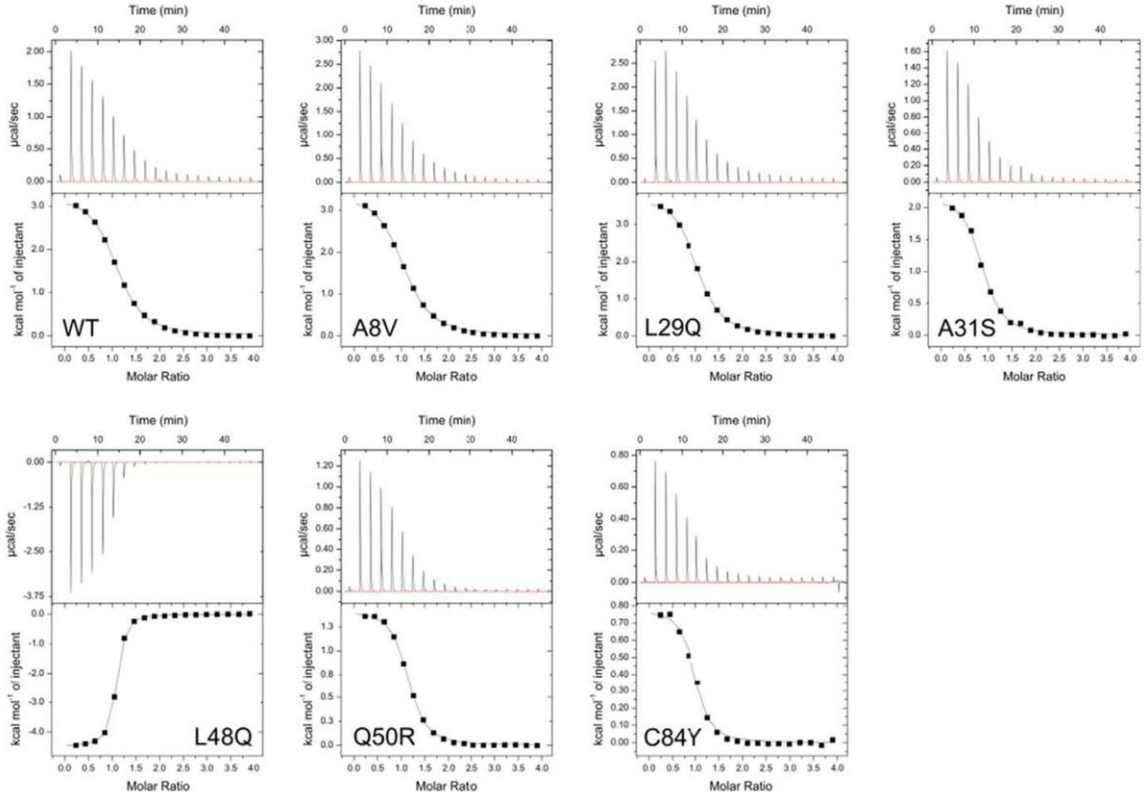

Figure 4-2 Representative isotherms for each of the TnC constructs at 25ºC
The isotherms for WT and each mutant are endothermic, except for the exothermic L48Q isotherm.

4.4.2. Melting Points

The melting points for all Apo TnC constructs were approximately 65ºC, with the exceptions of A8V at 58.5ºC and L48Q at 42.5ºC (**Table S4-2**).

4.4.3. TnC+Ca^{2+} Simulations

Each of the simulations diverged from the original coordinates (**Figure S4-1**). The representative structures are very similar with a total backbone RMSD of 1.9 Å. The local backbone dynamics are similar over 100 ns (**Figure S4-1**). The mutations produce small backbone perturbations compared to WT in their respective local regions and have backbone rmsd values that differ only by between 1.2 Å and 2.4 Å. The mutations can; however, substantially disrupt the packing of interacting side-chains for mutated residues that are not solvent exposed, A8V, L48Q, Q50R and C84Y. The L29Q and A31S substitutions affect fewer residues, but each introduces a hydrogen bond absent from the WT structure (**Figure 4-3**). Compared with WT, the A8V model has a modified interaction between the N and D helices, specifically a hydrophobic interaction with that involves residues Y5, A8, V9, and L12 on the N-helix and L78, V79, and V82 on the D helix. In the L29Q model, Q29 is solvent exposed, but the side chain amide is within hydrogen bonding distance of the I26 backbone O. The A31S substitution is in the EF-hand site I loop, and S31 is within interacting distance of the C35 backbone O, which, in the WT model, interacts with the backbone O of L29. The L48Q substitution disrupts a hydrophobic network in the core of the AB-helical interface that is composed of F19, A23, C35, V44, E76 and M80. The side chain amide of Q49 is within interacting distance of the backbone O of M47. The Q50R substitution, located between helices B and C alters helix C of the molecule, an interaction between Q50 and the backbone O of L48 is replaced by a series of hydrogen bonds between R50 and C84, in addition to both side chain O atoms of E56. Finally, the C84Y substitution disrupts a hydrophobic interaction between C84 with M60, M45, P52 and Q50. Instead, Y84 is within interacting distance with the backbone O of M60.

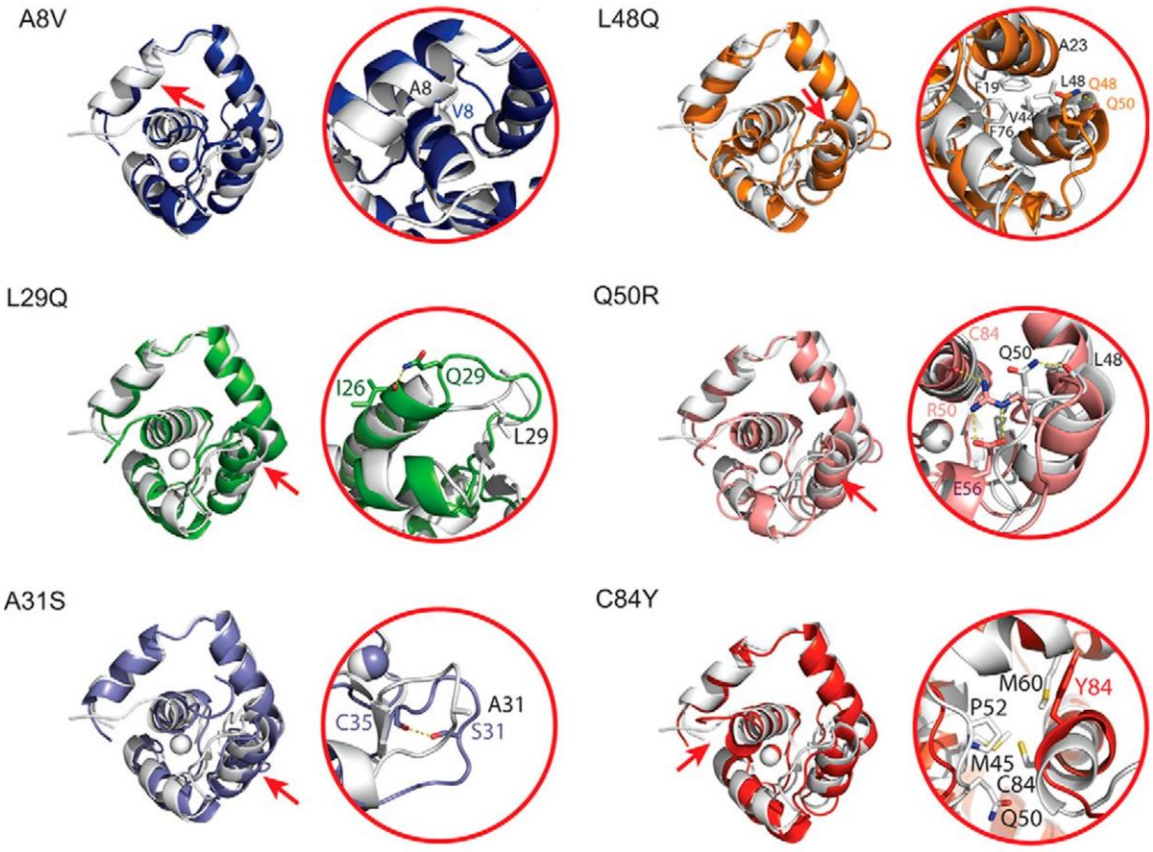

Figure 4-3 Structural changes induced by each of the mutations
In each panel, the left side contains a representative structure of each mutation superimposed with the wild-type structure (white). To orient the reader, a red arrow indicates the location of the mutation on the structure. Changes to side chain packing in the immediate area of each mutation are demonstrated on the right for each of the mutations. While the changes to the backbone are very subtle, there are side chain rearrangements in the local vicinity of the mutations, particularly for the mutations that occur at helix-helix interfaces such as A8V, L48Q and Q50R.

The Ca^{2+} coordination geometry and distances are similar for all constructs with the exception of A8V, which has tighter Ca^{2+} coordination geometry (**Table S4-3**). This is likely correlated with the PMF results discussed in detail below.

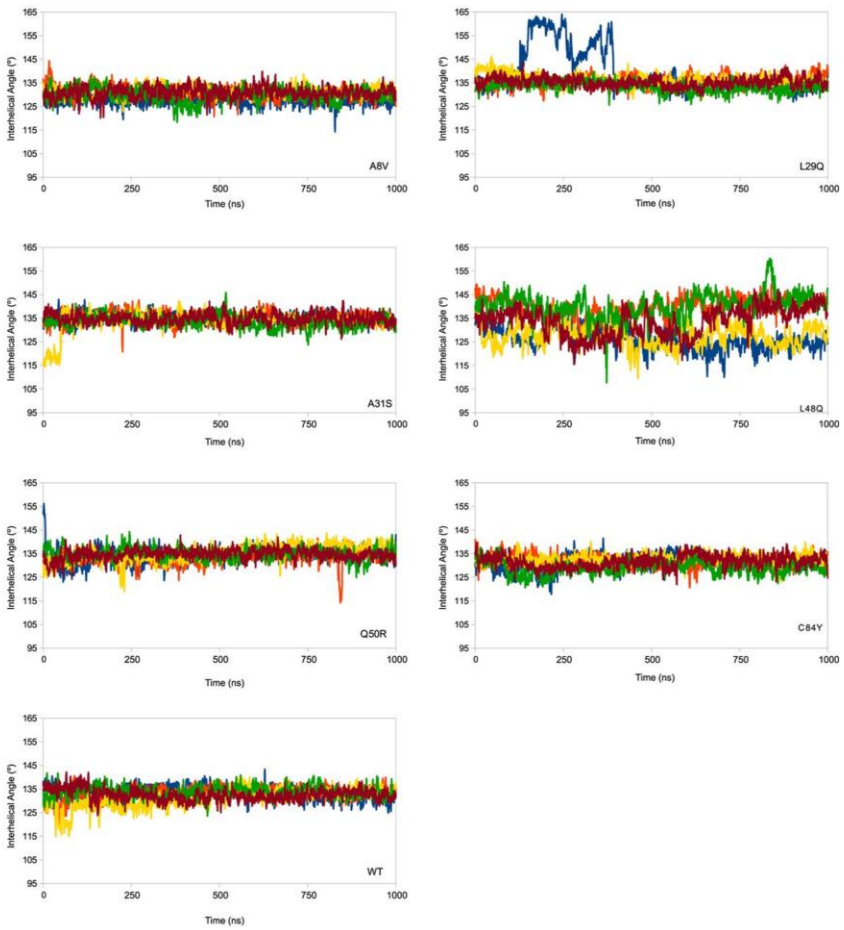

Figure 4-4 The A/B interhelical angle is plotted as a function of time for 5 replicated simulations of for each mutated model

Plots are a rolling average of 250 ps. An interhelical angle less than 110º is considered open, and above 130º is considered closed. There is little difference between WT and most of the constructs, with the exception of the L48Q model. The large angle values in one replicate of the L29Q simulations is an artifact due to a transient loss and recovery of secondary structure in one of the replicated simulations, the hydrophobic solvent accessible surface is not increased as a function of this change. The h-sasa as a function of time is reported in figure S4-4.

The average number of H-bonds in each mutant structure is the same over the course of each simulation, as are the average h-sasa in the closed and open forms (**Table S4-4**); however, monitoring the A/B interhelical angle (**Figure 4-4**) and h-sasa (**Figure S4-3**) over repeated 1 μs simulations demonstrates the frequency with which the TnC protein exposes the hydrophobic patch. The L29Q construct is least frequently open, followed in order by C84Y < A8V < WT < Q50R <A31S, and <L48Q. One of the replicated L29Q simulations had very high AB interhelical angles for a time; this was due to a transient loss of secondary structure, though it did not affect the exposed hydrophobic sasa (**Figure S4-2**). The interhelical angle data can be expressed as the

probability of observing the open conformation of the protein. An angle of 110º has been described as the maximum angle that can be considered open. The proportion of frames in which the N-cTnC molecule had an open AB interhelical angle was 0 for the A8V, L29Q, and C84Y constructs, 0.004% for the Q50R construct, 0.008% for WT, 0.016% for A31S and 0.07% for the L48Q N-cTnC (**Figure 4-5**). By defining cutoff angles for the transition between closed and open at 130º and 110º we can determine the probability of observing the N-cTnC molecule in the closed state (AB interhelical angle >130º) and gain insight on the relative stability of the closed conformation (**Figure 4-5**). The A8V construct has the lowest closed probability at 58%, followed by C84Y at 65%, WT and L48Q at 76%, Q50R and A31S at 86% and 88%, respectively, and finally L29Q at 92%.

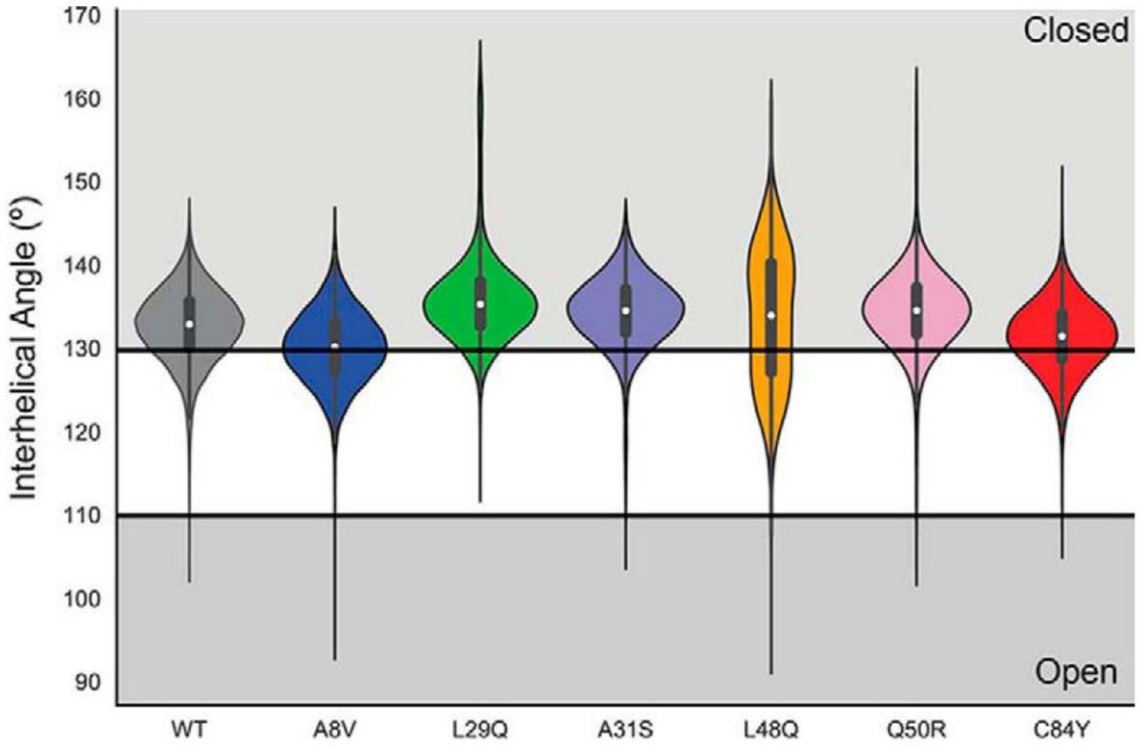

Figure 4-5 Violin plot demonstrating the distribution of open and closed N-cTnC structures

Observations over 5 replicated 1 µs simulations. The open conformation was defined by an AB interhelical angle less than 110º, while the closed conformation defined by an AB interhelical angle greater than 130º. The proportion of open frames is not correlated with the proportion of closed frames. The L48Q construct has the most frames in the open conformation while the A8V is the least closed. This suggests that the destabilization of the closed conformation does not necessarily imply that the open conformation is stabilized.

4.4.4. TnC+Ca^{2+}+TnI_{SW} simulations

The effects on the structural interactions between the TnC molecule and TnI_{SW} are subtle when averaged across the simulations (**Figure 4-6**), and as expected, the majority of the specific contacts are maintained when each of the N-cTnC mutants are compared to WT N-cTnC. The TnI_{SW} remains in contact with the TnC molecule for the duration of the simulations, but the specificity of that contact is somewhat different in response to certain mutations. For example: L29Q, A31S and Q50R make more common contacts between the N-terminal region of TnI_{SW} and the N-helix of TnC than WT, whereas L48Q and C84Y make fewer contacts than WT in this region. These results suggest that alterations in this binding interface may be due to modified interactions between the TnI_{SW} and other regions of the protein near the mutation sites.

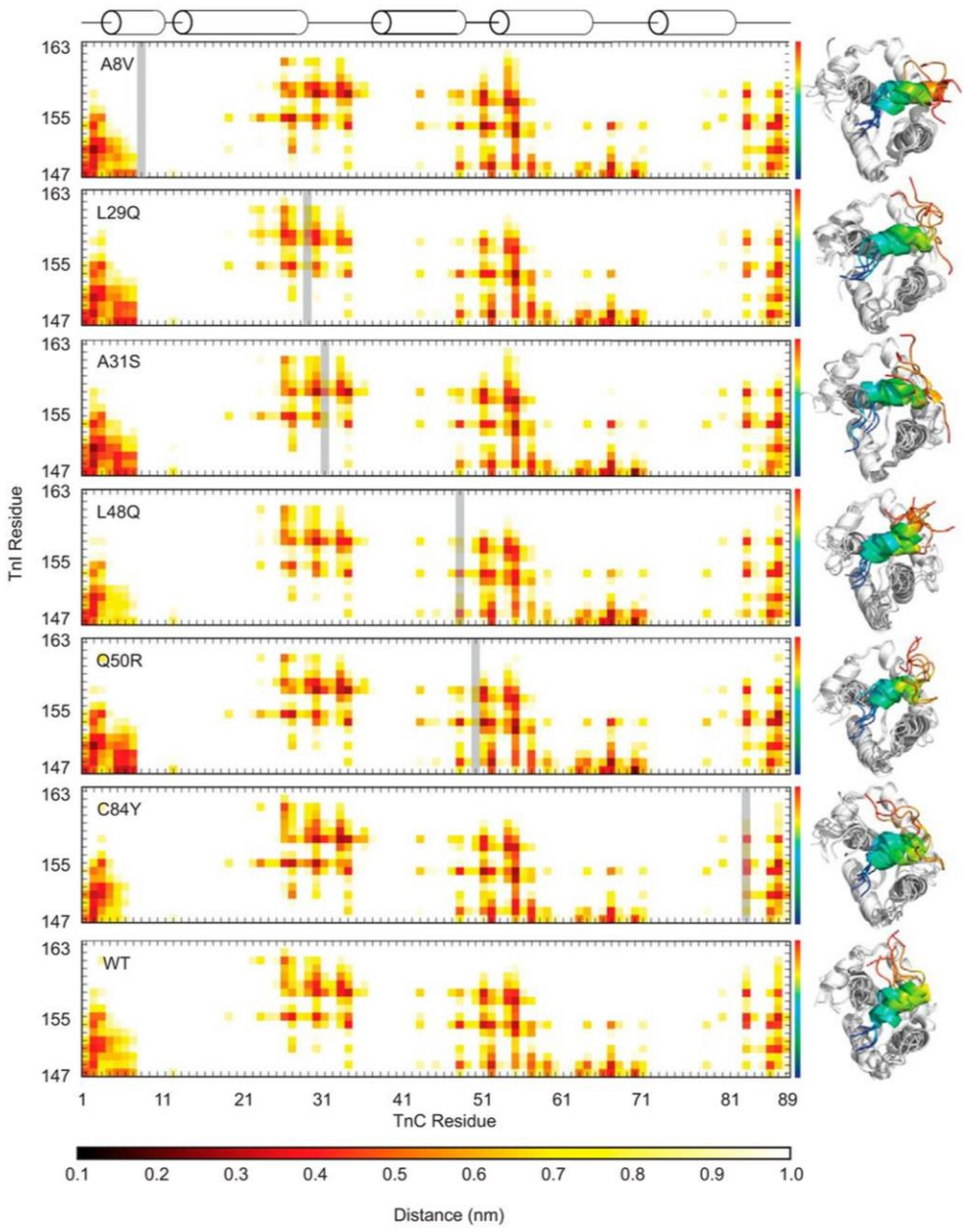

Figure 4-6 Average distance between cTnC and cTnI residues

The mutated TnC residue in each plot is indicated by a grey bar. The structures to the right are representative structures of independent simulations and indicate the differences in the orientation and variability of the $cTnI_{SW}$ peptide across replicates for each mutant. The TnI_{SW} is colored as a spectrum from blue at the N-terminus to red at the C-terminus. The calculated ΔG of interaction is maintained across mutations despite differences in the interaction distance profiles, which suggests a nonspecific interaction. The A31S mutant has a ΔG of interaction with the TnI_{SW} approximately 25% lower than WT (Table 4-2), perhaps due to shorter interaction distances with the N-terminal region of N-cTnC, but longer interaction distances in the vicinity of the A31S mutation and C-terminal portion of the TnI_{SW}.

4.4.5. Free Energy Calculations

The free energy change in Ca^{2+} binding, measured by potential of mean force (PMF) calculations (**Figure 4-7**) indicates that the highest free energy change was observed in the A8V construct (-72 ± 5 kJ*mol^{-1}), followed by Q50R (-41 ± 3 kJ*mol^{-1}) and C84Y (-46 ± 3 kJ*mol^{-1}), A31S (-46 ± 2 kJ*mol^{-1}) and L29Q (-46 ± 2 kJ*mol^{-1}), and finally L48Q (-32 ± 3 kJ*mol^{-1}) and WT (-32 ± 4 kJ*mol^{-1}). A representative structure from the 5 replicated 1 μs simulations of the A8V mutation yielded Ca^{2+} coordination distances that were similar to the other mutant constructs and a PMF derived Ca^{2+} interaction ΔG of 46 ± 5 kJ*mol^{-1}.

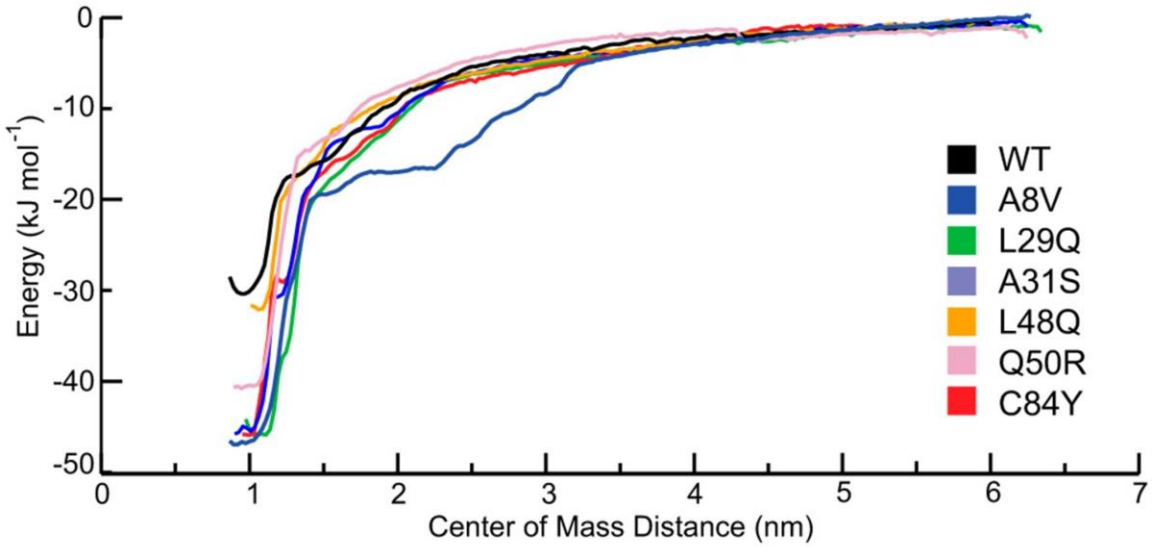

Figure 4-7 The potential of mean force profile of each of the mutated constructs as a function of center of mass distance between the TnC molecule and Ca^{2+} ion

Each of the mutated constructs has an increased ΔG of Ca^{2+} interaction. L48Q (-32 ± 3 kJ/mol) is the closest to WT (-32 ± 4 kJ*mol^{-1}), followed by Q50R (-41.3 ± 3 kJ*mol^{-1}), L29Q (-46 ± 2 kJ*mol^{-1}), C84Y (-46 ± 3 kJ*mol^{-1}), A31S (-46 ± 2 kJ*mol^{-1}), and A8V (-46 ± 5 kJ*mol^{-1}), which are similar to each other.

Interaction energies between TnC and the TnI_{SW} were estimated by Molecular Mechanics/Poisson Boltzmann Surface Area (MM/PBSA) calculations. The energies reported are much larger than could be reasonably expected, although this method has been used as a means to score the relative strength interactions with some success (Lindert, Cheng et al. 2015). The values are similar for each of the constructs, with the

exception of the A31S mutant, which has a weaker calculated binding interaction (**Table 4-2**).

Table 4-2 MM/PBSA results for the WT and mutant N-cTnC/TnI$_{SW}$ interaction

	Van der Waals	Electrostatic	Polar	sasa	Total
A8V	−3.0E2 ± 3.5E1	−1.7E3 ± 2.8E2	8.1E2 ± 2.3E2	−3.9E1 ± 3.2E0	−1.3E3 ± 1.2E2
L29Q	−3.2E2 ± 4.1E1	−2.0E3 ± 2.8E2	1.0E3 ± 2.7E2	−4.1E1 ± 4.7E0	−1.3E3 ± 6.3E1
A31S	−3.0E2 ± 6.4E1	−1.7E3 ± 2.9E2	1.1E3 ± 2.0E2	−3.9E1 ± 7.7E0	−9.6E2 ± 2.2E2
L48Q	−3.1E2 ± 5.2E1	−1.9E3 ± 2.6E2	1.0E3 ± 2.1E2	−4.0E1 ± 4.5E0	−1.3E3 ± 6.7E1
Q50R	−3.1E2 ± 2.7E1	−2.0E3 ± 1.8E2	1.1E3 ± 2.0E2	−4.1E1 ± 3.0E0	−1.2E3 ± 5.4E1
C84Y	−3.2E2 ± 3.9E1	−1.7E3 ± 2.2E2	8.4E2 ± 1.9E2	−4.0E1 ± 4.3E0	−1.2E3 ± 8.1E1
WT	−3.2E2 ± 2.6E1	−1.9E3 ± 2.8E2	1.0E3 ± 3.2E2	−4.1E1 ± 3.1E0	−1.2E3 ± 1.4E2

4.5. Discussion

The measurements described in this study have provided novel information about the molecular basis of N-cTnC function in the regulation of cardiac muscle contraction. Muscle contraction begins when N-cTnC binds to Ca^{2+}, opens, and interacts with TnI$_{SW}$. The cTnC molecule also interacts with the cardiac-specific N-terminal extension of TnI (Hwang, Cai et al. 2014), which responds to the phosphorylation of TnI residues 22 and 23 (Li, Stevens et al. 2013). In the presence of the Tn complex, the cTnC Ca^{2+} affinity increases by 10-fold over the isolated cTnC molecule. Improved affinity was attributed to the stabilized open conformation (Johnson, Collins et al. 1980, Pinto, Parvatiyar et al. 2009). Our hypothesis was that the Ca^{2+} sensitizing mutations would directly increase Ca^{2+} affinity of the isolated N-cTnC, while de-sensitizing mutations reduce the N-cTnC Ca^{2+} affinity. Mutations were hypothesized to affect TnC function through directly modifying Ca^{2+} coordination or modifying the energetic cost of the N-cTnC conformational change. Mutations in the Tn complex have been shown to modify Ca^{2+} affinity indirectly through altering the interaction between N-cTnC and the TnI$_{SW}$ (Johnson, Collins et al. 1980, Pinto, Parvatiyar et al. 2009). We have explored this

hypothesis through ITC measurements of Ca^{2+} affinity and MD simulations that: 1) assess the strength of the Ca^{2+} binding interaction, 2) describe the properties of the N-cTnC conformational change, and 3) measure the strength of the interaction between N-cTnC and TnI_{SW}.

It is challenging to directly measure the N-cTnC Ca^{2+} interaction. Fluorescence-based experiments employ reporters such as IAANS (Dong, Wang et al. 1997, Hazard, Kohout et al. 1998, Li, Stevens et al. 2013), or an F27W mutation (Gillis, Blumenschein et al. 2003). Upon titration with Ca^{2+}, the fluorophore reports the N-cTnC conformational change as a measure of N-cTnC Ca^{2+} affinity, while measurements made using stopped flow fluorospectroscopy report rates of Ca^{2+} dissociation (Tikunova, Liu et al. 2010). The K_d for WT TnC has been previously reported fluorometrically as 11.3 μM for WT N-cTnC, which was lowered to 8 μM with the L29Q mutation (Liang, Chung et al. 2008). Similarly, fluorescence titration of the N-cTnC/Ca^{2+} interaction yielded midpoint values of 12.3 μM for WT N-cTnC, 12.9 μM for A8V, and 37.2 μM for C84Y (Pinto, Parvatiyar et al. 2009). Our ITC experiments, which consider the unmodified N-cTnC molecule, demonstrated no statistically significant differences in K_d between WT and the FHC-associated mutants, with the exception of C84Y (**Table 1**). Our measurements of the DCM associated mutant Q50R and engineered Ca^{2+}-sensitizing mutation L48Q have shown a three-fold and ten-fold increase in affinity for Ca^{2+}, respectively. Our results agree with the previously reported K_d for full-length cTnC at 24 μM (Tikunova and Davis 2004), which decreased to 1.9 μM in the L48Q construct (Tikunova and Davis 2004). When compared to another ITC study of the WT N-cTnC/Ca^{2+} interaction, the ΔGs are approximately 3 $kJ*mol^{-1}$ lower (Skowronsky, Schroeter et al. 2013). Each of A31S, L48Q, Q50R, and C84Y, produce increased ΔH and decreased ΔS values relative to WT, although the molecular basis of these changes is not necessarily the same. The A31S mutation stabilizes the loop between helices A and B with a hydrogen bond, which accounts for changes in both ΔH and ΔS. The L48Q, Q50R and C84Y mutations are along the interface between the NAD and BC helical bundles, which likely reduces the entropic cost of the closed/open transition by introducing a polar residue into a hydrophobic region. Each of these substitutions also creates at least one new hydrogen bond that affects ΔH (**Figure 4-3**).

The increases in Ca^{2+} affinity of L48Q and Q50R N-cTnC were attributed to the reduced cost of exposing the hydrophobic patch. Our ITC experiments reported lower

ΔS values for these mutants (**Table 4-1**), associated with the exposure of hydrophobic residues. The changes in ΔS are consistent with our measurement of the A/B interhelical angle, as the molecule transitions into the open form; hydrophobic residues in the interface between the NAD helical bundle and the BC helical bundle are exposed. This has been demonstrated in another MD-based study of the L48Q and V44Q N-cTnC mutation (Kekenes-Huskey, Lindert et al. 2012). In the A31S mutation the ΔS value is lower than that of WT, perhaps due to the hydrogen bond formed by the serine, which reduces the mobility of the loop, a finding consistent with a previous exploration of A31S (Parvatiyar, Landstrom et al. 2012). The C84Y mutant disrupts the side-chain packing between C84 and several residues between helices C and D, and produces a more favorable open conformation (**Figure 4-3**). Despite the overall structural similarity of the mutant constructs, there are changes in side-chain packing due to each substitution compared to the WT model (**Figure 4-3**). The melting points were lower for the A8V and L48Q mutants, consistent with the observation that they spend the least time in the closed conformation. The hydrophobic interactions disrupted by these mutations play an important role in the stability of the N-TnC molecule (**Figure 4-5**).

Small-angle X-ray scattering (SAXS) has been used to investigate tertiary protein contacts in the apo and Ca^{2+}-bound states of the A8V and A31S mutants. Despite minimal structural changes in these mutants, this technique can be used to uncover potentially lower stability resulting from salient local changes in FHC mutants (Marques, Pinto et al. 2017).

The strengths of the charge-charge interactions that govern the direct Ca^{2+}/N-cTnC interaction are proportional to the distance between the Ca^{2+} ion and the coordinating oxygen atoms (**Table S4-2**). The PMF-derived ΔG of Ca^{2+} binding of the L48Q mutation was most similar to the WT protein, and the remaining mutations each yielded stronger Ca^{2+} interactions (**Figure 4-7**). Notably the A8V interaction was the strongest, and the Ca^{2+} coordination was the tightest in 100 ns simulations, however this was not found in the Potential of Mean Force (PMF) calculation based on the 1 μs simulation (**Figure 4-7**). The absolute values of the interaction energies are overestimated due to the parameterization of Ca^{2+} in the simulation; however, the results are useful as a relative measure of the change in free energy of binding (Li, Ngo et al. 2015).

In skeletal TnC, the affinity for Ca^{2+} is inversely related to protein stability. It is reasonable to assume that similar mechanisms govern the cardiac isoforms of this protein (Suarez, Machado et al. 2003). The affinity of N-cTnC for Ca^{2+} is set by a balance between the conformational strain induced by Ca^{2+} binding that is acting to open the N-cTnC molecule and the energetic cost of exposing a hydrophobic cleft (Gifford, Walsh et al. 2007). Introduction of a polar amino acid into the hydrophobic cleft reduces the cost of opening N-cTnC by destabilizing the closed conformation or stabilizing the open conformation (Tikunova, Rall et al. 2002). Ca^{2+} binding causes a change in the dynamic equilibrium of the populations of open and closed TnC molecules. When Ca^{2+} is bound, 20-27% of the N-cTnC population is open (McKay, Saltibus et al. 2000, Cordina, Liew et al. 2013). Previous MD simulations have estimated the ΔG of the WT cTnC open/closed transition at 33.5 $kJ*mol^{-1}$ (Lindert, Kekenes-Huskey et al. 2012). The N-cTnC conformational change necessarily precedes the TnI_{SW} interaction and therefore changes in the favorability of the conformational change are related to the probability of N-cTnC binding to the TnI_{SW} (Lindert, Kekenes-Huskey et al. 2012).

Monitoring the A/B interhelical angle through 1 μs simulations has revealed that mutations affect the conformational dynamics of N-cTnC (**Figure 4-5**). A previous study had defined the N-cTnC molecule as “open” with an AB interhelical angle <110º (Lindert, Kekenes-Huskey et al. 2012). We define a closed structure as any with an AB interhelical angle >130º, similar to the NMR structure of N-cTnC (Spyracopoulos, Li et al. 1997). This allows for the quantification of the relative stability of the closed state (**Figure 4-5**). The open conformation is found most frequently in simulations of the L48Q construct, followed by the A31S mutation. Work by Marques et al. shows that A31S may cause greater exposure in the primed state of the full length TnC (ie. when Ca^{2+} is bound to sites III/IV) (Marques, Pinto et al. 2017). A similar degree of openness was observed for the remaining constructs, a finding corroborated by the hydrophobic solvent accessible surface (h-sasa) (**Figure S4-3**). The L29Q mutant was the least open; interhelical angles below 115º were not observed, and had the highest closed probability. The closed state was least frequently observed in the A8V construct, which is consistent with paramagnetic NMR data that show that A8V cTnC opened more readily than WT N-cTnC (Cordina, Liew et al. 2013), and contribute to the increased affinity between A8V TnC and TnI_{SW} (Zot, Hasbun et al. 2016). These data suggest that

the molecular etiology is different for each mutation, despite producing a similar disease phenotype.

The ΔG of N-cTnC and TnI_{SW} interaction is similar to WT for each of the N-cTnC mutants with the exception of A31S, which is approximately 75% of the WT ΔG (**Table 4-2**). As with the PMF calculations, the ΔG values derived from MM/PBSA calculations provide insight into the relative strengths, but the absolute values are not expected to correspond to more computationally expensive calculations, or experimentally derived measurements (Lindert, Cheng et al. 2015). The A31S N-cTnC has a modified interface with TnI_{SW}, which favors closer interactions with the N-terminal region of TnC and longer distance interactions with remainder of N-cTnC, particularly in the vicinity of the mutation (**Figure 4-6**). Relative to WT, each mutant has a slightly different interaction with TnI_{SW}, but did not produce a change in interaction energy. We have previously observed a similar effect in the zebrafish TnC/TnI_{SW} interaction in which TnI substitution had a greater effect on the interaction than TnC substitution (Genge, Stevens et al. 2016). There is fluorescence-based evidence that each of the L48Q (Wang, Robertson et al. 2012) and A8V (Zot, Hasbun et al. 2016) N-cTnC mutations increase the affinity of N-cTnC for the TnI_{SW}, our results suggest that this affinity change may be due, in part, to the ability of these mutants to open more readily than WT which generates more opportunity for TnC-TnI interaction.

This work provides insight into how the dynamics of N-cTnC can govern the interactions with each of Ca^{2+} and cTnI, which in turn, influence sarcomeric Ca^{2+} sensitivity. The engineered L48Q mutation has the most salient effect on the N-cTnC ITC-derived Ca^{2+} binding and on the dynamics of the N-cTnC molecule. A finding that has been corroborated, experimentally (Tikunova and Davis 2004, Wang, Robertson et al. 2012), *in silico* (Kekenes-Huskey, Lindert et al. 2012) and *in vivo* (Davis, Davis et al. 2016, Shettigar, Zhang et al. 2016). The L48Q mutation has a large disruptive effect on the hydrophobic interactions that maintain N-cTnC in the closed conformation, which creates increased Ca^{2+} affinity through a modification of the thermodynamic landscape of the conformational change, and allows the TnI_{SW} to bind to N-cTnC more readily (Wang, Robertson et al. 2012). Through these molecular changes, the L48Q mutation can produce a positive inotropic effect, or with higher sarcomere incorporation and β-blocking drugs, can produce hypertrophy in murine models (Davis, Davis et al. 2016, Shettigar, Zhang et al. 2016). The L29Q mutation was similar to WT in each of our

measurements; However, L29Q has been shown to affect length-dependent activation and modify the response to phosphorylation of serine 22/23 of cTnI (Li, Stevens et al. 2013, Messer and Marston 2014, Robertson, Sevrieva et al. 2014, Robertson, Sevrieva et al. 2015). The A8V and C84Y mutations are near the interface with the N-helix of TnI (**Figure 4-1**), and may have a more pronounced effect on the orientation of N-cTnC in the Tn complex (Sevrieva, Knowles et al. 2014).

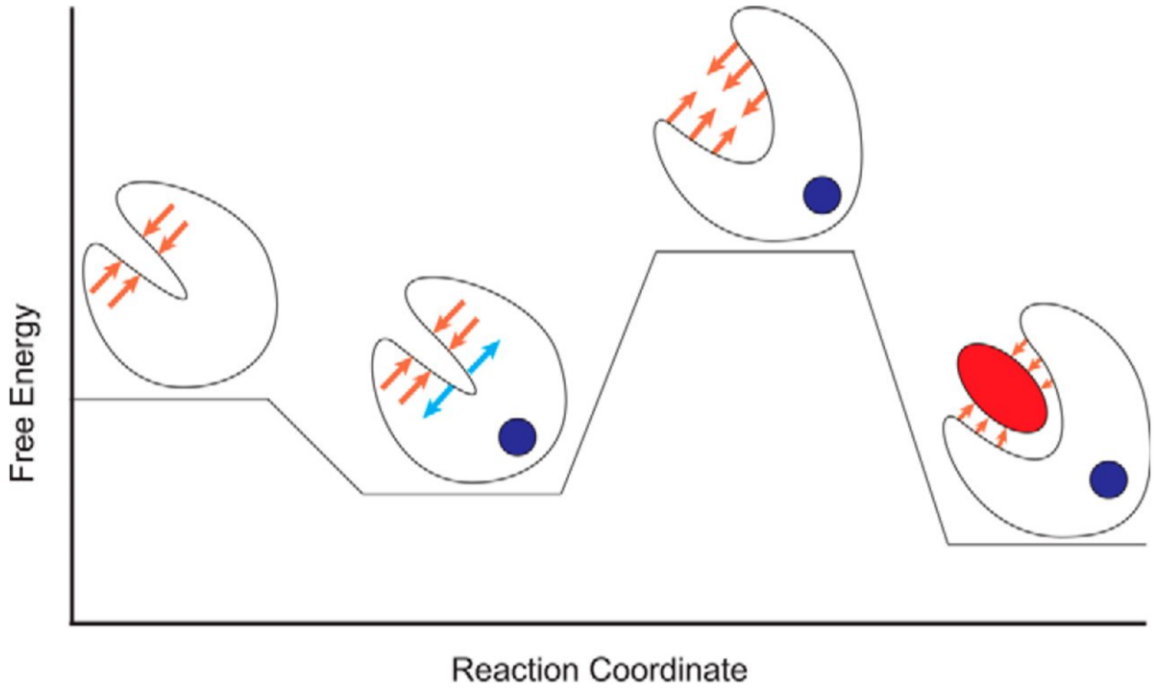

Figure 4-8 Schematic of the energetic landscape of N-cTnC activation
N-cTnC is shown as a cartoon, Ca^{2+} is a blue circle, and the TnI switch peptide is represented as a red ellipse. Lower energy states are more favorable. The orange arrows represent the resistance to the conformational change due to the hydrophobic cleft. Blue arrows indicate conformational strain introduced by Ca^{2+} binding. The Ca^{2+} bound, open conformation relieves the conformational strain, while occluding the hydrophobic cleft and is therefore the most favorable conformation. Mutations that affect the relative stabilities of these states will modify the probability of transitions between them and increase or decrease the Ca^{2+} sensitivity of the myofilament

Our results support the model for the molecular mechanism of Ca^{2+} binding which is dictated by the favorability of the conformational change and the stability of the TnI-TnC (Li and Hwang 2015) interaction. Mutations modify the structural dynamics of TnC, rather than the regulatory Ca^{2+} binding site. The changes are observed in the relative favorability of the protein conformations that transduce the contraction signal (**Figure 4-8**). This can increase Ca^{2+} sensitivity of contraction by destabilizing the closed conformation of N-cTnC, stabilizing the open conformation, or stabilizing the TnI_{SW}

interaction. These changes lead to an increase in the Ca^{2+} buffering capacity of the myofilament that may increase the duration of the Ca^{2+} transient, and is consistent with observations of the greater capacity of the Tn complex to bind Ca^{2+} than the isolated N-cTnC molecule (Johnson, Collins et al. 1980, Tikunova and Davis 2004, Davis, Norman et al. 2007). The complimentary use of MD, ITC, and fluorometric techniques provides detailed information about the molecular etiology of cTnC mutations. A complete understanding of the molecular and thermodynamic basis for myofilament Ca^{2+} sensitivity will inform the risk stratification of existing and novel FHC-associated mutations, the selection of appropriate therapeutics and enable rational drug development that specifically target or compensate for the unique deleterious effects of these disease mutations.

4.6. Supplementary Material

Supplemental Table 4-1 Dimensions and composition of the simulated systems

		100 ns (Ca^{2+}-bound)	PMF Simulations	100 ns (TnC+Ca^{2+}+TnI_{sw})	1 microsecond (Ca^{2+} Bound)
WT	Box Dimensions (nm)	6 x 6 x 6	15 x 6 x 6	7.65 x 7.65 x 7.65	6 x 6 x 6
	K^+ Ions	14	13	11	14
	Cl^- Ions	1	0	0	1
	Ca^{2+} Ions	1	1	1	1
	Water Atoms	20077	52044	39891	20077
A8V	Box Dimensions (nm)	6 x 6 x 6	15 x 6 x 6	7.65 x 7.65 x 7.65	6 x 6 x 6
	K^+ Ions	14	13	11	14
	Cl^- Ions	1	0	0	1
	Ca^{2+} Ions	1	1	1	1
	Water Atoms	20031	52023	39882	20031
L29Q	Box Dimensions (nm)	6 x 6 x 6	15 x 6 x 6	7.65 x 7.65 x 7.65	6 x 6 x 6
	K^+ Ions	14	13	11	14
	Cl^- Ions	1	0	0	1
	Ca^{2+} Ions	1	1	1	1
	Water Atoms	20043	52038	39885	20043
A31S	Box Dimensions (nm)	6 x 6 x 6	15 x 6 x 6	7.65 x 7.65 x 7.65	6 x 6 x 6
	K^+ Ions	14	13	11	14
	Cl^- Ions	1	0	0	1
	Ca^{2+} Ions	1	1	1	1
	Water Atoms	20034	52029	39894	20034
L48Q	Box Dimensions (nm)	6 x 6 x 6	15 x 6 x 6	7.65 x 7.65 x 7.65	6 x 6 x 6
	K^+ Ions	14	13	11	14
	Cl^- Ions	1	0	0	1
	Ca^{2+} Ions	1	1	1	1
	Water Atoms	20034	52041	39894	20034
Q50R	Box Dimensions (nm)	6 x 6 x 6	15 x 6 x 6	7.65 x 7.65 x 7.65	6 x 6 x 6
	K^+ Ions	14	13	11	14
	Cl^- Ions	1	0	0	1
	$Ca2^+$ Ions	1	1	1	1
	Water Atoms	20040	52032	39891	20040
C84Y	Box Dimensions (nm)	6 x 6 x 6	15 x 6 x 6	7.65 x 7.65 x 7.65	6 x 6 x 6
	K^+ Ions	14	13	11	14
	Cl^- Ions	1	0	0	1
	Ca^{2+} Ions	1	1	1	1
	Water Atoms	20022	52020	39876	20022

Supplemental Table 4-2 Melting Temperatures of APO TnC constructs

Construct	WT	A8V	L29Q	A31S	L48Q	Q50R	C84Y
Melt Temp (°C)	64	58.5	65	65	42.5	65.5	64.5

Supplemental Table 4-3 MD derived Ca^{2+} Coordination Distances (Å). Distances are the average of 5 replicated 100 ns simulations.

	WT	A8V	L29Q	A31S	L48Q	Q50R	C84Y
Ca-65ASP-OD1	3.4 ± 0.3	2.26 ± 0.2	2.99 ± 0.4	2.92 ± 0.3	3.07 ± 0.3	3.94 ± 0.5	2.89 ± 0.3
Ca-65ASP-OD2	2.96 ± 0.3	3.03 ± 0.2	3.13 ± 0.2	3.58 ± 0.3	3.25 ± 0.3	3.94 ± 0.4	3.86 ± 0.3
Ca-66GLU-OE1	8.58 ± 0.5	6.86 ± 0.3	8.56 ± 0.8	8.97 ± 0.5	8.67 ± 0.4	8.19 ± 0.5	8.09 ± 0.5
Ca-66GLU-OE2	8.59 ± 0.4	6.86 ± 0.3	8.57 ± 0.8	8.95 ± 0.5	8.67 ± 0.4	8.1 ± 0.6	8.08 ± 0.5
Ca-67ASP-OD1	2.8 ± 0.2	2.44 ± 0.2	2.81 ± 0.3	2.98 ± 0.3	3.17 ± 0.2	3.33 ± 0.3	4.15 ± 0.3
Ca-67ASP-OD2	2.94 ± 0.2	2.3 ± 0.2	2.63 ± 0.3	2.72 ± 0.1	2.7 ± 0.1	3.45 ± 0.5	4.14 ± 0.3
Ca-69SER-OG	4.42 ± 0.3	3.29 ± 0.3	3.98 ± 0.5	4.35 ± 0.7	4.74 ± 0.4	4.91 ± 0.5	5.8 ± 0.6
Ca-69SER-O	6.96 ± 0.3	5.44 ± 0.2	6.71 ± 0.6	7.05 ± 0.4	7.23 ± 0.2	7.49 ± 0.3	7.59 ± 0.3
Ca-71THR-OG1	5.57 ± 0.3	3.96 ± 0.2	4.8 ± 0.4	5.07 ± 0.3	5.47 ± 0.3	5.11 ± 0.3	4.95 ± 0.2
Ca-71THR-O	3.36 ± 0.3	2.2 ± 0.1	2.75 ± 0.2	2.85 ± 0.2	3.18 ± 0.1	3.14 ± 0.2	2.79 ± 0.2
Ca-73ASP-OD1	4.73 ± 0.5	3.46 ± 0.3	4.63 ± 0.7	4.7 ± 0.7	5.43 ± 0.6	4.89 ± 1.0	3.65 ± 0.5
Ca-73ASP-OD2	4.19 ± 0.5	3.36 ± 0.7	4.6 ± 0.6	4.19 ± 0.3	5.85 ± 0.5	4.59 ± 1.1	3.77 ± 0.4
Ca-76GLU-OE1	2.68 ± 0.1	2.14 ± 0.1	2.59 ± 0.2	2.7 ± 0.1	2.67 ± 0.1	2.67 ± 0.1	2.63 ± 0.1
Ca-76GLU-OE2	2.7 ± 0.1	2.12 ± 0.1	2.54 ± 0.2	2.7 ± 0.1	2.67 ± 0.1	2.71 ± 0.1	2.68 ± 0.1

Supplemental Table 4-4 Simulation-derived properties of WT cTnC and mutant constructs

	WT	A8V	L29Q	A31S	L48Q	Q50R	C84Y
Average h-sasa TnC+Ca (Closed) (nm^2)	22.6 ± 0.3	22.6 ± 0.4	22.9 ± 0.4	22.3 ± 0.5	22.7 ± 0.6	22.5 ± 0.2	22.5 ± 0.4
Average h-sasa TnC+Ca (Open) (nm^2)	25.3 ± 0.7	24.8 ± 0.5	25.4±0.6	25.0 ± 0.6	25.6 ± 0.3	25.4 ± 0.3	25.5 ± 0.4
Number of H-bonds (Closed)	58.5±0.9	59.5 ± 1.7	58.9 ± 1.5	59.5 ± 1.4	59.7 ± 0.9	60.6 ± 2.0	60.6 ± 1.6

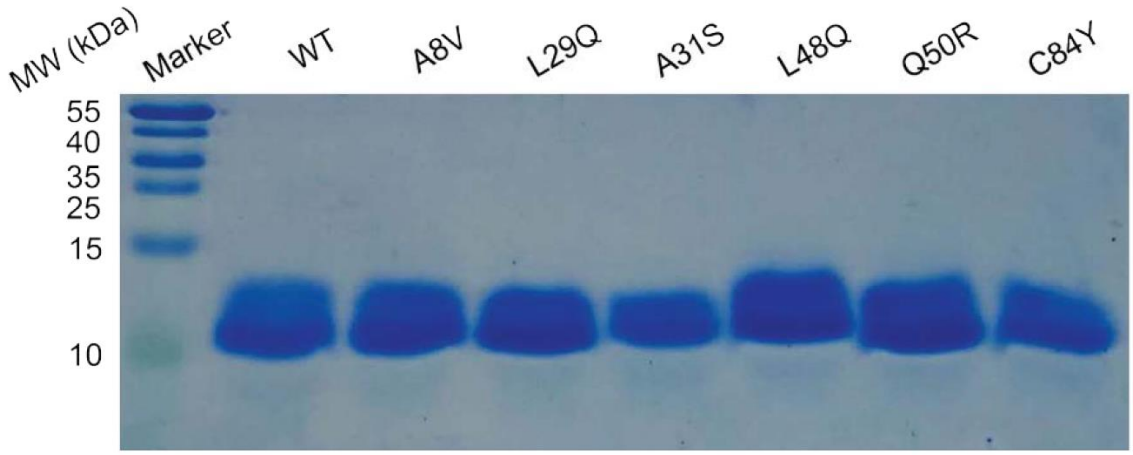

Supplemental Figure 4-1 SDS PAGE of the N-cTnC constructs used in ITC.
Each sample of WT and mutant N-cTnC samples was pure, free of degraded protein and ran at ~10.1 kDa.

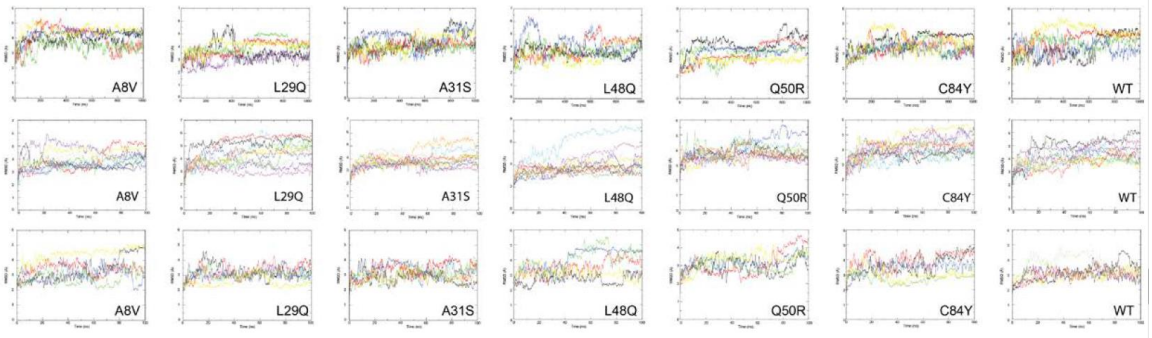

Supplemental Figure 4-2 RMSD as a function of time for 1 µs and 100 ns simulations of TnC+Ca^{2+}, and 100 ns of TnC+Ca^{2+}+TnI_{SW} for each mutant construct.
These indicate that each of the simulations has diverged substantially from the starting coordinates. Plots are a running average over 0.5% of the total number of data points.

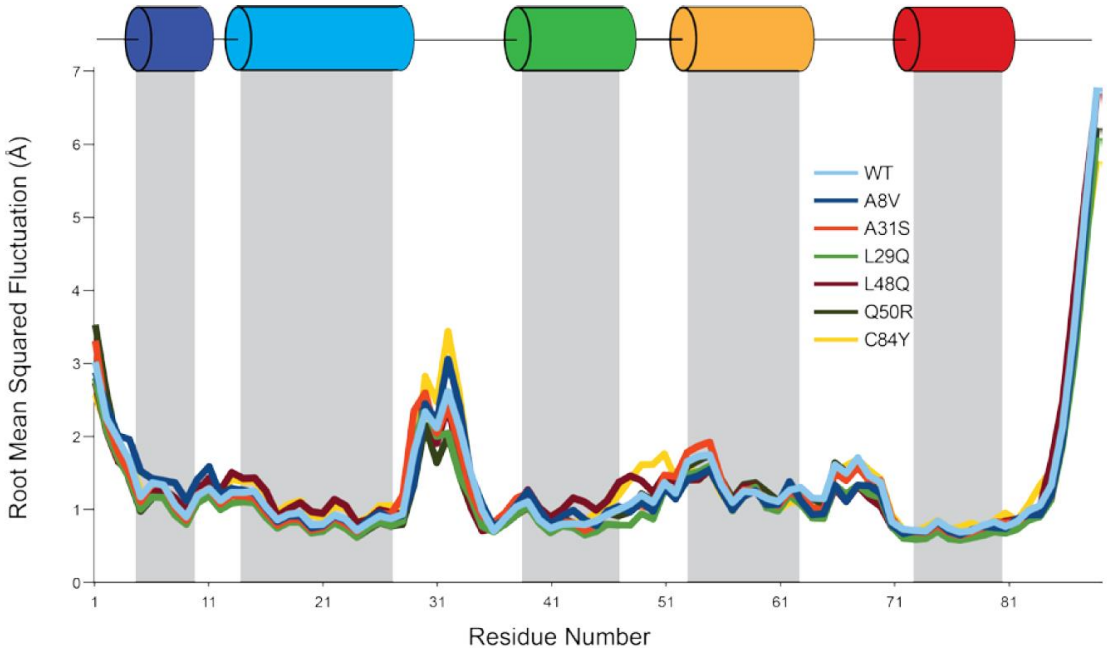

Supplemental Figure 4-3 Root mean squared fluctuations (RMSF) plotted by residue for the models of WT NcTnC and each of the mutated constructs from 100 ns simulations.

The local flexibility is similar for each for these constructs and is highest at the termini and loop regions between helices A and B.

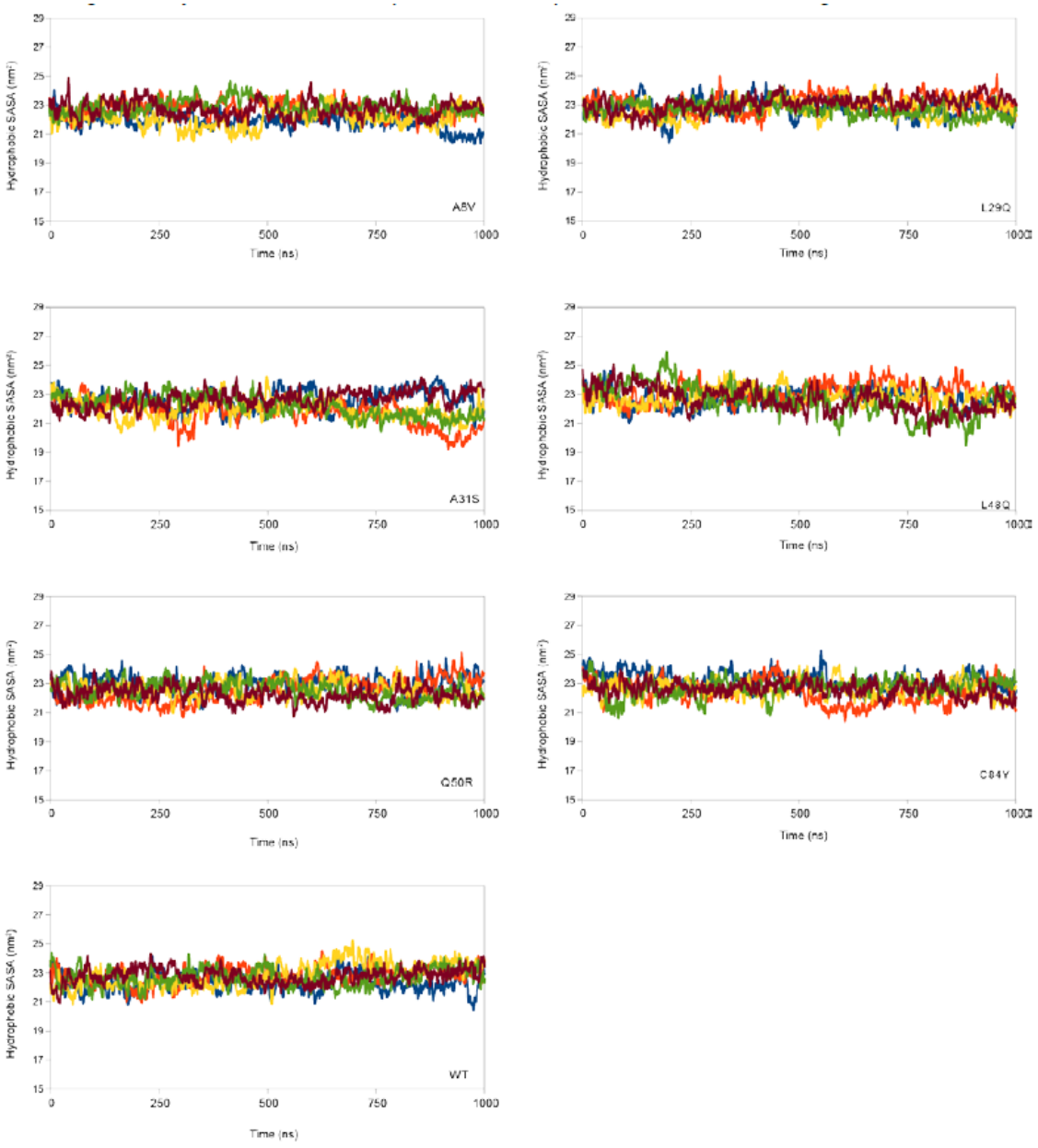

Supplemental Figure 4-4 Hydrophobic solvent accessible surface area plotted as a function of time for 5 replicated simulations for models of WT NcTnC and each of the mutated constructs.

Plots are a rolling average of 250 ps. There is little difference between WT and most of the constructs, with the exception of L48Q and A31S.

4.7. References

Berendsen, H. J. C., J. P. M. Postma, W. F. v. Gunsteren, A. DiNola and J. R. Haak (1984). "Molecular dynamics with coupling to an external bath." The Journal of Chemical Physics **81**(8): 3684-3690.

Bers, D. M. (2000). "Calcium Fluxes Involved in Control of Cardiac Myocyte Contraction." Circulation Research **87**(4): 275-281.

Bordoli, L. and T. Schwede (2012). "Automated protein structure modeling with SWISS-MODEL Workspace and the Protein Model Portal." Methods Mol Biol **857**: 107-136.

Bussi, G., D. Donadio and M. Parrinello (2007). "Canonical sampling through velocity rescaling." J Chem Phys **126**(1): 014101.

Cerutti, D. S., R. E. Duke, T. A. Darden and T. P. Lybrand (2009). "Staggered Mesh Ewald: An extension of the Smooth Particle-Mesh Ewald method adding great versatility." J Chem Theory Comput **5**(9): 2322.

Cordina, N. M., C. K. Liew, D. A. Gell, P. G. Fajer, J. P. Mackay and L. J. Brown (2013). "Effects of Calcium Binding and the Hypertrophic Cardiomyopathy A8V Mutation on the Dynamic Equilibrium between Closed and Open Conformations of the Regulatory N-Domain of Isolated Cardiac Troponin C." Biochemistry **52**(11): 1950-1962.

Daura, X., K. Gademann, B. Jaun, D. Seebach, W. F. van Gunsteren and A. E. Mark (1999). "Peptide Folding: When Simulation Meets Experiment." Angewandte Chemie International Edition **38**(1-2): 236-240.

Davis, J., L. C. Davis, R. N. Correll, C. A. Makarewich, J. A. Schwanekamp, F. Moussavi-Harami, D. Wang, A. J. York, H. Wu and S. R. Houser (2016). "A tension-based model distinguishes hypertrophic versus dilated cardiomyopathy." Cell **165**(5): 1147-1159.

Davis, J. P., C. Norman, T. Kobayashi, R. J. Solaro, D. R. Swartz and S. B. Tikunova (2007). "Effects of thin and thick filament proteins on calcium binding and exchange with cardiac troponin C." Biophysical journal **92**(9): 3195-3206.

Dewan, S., K. J. McCabe, M. Regnier, A. D. McCulloch and S. Lindert (2016). "Molecular Effects of cTnC DCM Mutations on Calcium Sensitivity and Myofilament Activation-An Integrated Multiscale Modeling Study." J Phys Chem B **120**(33): 8264-8275.

Dong, W.-J., C.-K. Wang, A. M. Gordon and H. C. Cheung (1997). "Disparate Fluorescence Properties of 2-[4′-(Iodoacetamido)anilino]-Naphthalene-6-Sulfonic Acid Attached to Cys-84 and Cys-35 of Troponin C in Cardiac Muscle Troponin." Biophysical Journal **72**(2, Part 1): 850-857.

Eisenhaber, F., P. Lijnzaad, P. Argos, C. Sander and M. Scharf (1995). "The double cubic lattice method: Efficient approaches to numerical integration of surface area and volume and to dot surface contouring of molecular assemblies." Journal of Computational Chemistry **16**(3): 273-284.

Feest, E. R., F. Steven Korte, A. Y. Tu, J. Dai, M. V. Razumova, C. E. Murry and M. Regnier (2014). "Thin filament incorporation of an engineered cardiac troponin C variant (L48Q) enhances contractility in intact cardiomyocytes from healthy and infarcted hearts." J Mol Cell Cardiol **72**: 219-227.

Genge, C. E., C. M. Stevens, W. S. Davidson, G. Singh, D. Peter Tieleman and G. F. Tibbits (2016). "Functional divergence in teleost cardiac troponin paralogs guides variation in the interaction of TnI switch region with TnC." Genome biology and evolution **8**(4): 994-1011.

Gifford, Jessica L., Michael P. Walsh and Hans J. Vogel (2007). "Structures and metal-ion-binding properties of the Ca²⁺-binding helix–loop–helix EF-hand motifs." Biochemical Journal **405**(2): 199-221.

Gillis, T. E., T. M. Blumenschein, B. D. Sykes and G. F. Tibbits (2003). "Effect of temperature and the F27W mutation on the Ca2+ activated structural transition of trout cardiac troponin C." Biochemistry **42**(21): 6418-6426.

Gillis, T. E., C. R. Marshall and G. F. Tibbits (2007). "Functional and evolutionary relationships of troponin C." Physiol Genomics **32**(1): 16-27.

Harada, K. and S. Morimoto (2004). "Inherited cardiomyopathies as a troponin disease." Jpn J Physiol **54**(4): 307-318.

Hazard, A. L., S. C. Kohout, N. L. Stricker, J. A. Putkey and J. J. Falke (1998). "The kinetic cycle of cardiac troponin C: calcium binding and dissociation at site II trigger slow conformational rearrangements." Protein Science **7**(11): 2451-2459.

Hess, B., H. Bekker, H. J. C. Berendsen and J. G. E. M. Fraaije (1997). "LINCS: A linear constraint solver for molecular simulations." Journal of Computational Chemistry **18**(12): 1463-1472.

Hoffmann, B., H. Schmidt-Traub, A. Perrot, K. J. Osterziel and R. Gessner (2001). "First mutation in cardiac troponin C, L29Q, in a patient with hypertrophic cardiomyopathy." Hum Mutat **17**(6): 524.

Hub, J. S., B. L. de Groot and D. van der Spoel (2010). "g_wham—A Free Weighted Histogram Analysis Implementation Including Robust Error and Autocorrelation Estimates." Journal of Chemical Theory and Computation **6**(12): 3713-3720.

Hwang, P. M., F. Cai, S. E. Pineda-Sanabria, D. C. Corson and B. D. Sykes (2014). "The cardiac-specific N-terminal region of troponin I positions the regulatory domain of troponin C." Proceedings of the National Academy of Sciences **111**(40): 14412-14417.

Johnson, J. D., J. H. Collins, S. P. Robertson and J. D. Potter (1980). "A fluorescent probe study of Ca2+ binding to the Ca2+-specific sites of cardiac troponin and troponin C." Journal of Biological Chemistry **255**(20): 9635-9640.

Kekenes-Huskey, P. M., S. Lindert and J. A. McCammon (2012). "Molecular basis of calcium-sensitizing and desensitizing mutations of the human cardiac troponin C regulatory domain: a multi-scale simulation study." PLoS Comput Biol **8**(11): e1002777.

Kirschenlohr, H. L., A. A. Grace, J. I. Vandenberg, J. C. Metcalfe and G. A. Smith (2000). "Estimation of systolic and diastolic free intracellular Ca2+ by titration of Ca2+ buffering in the ferret heart." Biochem J **346 Pt 2**: 385-391.

Kumari, R., R. Kumar and A. Lynn (2014). "g_mmpbsa--a GROMACS tool for high-throughput MM-PBSA calculations." J Chem Inf Model **54**(7): 1951-1962.

Landstrom, A. P., M. S. Parvatiyar, J. R. Pinto, M. L. Marquardt, J. M. Bos, D. J. Tester, S. R. Ommen, J. D. Potter and M. J. Ackerman (2008). "Molecular and functional characterization of novel hypertrophic cardiomyopathy susceptibility mutations in TNNC1-encoded troponin C." Journal of molecular and cellular cardiology **45**(2): 281-288.

Li, A. Y., C. M. Stevens, B. Liang, K. Rayani, S. Little, J. Davis and G. F. Tibbits (2013). "Familial hypertrophic cardiomyopathy related cardiac troponin C L29Q mutation alters length-dependent activation and functional effects of phosphomimetic troponin I*."

Li, H., V. Ngo, M. C. Da Silva, D. R. Salahub, K. Callahan, B. Roux and S. Y. Noskov (2015). "Representation of Ion–Protein Interactions Using the Drude Polarizable Force-Field." The Journal of Physical Chemistry B **119**(29): 9401-9416.

Li, M. X. and P. M. Hwang (2015). "Structure and function of cardiac troponin C (TNNC1): Implications for heart failure, cardiomyopathies, and troponin modulating drugs." Gene **571**(2): 153-166.

Li, M. X., L. Spyracopoulos and B. D. Sykes (1999). "Binding of Cardiac Troponin-I147-163 Induces a Structural Opening in Human Cardiac Troponin-C." Biochemistry **38**(26): 8289-8298.

Liang, B., F. Chung, Y. Qu, D. Pavlov, T. E. Gillis, S. B. Tikunova, J. P. Davis and G. F. Tibbits (2008). "Familial hypertrophic cardiomyopathy-related cardiac troponin C mutation L29Q affects Ca2+ binding and myofilament contractility." Physiological genomics **33**(2): 257-266.

Liang, B., F. Chung, Y. Qu, D. Pavlov, T. E. Gillis, S. B. Tikunova, J. P. Davis and G. F. Tibbits (2008). "Familial hypertrophic cardiomyopathy-related cardiac troponin C mutation L29Q affects Ca2+ binding and myofilament contractility." Physiol Genomics **33**(2): 257-266.

Lindert, S., Y. Cheng, P. Kekenes-Huskey, M. Regnier and J. A. McCammon (2015). "Effects of HCM cTnI mutation R145G on troponin structure and modulation by PKA phosphorylation elucidated by molecular dynamics simulations." Biophys J **108**(2): 395-407.

Lindert, S., P. M. Kekenes-Huskey, G. Huber, L. Pierce and J. A. McCammon (2012). "Dynamics and calcium association to the N-terminal regulatory domain of human cardiac troponin C: a multiscale computational study." The Journal of Physical Chemistry B **116**(29): 8449-8459.

Lindorff-Larsen, K., S. Piana, K. Palmo, P. Maragakis, J. L. Klepeis, R. O. Dror and D. E. Shaw (2010). "Improved side-chain torsion potentials for the Amber ff99SB protein force field." Proteins **78**(8): 1950-1958.

Mahoney, M. W. and W. L. Jorgensen (2000). "A five-site model for liquid water and the reproduction of the density anomaly by rigid, nonpolarizable potential functions." The Journal of Chemical Physics **112**(20): 8910-8922.

Maron, B. J., J. Shirani, L. C. Poliac, R. Mathenge, W. C. Roberts and F. O. Mueller (1996). "Sudden death in young competitive athletes: clinical, demographic, and pathological profiles." JAMA **276**(3): 199-204.

Marques, M. d. A., J. R. Pinto, A. H. Moraes, A. Iqbal, M. T. de Magalhães, J. Monteiro, M. M. Pedrote, M. M. Sorenson, J. L. Silva and G. A. de Oliveira (2017). "Allosteric transmission along a loosely structured backbone allows a cardiac Troponin C mutant to function with only one Ca2+ ion." Journal of Biological Chemistry: jbc. M116. 765362.

Martins, A. S., M. S. Parvatiyar, H. Z. Feng, J. M. Bos, D. Gonzalez-Martinez, M. Vukmirovic, R. S. Turna, M. A. Sanchez-Gonzalez, C. D. Badger, D. A. R. Zorio, R. K. Singh, Y. Wang, J. P. Jin, M. J. Ackerman and J. R. Pinto (2015). "In Vivo Analysis of Troponin C Knock-In (A8V) Mice: Evidence that TNNC1 Is a Hypertrophic Cardiomyopathy Susceptibility Gene." Circ Cardiovasc Genet **8**(5): 653-664.

McKay, R. T., L. F. Saltibus, M. X. Li and B. D. Sykes (2000). "Energetics of the Induced Structural Change in a Ca2+ Regulatory Protein: Ca2+ and Troponin I Peptide Binding to the E41A Mutant of the N-Domain of Skeletal Troponin C." Biochemistry **39**(41): 12731-12738.

Messer, A. E. and S. B. Marston (2014). "Investigating the role of uncoupling of troponin I phosphorylation from changes in myofibrillar Ca2+-sensitivity in the pathogenesis of cardiomyopathy." Frontiers in physiology **5**: 315.

Páll, S. and B. Hess (2013). "A flexible algorithm for calculating pair interactions on SIMD architectures." Computer Physics Communications **184**(12): 2641-2650.

Parmacek, M. S. and R. J. Solaro (2004). "Biology of the troponin complex in cardiac myocytes." Prog Cardiovasc Dis **47**(3): 159-176.

Parvatiyar, M. S., A. P. Landstrom, C. Figueiredo-Freitas, J. D. Potter, M. J. Ackerman and J. R. Pinto (2012). "A mutation in TNNC1-encoded cardiac troponin C, TNNC1-A31S, predisposes to hypertrophic cardiomyopathy and ventricular fibrillation." Journal of Biological Chemistry **287**(38): 31845-31855.

Pinto, J. R., M. S. Parvatiyar, M. A. Jones, J. Liang, M. J. Ackerman and J. D. Potter (2009). "A functional and structural study of troponin C mutations related to hypertrophic cardiomyopathy." J Biol Chem **284**(28): 19090-19100.

Pronk, S., S. Pall, R. Schulz, P. Larsson, P. Bjelkmar, R. Apostolov, M. R. Shirts, J. C. Smith, P. M. Kasson, D. van der Spoel, B. Hess and E. Lindahl (2013). "GROMACS 4.5: a high-throughput and highly parallel open source molecular simulation toolkit." Bioinformatics **29**(7): 845-854.

Robertson, I. M., I. Sevrieva, M. X. Li, M. Irving, Y.-B. Sun and B. D. Sykes (2014). "In Vitro and in Situ Structure and Function of the Cardiac Troponin C Familial Hypertrophic Cardiomyopathy-Linked Mutation, L29Q." Biophysical Journal **106**(2): 723a-724a.

Robertson, I. M., I. Sevrieva, M. X. Li, M. Irving, Y. B. Sun and B. D. Sykes (2015). "The structural and functional effects of the familial hypertrophic cardiomyopathy-linked cardiac troponin C mutation, L29Q." J Mol Cell Cardiol **87**: 257-269.

Schlecht, W., K. L. Li, D. Hu and W. Dong (2016). "Fluorescence Based Characterization of Calcium Sensitizer Action on the Troponin Complex." Chem Biol Drug Des **87**(2): 171-181.

Schmidtmann, A., C. Lindow, S. Villard, A. Heuser, A. Mügge, R. Geßner, C. Granier and K. Jaquet (2005). "Cardiac troponin C-L29Q, related to hypertrophic cardiomyopathy, hinders the transduction of the protein kinase A dependent phosphorylation signal from cardiac troponin I to C." FEBS Journal **272**(23): 6087-6097.

Seidman, C. E. and J. G. Seidman (2011). "Identifying sarcomere gene mutations in hypertrophic cardiomyopathy: a personal history." Circ Res **108**(6): 743-750.

Semsarian, C., J. Ingles, M. S. Maron and B. J. Maron (2015). "New perspectives on the prevalence of hypertrophic cardiomyopathy." Journal of the American College of Cardiology **65**(12): 1249-1254.

Sevrieva, I., A. C. Knowles, T. Kampourakis and Y. B. Sun (2014). "Regulatory domain of troponin moves dynamically during activation of cardiac muscle." J Mol Cell Cardiol **75**: 181-187.

Shettigar, V., B. Zhang, S. C. Little, H. E. Salhi, B. J. Hansen, N. Li, J. Zhang, S. R. Roof, H. T. Ho, L. Brunello, J. K. Lerch, N. Weisleder, V. V. Fedorov, F. Accornero, J. A. Rafael-Fortney, S. Gyorke, P. M. Janssen, B. J. Biesiadecki, M. T. Ziolo and J. P. Davis (2016). "Rationally engineered Troponin C modulates in vivo cardiac function and performance in health and disease." Nat Commun **7**: 10794.

Skowronsky, R. A., M. Schroeter, T. Baxley, Y. Li, J. M. Chalovich and A. M. Spuches (2013). "Thermodynamics and molecular dynamics simulations of calcium binding to the regulatory site of human cardiac troponin C: evidence for communication with the structural calcium binding sites." JBIC Journal of Biological Inorganic Chemistry **18**(1): 49-58.

Spyracopoulos, L., M. X. Li, S. K. Sia, S. M. Gagné, M. Chandra, R. J. Solaro and B. D. Sykes (1997). "Calcium-induced structural transition in the regulatory domain of human cardiac troponin C." Biochemistry **36**(40): 12138-12146.

Stevens, C. M., K. Rayani, C. E. Genge, G. Singh, B. Liang, J. M. Roller, C. Li, A. Y. Li, D. P. Tieleman and F. van Petegem (2016). "Characterization of Zebrafish Cardiac and Slow Skeletal Troponin C Paralogs by MD Simulation and ITC." Biophysical Journal **111**(1): 38-49.

Suarez, M. C., C. J. V. Machado, L. M. T. Lima, L. B. Smillie, J. R. Pearlstone, J. L. Silva, M. M. Sorenson and D. Foguel (2003). "Role of hydration in the closed-to-open transition involved in Ca2+ binding by troponin C." Biochemistry **42**(18): 5522-5530.

Takeda, S., A. Yamashita, K. Maeda and Y. Maéda (2003). "Structure of the core domain of human cardiac troponin in the Ca2+-saturated form." Nature **424**(6944): 35-41.

Tikunova, S. B. and J. P. Davis (2004). "Designing calcium-sensitizing mutations in the regulatory domain of cardiac troponin C." Journal of Biological Chemistry **279**(34): 35341-35352.

Tikunova, S. B., B. Liu, N. Swindle, S. C. Little, A. V. Gomes, D. R. Swartz and J. P. Davis (2010). "Effect of calcium-sensitizing mutations on calcium binding and exchange with troponin C in increasingly complex biochemical systems." Biochemistry **49**(9): 1975-1984.

Tikunova, S. B., J. A. Rall and J. P. Davis (2002). "Effect of hydrophobic residue substitutions with glutamine on Ca2+ binding and exchange with the N-domain of troponin C." Biochemistry **41**(21): 6697-6705.

van Spaendonck-Zwarts, K. Y., J. P. van Tintelen, D. J. van Veldhuisen, R. van der Werf, J. D. Jongbloed, W. J. Paulus, D. Dooijes and M. P. van den Berg (2010). "Peripartum cardiomyopathy as a part of familial dilated cardiomyopathy." Circulation **121**(20): 2169-2175.

Wang, D., I. M. Robertson, M. X. Li, M. E. McCully, M. L. Crane, Z. Luo, A.-Y. Tu, V. Daggett, B. D. Sykes and M. Regnier (2012). "Structural and functional consequences of the cardiac troponin C L48Q Ca2+-sensitizing mutation." Biochemistry **51**(22): 4473-4487.

Zhang, X. L., G. F. Tibbits and M. Paetzel (2013). "The structure of cardiac troponin C regulatory domain with bound Cd2+ reveals a closed conformation and unique ion coordination." Acta Crystallographica Section D: Biological Crystallography **69**(5): 722-734.

Zot, H. G., J. E. Hasbun, C. A. Michell, M. Landim-Vieira and J. R. Pinto (2016). "Enhanced troponin I binding explains the functional changes produced by the hypertrophic cardiomyopathy mutation A8V of cardiac troponin C." Arch Biochem Biophys **601**: 97-104.

Chapter 5.

Binding of Calcium and Magnesium to Cardiac Troponin C Assessed Through Isothermal Titration Calorimetry

My contributions to this publication included design, implementation, and analysis of the ITC experiments, as well as manuscript preparation. The Simulations contained herein and the text pertaining to this work was prepared by Justin T. Seffernick under the guidance of Dr. Steffen Lindert.

5.1. Abstract

Cardiac troponin C (cTnC) is the calcium (Ca^{2+}) sensing component of the cardiac contractile apparatus. Binding of Ca^{2+} or magnesium (Mg^{2+}) to sites III and IV in the C-terminal domain of cTnC tethers this molecule to the rest of the thin filament. The dissociation constant (K_d) associated with binding of Ca^{2+} (~10^{-7} M) is 3 orders of magnitude lower than that of Mg^{2+} (~10^{-4} M). In the N-terminal domain, site II (~10^{-5} M) is unbound at $[Ca^{2+}]_{diastolic}$ (~0.1 µM) and subsequently bound at $[Ca^{2+}]_{systolic}$ (~0.6 - 1.2 µM). This interaction acts as a switch to initiate a series of conformational changes that culminate in force production within the myocardium.

We have utilized isothermal titration calorimetry (ITC) to determine the thermodynamics of the interaction between Ca^{2+} and N-terminal cTnC (K_d = 15.2 ± 0.5 µM). Mg^{2+} was not previously thought to bind to the N-terminus of cTnC, however these data strongly suggest that physiologically relevant concentrations of this divalent cation bind to site II (K_d = 652.8 ± 28.45 µM). Pre-incubation of the protein with increasing concentrations of Ca^{2+} significantly decreased Mg^{2+} binding and a similar effect was seen for pre-incubation with Mg^{2+}. This, combined with a significant reduction in the binding of both cations to a double mutant (D67A/D73A) in the EF-hand motif of site II, strongly suggest that both cations interact with the same locus in the N-cTnC. These results were corroborated by thermodynamic integration simulations on the same system.

In full-length cTnC, as expected, Ca^{2+} was found to interact with greater affinity (K_d = 0.12 ± 0.02 µM) with structural sites III/IV compared to Mg^{2+} (K_d =16.7 ± 0.7 µM). However, Mg^{2+} was also found to bind site II (K_d = 406.1 ± 7.9 µM) in competition with Ca^{2+} (K_d = 22.7 ± 0.5 µM). Given these findings and work by other groups, it is highly likely that cytosolic concentrations of free Mg^{2+} (~ 1 mM) occupies a significant percentage of the available population of cTnC site II's as this concentration of Mg^{2+} was found to increase the K_d of Ca^{2+} binding by 1.4-fold.

Approximately 90% of total cellular Mg^{2+} (~10 mM) is normally buffered by cellular components such as ATP. However, under ischemic conditions, the free Mg^{2+} may increase significantly and compete for binding to site II. In full-length cTnC, we found that 3 mM Mg^{2+} increased the K_d of Ca^{2+} binding to site II 1.6-fold. Pending further exploration of the implications of these results, our findings suggest that Mg^{2+} may interact with site II of cTnC to play a physiologically significant role in cardiac contractility.

5.2. Introduction

The troponin (Tn) complex is a heterotrimeric unit that includes components for: calcium (Ca^{2+}) binding (troponin C – TnC), inhibition of contraction (troponin I – TnI), and tropomyosin binding (troponin T – TnT) (Parmacek and Solaro 2004). Binding of Ca^{2+} to site II within TnC is the molecular precursor to a series of structural alterations within the Tn complex that initiate contraction (Kawasaki and van Eerd 1972, Murray and Kay 1972, Potter and Gergely 1975). Conformational perturbations which follow binding cause further changes in the rest of the thin filament (TF), culminating in rigour state between the actin filament and myosin heads to allow for force production (Potter and Gergely 1975, Filatov, Katrukha et al. 1999, Parmacek and Solaro 2004).

TnC is formed by a 14 residue N-helix and 8 other helices (labelled A-H). within each binding site, Ca^{2+} is coordinated by negatively charged sidechains from EF-hand motifs that consist of 29 amino acids (Strynadka and James 1989). 12 amino acids within this motif form a helix-loop-helix, with residues in positions 1 (+x), 3 (+y), 5 (+z), 7 (-y), 9 (-x), and 12 (-z) containing six oxygen atoms arranged at the helices of a pentagonal bipyramid. Specific residues, especially aspartic acids contribute greatly (Yap, Ames et al. 1999, Lewit-Bentley and Rety 2000). Steric arrangements may also

contribution to Ca^{2+} coordination (Kretsinger and Nockolds 1973). Skeletal muscle troponin TnC (sTnC) has 4 functional Ca^{2+} binding motifs (Seamon, Hartshorne et al. 1977, Ebashi, Nonomura et al. 1980). Cardiac TnC (cTnC) has a similar overall structure but a slightly different primary sequence. Insertion of a valine at residue 28, substitution of a leucine for the aspartic acid at residue 29, and an alanine in place of aspartic acid at residue 31; have rendered the site I of cTnC non-receptive to Ca^{2+} binding that normally occurs in sTnC without these three changes (**Figure 5-1**) (van Eerd and Takahshi 1976, Farah and Reinach 1995).

	x		**y**		**z**		**-y**		**-x**			**-z**
Site I (29-40)	**L**	G	**A**	E	**D**	G	**C**	I	**S**	T	K	**E**
Site II (65-76)	**D**	E	**D**	G	**S**	G	**T**	V	**D**	F	D	**E**
Site III (105-116)	**D**	K	**N**	A	**D**	G	**Y**	I	**D**	L	D	**E**
Site IV (141-152)	**D**	K	**N**	N	**D**	G	**R**	I	**D**	Y	D	**E**

Figure 5-1 Sequence alignment of the 4 EF hand binding motifs in cTnC
The coordinating residues within EF hands I-IV are shown with the residue number listed in brackets. Each of residues x, y, z, -y, -x, and -z, that make up the helices of the pentagonal bipyramid are indicated. The conservation of the amino acids in each of the coordinating residues between sites II, III, and IV is striking as is the clear differences seen in site I.

cTnC is one of the major cytosolic buffers of Ca^{2+} and is prevalent throughout the contractile filaments of cardiomyocytes (Schober, Huke et al. 2012). Ca^{2+} binding to the C-terminal domain occurs with high affinity (~10^7 M^{-1}) (~10x the N-domain) and slow exchange rate (~100x the N-domain) (Johnson, Charlton et al. 1979, Johnson, Nakkula et al. 1994). As such, Ca^{2+} is always bound to sites III and IV by cytosolic concentrations of free Ca^{2+} (0.1 – 1 µM) (Bers 2000). Lower affinity (K_A~10^4 M^{-1}) Mg^{2+} binding also occurs at sites III and IV (Potter and Gergely 1975). Given the slow off-rate (K_{off}) of Ca^{2+} dissociation from III and IV, the cellular concentrations of Mg^{2+}, and the binding affinity of Mg^{2+}, this ion competes with and reduces Ca^{2+} binding to these “structural” sites (Leavis and Kraft 1978, Robertson, Johnson et al. 1981). The binding of both Ca^{2+} and Mg^{2+} ions to sites III and IV is cooperative and alters the structure of TnC, allowing for it to be tethered to the TnI, TnT, and the rest of the TF (Sturtevant 1977, Tikunova and Davis 2004).

The C-terminus of cTnC is linked to the N-terminus by a flexible linker region composed of a nine turn α-helix (Sundaralingam, Bergstrom et al. 1985, Sia, Li et al.

1997). Within the N-terminal domain of cTnC (N-cTnC), Ca^{2+} binds to the low affinity (~10^{-5} M) site II such that this site is unbound at diastolic concentrations (~0.1 μM) (Cheung, Tillotson et al. 1989) and bound at systolic concentrations (~ 1 μM) of the ion (Kirschenlohr, Grace et al. 2000). Favourable binding at site II, which relieves tension in the protein is coupled to thermodynamically unfavorable exposure of a hydrophobic pocket (Gifford, Walsh et al. 2007). This results when helices B and C (BC domain) move away from helices N, A, and D (NAD domain) with a short anti-parallel β-sheet between EF-hands I and II acting as the hinge (Herzberg and James 1985, Slupsky and Sykes 1995, Houdusse, Love et al. 1997). While the exposure of this hydrophobic cleft is much reduced in cTnC in the absence of Ca^{2+} (Sia, Li et al. 1997, Spyracopoulos, Li et al. 1997), binding to the regulatory domain by C-terminal $TnI_{147-163}$ (also called the switch peptide) stabilizes N-cTnC to facilitate exposure of the hydrophobic cleft (Li, Spyracopoulos et al. 1999). The exposure of hydrophobic residues to the aqueous environment must be offset by the favourable energetics of Ca^{2+} binding to site II. However, changes in solvent accessibility of hydrophobic residues may not play a pivotal role in determining Ca^{2+} binding as has often been supposed (Tikunova, Rall et al. 2002, Tikunova and Davis 2004). This suggest may be due in part to the less open Ca^{2+}-bound state of cTnC compared to that seen in the holo-state of skeletal TnC. Many of the studies on dynamics of contraction were initially carried out on skeletal TnC. More recently however, NMR analysis has shown that skeletal TnC is more open than cTnC in the holo-state; possibly due in part to the conformational flexibility induced by a functional site I within this protein (Spyracopoulos, Li et al. 1997).

The total $[Mg^{2+}]_i$ is ~10 mM but most of this is bound to cellular components such as ATP and only ~0.5 – 1.0 mM is free (Romani and Scarpa 1992, Dai, Friedman et al. 1997). In conditions with diminished buffering capacity, such as ATP depleted states, the free $[Mg^{2+}]$ could increase significantly (Murphy, Steenbergen et al. 1989, Hongo, Konishi et al. 1994, Tessman and Romani 1998) and would then be extruded from the cell (Laires, Monteiro et al. 2004), but may also provide more significant competition with Ca^{2+} for binding to cTnC. Increase in Mg-ATP in both skeletal and cardiac tissue causes elevation in Ca^{2+} sensitivity of skinned fibers (Godt 1974, Best, Donaldson et al. 1977, Godt and Morgan 1984).

In skeletal muscle, Mg^{2+} binds the low affinity sites of TnC competitively and with a relatively high affinity (K_d ~1.9 mM). The F27W fluorophore was used to investigate the

effects of Mg^{2+} binding to cTnC, whereby conformational changes occur, albeit in response to much lower than Ca^{2+} binding affinities (K_d ~300 µM and 2 µM). At low concentrations (1-3 mM), Mg^{2+} was not found to change fluorescence, therefore binding of Mg^{2+} to N-cTnC does not result in structural changes seen with Ca^{2+} binding. 3 mM Mg^{2+} was found to lower the Ca^{2+} affinity of cTnC more than 3-fold (Tikunova and Davis 2004). This effect was also maintained at higher levels of complexity; in skinned rabbit psoas muscles, addition of Mg^{2+} was found to decrease the Ca^{2+} sensitivity of force production (Davis, Rall et al. 2002).

Further evidence has been obtained through fluorescence-based studies of isolated cTnC (Potter, Robertson et al. 1981, Ogawa 1985, Zot and Potter 1987, Morimoto 1991, Francois, Gerday et al. 1993, She, Dong et al. 1998), the Tn complex (Potter, Robertson et al. 1981, Zot and Potter 1987), and reconstituted fibers (Zot and Potter 1987, Allen, Yates et al. 1992) where Mg^{2+} seems to decrease Ca^{2+} sensitivity. In isolated cTnC K_A for Mg^{2+} was measured to be 4.4e2 M^{-1} (Ogawa 1985).

Detection of heat changes associated with the interactions of metal ions and proteins is challenging and highly dependent on the technique/instrumentation (Yamada 1978, Kometani and Yamada 1983). The interaction of Ca^{2+}/Mg^{2+} with sites III/IV results in large ΔH, the changes resulting from site I/II binding are at times, at the detection limit of instruments and may thus be deemed negligible (Yamada and Kometani 1982). However, isothermal titration calorimetry (ITC) provides great sensitivity in detecting minute thermodynamic fluctuations and may thus be utilized to detect these changes down to 0.1 µcal (Yamada 2003, Wilcox 2008, Grossoehme, Spuches et al. 2010, Sacco, Skowronsky et al. 2012). Moreover, the study of isolated N-cTnC allows for study of binding to a single site.

As yet, the implications of Mg^{2+} competition with Ca^{2+} for site II are unclear. We have used ITC to explore the thermodynamics of the interaction between Ca^{2+} and Mg^{2+} at the level of N-cTnC and full length cTnC. The binding of each cation was analyzed to establish a baseline. In the N-terminus, these interactions were significantly diminished through two mutations in site II. Competitive binding also caused a reduction in the apparent affinity and further indicated interaction of both cations with the same locus in the protein. At the level of full length cTnC, Mg^{2+} seems to compete with and reduce Ca^{2+} binding to all three binding sites.

Total cytosolic Ca^{2+} is in the 2.1 – 2.6 mM range but free concentration is tightly regulated and kept in the 0.1 – 1 µM range at rest (Brini, Cali et al. 2012). Mg^{2+} is also abundant in the cell but is less tightly controlled, and it has been thought to bind only the structural sites of cTnC under physiological concentrations. We have quantified the affinity of cTnC for this ion. Based on our results, and given the previous studies cited herein, Mg^{2+} may also compete with Ca^{2+} in binding to the regulatory site II. The thermodynamic landscape that characterizes the interaction of Ca^{2+}/Mg^{2+} with site II is endothermic and driven by a favourable change in entropy (ΔS). While, the Mg^{2+}-site II interaction occurs with lower affinity compared to Ca^{2+} binding, at physiological concentrations or with energy depletion induced elevated states, it may enact structural perturbations or further reduce Ca^{2+} binding and thus modify contraction.

5.3. Methods

5.3.1. Construct preparation and protein expression

The TNNC1 gene (Uniprot ID P63316) had previously been cloned into pET21a(+) vector and had a stop codon inserted at the 90th residue to create the N-cTnC construct using the Phusion site directed mutagenesis protocol (Thermo Scientific). This construct was transformed into the BL21(DE3) expression strain. The D76A/D73A construct was made using site directed mutagenesis carried out by GenScript (New Jersey, USA). Expression and purification of all constructs were carried out as described previously (Stevens, Rayani et al. 2016, Stevens, Rayani et al. 2017). In brief, 100 mL of lysogeny broth was supplemented with 50 µg/mL ampicillin and a glycerol stock stab and grown over-night at a shaking speed of 250 rpm and 37ºC. In the morning the same conditions were provided to 1 L cultures that were grown for ~3 hrs to an OD_{600} of 0.8 – 1.0 followed by induction with β-D-1-thiogalactopyranoside (IPTG). After 3 hrs, the cells were harvested by centrifugation and stored at -80 ºC.

5.3.2. Protein purification

The cell pellet was thawed and suspended in 50 mM Tris-Cl pH 8.0, 5 mM ethylenediamine-tetraacetic acid (EDTA) and sonicated on ice, 5 times 30 sec each, with intervals of rest between to avoid overheating. The lysate was centrifuged for 15 mins at 30k rpm and the supernatant separated twice to remove all cell debris. The supernatant

was applied to a fast-flow Q-Sepharose column pre-equilibrated with the suspension buffer and 1 mM dithiothreitol (DTT). The protein was eluted from the column by applying a 180 mL ramp gradient using the same buffer with the addition of a 0.5 M NaCl. The gradient was applied using an AKTA FPLC machine that was also used to fractionate the eluted samples. Following analysis by SDS-PAGE, the samples containing N-cTnC were pooled and concentrated using Amicon centrifugal concentrators with a 3 KDa molecular weight cut-off (Millipore).

The full-length protein was purified in the same way, with the exception of a 30% ammonium sulphate cut following the sonication step. Centrifugation was used to remove insoluble components and the supernatant was then dialyzed overnight against 4 L of NaCl-free column buffer.

The concentrated protein was the applied to a HiPrep 26/60 Sephacryl S-100 column (DEAE FF) (GE healthcare) which was equilibrated with the re-suspension buffer supplemented with 100 mM NaCl. SDS-PAGE analysis of the fractions was used to identify and pool those containing cTnC. The protein was stored at -80 ºC prior to pre-ITC dialysis.

5.3.3. Dialysis and ITC experiments

To generate the apo-state protein, it was dialyzed into 2 L of 50 mM 4-(2-hydroxyethyl)-1-piperazineethanesulfonic acid (HEPES) pH 7.2, 150 mM KCl, 2 mM EDTA, and 15 mM β-mercaptoethanol (BME). In the next 2 L buffer exchange, no EDTA was added. In the last buffer exchange of the same volume, no EDTA was added and the amount of BME was decreased such that the final concentration was 2 mM.

An extinction coefficient of 1490 $M^{-1}cm^{-1}$ and 4595 $M^{-1}cm^{-1}$, and a molecular weight of 10.1 kDa and 18.4 KDa were used to determine protein concentration for the N-cTnC and full length cTnC constructs respectively, by UV-vis spectroscopy using a NanoDrop 2000 spectrophotometer (Thermo Scientific). The final dialysis buffer was used to dilute the protein samples to a final concentration of 200 µM for the N-terminal construct and 150 µM for full length cTnC. The protein concentration was further checked through a Bradford assay and again through the Edelhoch method as previously described (Stevens, Rayani et al. 2017).

5.3.4. Experimental Protocols

Full-length cTnC

Standard 1.0 M $CaCl_2$ and $MgCl_2$ stock solutions (Sigma, USA) were serially diluted in the final dialysis buffer to produce 6 mM Ca^{2+} and 40 mM Mg^{2+} for the full length cTnC titrations. 6 mM Ca^{2+} was titrated into 100 µM apo-state full length human cTnC as the baseline condition. The data was fit with a two sets-of-binding-sites model. The same amount of protein was diluted in the ITC buffer and used for all subsequent conditions that were fit with the same model. Supra-physiological concentrations Ca^{2+} were selected for the pre-incubation experiements and justified as the goals of these experiments were not violated. The goals of these experiements were to explore possible competition between Ca^{2+} and Mg^{2+} in binding to cTnC and N-cTnC. Higher concentrations could thus be used to observe clearer results. Also, the amounts of cTnC and N-cTnC are above what is available in the cell and the affinity of their binding sites is lowered as they exist in isolation in these experiments ie. their affinities would be elevated by the presence of other cTn complex proteins. The concentrations of Mg^{2+} pre-incubated (1 and 3 mM) is not far beyond what would be expected in normal cellular conditions.

N-terminal cTnC

The same standards were used to produce 4 mM Ca^{2+} and 20 mM Mg^{2+} titrants for the N-cTnC experiments. 4 mM Ca^{2+} was titrated into 200 µM apo-state N-cTnC as the baseline condition with subsequent titrations using the same amount of protein. The isotherms were all fit with a single binding site model.

Titrations

The ITC experiments were carried out in a MicroCal ITC_{200} instrument (Malvern, UK). Repeat titrations were used to ensure reproducibility. The sample cell was set at 25 ºC, 200 µL of the protein was loaded and the experiment was carried out at the same temperature. For the N-terminal constructs, 19 injections of the titrant were used with the first being a dummy injection of 0.4 µL and the subsequent 18 injections, 2 µL each. For the full-length constructs, the same volume of sample was titrated with a dummy injection of 0.5 µL and 38 injections of 1 µL. The time interval between injections was 120 sec and stirring speed was set at 1000 rpm throughout each experiment.

5.3.5. Analysis of results

Titration data obtained from ITC was fit using Origin 8.0 (OriginLab, Northampton, MA) to calculate the thermodynamic parameters using a least-squares algorithm as described previously. In this method, if multiple ligands are simultaneously present in the reaction mixture, an “apparent affinity” is determined for the injected titrant. Origin also allows for fitting of more complex models of interactions which were utilized in the case of multiple binding sites for the full length cTnC experiments.

When fitting the data for the N-cTnC constructs (apart from the Ca^{2+} into Apo-state N-cTnC condition), the N associated with each interaction was necessarily constrained to equal 1.00 to facilitate curve fitting without altering protein concentration. The baseline condition was repeated daily to monitor fluctuations in concentration of properly folded and functional protein.

Protein concentration plays a large role in determination of affinity. The concentration of the titrant may be affected by pipetting errors, albeit this effect is minimal. The ratio of the ligand to titrant in the single binding site condition (as given by the stoichiometry – n) is a measure of the functional moles of protein and was approximately 1.00 in all the N-cTnC titrations. Given the method of concentration determination, the number of binding sites, cooperativity, and the variable binding strength of each titrants, the N cannot be used in the same way for the full-length cTnC experiments. Therefore, the values presented can be compared between conditions but care should be taken when comparing these to other systems. Ease of manipulation of the N-cTnC/cTnC system contrasts with those that include the cTn/TF. Thus, the binding parameters measured here may not translate in absolute term when cTnC is incorporated into a more complex system.

5.3.6. Thermodynamic Integration (TI)

Starting from the representative model of PDB:1AP4 (Spyracopoulos, Li et al. 1997), thats contains N-cTnC with a single Ca^{2+} ion bound, the system was solvated with a 12 Å padded TIP3P water box and neutralized with Na^{+} in Amber16 (D.A. Case, R.M. Betz et al. 2016). The system was also prepared similarly for only the Ca^{2+} ion in a 12 Å padded TIP3P water box. The alchemical thermodynamic cycle used for ligand binding

was described in detail previously (Leelananda and Lindert 2016). In short, TI was performed using the following three steps for Ca^{2+} in protein: turn on restraints, turn off charge, and turn off van der Waals forces. The specific distance restraints used in all systems can be found in **Supplementary Table 5-3**. Additionally, TI was performed for the following two steps for Ca^{2+} in water: turn off charge and turn off van der Waals forces. Each step of the thermodynamic cycle was performed with the coupling parameter (λ) ranging from 0.0-1.0 in increments of 0.1. For each simulation, the system was minimized (2000 cycles) and heated (0.5 ns) before the 5 ns production run at 300 K using the ff14SB force field (Maier, Martinez et al. 2015). These calculations were also performed on the D67A/D73A mutated system. The mutations were imposed on the 1AP4 representative model using PyMOL (L DeLano 2002).

For the calculation of Mg^{2+} binding affinity, Ca^{2+} was replaced with Mg^{2+} in the 1AP4 representative model since no Mg^{2+}-bound N-cTnC structure was available in the protein databank. In order to generate more accurate restraints and starting coordinates for the TI calculations, a minimization was performed on the structure in Amber. Following the minimization, TI simulations were run similarly as for Ca^{2+}. However, due to previously documented errors in the default Mg^{2+} parameters, the $\Delta G_{solvation}$-optimized Mg^{2+} parameters from Li *et. al.* were used (Li, Roberts et al. 2013, Panteva, Giambasu et al. 2015). These calculations were also performed on the D67A/D73A mutated system.

To calculate absolute binding affinities for the ions, the change in free energy (ΔG) was calculated for each step in the thermodynamic cycle by integrating the potential energy with respect to the coupling parameter, λ (Shirts, Mobley, et al. 2010). Two corrections were made to these calculated ΔG values. The first correction was necessary due to the introduction of the distance restraints (as described in Boresch et al.) which quantified the free energy cost of restraining the ion to the binding site (Boresch, Tettinger et al. 2003). The second correction was performed to correct the charged system (as described in Rocklin et al.) to revise the free energy for the fact that the system is charged during the disappearance of the charged ions (Rocklin, Mobley et al. 2013). The overall ΔG of binding was the change in free energy between the ions in complex with the protein (ion in protein steps 1, 2, and 3) and the ions in water (ion in water steps 1 and 2). For each system, 5 independent runs were performed and results were averaged.

5.4. Results

5.4.1. Full length cTnC

Ca^{2+} binding to apo-state full length cTnC

The binding of Ca^{2+} to sites III/IV occurred with a K_d of 0.12 ± 0.02 µM, this interaction was characterized by an exothermic interaction (ΔH = -8.12 ± 0.07 kcal*mol^{-1}) with a positive change in entropy (T*ΔS = 1.24± 0.07 kcal*mol^{-1}) and was spontaneous (ΔG = -9.44 ± 0.61 kcal*mol^{-1}).

In the N-terminal domain, the K_d associated with binding of Ca^{2+} to site II was 22.7 ± 0.5 µM; significantly lower binding affinity. It also had positive ΔH (3.71 ± 0.06 kcal*mol^{-1}). This reaction was entropically driven (T*ΔS = 10.0 ± 0.07 kcal*mol^{-1}) and spontaneous (-6.29 ± 0.20 kcal*mol^{-1}) (**Table S5-1 and Figure S5-1**).

Mg^{2+} binding to apo-state full length cTnC

Mg^{2+} binding to site II (K_d = 406.1 ± 7.9 µM) and sites III/IV (K_d = 16.7 ± 0.7 µM) was characterized by a positive ΔH (0.091 ± 0.001 kcal*mol^{-1}) and negative ΔH (-0.23 ± 0.01 kcal*mol^{-1}) respectively (**Table S5-1**). Based on these enthalpy values, it is clear that for any given Mg^{2+} concentration, significantly greater amounts of binding occur at the C-terminus in comparison to the N-terminus.

The interaction of Mg^{2+} with sites III/IV occurs at much lower affinity (two orders of magnitude) than that seen for Ca^{2+}. The interaction with site II and sites III/IV were both entropically favourable (T*ΔS = 4.71 ± 0.01 kcal*mol^{-1} and T*ΔS = 6.28 ± 0.03 kcal*mol^{-1}) and resulted in spontaneous interactions (ΔG = -4.62 ± 0.11 kcal*mol^{-1} and ΔG = -6.51 ± 0.31 kcal*mol^{-1}). These all differed significantly from those observed for Ca^{2+} binding, $p<0.05$.

Ca^{2+} binding to Mg^{2+} pre-incubated full length cTnC

Increasing concentrations of Mg^{2+} occupied a greater proportion of binding sites and limited binding Ca^{2+} to cTnC at all sites (**Table S5-1**). Binding of Ca^{2+} to site II was significantly reduced by pre-incubation with 1 mM and 3 mM Mg^{2+} as indicated by an increase in K_d and a lowering of the ΔH (**Table S5-1 and Figure 5-2**). Binding of Ca^{2+} to sites III/IV in the presence of 1 mM Mg^{2+} resulted in a K_d (0.14 ± 0.01 µM) that was not

significantly different than seen for the 3 mM Mg^{2+} preincubation (K_d = 0.08 ± 0.01 µM) (**Table S5-1 and Figure 5-2**).

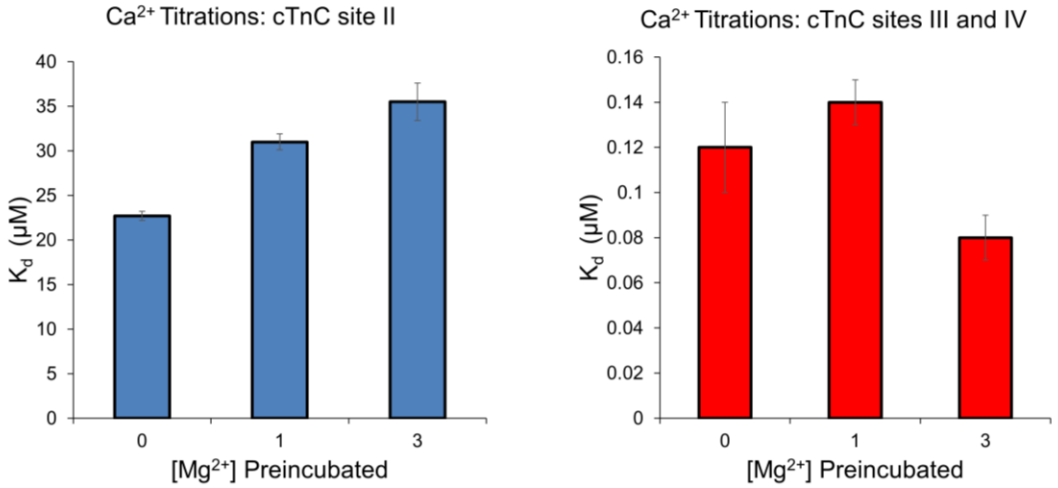

Figure 5-2 Binding of Ca^{2+} and Mg^{2+} to site II and Site III/IV of full length cTnC
Left panel: The affinity of site II for Ca^{2+} is compared in the apo-state and with Mg^{2+} preincubation in full length cTnC; Right Panel: The affinity of sites III/IV for Ca^{2+} is compared in the apo-state and with Mg^{2+} preincubation in full length cTnC. The 3 mM Mg^{2+} preincubation condition caused a decrease in K_d but when testing the difference between this condition and the 1 mM Mg^{2+} pre-incubation, given the relatively large SEM, the K_d was not significantly different ($p < 0.05$). Statistical differences were assessed through ANOVA followed by Tukey's post hoc test.

For the 1 mM Mg^{2+} pre-incubation, the exothermic interaction (ΔH = -6.87 ± 0.09 kcal*mol^{-1}) was entropically favourable (T*ΔS = 2.50 ± 0.10 kcal/mol) and resulted in a spontaneous interaction (ΔG = -9.37 ± 0.50 kcal*mol-1). For the 3 mM Mg^{2+} condition, the reaction was again exothermic (ΔH = -6.19 ± 0.06 kcal*mol-1) with a positive change in T*ΔS (3.50 ± 0.06 kcal/mol) and resulted in spontaneous binding (ΔG = -9.79 ± 0.26 kcal*mol-1).

The difficulty associated with the separation of the binding interaction containing two sets of sites, resulting in part from the conformational flexibility induced by the DE linker induced us to continue our studies exclusively at the regulatory domain.

5.4.2. N-terminal cTnC

The interaction between Ca^{2+}/Mg^{2+} and N-cTnC was found to be associated with a positive ΔH and negative ΔG, characteristic of a reaction driven by a positive ΔS (**Figure 5-3**). Despite some differences in the absolute values observed, which is consistent with differences in buffer and experimental conditions, our baseline values

comparing Ca^{2+} binding to apo-state N-cTnC are consistent with previously published data (Skowronsky, Schroeter et al. 2013, Tanaka, Takahashi et al. 2013, Stevens, Rayani et al. 2016, Stevens, Rayani et al. 2017).

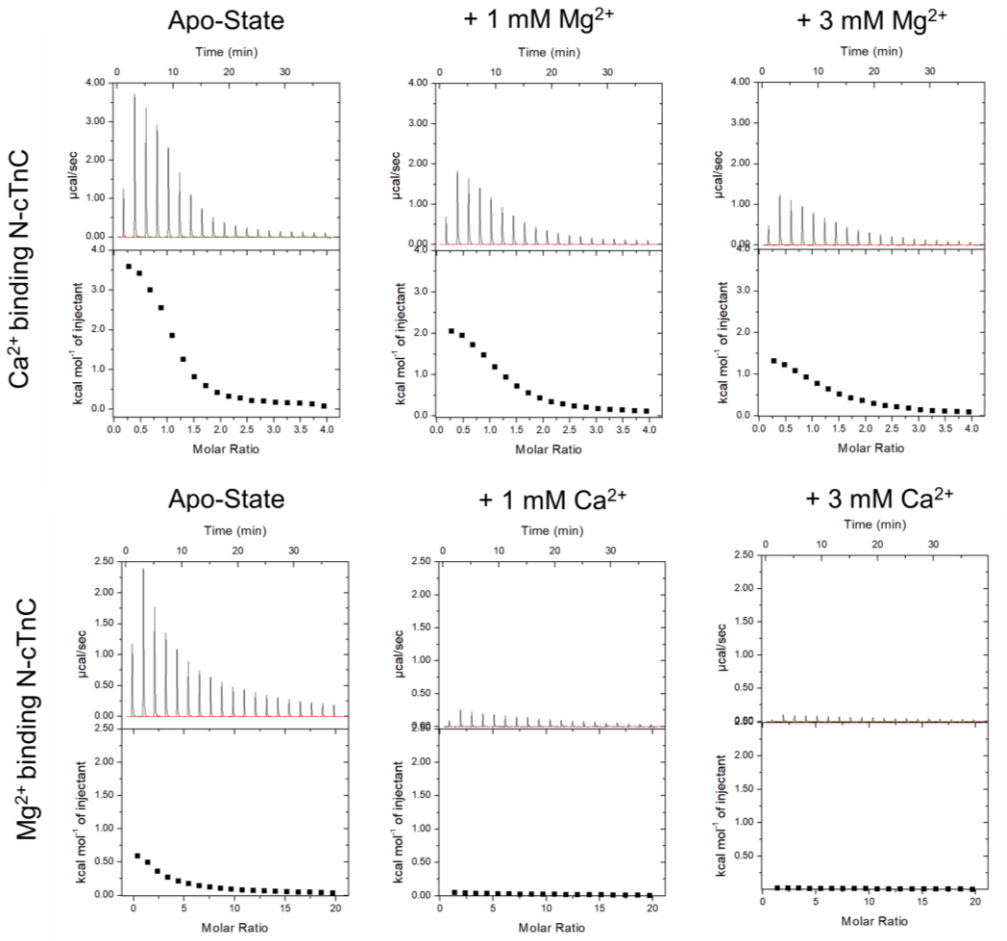

Figure 5-3 Representative isotherms for N-cTnC ITC titrations
Upper panels show the heat recorded during the titration and lower panels plot the integrated heat signal against the molar ratio of titrant added. For all titrations: 19 injections were used with the first being 0.8 µL and the subsequent 18 being 2 µL each. The top row shows the titration of 4 mM Ca^{2+} into apo-state N-cTnC, following by the same titration into 1 mM and 3 mM Mg^{2+} pre-incubated N-cTnC; these isotherms are scaled to 4 µcal*s^{-1} to help visualize the relative heat change. The bottom row shows the titration of 20 Mg^{2+} into apo-state N-cTnC, followed by 1 and 3 mM Ca^{2+} pre-incubated N-cTnC; these isotherms are scaled to 2.5 µcal*s^{-1} to help visualize the relative heat change.

Ca^{2+} and Mg^{2+} binding to apo-state N-cTnC

The affinity of N-cTnC for Ca^{2+} (K_A = 66.1 ± 2.0 *10^3 M^{-1}) was found to be well over an order of magnitude greater than for Mg^{2+} (K_A = 1.54 ± 0.06 *10^3 M^{-1}), corresponding to a more than 40-fold difference (**Table S5-2 and Figure 5-4**). The

steepness of the binding curve and the midpoint can be compared between the representative isotherms to provide some indication of these differences (**Figure 5-3**).

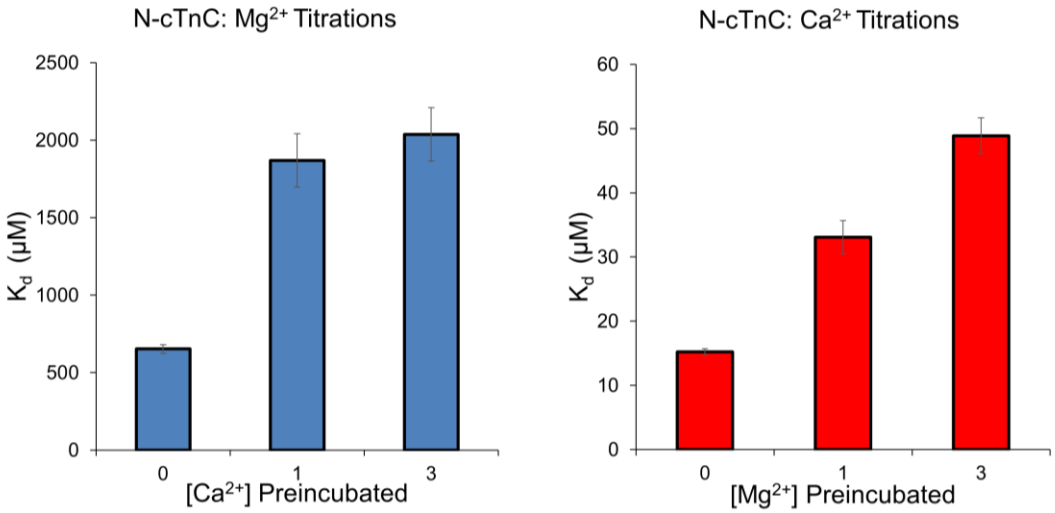

Figure 5-4 Binding of Ca^{2+} and Mg^{2+} to site II of N-cTnC
Left panel: The affinity of site II for Mg^{2+} is compared in the apo-state and with Ca^{2+} preincubation in N-cTnC; Right Panel: The affinity of site II for Ca^{2+} is compared in the apo-state and with Mg^{2+} preincubation in N-cTnC. Statistical differences were assessed through ANOVA followed by Tukey's post hoc test. Ca^{2+} tirations were not significantly different but Mg^{2+} with pre-incubation was different from the apo-state titration when either 1 mM or 3 mM Ca^{2+} were preincubated.

The ΔH of the Ca^{2+}-N-cTnC interaction was significantly greater (3.82 ± 0.04 kcal*mol^{-1}) than that with Mg^{2+} (2.64 ± 0.1 kcal*mol^{-1}). Both reactions increase the ΔS of the system, but this was more apparent for the Ca^{2+} titration (T*ΔS = 10.4 ± 0.03 kcal*mol^{-1}) than for Mg^{2+} (T*ΔS = 6.99 ± 0.07 kcal*mol^{-1}), resulting in spontaneous reactions as characterized by negative ΔG values (-6.57 ± 0.02 kcal*mol^{-1} for Ca^{2+} and -4.35 ± 0.03 kcal*mol^{-1} for Mg^{2+}) (**Table S5-2**).

The spontaneity of the reaction is derived from the ΔH and ΔS by the following equation:

$$\Delta G = \Delta H - T*\Delta S$$

Moreover, the affinity also determines spontaneity through the following relationship:

$$\Delta G = - RT*\ln(K_A)$$

With R being the universal gas constant and T the temperature (Kelvin).

As expected, the affinity of Ca^{2+} binding to apo-state N-cTnC was also found to be significantly higher than all other conditions and was thus characterized by the lowest observed dissociation constant (K_d) (15.2 ± 0.5 µM) (**Figure 5-4 and Table S5-2).**

Mg^{2+} binding to Ca^{2+}pre-incubated N-cTnC

To investigate the site of Mg^{2+} binding, apo-state N-cTnC was pre-incubated with increasing concentrations of Ca^{2+}, then titrated with 20 mM Mg^{2+} in each case; 1 mM and 3 mM preincubations are compared (**Figure 5-4**). These titrations, in addition to those with 2 mM and 5 mM Ca^{2+} were compared and showed the same general pattern of decreased binding (**Table S5-2**). The affinity decreased with increasing concentration of Ca^{2+} pre-incubated but the differences were not statistically significant. However, the heat change in these conditions was significantly lower between 1 and 3 mM Ca^{2+} pre-incubation conditions (0.48 ± 0.04 and 0.24 ± 0.02 kcal*mol^{-1}, respectively).

These values were lower than the Mg^{2+} into apo-protein condition that yielded a ΔH = 2.64 ± 0.1 kcal*mol^{-1}. The ΔH was also an order of magnitude lower than Ca^{2+} into apo-protein which liberated 3.82 ± 0.04 kcal*mol^{-1}. Moreover, the K_d values were 1870.0 and 2037.5 µM for the 1 mM and 3 mM Ca^{2+} conditions, showing a decrease in affinity with increasing concentrations of Ca^{2+} pre-incubated with the protein sample and a more than 2 orders of magnitude lower affinity compare to the Ca^{2+} into WT condition. The significant reduction in affinity, ΔH, and increasingly smaller ΔS associated with higher Ca^{2+} pre-incubation suggests that both metal cations may be binding to the same EF-hand binding motif in site II of N-cTnC.

Ca^{2+} binding to Mg^{2+} pre-incubated N-cTnC

Apo-protein pre-incubated with Mg^{2+} was titrated with Ca^{2+} to gain a measure of the “apparent” affinity of the protein for Ca^{2+} when the site might be occupied with the other divalent cations. As expected, increasing the Mg^{2+} reduced the amount of binding (monitored by ΔH). the Ca^{2+} affinity was lower compared to the apo-N-cTnC binding condition and decreased with higher concentrations of Mg^{2+} (**Table S5-2 and Figure 5-4**).

Ca^{2+} and Mg^{2+} binding to apo-D67A/D73A N-cTnC

Point mutations (D67A and D73A) were made, changing two negatively charged aspartic acid residues into hydrophobic alanines in the binding EF-hand motif of site II (**Figure 5-5**). Binding of both divalent cations was reduced by these mutations with the K_A being greater for Ca^{2+} binding (5.9 ± 0.5 *10^3 M^{-1}) compared to Mg^{2+} binding (0.90 ± 0.08 *10^3 M^{-1}) (**Table S5-2; Figure S5-2 and Figure 5-6**). Compared to the WT binding, Ca^{2+} binding was reduced almost 12-fold and Mg^{2+} binding was reduced nearly 2-fold by the double mutation.

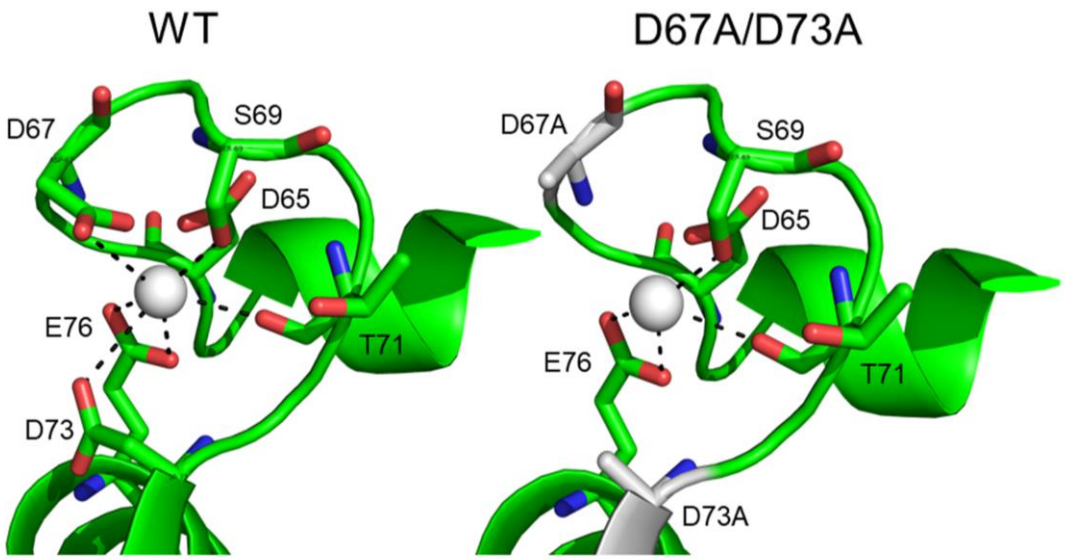

Figure 5-5 Depiction of WT and D67A/D73A mutant coordination of Ca^{2+}/ Mg^{2+}
The D67A/D73A double mutant removes two of the coordinating residues within the EF hand of site II in N-cTnC. The goal of this double mutation was to compare the reduced amount of binding of Ca^{2+} and Mg^{2+} and to gain insight into the locus of binding for each cation. The figure was generated using Pymol and adapted from the PDB:1J1E x-ray structure.

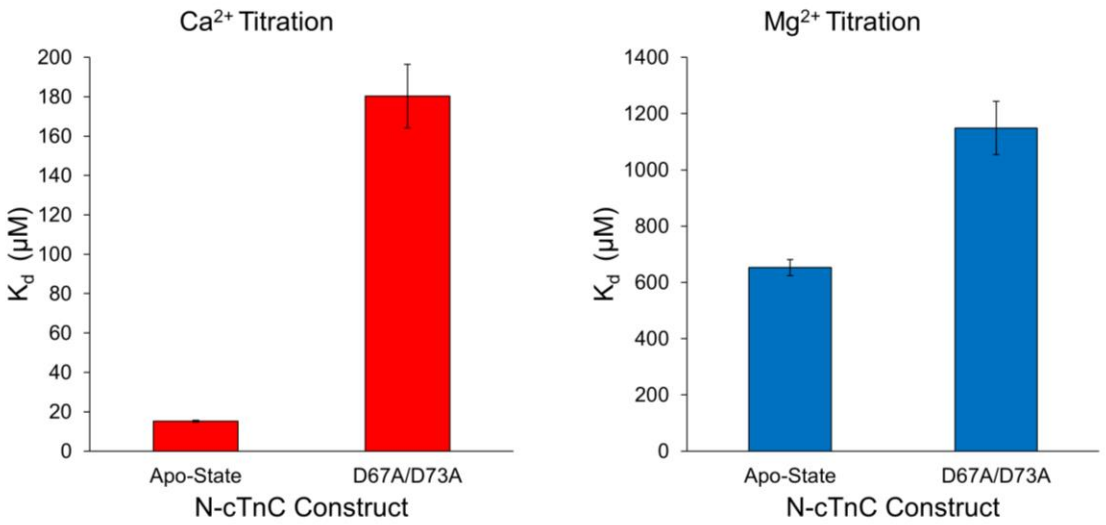

Figure 5-6 Effect of D67A/D73A on the Ca^{2+}/ Mg^{2+} binding affinity of the site II of N-cTnC

The effect of the D67A/D73A on Ca^{2+} and Mg^{2+} binding is assessed. The affinity of binding for both cations to N-cTnC was lower when comparing the mutant and the WT. The effect on Ca^{2+} binding was more pronounced (11-fold reduction) compared to Mg^{2+} (1.7-fold reduction) but this is reconcilable with the number of coordinating residues needed to bind Ca^{2+} (6) vs. Mg^{2+} (5); therefore 4 coordinating residues should affect Ca^{2+} binding to a greater extent. Ca^{2+} still binds the mutant with greater affinity in the double mutant (Falke, Drake et al. 1994).

The ΔS associated with each interaction can be expected to be greatest in conditions that expose a more hydrophobic patch (between helices A and B) in N-cTnC. While neither mutation directly affected this area of the protein, they may be expected to create a more hydrophobic region in the protein by introducing a non-polar alanine residue that would hypothetically decrease the number of hydrogen bond forming moieties. To this end the ΔS associated with the double mutant was shown to be significantly lower than the apo-state WT N-cTnC (**Table S5-2**) protein but it should also be considered that the mutations alter both the baseline and the post conformational change enthalpies in ways that are dependent on the kinetics of the structural change.

5.4.3. Ca^{2+} and Mg^{2+} binding affinities from Thermodynamic Integration

Thermodynamic Integration was performed to calculate absolute binding affinities for the ions in the following systems: Ca^{2+} to WT N-cTnC, Ca^{2+} to D67A/D73A N-cTnC, Mg^{2+} to WT N-cTnC, and Mg^{2+} to D67A/D73A N-cTnC. The average calculated binding affinities over 5 independent runs were -6.9 ± 1.3, -4.5 ± 2.4, -0.6 ± 2.8, and +0.4 ± 2.3

kcal*mol^{-1} respectively. The Ca^{2+} binding affinities were in good agreement with the ITC data. While the calculated absolute Mg^{2+} binding affinities were not in perfect agreement with the ITC data, they did show the same trend. Mg^{2+} had a weaker binding affinity than Ca^{2+} for all systems (-6.57 to -4.38 kcal*mol^{-1} and -6.9 to -0.6 kcal*mol^{-1} for ITC and TI respectively for WT system and -5.12 to -4.02 kcal*mol^{-1} and -4.5 to +0.4 kcal*mol^{-1} for ITC and TI respectively for D67A/D73A system). Additionally, between the Mg^{2+} binding affinities, the binding affinity was consistently weaker for the D67A/D73A mutation. The ΔΔG values comparing ΔG between WT and D67A/D73A systems were similar for ITC and TI (0.36 kcal*mol^{-1} and 1.0 kcal*mol^{-1} respectively).

Table 5-1 Average calculated binding affinities for each system

System	ΔG_{TI} (kcal/mol)
Ca^{2+} to WT	-6.9 ± 1.3
Ca^{2+} to D67A/D73A	-4.5 ± 2.4
Mg^{2+} to WT	-0.6 ± 2.8
Mg^{2+} to D67A/D73A	+0.4 ± 2.0

Averages were calculated over 5 independent runs

5.5. Discussion

This study provides novel information regarding the thermodynamics that underlie the interaction between cTnC and metallic cations. The presence of cTnI and cTnT increases Ca^{2+} affinity of cTnC by a full order of magnitude at diastolic concentrations of each. Moreover, binding of systolic concentrations of Ca^{2+} to site II of cTnC strengthens the interaction with cTnI and the rest of the cTn complex (Potter and Gergely 1975, Ramos 1999, Pinto, Parvatiyar et al. 2009). Therefore, care must be taken when translating observations on cTnC to more complex systems such as the cTn complex or the cardiac TF.

As seen in previous reports, we have found that the binding of Ca^{2+} to N-cTnC is favorable and results from an entropically driven, endothermic process (**Figure 5-3** and **Table S5-2**) (Stevens, Rayani et al. 2017, Johnson, Fulcher et al. 2019). The favorable

ΔS may be due in part to the dehydration ΔS of Ca^{2+} which is thought to be on the order of ~350 kcal/mol and slightly lower than that of Mg^{2+} (~450 kcal/mol) (Smith DW, 1977). It is also possible that the endothermic nature of these interactions results from other factors such as the exchange of protons that are transferred from the ligand to the buffer upon Ca^{2+} binding (Skowronsky, Schroeter et al. 2013).

Measurement of Ca^{2+} binding to cTnC is often achieved indirectly by measuring the fluorescence change and correlating this to the conformational change that results from the interaction. Fluorescent molecules such as 2-[4'-(iodoacetamido)anilino]-naphthalene-6-sulfonic acid (IAANS) (Wang, Huang et al. 1997, Hazard, Kohout et al. 1998, Li, Stevens et al. 2013) or reporters such as F27W (Gillis, Blumenschein et al. 2003) can be used to quantify this binding interaction. At 21°C in bovine F27W cTnC had a K_d of ~5 µM and IAANS labelled C35S cTnC had a K_d of ~7 µM (Gillis, Marshall et al. 2000, Tikunova and Davis 2004). Through fluorescence-based measurement, the K_d of N-cTnC for Ca^{2+} was previously reported to be between 11.3 µM - 12.3 µM (Liang, Chung et al. 2008, Pinto, Parvatiyar et al. 2009). These parameters agree with our measured Ca^{2+} binding to apo-state N-cTnC and apo-state cTnC (**Tables S5-1 and S5-2**), deviating slightly due to buffer and temperature conditions.

Normally, cytosolic $[Mg^{2+}]_{free}$ is tightly controlled around ~0.5 – 1 mM (Romani 2011). At these concentrations, Mg^{2+} is known to compete with Ca^{2+} for sites III and IV. Circular dichroism has been used to show that Ca^{2+} binding to sites III/IV increases the α-helical content of cTnC, from 19 to 41 percent (Herzberg and James 1985, Yumoto, Nara et al. 2001) and causes conformational changes that remove non-polar amino acids from the solvent exposed environment (Sturtevant 1977). This contrasts with NMR based visualization of N-cTnC, where the apo-state and Ca^{2+}-bound forms showed minimal structural deviation (Spyracopoulos, Li et al. 1997).

Ca^{2+} has many times greater polarizability than Mg^{2+} and lower hydration energy (Carafoli and Krebs 2016). The radius of Mg^{2+} (0.65 Å) is also smaller than Ca^{2+} (0.99 Å) (Lockless, Zhou et al. 2007), however, in its hydrated form, Mg^{2+} is 400x larger whereas Ca^{2+} is only 25x times larger (Maguire 2006). In Calmodulin (CaM), metals with similar ionic radii are able to substitute for Ca^{2+} (Chao, Suzuki et al. 1984, Malmendal, Linse et al. 1999). Mg^{2+} is able to bind to CaM, but does not induce the conformational change associated with Ca^{2+} binding (Follenius and Gerard 1984, Gilli, Lafitte et al. 1998).

Normally, six oxygen atoms arranged in an octahedral geometry are thought to coordinate Mg^{2+} (Linse and Forsen 1995). This is one less oxygen molecule than needed to coordinate Ca^{2+} through a pentagonal bipyramid (Cates, Berry et al. 1999). However, Ca^{2+} can be coordinated by 6 – 8 coordinating residues (but also by as many as 12) at a distance that can vary greatly (0.229 – 0.265 nm) compared to a much smaller variance for Mg^{2+} coordination (0.200 – 0.216 nm) (Brini, Cali et al. 2012).

Ca^{2+} and Mg^{2+} are most often coordinated by oxygen atoms, this is usually a hydroxyl group for Mg^{2+} and a carboxyl group for Ca^{2+} (Harding 2002). Ca^{2+} is most frequently coordinated by side chains of aspartic acid, glutamic acid, asparagine, followed by serine/threonine, while Mg^{2+} is most frequently coordinated by aspartic acid, glutamic acid, histidine, threonine, serine, and asparagine respectively (Dokmanic, Sikic et al. 2008). EF hand containing proteins have also been shown to bind Mg^{2+} when there are appropriately placed negatively charged amino residues (especially in the +z and - z positions) (Reid and Procyshyn 1995, Tikunova, Black et al. 2001, Davis, Rall et al. 2002). In site II of mammalian cTnC, there is a polar serine at the +z position (residue 69) and a negatively charged glutamic acid residue at the –z position (residue 76).

Similarities exist between the coordinating residue of site II in cTnC and S100 proteins where an N-terminal “pseudo-EF hand” is formed by 14-residue loop that coordinates Ca^{2+} with low affinity (Bhattacharya, Bunick et al. 2004). These loops can also be bound by other cations such as zinc and cooper, which while less abundant in the cell, have similar biophysical properties to Mg^{2+} (Heizmann and Cox 1998, Dokmanic, Sikic et al. 2008). Moreover, the interaction of other, similarly unabundant cations (such as Strontium) with TnC has previously been established (Kerrick, Zot et al. 1985).

It was initially concluded that Mg^{2+} only binds to sites III and IV in TnC (Potter and Gergely 1975). Equilibrium dialysis was used to show that Mg^{2+} does not compete with Ca^{2+} for the N-terminal sites of cTnC, instead, other binding sites were suggested (Holroyde, Robertson et al. 1980). Enthalpic titrations were not able to visualize a discernable change in Mg^{2+} binding to the low affinity sites of skeletal TnC (Yamada and Kometani 1982, Li, Chandra et al. 1994). However, at room temperature, the K_d associated with Mg^{2+} binding was determined to be about 4 mM, using fluorescence and assuming competitive binding (Johnson, Collins et al. 1980). More recently, Ca^{2+}

sensitivity of the actomyosin ATPase and force production of skinned rat cardiac cells was unaltered when Mg^{2+} was increased from 1 to 8 mM (Allen, Xu et al. 2000). These findings were questioned by some who used metallochromic indicators to deduce a sufficiently high Mg^{2+}-affinity in the regulatory sites I/II of skeletal TnC (Ogawa 1985).

The observation of Mg^{2+} binding to the low affinity sites of N-cTnC has led to the suggestion that differences in affinity may be due at least in part to the Ca^{2+} buffering and thus the free concentration of the ion in these experiments. Given the kinetic rates associated with these interactions, it is difficult to have confidence in EGTA determined rates of binding (Ebashi and Ogawa 1988). Moreover, given the temperature sensitivity of cTnC, this factor alone can alter experimental outcomes by orders of magnitude (Kohama 1980, Gillis, Moyes et al. 2003). The change in sensitivity in the face of altered temperature has been suggested to result mostly from binding to the low affinity sites and possibly through interactions with other members of the Tn complex (Godt and Lindley 1982, Stephenson and Williams 1982, Wnuk, Schoechlin et al. 1984).

Fabiato and Fabiato showed that increasing concentration of free Mg^{2+} decreases myofilament Ca^{2+} sensitivity of skinned cardiomyocytes (Fabiato and Fabiato 1975). $[Mg^{2+}]$ affects the Ca^{2+}-sensitivity of the myofibrillar ATPase as well as actomyosin tension development in both skeletal and cardiac muscle preparations (Donaldson and Kerrick 1975, Kerrick and Donaldson 1975, Solaro and Shiner 1976, Ashley and Moisescu 1977, Best, Donaldson et al. 1977, Donaldson, Best et al. 1978, Ebashi, Nonomura et al. 1980, Morimoto 1991). Given these corroborative findings, through multiple experimental setups and by different groups increases their credibility.

Mg^{2+} affinity of sites III/IV alone is not sufficient to fully explain the change in the force-pCa relationship caused by Mg^{2+} In skinned skeletal muscle fibers (Ebashi and Endo 1968). In rabbit fast skeletal muscle, Mg^{2+} competes with Ca^{2+} for low affinity binding sites of TnC where it binds with an affinity of 1.94e2 M^{-1} (much lower than the 6.20e6 M^{-1} seen for Ca^{2+}). The K_A associated with sites III and IV was measured to be 1.2e6 M^{-1} for Ca^{2+} and 1.1e2 M^{-1} for Mg^{2+} in canine ventricular skinned myocytes (Pan and Solaro 1987).

In isolated cTnC, Mg^{2+} was found to interact with site II of cTnC with an apparent binding constant of 5.2e2 M^{-1}. This was only slightly lower than the constant associated

with Mg^{2+} binding to sites III/IV (~10^3 M^{-1}), Ca^{2+} binding to sites III/IV (~10^6 M^{-1}), and Ca^{2+} binding to site II (~10^4 M^{-1}) (Ogawa 1985).

Fluorescence was used to measure the Mg^{2+} affinity of site II at 15 °C (~1.2-1.9 mM) (Tikunova and Davis 2004). In the presence of 3 mM Mg^{2+}, the K_d associated with binding of Ca^{2+} to site II of full length cTnC was reduced from 7 µM in the apo-state to 24 µM (Tikunova and Davis 2004). A system containing cTnC-cTnI had 2.5-fold lower Ca^{2+} affinity in the presence of 3 mM Mg^{2+} (Siddiqui, Tikunova et al. 2016). Given these affinities, Tikunova and Davis hypothesized that site II would be 33-44% saturated by 1 mM cellular Mg^{2+} at diastolic Ca^{2+} concentrations (Tikunova and Davis 2004).

In a recent ITC study, the Mg^{2+} binding affinity of site II in lobster TnC isoforms, which are similar in sequence to human variants was explored. Mg^{2+} affinity of site II was one order of magnitude lower than that of Ca^{2+}, such that it would compete with Ca^{2+} for binding (Tanaka, Takahashi et al. 2013).

We measured site II binding affinity of Mg^{2+} in N-cTnC (K_A = 1.54e3 ± 0.06e3 M^{-1}) and in full length cTnC (K_A = 2.47e3 ± 0.5e3 M^{-1}). These values were lower than the binding affinity of Ca^{2+} in N-cTnC (K_A = 66.1e3 ± 2.0e3 M^{-1}) and full length cTnC (K_A = 44.3e3 ± 1.0e3 M^{-1}) (**Tables S5-1 and 5-3**). At these affinities and given the relatively high cytosolic $[Mg^{2+}]_{free}$ (~1 mM) (Linse and Forsen 1995, Malmendal, Linse et al. 1999), this cation would compete for binding to site II of cTnC (Nara, Morii et al. 2013). We also observed reduced Ca^{2+} binding to site II in the presence of Mg^{2+} at the N-cTnC level (**Figure 5-4**). In full length cTnC, Mg^{2+} reduced Ca^{2+} binding to all three sites II/III/IV (**Figure 5-3**). We found that Mg^{2+} binds sites III/IV of cTnC with a K_d = 16.7 ± 0.7 µM.

In order to further validate the ITC data, we also performed thermodynamic integration (TI) to calculate absolute binding affinities computationally. We performed these calculations for both Ca^{2+} and Mg^{2+} binding separately for both WT N-cTnC and D67A/D73A N-cTnC. For both sets of simualtions, the structure of Ca^{2+}-bound N-cTnC (PDB:1AP4) was used as the starting parameter and restrained throughout the simulation. ITC measures the thermodynamically quantifiable closed to open transition of the N-cTnC molecule. TI does not allow for such a transition, rather, it quantifies only the binding interaction. In the future, the closed structure of N-cTnC (PDB:1SPY) can be simulated to quantify the presumably lower affinity it has for each of Ca^{2+} and Mg^{2+}. The

difference between these sets of simulations could then, potentially be used to better corroborate the ITC data.

For Ca^{2+} binding, our TI results agreed very well with the binding affinities from ITC. Binding affinities for the wild-type system were -6.57 ± 0.02 and -6.9 ± 1.3 kcal*mol^{-1} for ITC and TI respectively. For the D67A/D73A mutated system, binding affinities were -5.12 ± 0.02 and -4.5 ± 2.4 kcal*mol^{-1} respectively. For Mg^{2+} binding, the calculated absolute binding affinities were consistently underestimated by about 4 kcal*mol^{-1}, but showed the same relative trends. Mg^{2+} was calculated to bind weaker than Ca^{2+} and bind weaker for the D67A/D73A mutation similarly to ITC. The Mg^{2+} absolute binding affinities were likely underestimated for multiple reasons. First, the crystal structure of WT N-cTnC (1AP4) contained Ca^{2+} bound and no structure of Mg^{2+} bound WT N-cTnC was available. We attempted to correct for this issue by minimizing the structure with Mg^{2+} bound. Due to the lack of an exact starting structure and restraints chosen, there is still likely some error. Additionally, while we did try to choose the most accurate Mg^{2+} parameters for binding affinity calculation, there are well documented difficulties in free energy calculations for Mg^{2+}, most notably that the free energy of solvation ($\Delta G_{solvation}$) is consistently underestimated (Steinbrecher, Joung et al. 2011, Panteva, Giambasu et al. 2015). Even when using the same Mg^{2+} force field, solvation ΔG values are also known to have large variations for Mg^{2+} depending on the exact simulation parameters used. For example, Panteva *et al.* and Li *et al.* both tried to reproduce Mg^{2+} solvation free energy using the same parameters as Åqvist, but saw variations on the order of 20 kcal*mol^{-1} (Åqvist 1990). While this may be an extreme example, it illustrates the difficulty in calculation of free energy changes with Mg^{2+} ions involved. Given these potential errors in TI for $\Delta G_{solvation}$ for Mg^{2+}, the fact that we still see relatively good agreement with the ITC data for absolute binding affinity of Mg^{2+} helps further validates the experimental results.

We have tested the hypothesis that similarly charged Ca^{2+} and Mg^{2+} both interact with all the functional EF-hand motifs in cTnC. The interaction with sites III and IV has been established for some time (Johnson, Collins et al. 1980), but site II may also bind Mg^{2+}. Interestingly, a hypothesis that is reconcilable with our own was initially put forth; that of six binding sites. In this scenario there were: two Ca^{2+} specific sites, two Mg^{2+} specific sites, and two sites that can bind both cations. During these experiments, only

the absence of Mg^{2+} allowed for the binding sites in cTnC to be separated into low affinity sites (~10^5 M^{-1}) and high affinity sites (~10^7 M^{-1}) (Potter and Gergely 1975).

Binding to site II is not expected to induce significant structural changes in N-cTnC based on previous Molecular Dynamics Simulation data (Spyracopoulos, Li et al. 1997, Skowronsky, Schroeter et al. 2013, Stevens, Rayani et al. 2017). Therefore, it is likely that the favourable ΔS associated with the interaction is due to increased degrees of freedom for the water molecules that would result when stabilizing hydrogen bonds are transferred from the positively charged metal cation and the negatively charged amino acid side chains in the binding site II to the buffered environment (Skowronsky, Schroeter et al. 2013).

Representative isotherms for the pre-incubation of both Ca^{2+} and Mg^{2+} with the apo-protein are shown in **Figure 5-3**. It was observed that the apparent affinity of N-cTnC decreased for the titrant in both cases (**Table S5-2**). The D67A/D73A mutant condition also reduced binding of both divalent cations (**Figure 5-6**), though the effect differed slightly between the Ca^{2+} and Mg^{2+}. There was a 12-fold lower Ca^{2+} affinity in the mutant compared to the WT protein, which was greater than the 1.7-fold change in Mg^{2+} binding affinity.

Our ITC data on the full length cTnC show that both Ca^{2+} and Mg^{2+} bind to site III/IV as expected and that the affinity of the former is greater than that of the later. Mg^{2+} also competes with Ca^{2+} for binding to site II, with the caveat that Mg^{2+} binding is not thought to cause the requisite conformational changes in the N-terminus of cTnC to facilitate interaction with cTnI and allow for force production to occur (Tikunova and Davis 2004). The amount of Mg^{2+} that binds the regulatory site II is likely to be highly dependent on technique, system, and buffer conditions. In N-cTnC, occupation of site II by Mg^{2+} was again seen to reduce the amount of Ca^{2+} which was able to bind this protein, at concentrations that may have physiologically relevant consequences under normal conditions and even more so in the face of diseases which alter the Ca^{2+} sensitivity of contraction.

Moreover, increases in cAMP in the cell through α- and β-adrenergic stimulation elicits extrusion of Mg^{2+} from the cell in mammalian tissues (Wolf, Di Francesco et al. 1996, Fagan and Romani 2001, Cefaratti and Romani 2007) including cardiomyocytes

(Vormann and Günther 1987, Howarth, Waring et al. 1994). If shown in the heart, both sodium-dependent and independent removal of Mg^{2+} from the cytosol under stressful conditions would lower cytosolic presence of this cation. Despite this, free Mg^{2+} does not fluctuate greatly under such stimulation, suggesting that buffered Mg^{2+} is removed from the cell (Amano, Matsubara et al. 2000). Nevertheless, this altered pool of Mg^{2+} may lead to changed competition with Ca^{2+} for binding to troponin and affect changes in force production.

5.6. Conclusions

Our studies provide insights regarding the thermodynamics of metal cation binding to N-cTnC. Competitive binding of Ca^{2+} and Mg^{2+} is observed at the site II of cTnC. These endothermic and entropically driven interactions are characterized by differences in K_A, ΔH, and ΔS consistent with the differences in ionic radius, number of required coordinating residues, as well as the energic cost of exposing hydrophobicity amino acids to an aqueous environment. In the cell, these differences are functionally necessitated by dissimilar cytosolic prevalence of each cation. Cellular concentrations of Mg^{2+} are not necessarily high enough to directly regulate contraction and are not thought to cause a conformational change upon binding to cTnC. However, given the site II binding affinity we have observed, its occupation of the binding site may restrict Ca^{2+} binding. Our findings suggest that Mg^{2+} binding may conceivably alter the availability of site II to Ca^{2+} or alter the interaction of cTnC with other cTn complex proteins such as the switch arm of cTnI and in so doing affect changes in the force production capabilities of cardiac tissue.

5.7. Supplementary Appendix

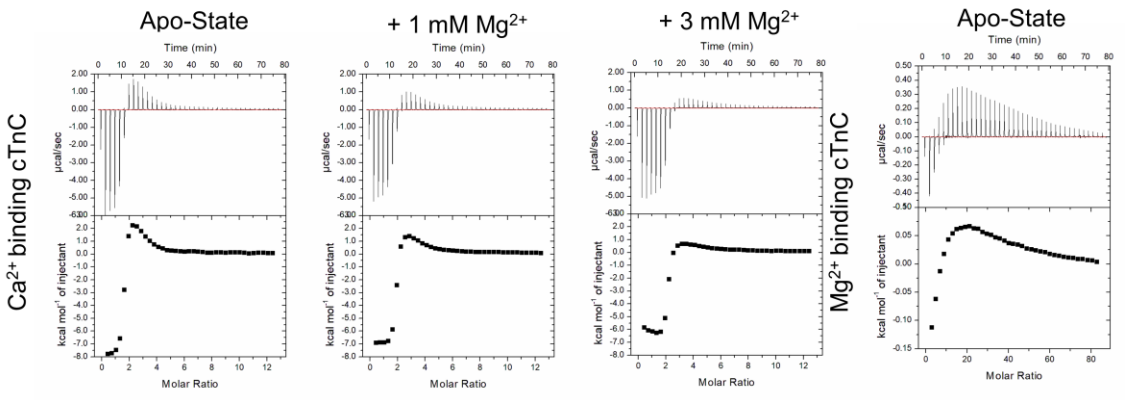

Supplemental Figure 5-1 Representative isotherms for full length cTnC ITC titrations

Representative isotherms for each full-length cTnC titration condition are shown. Upper panels show the heat recorded during the titration and lower panels plot the integrated heat signal against the molar ratio of titrant added. For all titrations 39 injections were used with the first being 0.5 µL and the subsequent 38 being 1 µL each. In the top row, from left to right, the panels show: the titration of 6 mM Ca^{2+} into: apo-state full length cTnC, 1 mM Mg^{2+} incubated cTnC, and 3 mM Mg^{2+} incubated cTnC. The bottom row shows the titration of 40 mM Mg^{2+} into the apo-state full length cTnC. The isotherms can be used to visually determine the decreased amount of binding to site II in the presence of increasing Mg^{2+}.

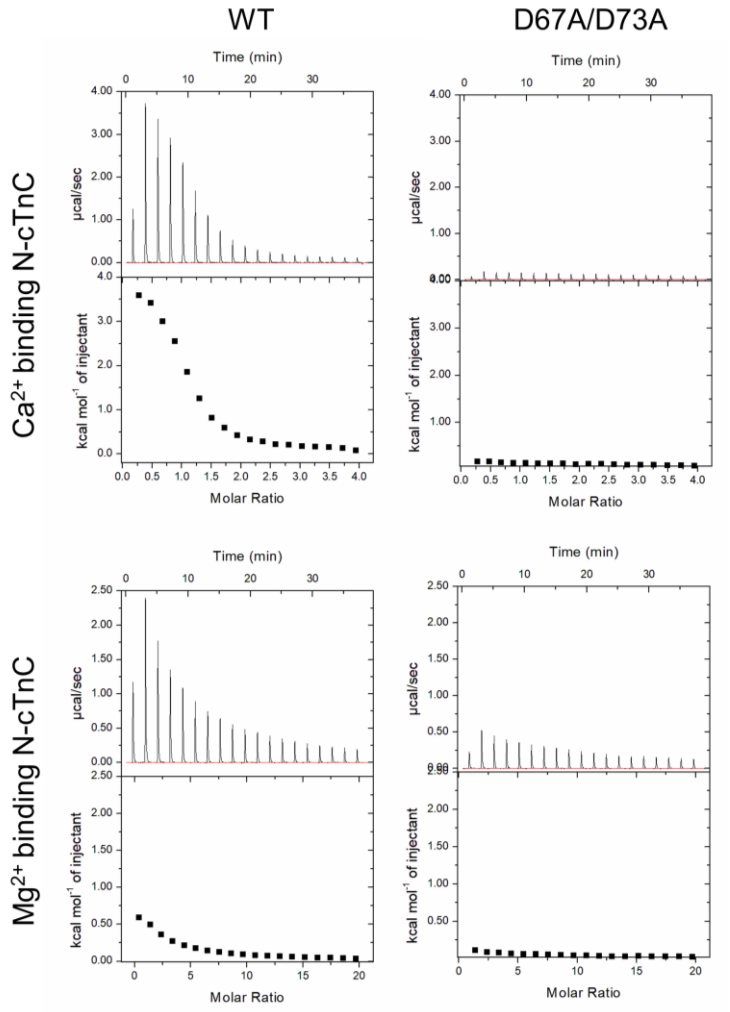

Supplemental Figure 5-2 Representative binding isotherms for binding of Ca^{2+} and Mg^{2+} to site II of N-cTnC

The top row shows the titration of 4 mM Ca^{2+} into apo-state N-cTnC, following by the same titration into the D67A/D73A mutant; these isotherms are scaled to 4 µcal*s^{-1} to help visualize the relative heat change. The bottom row shows the titration of 20 Mg^{2+} into apo-state N-cTnC, followed by the same titration into the D67A/D73A mutant; these isotherms are scaled to 2.5 µcal*s^{-1} to help visualize the relative heat change.

Supplemental Table 5-1 Thermodynamic Parameters Derived for Ca^{2+} and Mg^{2+} binding to full-length cTnC

	Titrant	cTnC condition	n	N	K_A $*10^3$ (M^{-1})	K_d (μM)	ΔH (kcal*mol^{-1})	T*ΔS (kcal*mol^{-1})	ΔG (kcal*mol^{-1})
Site II	Ca^{2+}	Apo-State	7	1.91 ± 0.07	44.3 ^{A} ± 1.0	22.7 ^{B} ± 0.5	3.71 ^{A} ± 0.06	10.0 ^{A} ± 0.07	-6.29 ^{C} ± 0.20
	Mg^{2+}	Apo-State	8	32.9 ± 0.5	2.47 ^{C} ± 0.05	406.1 ^{A} ± 7.9	0.091 ^{D} ± 0.001	4.71 ^{D} ± 0.01	-4.62 ^{A} ± 0.11
	Ca^{2+}	+ 1 mM Mg^{2+}	8	2.10 ± 0.05	32.4 ^{B} ± 0.9	31.0 ^{B} ± 0.9	1.93 ^{B} ± 0.09	8.09 ^{B} ± 0.08	-6.16 ^{B} ± 0.59
	Ca^{2+}	+ 3 mM Mg^{2+}	10	2.96 ± 0.06	29.1 ^{B} ± 1.7	35.5 ^{B} ± 2.1	0.75 ^{C} ± 0.03	6.83 ^{C} ± 0.04	-6.08 ^{B} ± 0.54
Sites III/IV	Ca^{2+}	Apo-State	7	2.19 ± 0.05	8757.1 ^{B} ± 951.4	0.12 ^{B} ± 0.02	-8.20 ^{D} ± 0.07	1.24 ^{D} ± 0.07	-9.44 ^{B} ± 0.61
	Mg^{2+}	Apo-State	8	4.92 ± 0.15	60.5 ^{C} ± 3.0	16.7 ^{A} ± 0.7	-0.23 ^{A} ± 0.01	6.28 ^{A} ± 0.03	-6.51 ^{A} ± 0.31
	Ca^{2+}	+ 1 mM Mg^{2+}	8	2.02 ± 0.04	7526.3 ^{B} ± 333.5	0.14 ^{B} ± 0.01	-6.87 ^{C} ± 0.09	2.50 ^{C} ± 0.10	-9.37 ^{B} ± 0.50
	Ca^{2+}	+ 3 mM Mg^{2+}	10	1.94 ± 0.04	12870.0 ^{A} ± 939.6	0.08 ^{B} ± 0.01	-6.19 ^{B} ± 0.06	3.50 ^{B} ± 0.06	-9.79 ^{C} ± 0.26

6 mM Ca^{2+} and 40 mM Mg^{2+} titrations into 100 μM N-cTnC were the baseline conditions. Ca^{2+} was also titrated into protein pre-incubated with 1 and 3 mM Mg^{2+} to study the competition for all three binding sites. Binding to site II was analyzed separately from binding to sites IIII/IV where analysis of variance was used to test for a significant difference in the means for each thermodynamic parameter. At the level of each parameter, Tukey's post hoc test was carried out. The results of this test are indicated by superscripted letters, where conditions with unique letters are significantly different ($p < 0.05$).

Supplemental Table 5-2 Thermodynamic Parameters Derived from ITC for Each N-cTnC Titration Condition

Titrant	N-cTnC Condition	n	N	K_A*10^3 (M^{-1})	K_d (μM)	ΔH (kcal*mol^{-1})	T*ΔS (kcal*mol^{-1})	ΔG (kcal*mol^{-1})
Ca^{2+}	Apo-State	7	1.01 ± 0.01	66.1 ^{A} ± 2.0	15.2 ^{C} ± 0.5	3.82 ^{A} ± 0.04	10.39 ^{A} ± 0.03	-6.57 ^{H} ± 0.02
	D67A/D73A	8	1.00	5.9 $^{E, F}$ ± 0.5	180.3 ^{C} ± 16.2	0.23 $^{H, I}$ ± 0.02	5.36 ^{G} ± 0.05	-5.12 ^{D} ± 0.05
	+ 1 mM Mg^{2+}	6	1.00	31.2 ^{B} ± 2.7	33.1 ^{C} ± 2.57	2.47 ^{B} ± 0.05	8.58 ^{B} ± 0.01	-6.12 ^{G} ± 0.05
	+ 3 mM Mg^{2+}	7	1.00	20.9 ^{C} ± 1.3	48.9 ^{C} ± 2.81	1.73 ^{C} ± 0.05	7.62 ^{C} ± 0.03	-5.89 ^{G} ± 0.04
	+ 5 mM Mg^{2+}	7	1.00	14.0 ^{D} ± 0.7	72.3 ^{C} ± 3.17	1.52 ^{D} ± 0.05	7.17 ^{D} ± 0.04	-5.65 ^{F} ± 0.02
	+ 10 mM Mg^{2+}	7	1.00	9.7 $^{D, E}$ ± 0.5	105.3 ^{C} ± 5.54	1.13 ^{E} ± 0.04	6.57 ^{E} ± 0.02	-5.43 $^{E, F}$ ± 0.03
	+ 20 mM Mg^{2+}	5	1.00	8.2 ^{E} ± 0.1	122.8 ^{C} ± 2.06	0.78 ^{F} ± 0.04	6.13 ^{F} ± 0.03	-5.35 $^{D, E}$ ± 0.01
Mg^{2+}	Apo-State	5	1.00	1.54 $^{F, G}$ ± 0.06	652.8 $^{B, C}$ ± 28.4	2.64 ^{B} ± 0.1	6.99 ^{D} ± 0.07	-4.35 ^{C} ± 0.03
	D67A/D73A	5	1.00	0.90 $^{F, G}$ ± 0.08	1148.6 ^{A} ± 95.0	0.76 ^{F} ± 0.04	4.78 ^{H} ± 0.03	-4.02 ^{B} ± 0.05
	+ 1 mM Ca^{2+}	5	1.00	0.55 ^{G} ± 0.05	1870.0 ^{A} ± 171.5	0.48 ^{G} ± 0.04	4.22 ^{I} ± 0.03	-3.73 ^{A} ± 0.05
	+ 2 mM Ca^{2+}	6	1.00	0.47 ^{G} ± 0.05	2251.7 ^{A} ± 261.8	0.41 $^{G, H}$ ± 0.04	4.04 $^{I, J}$ ± 0.07	-3.63 ^{A} ± 0.07
	+ 3 mM Ca^{2+}	8	1.00	0.52 ^{G} ± 0.04	2037.5 ^{A} ± 172.2	0.24 $^{H, I}$ ± 0.02	3.92 ^{J} ± 0.04	-3.69 ^{A} ± 0.05
	+ 5 mM Ca^{2+}	9	1.00	0.50 ^{G} ± 0.08	2255.8 ^{A} ± 220.1	0.20 ^{I} ± 0.02	3.84 ^{J} ± 0.06	-3.64 ^{A} ± 0.07

4 mM Ca^{2+} and 20 mM Mg^{2+} titrations into 200 μM N-cTnC were the baseline conditions. For the Ca^{2+} titrations, pre-incubation with 1, 3, 5, 10, and 20 mM Mg^{2+} prior to titrations was used to study the site II occupation by both cations. The affinity and enthalpy change associated with the interaction was decreased with increasing amounts of Mg^{2+} incubated. For the Mg^{2+} titrations, pre-incubation with 1, 2, 3, 5 mM Ca^{2+} prior to titrations was used to study the binding of both cations to site II. Increasing the concentration of Ca^{2+} decreased the binding affinity of Mg^{2+} to site II and decreased the enthalpy change, therefore less Mg^{2+} binds N-cTnC in the presence of Ca^{2+}. The D67A/D73A mutant was used to reduce the binding of both cations to the EF hand of site II, albeit to a different extent for each. All parameters are displayed as mean ± SEM, with the exception of the stoichiometric ratio for the Mg^{2+} binding which was constrained to 1.00 to facilitate fitting. Titrations not linked with the same superscripted letter were significantly different ($p<0.05$). The first letter of the alphabet indicates the largest mean and each subsequent letter denotes a significantly lower mean.

Supplemental Table 5-3 Ion restraints used for thermodynamic integration.

System	Ca^{2+} to WT N-cTnC		Ca^{2+} to D67A/D73A N-cTnC		Mg^{2+} to WT N-cTnC		Mg^{2+} to D67A/D73A N-cTnC	
Restraint 1	ASP67 CG	2.7 Å	ALA67 CB	4.2 Å	ASP67 CG	2.3 Å	THR71 O	1.9 Å
Restraint 2	SER69 OG	2.6 Å	SER69 OG	2.6 Å	SER69 OG	3.7 Å	SER69 OG	2.0 Å
Restraint 3	GLU76 CD	2.8 Å	GLU76 CD	2.8 Å	THR71 OG1	4.5 Å	ASP65 CG	2.3 Å

For each system, 3 restraints to the ion were used. Table shows atom and distance to restrained ion.

5.8. References

Allen, K., Y. Y. Xu and W. G. Kerrick (2000). "Ca(2+) measurements in skinned cardiac fibers: effects of Mg(2+) on Ca(2+) activation of force and fiber ATPase." J Appl Physiol (1985) **88**(1): 180-185.

Allen, T. S., L. D. Yates and A. M. Gordon (1992). "Ca(2+)-dependence of structural changes in troponin-C in demembranated fibers of rabbit psoas muscle." Biophys J **61**(2): 399-409.

Amano, T., T. Matsubara, J. Watanabe, S. Nakayama and N. Hotta (2000). "Insulin modulation of intracellular free magnesium in heart: involvement of protein kinase C." British journal of pharmacology **130**(4): 731-738.

Åqvist, J. (1990). "Ion-water interaction potentials derived from free energy perturbation simulations." The Journal of Physical Chemistry **94**(21): 8021-8024.

Ashley, C. C. and D. G. Moisescu (1977). "Effect of changing the composition of the bathing solutions upon the isometric tension-pCa relationship in bundles of crustacean myofibrils." J Physiol **270**(3): 627-652.

Bers, D. M. (2000). "Calcium Fluxes Involved in Control of Cardiac Myocyte Contraction." Circulation Research **87**(4): 275-281.

Best, P. M., S. K. Donaldson and W. G. Kerrick (1977). "Tension in mechanically disrupted mammalian cardiac cells: effects of magnesium adenosine triphosphate." J Physiol **265**(1): 1-17.

Bhattacharya, S., C. G. Bunick and W. J. Chazin (2004). "Target selectivity in EF-hand calcium binding proteins." Biochim Biophys Acta **1742**(1-3): 69-79.

Boresch, S., F. Tettinger, M. Leitgeb and M. Karplus (2003). "Absolute Binding Free Energies: A Quantitative Approach for Their Calculation." The Journal of Physical Chemistry B **107**(35): 9535-9551.

Brini, M., T. Cali, D. Ottolini and E. Carafoli (2012). "Calcium pumps: why so many?" Compr Physiol **2**(2): 1045-1060.

Carafoli, E. and J. Krebs (2016). "Why Calcium? How Calcium Became the Best Communicator." J Biol Chem **291**(40): 20849-20857.

Case, D.A., Betz, R.M., Cerutti, D.S., Cheatham, III, T.E., Darden, T.A., Duke, R.E., Giese, T.J. , Gohlke, H., Goetz, A.W., Homeyer, N., Izadi, S., Janowski, P., Kaus, J., Kovalenko, A., Lee, T.S., LeGrand, S., Li, P., Lin, C., Luchko, T., Luo, R., Madej, B., Mermelstein, D., Merz, K.M., Monard, G., Nguyen, H., Nguyen, H.T., Omelyan, I., Onufriev, A., Roe, D.R., Roitberg, A., Sagui, C, Simmerling, C.L., Botello-Smith, W.M., Swails, J., Walker, R.C., Wang, J., Wolf, R.M., Wu, X., Xiao, L. and Kollman, P.A. (2016), AMBER 2016, University of California, San Francisco.

Cates, M. S., M. B. Berry, E. L. Ho, Q. Li, J. D. Potter and G. N. Phillips, Jr. (1999). "Metal-ion affinity and specificity in EF-hand proteins: coordination geometry and domain plasticity in parvalbumin." Structure **7**(10): 1269-1278.

Cefaratti, C. and A. M. Romani (2007). "Functional characterization of two distinct Mg2+ extrusion mechanisms in cardiac sarcolemmal vesicles." Molecular and cellular biochemistry **303**(1-2): 63-72.

Chao, S. H., Y. Suzuki, J. R. Zysk and W. Y. Cheung (1984). "Activation of calmodulin by various metal cations as a function of ionic radius." Mol Pharmacol **26**(1): 75-82.

Cheung, J. Y., D. L. Tillotson, R. Yelamarty and R. Scaduto (1989). "Cytosolic free calcium concentration in individual cardiac myocytes in primary culture." American Journal of Physiology-Cell Physiology **256**(6): C1120-C1130.

Dai, L. J., P. A. Friedman and G. A. Quamme (1997). "Cellular mechanisms of chlorothiazide and cellular potassium depletion on Mg2+ uptake in mouse distal convoluted tubule cells." Kidney Int **51**(4): 1008-1017.

Davis, J. P., J. A. Rall, P. J. Reiser, L. B. Smillie and S. B. Tikunova (2002). "Engineering competitive magnesium binding into the first EF-hand of skeletal troponin C." J Biol Chem **277**(51): 49716-49726.

Dokmanic, I., M. Sikic and S. Tomic (2008). "Metals in proteins: correlation between the metal-ion type, coordination number and the amino-acid residues involved in the coordination." Acta Crystallogr D Biol Crystallogr **64**(Pt 3): 257-263.

Donaldson, S. K., P. M. Best and G. L. Kerrick (1978). "Characterization of the effects of Mg2+ on Ca2+- and Sr2+-activated tension generation of skinned rat cardiac fibers." J Gen Physiol **71**(6): 645-655.

Donaldson, S. K. and W. G. Kerrick (1975). "Characterization of the effects of Mg2+ on Ca2+- and Sr2+-activated tension generation of skinned skeletal muscle fibers." J Gen Physiol **66**(4): 427-444.

Ebashi, S. and M. Endo (1968). "Calcium ion and muscle contraction." Prog Biophys Mol Biol **18**: 123-183.

Ebashi, S., Y. Nonomura, K. Kohama, T. Kitazawa and T. Mikawa (1980). "Regulation of muscle contraction by Ca ion." Mol Biol Biochem Biophys **32**: 183-194.

Ebashi, S. and Y. Ogawa (1988). "Ca2+ in contractile processes." Biophys Chem **29**(1-2): 137-143.

Fabiato, A. and F. Fabiato (1975). "Effects of magnesium on contractile activation of skinned cardiac cells." J Physiol **249**(3): 497-517.

Fagan, T. E. and A. Romani (2001). "α1-Adrenoceptor-induced Mg2+ extrusion from rat hepatocytes occurs via Na+-dependent transport mechanism." American Journal of Physiology-Gastrointestinal and Liver Physiology **280**(6): G1145-G1156.

Farah, C. S. and F. C. Reinach (1995). "The troponin complex and regulation of muscle contraction." Faseb j **9**(9): 755-767.

Filatov, V. L., A. G. Katrukha, T. V. Bulargina and N. B. Gusev (1999). "Troponin: structure, properties, and mechanism of functioning." Biochemistry (Mosc) **64**(9): 969-985.

Follenius, A. and D. Gerard (1984). "Fluorescence investigations of calmodulin hydrophobic sites." Biochem Biophys Res Commun **119**(3): 1154-1160.

Francois, J. M., C. Gerday, F. G. Prendergast and J. D. Potter (1993). "Determination of the Ca2+ and Mg2+ affinity constants of troponin C from eel skeletal muscle and positioning of the single tryptophan in the primary structure." J Muscle Res Cell Motil **14**(6): 585-593.

Gifford, Jessica L., Michael P. Walsh and Hans J. Vogel (2007). "Structures and metal-ion-binding properties of the Ca²⁺-binding helix–loop–helix EF-hand motifs." Biochemical Journal **405**(2): 199-221.

Gilli, R., D. Lafitte, C. Lopez, M. Kilhoffer, A. Makarov, C. Briand and J. Haiech (1998). "Thermodynamic analysis of calcium and magnesium binding to calmodulin." Biochemistry **37**(16): 5450-5456.

Gillis, T. E., T. M. Blumenschein, B. D. Sykes and G. F. Tibbits (2003). "Effect of temperature and the F27W mutation on the Ca2+ activated structural transition of trout cardiac troponin C." Biochemistry **42**(21): 6418-6426.

Gillis, T. E., C. R. Marshall, X.-H. Xue, T. J. Borgford and G. F. Tibbits (2000). "Ca2+ binding to cardiac troponin C: effects of temperature and pH on mammalian and salmonid isoforms." American Journal of Physiology-Regulatory, Integrative and Comparative Physiology **279**(5): R1707-R1715.

Gillis, T. E., C. D. Moyes and G. F. Tibbits (2003). "Sequence mutations in teleost cardiac troponin C that are permissive of high Ca 2+ affinity of site II." American Journal of Physiology-Cell Physiology **284**(5): C1176-C1184.

Godt, R. E. (1974). "Calcium-activated tension of skinned muscle fibers of the frog. Dependence on magnesium adenosine triphosphate concentration." J Gen Physiol **63**(6): 722-739.

Godt, R. E. and B. D. Lindley (1982). "Influence of temperature upon contractile activation and isometric force production in mechanically skinned muscle fibers of the frog." J Gen Physiol **80**(2): 279-297.

Godt, R. E. and J. L. Morgan (1984). "Contractile responses to MgATP and pH in a thick filament regulated muscle: studies with skinned scallop fibers." Adv Exp Med Biol **170**: 569-572.

Grossoehme, N. E., A. M. Spuches and D. E. Wilcox (2010). "Application of isothermal titration calorimetry in bioinorganic chemistry." J Biol Inorg Chem **15**(8): 1183-1191.

Harding, M. M. (2002). "Metal-ligand geometry relevant to proteins and in proteins: sodium and potassium." Acta Crystallogr D Biol Crystallogr **58**(Pt 5): 872-874.

Hazard, A. L., S. C. Kohout, N. L. Stricker, J. A. Putkey and J. J. Falke (1998). "The kinetic cycle of cardiac troponin C: calcium binding and dissociation at site II trigger slow conformational rearrangements." Protein Science **7**(11): 2451-2459.

Heizmann, C. W. and J. A. Cox (1998). "New perspectives on S100 proteins: a multi-functional Ca(2+)-, Zn(2+)- and Cu(2+)-binding protein family." Biometals **11**(4): 383-397.

Herzberg, O. and M. N. James (1985). "Structure of the calcium regulatory muscle protein troponin-C at 2.8 Å resolution."

Holroyde, M., S. Robertson, J. Johnson, R. Solaro and J. Potter (1980). "The calcium and magnesium binding sites on cardiac troponin and their role in the regulation of myofibrillar adenosine triphosphatase." Journal of Biological Chemistry **255**(24): 11688-11693.

Hongo, K., M. Konishi and S. Kurihara (1994). "Cytoplasmic free Mg2+ in rat ventricular myocytes studied with the fluorescent indicator furaptra." Jpn J Physiol **44**(4): 357-378.

Houdusse, A., M. L. Love, R. Dominguez, Z. Grabarek and C. Cohen (1997). "Structures of four Ca2+-bound troponin C at 2.0 A resolution: further insights into the Ca2+-switch in the calmodulin superfamily." Structure **5**(12): 1695-1711.

Howarth, F., J. Waring, B. Hustler and J. Singh (1994). "Effects of extracellular magnesium and beta adrenergic stimulation on contractile force and magnesium mobilization in the isolated rat heart." Magnesium research **7**(3-4): 187-197.

Johnson, J. D., S. C. Charlton and J. D. Potter (1979). "A fluorescence stopped flow analysis of Ca2+ exchange with troponin C." J Biol Chem **254**(9): 3497-3502.

Johnson, J. D., J. H. Collins, S. P. Robertson and J. D. Potter (1980). "A fluorescent probe study of Ca2+ binding to the Ca2+-specific sites of cardiac troponin and troponin C." Journal of Biological Chemistry **255**(20): 9635-9640.

Johnson, J. D., R. J. Nakkula, C. Vasulka and L. B. Smillie (1994). "Modulation of Ca2+ exchange with the Ca(2+)-specific regulatory sites of troponin C." J Biol Chem **269**(12): 8919-8923.

Johnson, R. A., L. M. Fulcher, K. Vang, C. D. Palmer, N. E. Grossoehme and A. M. Spuches (2019). "In depth, thermodynamic analysis of Ca(2+) binding to human cardiac troponin C: Extracting buffer-independent binding parameters." Biochim Biophys Acta Proteins Proteom **1867**(4): 359-366.

Kawasaki, Y. and J.-P. van Eerd (1972). "The effect of Mg++ on the conformation of the Ca++-binding component of troponin." Biochemical and Biophysical Research Communications **49**(4): 898-905.

Kerrick, W. G., H. G. Zot, P. E. Hoar and J. D. Potter (1985). "Evidence that the Sr2+ activation properties of cardiac troponin C are altered when substituted into skinned skeletal muscle fibers." J Biol Chem **260**(29): 15687-15693.

Kerrick, W. G. L. and S. K. B. Donaldson (1975). "The comparative effects of [Ca2+] and [Mg2+] on tension generation in the fibers of skinned frog skeletal muscle and mechanically disrupted rat ventricular cardiac muscle." Pflügers Archiv **358**(3): 195-201.

Kirschenlohr, H. L., A. A. Grace, J. I. Vandenberg, J. C. Metcalfe and G. A. Smith (2000). "Estimation of systolic and diastolic free intracellular Ca2+ by titration of Ca2+ buffering in the ferret heart." Biochem J **346 Pt 2**: 385-391.

Kohama, K. (1980). "Role of the high affinity Ca binding sites of cardiac and fast skeletal troponins." J Biochem **88**(2): 591-599.

Kometani, K. and K. Yamada (1983). "Enthalpy, entropy and heat capacity changes induced by binding of calcium ions to cardiac troponin C." Biochemical and biophysical research communications **114**(1): 162-167.

Kretsinger, R. H. and C. E. Nockolds (1973). "Carp muscle calcium-binding protein. II. Structure determination and general description." J Biol Chem **248**(9): 3313-3326.

L DeLano, W. (2002). The PyMOL Molecular Graphics System (2002) DeLano Scientific, Palo Alto, CA, USA. http://www.pymol.org.

Laires, M. J., C. P. Monteiro and M. Bicho (2004). "Role of cellular magnesium in health and human disease." Front Biosci **9**: 262-276.

Leavis, P. and E. L. Kraft (1978). "Calcium binding to cardiac troponin C." Archives of biochemistry and biophysics **186**(2): 411-415.

Leelananda, S. P. and S. Lindert (2016). "Computational methods in drug discovery." Beilstein J Org Chem **12**: 2694-2718.

Lewit-Bentley, A. and S. Rety (2000). "EF-hand calcium-binding proteins." Curr Opin Struct Biol **10**(6): 637-643.

Li, A. Y., C. M. Stevens, B. Liang, K. Rayani, S. Little, J. Davis and G. F. Tibbits (2013). "Familial hypertrophic cardiomyopathy related cardiac troponin C L29Q mutation alters length-dependent activation and functional effects of phosphomimetic troponin I*."

Li, M. X., M. Chandra, J. R. Pearlstone, K. I. Racher, G. Trigo-Gonzalez, T. Borgford, C. M. Kay and L. B. Smillie (1994). "Properties of isolated recombinant N and C domains of chicken troponin C." Biochemistry **33**(4): 917-925.

Li, M. X., L. Spyracopoulos and B. D. Sykes (1999). "Binding of Cardiac Troponin-I147-163 Induces a Structural Opening in Human Cardiac Troponin-C." Biochemistry **38**(26): 8289-8298.

Li, P., B. P. Roberts, D. K. Chakravorty and K. M. Merz, Jr. (2013). "Rational Design of Particle Mesh Ewald Compatible Lennard-Jones Parameters for +2 Metal Cations in Explicit Solvent." J Chem Theory Comput **9**(6): 2733-2748.

Liang, B., F. Chung, Y. Qu, D. Pavlov, T. E. Gillis, S. B. Tikunova, J. P. Davis and G. F. Tibbits (2008). "Familial hypertrophic cardiomyopathy-related cardiac troponin C mutation L29Q affects Ca2+ binding and myofilament contractility." Physiological genomics **33**(2): 257-266.

Linse, S. and S. Forsen (1995). "Determinants that govern high-affinity calcium binding." Adv Second Messenger Phosphoprotein Res **30**: 89-151.

Lockless, S. W., M. Zhou and R. MacKinnon (2007). "Structural and thermodynamic properties of selective ion binding in a K+ channel." PLoS Biol **5**(5): e121.

Maguire, M. E. (2006). "Magnesium transporters: properties, regulation and structure." Front Biosci **11**: 3149-3163.

Maier, J. A., C. Martinez, K. Kasavajhala, L. Wickstrom, K. E. Hauser and C. Simmerling (2015). "ff14SB: Improving the Accuracy of Protein Side Chain and Backbone Parameters from ff99SB." J Chem Theory Comput **11**(8): 3696-3713.

Malmendal, A., S. Linse, J. Evenas, S. Forsen and T. Drakenberg (1999). "Battle for the EF-hands: magnesium-calcium interference in calmodulin." Biochemistry **38**(36): 11844-11850.

Morimoto, S. (1991). "Effect of myosin cross-bridge interaction with actin on the Ca2+-binding properties of troponin C in fast skeletal myofibrils." The Journal of Biochemistry **109**(1): 120-126.

Murray, A. C. and C. M. Kay (1972). "Hydrodynamic and optical properties of troponin A. Demonstration of a conformational change upon binding calcium ion." Biochemistry **11**(14): 2622-2627.

Nara, M., H. Morii and M. Tanokura (2013). "Infrared study of synthetic peptide analogues of the calcium-binding site III of troponin C: The role of helix F of an EF-hand motif." Biopolymers **99**(5): 342-347.

Ogawa, Y. (1985). "Calcium binding to troponin C and troponin: effects of Mg2+, ionic strength and pH." The Journal of Biochemistry **97**(4): 1011-1023.

Pan, B. S. and R. J. Solaro (1987). "Calcium-binding properties of troponin C in detergent-skinned heart muscle fibers." J Biol Chem **262**(16): 7839-7849.

Panteva, M. T., G. M. Giambasu and D. M. York (2015). "Comparison of structural, thermodynamic, kinetic and mass transport properties of Mg(2+) ion models commonly used in biomolecular simulations." J Comput Chem **36**(13): 970-982.

Parmacek, M. S. and R. J. Solaro (2004). "Biology of the troponin complex in cardiac myocytes." Prog Cardiovasc Dis **47**(3): 159-176.

Pinto, J. R., M. S. Parvatiyar, M. A. Jones, J. Liang, M. J. Ackerman and J. D. Potter (2009). "A functional and structural study of troponin C mutations related to hypertrophic cardiomyopathy." J Biol Chem **284**(28): 19090-19100.

Potter, J. D. and J. Gergely (1975). "The calcium and magnesium binding sites on troponin and their role in the regulation of myofibrillar adenosine triphosphatase." Journal of Biological Chemistry **250**(12): 4628-4633.

Potter, J. D., S. P. Robertson and J. D. Johnson (1981). "Magnesium and the regulation of muscle contraction." Fed Proc **40**(12): 2653-2656.

Ramos, C. H. (1999). "Mapping subdomains in the C-terminal region of troponin I involved in its binding to troponin C and to thin filament." J Biol Chem **274**(26): 18189-18195.

Reid, R. E. and R. M. Procyshyn (1995). "Engineering magnesium selectivity in the helix-loop-helix calcium-binding motif." Arch Biochem Biophys **323**(1): 115-119.

Robertson, S., J. D. Johnson and J. Potter (1981). "The time-course of Ca2+ exchange with calmodulin, troponin, parvalbumin, and myosin in response to transient increases in Ca2+." Biophysical journal **34**(3): 559.

Rocklin, G. J., D. L. Mobley, K. A. Dill and P. H. Hunenberger (2013). "Calculating the binding free energies of charged species based on explicit-solvent simulations employing lattice-sum methods: an accurate correction scheme for electrostatic finite-size effects." J Chem Phys **139**(18): 184103.

Romani, A. and A. Scarpa (1992). "Regulation of cell magnesium." Arch Biochem Biophys **298**(1): 1-12.

Romani, A. M. P. (2011). Intracellular magnesium homeostasis. Magnesium in the Central Nervous System. R. Vink and M. Nechifor. Adelaide (AU), University of Adelaide Press (c) 2011 The Authors.

Sacco, C., R. A. Skowronsky, S. Gade, J. M. Kenney and A. M. Spuches (2012). "Calorimetric investigation of copper(II) binding to Abeta peptides: thermodynamics of coordination plasticity." J Biol Inorg Chem **17**(4): 531-541.

Schober, T., S. Huke, R. Venkataraman, O. Gryshchenko, D. Kryshtal, H. S. Hwang, F. J. Baudenbacher and B. C. Knollmann (2012). "Myofilament Ca sensitization increases cytosolic Ca binding affinity, alters intracellular Ca homeostasis, and causes pause-dependent Ca-triggered arrhythmia." Circulation research **111**(2): 170-179.

Seamon, K. B., D. J. Hartshorne and A. A. Bothner-By (1977). "Ca2+ and Mg2+ dependent conformations of troponin C as determined by 1H and 19F nuclear magnetic resonance." Biochemistry **16**(18): 4039-4046.

She, M., W. J. Dong, P. K. Umeda and H. C. Cheung (1998). "Tryptophan mutants of troponin C from skeletal muscle: an optical probe of the regulatory domain." European journal of biochemistry **252**(3): 600-607.

Shirts, M. R., Mobley, D. L., & Brown, S. P. (2010). Free-energy calculations in structure-based drug design. Drug design: structure-and ligand-based approaches, 61-86.

Sia, S. K., M. X. Li, L. Spyracopoulos, S. M. Gagné, W. Liu, J. A. Putkey and B. D. Sykes (1997). "Structure of cardiac muscle troponin C unexpectedly reveals a closed regulatory domain." Journal of Biological Chemistry **272**(29): 18216-18221.

Siddiqui, J. K., S. B. Tikunova, S. D. Walton, B. Liu, M. Meyer, P. P. de Tombe, N. Neilson, P. M. Kekenes-Huskey, H. E. Salhi, P. M. Janssen, B. J. Biesiadecki and J. P. Davis (2016). "Myofilament Calcium Sensitivity: Consequences of the Effective Concentration of Troponin I." Front Physiol **7**: 632.

Skowronsky, R. A., M. Schroeter, T. Baxley, Y. Li, J. M. Chalovich and A. M. Spuches (2013). "Thermodynamics and molecular dynamics simulations of calcium binding to the regulatory site of human cardiac troponin C: evidence for communication with the structural calcium binding sites." JBIC Journal of Biological Inorganic Chemistry **18**(1): 49-58.

Slupsky, C. M. and B. D. Sykes (1995). "NMR solution structure of calcium-saturated skeletal muscle troponin C." Biochemistry **34**(49): 15953-15964.

Solaro, R. J. and J. S. Shiner (1976). "Modulation of Ca2+ control of dog and rabbit cardiac myofibrils by Mg2+. Comparison with rabbit skeletal myofibrils." Circ Res **39**(1): 8-14.

Spyracopoulos, L., M. X. Li, S. K. Sia, S. M. Gagné, M. Chandra, R. J. Solaro and B. D. Sykes (1997). "Calcium-induced structural transition in the regulatory domain of human cardiac troponin C." Biochemistry **36**(40): 12138-12146.

Steinbrecher, T., I. Joung and D. A. Case (2011). "Soft-core potentials in thermodynamic integration: comparing one- and two-step transformations." J Comput Chem **32**(15): 3253-3263.

Stephenson, D. G. and D. A. Williams (1982). "Effects of sarcomere length on the force-pCa relation in fast- and slow-twitch skinned muscle fibres from the rat." J Physiol **333**: 637-653.

Stevens, C. M., K. Rayani, C. E. Genge, G. Singh, B. Liang, J. M. Roller, C. Li, A. Y. Li, D. P. Tieleman and F. van Petegem (2016). "Characterization of Zebrafish Cardiac and Slow Skeletal Troponin C Paralogs by MD Simulation and ITC." Biophysical Journal **111**(1): 38-49.

Stevens, C. M., K. Rayani, G. Singh, B. Lotfalisalmasi, D. P. Tieleman and G. F. Tibbits (2017). "Changes in the dynamics of the cardiac troponin C molecule explain the effects of Ca2+-sensitizing mutations." Journal of Biological Chemistry **292**(28): 11915-11926.

Strynadka, N. C. and M. N. James (1989). "Crystal structures of the helix-loop-helix calcium-binding proteins." Annu Rev Biochem **58**: 951-998.

Sturtevant, J. M. (1977). "Heat capacity and entropy changes in processes involving proteins." Proc Natl Acad Sci U S A **74**(6): 2236-2240.

Sundaralingam, M., R. Bergstrom, G. Strasburg, S. T. Rao, P. Roychowdhury, M. Greaser and B. C. Wang (1985). "Molecular structure of troponin C from chicken skeletal muscle at 3-angstrom resolution." Science **227**(4689): 945-948.

Tanaka, H., H. Takahashi and T. Ojima (2013). "Ca(2)+-binding properties and regulatory roles of lobster troponin C sites II and IV." FEBS Lett **587**(16): 2612-2616.

Tessman, P. A. and A. Romani (1998). "Acute effect of EtOH on Mg2+ homeostasis in liver cells: evidence for the activation of an Na+/Mg2+ exchanger." Am J Physiol **275**(5): G1106-1116.

Tikunova, S. B., D. J. Black, J. D. Johnson and J. P. Davis (2001). "Modifying Mg2+ binding and exchange with the N-terminal of calmodulin." Biochemistry **40**(11): 3348-3353.

Tikunova, S. B. and J. P. Davis (2004). "Designing calcium-sensitizing mutations in the regulatory domain of cardiac troponin C." Journal of Biological Chemistry **279**(34): 35341-35352.

Tikunova, S. B., J. A. Rall and J. P. Davis (2002). "Effect of hydrophobic residue substitutions with glutamine on Ca2+ binding and exchange with the N-domain of troponin C." Biochemistry **41**(21): 6697-6705.

van Eerd, J. P. and K. Takahshi (1976). "Determination of the complete amino acid sequence of bovine cardiac troponin C." Biochemistry **15**(5): 1171-1180.

Vormann, J. and T. Günther (1987). "Amiloride-sensitive net Mg2+ efflux from isolated perfused rat hearts." Magnesium **6**(4): 220-224.

Wang, S.-Q., Y.-H. Huang, K.-S. Liu and Z.-Q. Zhou (1997). "Dependence of myocardial hypothermia tolerance on sources of activator calcium." Cryobiology **35**(3): 193-200.

Wilcox, D. E. (2008). "Isothermal titration calorimetry of metal ions binding to proteins: An overview of recent studies." Inorganica Chimica Acta **361**(4): 857-867.

Wnuk, W., M. Schoechlin and E. A. Stein (1984). "Regulation of actomyosin ATPase by a single calcium-binding site on troponin C from crayfish." J Biol Chem **259**(14): 9017-9023.

Wolf, F. I., A. Di Francesco, V. Covacci, D. Corda and A. Cittadini (1996). "Regulation of intracellular magnesium in ascites cells: Involvement of different regulatory pathways." Archives of biochemistry and biophysics **331**(2): 194-200.

Yamada, K. (1978). "The enthalpy titration of troponin C with calcium." Biochimica et Biophysica Acta (BBA)-Protein Structure **535**(2): 342-347.

Yamada, K. (2003). "Calcium binding to troponin C as a primary step of the regulation of contraction. A microcalorimetric approach." Adv Exp Med Biol **538**: 203-212; discussion 213.

Yamada, K. and K. Kometani (1982). "The changes in heat capacity and entropy of troponin C induced by calcium binding." The Journal of Biochemistry **92**(5): 1505-1517.

Yap, K. L., J. B. Ames, M. B. Swindells and M. Ikura (1999). "Diversity of conformational states and changes within the EF-hand protein superfamily." Proteins **37**(3): 499-507.

Yumoto, F., M. Nara, H. Kagi, W. Iwasaki, T. Ojima, K. Nishita, K. Nagata and M. Tanokura (2001). "Coordination structures of Ca2+ and Mg2+ in Akazara scallop troponin C in solution. FTIR spectroscopy of side-chain COO- groups." Eur J Biochem **268**(23): 6284-6290.

Zot, A. S. and J. D. Potter (1987). "Structural aspects of troponin-tropomyosin regulation of skeletal muscle contraction." Annual review of biophysics and biophysical chemistry **16**(1): 535-559.

Chapter 6.

The Effect of Magnesium on Calcium Binding to Mutant Troponin C

6.1. Abstract

Cardiac troponin C (cTnC) is the calcium (Ca^{2+}) sensing component of the heterotrimeric cardiac troponin (cTn) complex, where binding of this cation during systole causes a series of conformational changes that culminate in force production. Mutations in cTnC allosterically alter the binding properties of this protein to increase or decrease affinity. It has been proposed that elevated force production and duration of time spent in contraction may lead to the hypertrophic phenotype in what is likely a collective of diseases termed Hypertrophic Cardiomyopathies (HCM).

Regulation of contraction has long been though to occur exclusively through Ca^{2+} binding to site II of cTnC, however the relative abundance of cellular magnesium (Mg^{2+}), coupled with sequence similarities between Ca^{2+} and Mg^{2+} binding motifs makes this divalent cation a potential competitor for binding to the same sites. Despite findings by a number of groups, the existing dogma still precludes the binding of Mg^{2+} to site II of cTnC. We have used isothermal titration calorimetry (ITC) to explore the thermodynamic properties associated with the interaction between Ca^{2+}/Mg^{2+} and the regulatory (N-terminal) domain of cTnC (N-cTnC). Our data suggest that physiological concentrations of Mg^{2+} may bind to N-cTnC to compete with Ca^{2+} at site II.

We also explored the effect of a series of mutations located in N-cTnC. Three of the mutants (A8V, L29Q, and A31S) had only slightly elevated affinity for Ca^{2+} and Mg^{2+} relative to the WT construct. The other mutations (L48Q, Q50R, and C84Y), that are closer to the C-terminal domain and surrounding the EF hand binding motif of site II had a more dramatic effect on affinity and altered the thermodynamics of the binding interaction.

Our results suggest a physiologically significant role for cellular Mg^{2+} at baseline conditions and when elevated on the Ca^{2+} binding properties of the contractile

apparatus. This may be especially true in diseased states which alter the binding properties of both Ca^{2+} and Mg^{2+}, to alter contractile function.

6.2. Introduction

Familial Hypertrophic Cardiomyopathy (FHC) is the inherited subset of Hypertrophic Cardiomyopathy (HCM). FHC is thought to afflict between 1 in 500 (Maron, Gardin et al. 1995) and 1 in 200 (Semsarian, Ingles et al. 2015) and is the most common cause of sudden cardiac death in young athletes (Maron, Shirani et al. 1996). To date over 1000 mutations have been found in a variety of mostly sarcomeric proteins with over 100 mutations in the cardiac troponin (cTn) complex (Harada and Morimoto 2004, Ashrafian and Watkins 2007, Seidman and Seidman 2011). Despite such a wide range of molecular precursors, the disease is consistently characterized by hypertrophy, myocyte disarray, and fibrosis (Elliott and McKenna 2004). The devastating nature of this disease is rooted in the frequent absence of overt symptoms combined with the age of initial outward manifestation. The first sign is often sudden cardiac death, which is normally attributed to ventricular tachycardia and/or fibrillation following premature ventricular contractions (Davis, Davis et al. 2016).

It is generally believed that central to the mechanism of this disease is mishandling of calcium (Ca^{2+}), whereby increased sensitivity is thought to prolong the contractile phase and reduce relaxation thus causing diastolic dysfunction and leading to hypertrophy. Free Ca^{2+} in the cardiomyocyte is tightly regulated and fluctuates from 100 nM during diastole up to 1 µM in systole (Bers 2000).

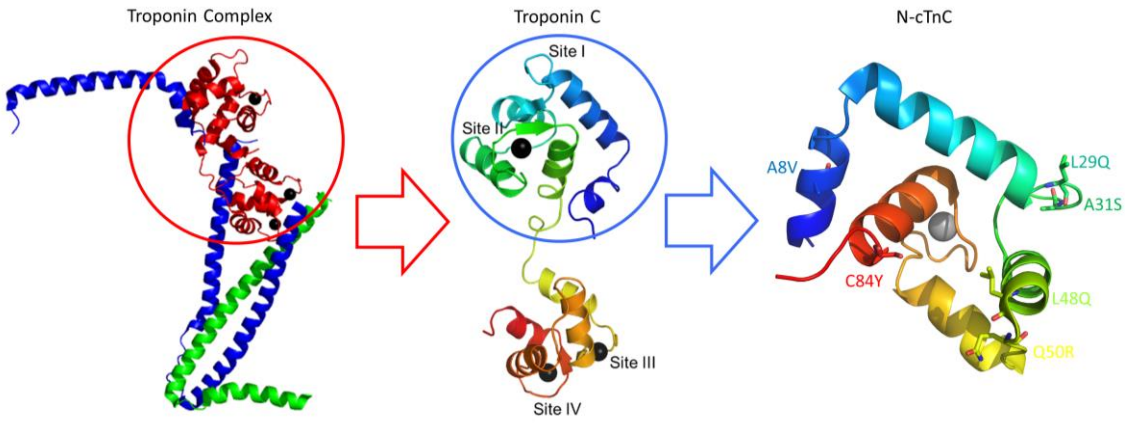

Figure 6-1 N-cTnC within cTnC and the Troponin complex
The cTn complex is shown on the left panel. This complex includes the Ca^{2+} binding cTnC in red, the inhibitory cTnI in blue, and the tropomyosin binding cTnT in green. Black spheres depict the bound cations that interact with sites III/IV in the C-terminal domain and site II in the N-terminal domain. cTnC, shown in the middle panel in rainbow colors with the N-terminal domain in blue and the C-terminal domain in red. The black spheres again depict the bound cations. The focus of this work is on the N-domain of cTnC which is depicted in the right-most panel with each of the 6 studied mutations highlighted and labelled.

The heterotrimeric cardiac troponin (cTn) complex is the link between Ca^{2+} signaling and contraction. This complex includes: Ca^{2+} sensing troponin C (TnC), inhibitory troponin I (TnI), and tropomyosin-binding troponin T (TnT) (**Figure 6-1**). The cTn complex, along with actin and tropomyosin forms the cardiac thin filament (TF). The TF interacts with multiple proteins such as myosin, myosin binding protein C, and titin that form the thick filament of the cardiac contractile apparatus (Katrukha 2013).

TnC is a globular protein with 4 Ca^{2+}/magnesium (Mg^{2+}) binding EF hands. Structural sites III and IV, in the C-terminal domain bind Ca^{2+} (K_A ~10^7 M^{-1}) and Mg^{2+} (K_A ~10^4 M^{-1}) with high affinity to tether cTnC to the other components of the cTn complex (Potter and Gergely 1975, Sturtevant 1977, Tikunova and Davis 2004). The N-terminal domain of cTnC also contains two EF hand motifs, however site I, which binds Ca^{2+} in skeletal tissue is dysfunctional in cardiac muscle leaving site II as the sole regulatory site. Low affinity (K_A ~10^5 M^{-1}) binding to site II allows for this site to be unbound during diastole and bound during systole. This binding acts as a switch, setting off a series of conformational changes in the cTn complex.

Binding to site II, results in the movement of helices NAD away from BC, exposing a hydrophobic cleft. This region is then bound and stabilized by the switch peptide of TnI (residues 147–163) (TnI_{sw}). This leads to movement within the cTn

complex and the rest of the TF exposing binding sites on actin and allowing for contact with myosin heads, ultimately resulting in force production (Sia, Li et al. 1997, Kirschenlohr, Grace et al. 2000).

Multiple FHC-associated mutations have been found in the N-terminal domain of cTnC (residues 1-89) (Kalyva, Parthenakis et al. 2014). In this study we have focused on A8V (Cordina, Liew et al. 2013), L29Q (Hoffmann, Schmidt-Traub et al. 2001), A31S (Parvatiyar, Landstrom et al. 2012), and C84Y (Landstrom, Parvatiyar et al. 2008) in addition to the engineered mutation L48Q (Tikunova and Davis 2004) and the Dilated Cardiomyopathy (DCM) associated mutation Q50R (van Spaendonck-Zwarts, van Tintelen et al. 2010) (**Figure 6-1**).

We have previously studied this series of mutations through isothermal titration calorimerty (ITC) and Molecular Dynamics (MD) Simulations (Stevens, Rayani et al. 2017). ITC allows for the measurement of the thermodynamic parameters which underly a binding interaction. Using this technique, we can elucidate the reaction stoichiometry (N) as well as the affinity (K_A) and thus the dissociation constant (K_d), the change in enthalpy (ΔH), change in entropy (ΔS), and change in Gibbs free energy (ΔG) (Freire, Mayorga et al. 1990). A prevalent hypothesis in this field posits that mutations that destabilized the closed conformation of the protein (prior to Ca^{2+} binding) and/or those that favor the open (Ca^{2+} bound) state confer an increase in affinity (Willott, Gomes et al. 2010).

A8V is located in the N-helix of N-cTnC and causes a slightly elevated Ca^{2+} binding affinity relative to WT. L29Q and A31S are located between helices A and B and caused a greater increase in Ca^{2+} affinity with the reaction coordinates largely maintained. Q50R and L48Q are located between helices B and C and significantly increased the affinity of the protein for Ca^{2+} and altered the energetics of the binding interaction. C84Y which is located immediately before the DE linker also significantly increased the affinity of the protein for Ca^{2+} to well above the values observed in the WT (Stevens, Rayani et al. 2017).

After potassium, Mg^{2+} is the second most abundant cellular cation with a total concentration of ~15 - 20 mM, but it is also tightly regulated with the majority buffered by cytosolic components such as ATP. Even still, free Mg^{2+} measures approximately 1 mM

and is about 1000 times as abundant as systolic Ca^{2+} (Romani and Scarpa 1992, Dai, Friedman et al. 1997, Maguire 2006).

Davis et al. have shown that Mg^{2+} concentrations of 3 mM decrease the Ca^{2+} affinity in isolated cTnC (Tikunova and Davis 2004), and skinned psoas muscles (Davis, Rall et al. 2002). Interestingly, in these fluorescence-based studies, Mg^{2+} did not seem to cause structural changes in cTnC (Tikunova and Davis 2004). We sought to further explore the effects of Mg^{2+} on Ca^{2+} binding to the regulatory domain of cTnC and possible modifying affects on the previously listed series of mutations.

Sequence variations outside the coordinating residues of the EF hands of cTnC allosterically induce alterations in Ca^{2+} affinity (Liang, Chung et al. 2008, Tikunova, Liu et al. 2010). These changes in Ca^{2+} binding have previously been linked to FHC and DCM-associated mutations, thus insight regarding the underlying thermodynamics of this foundational interaction may have far reaching implications (Gomes and Potter 2004, Li, Stevens et al. 2013, Stevens, Rayani et al. 2017). In contrast, mutations outside the binding residues of each EF hand are not thought to allosterically modify Mg^{2+} binding (Andersson, Malmendal et al. 1997, Ohki, Ikura et al. 1997, Malmendal, Evenas et al. 1998), therefore the role of this cation in FHC is currently unclear.

Our ITC studies on the binding of Ca^{2+} and Mg^{2+} to mutant N-cTnC suggest that Mg^{2+} may interact with this protein even at normal cytosolic free concentrations. The affinity of each of the 6 mutants for Mg^{2+} was higher than the WT which was measured to have a physiological significant affinity for Mg^{2+}. Therefore, the presence of Mg^{2+} at baseline levels may play a physiologically significant role. Higher than baseline concentrations of Mg^{2+} that accompany certain energy-depleted states may further accentuate the effects of inherited mutations and exacerbate disease phenotypes.

6.3. Methods

6.3.1. Construct Preparations

Recombinant proteins were expressed and purified as described previously (Stevens, Rayani et al. 2016). In brief, the human cTnC gene (*TNNC1*) within the pET-21a(+) vector was ordered from Novagen and the Phusion site directed mutagenesis kit (Thermo) used to introduce a stop codon at residue 90, followed by single base pair

changes to introduce all 6 mutations of interest (A8V, L29Q, A31S, L48Q, Q50R, and C84Y) on separate N-terminal constructs ($cTnC_{1-89}$). Mutagenesis was carried out with preliminary steps using the DH5α *E. coli* strain to house the plasmids. Following the mutagenesis and confirmation by sequencing, the constructs were transformed into the BL21(DE3) expression strain and stored as glycerol stocks.

6.3.2. Protein Expression

100 mL of Lysogeny Broth (LB) supplemented with 50 µg/mL of Ampicillin and a stab of the glycerol stock was grown overnight at 37˚C for 16 – 20 hrs with shaking at 225-250 rpm. 1 L flasks of LB were induced with 1-5% of the over night culture and supplemented with the same concentration of antibiotic and grown under the same conditions for ~3 hrs (until OD_{600} was between 0.8-1.0). The culture was then supplemented with 1 mM Isopropyl β-D-1-thiogalactopyranoside (IPTG) and grown for a further 3 – 4 hrs. Cells were then harvested by centrifugation and resuspended in the Lysis Buffer (50 mM Tris-Cl and 100 mM NaCl at pH 8.0). The suspended pellet was stored at -80˚C until purification.

6.3.3. Protein Purification

The pellet was thawed and sonicated at ~80% amplitude in 30 second intervals for a total time of 3 – 4 mins with each intermittent period spent on ice. The cells were then spun 2 times, for 15 minutes each at 30,000 xg and the supernatant kept and the pellet discarded. The supernatant was filtered as needed and applied to a 15 mL fast-flow DEAE or Q Sepharose column (GE Healthcare), pre-equilibrated with Buffer A (50 mM Tris-Cl, 100 mM NaCl, and 1 mM Dithiothreitol (DTT) at pH 8.0). Buffer B (Buffer A + 0.55 M NaCl) was applied over a 180 mL protocol, where the concentration was ramped up from 0 to 100% to elute the proteins of interest. Fractions containing the N-terminal cTnC construct were identified by SDS PAGE and pooled. An Amicon centrifugal concentrator (Millipore) with a 3 KDa cut-off was used to concentrate the pooled samples to a volume of 3 – 5 mL. The pooled samples were then applied to a HiPrep 26/60 Sephacryl S-100 column (GE Healthcare) equilibrated with Buffer A. The fractions were again analyzed by SDS PAGE and those containing the protein of interest, free of contaminants were pooled, concentrated, and stored at -80˚C.

6.3.4. Preparation for ITC Experiments

The protein was dialyzed against 3 exchanges of 2 L for at least 6 hrs each with ITC Buffer 1 containing 50 mM HEPES, 150 mM KCl, 2 mM of EDTA, and 15 mM β-mercaptoethanol (BME) at pH 7.2. ITC Buffer 2 was identical to the first but did not contain EDTA. ITC Buffer 3 was identical to the second but contained 2 mM BME. The nanodrop was used to gain a preliminary measure of the protein concentration using an extinction coefficient of 1490 $M^{-1}*cm^{-1}$ and a molecular weight of 10.4 kDa. An initial ITC run, was used to determine the molar ratio (N). Given that the concentration of the titrant is known and the number of binding sites in N-cTnC is 1, the concentration of folded, functional protein can be determined and adjusted in subsequent runs to give an N of 1.0.

The protein was diluted in the final dialysis buffer to a final concentration of 100 µM. The titrating solutions were prepared from 1.00 M Ca^{2+} and Mg^{2+} stocks (Sigma) by serial dilution in the final dialysis buffer.

6.3.5. ITC Protocol

The titrations were done with 2 mM Ca^{2+} and 20 mM Mg^{2+}, with the exception of the L48Q which was titrated with 2 mM Mg^{2+}. 19 titrations, 60 seconds apart were performed with the first being 0.8 µL and each subsequent injection 2 µL. The cell contents were mixed at 750 rpm throughout the titration. All titrations were carried out at 25°C.

6.3.6. Data Processing and Statistical Analysis

Data were imported and analyzed in Origin 8.0 software for Microcal ITC_{200} (Northampton, MA). After saturation, the final 2-3 data points were averaged, the heat was subtracted from all injections as a control for heat of dilution and non-specific interactions. Least-squares regression was used to fit each titration after the first (dummy) injection was removed with minimization of chi-square and visual evaluation used to determine the goodness-of-fit for a single binding site model. Following establishment of the protein concentration based on the obtained N value for each apo-state Ca^{2+} titration for each construct, the same dilution of protein was used for each

other titration and the N-value fixed to 1.00 to facilitate data fitting. The various thermodynamic parameters were averaged and reported as a mean ± SEM. The difference between the means was compared using a one-way ANOVA, where all the titration conditions had $p<0.001$. This was followed by Tukey's post-hoc test to determine where significant differences existed ($p<0.05$) (**Tables 6-1 and 6-2**).

6.4. Results

All of the studied mutations increased Ca^{2+} and Mg^{2+} binding affinity relative to the WT construct (**Tables 6-1 and 6-2**). The smallest increase was associated with A8V and the greatest with L48Q. In general, the mutations located most adjacent to site II (L48Q, Q50R, and C84Y) increased the affinity for each cation to a greater extent and altered the thermodynamic profile of the binding interaction more dramatically; the changes associated with the other mutants was subtler.

The K_A associated with Mg^{2+} binding was orders of magnitude lower than that with Ca^{2+} binding for all constructs (**Figure 6-2 and S6-5**). The addition of 1 mM Mg^{2+} generally decreased the affinity for Ca^{2+} but also decreased the extent to which Ca^{2+} was able to bind site II (as visualized through a reduction in ΔH) (**Table S6-5**). Addition of 3 mM Mg^{2+} further decreased both the K_A and ΔH (**Table S6-6**).

Mutations with the closest proximity to site II, namely Q50R and C84Y responded most dramatically to the presence of Mg^{2+}. Pre-incubation caused the reaction landscape to change significantly such that endothermic apo-state interactions became exothermic.

6.4.1. Titration Based comparison

Calcium binding

L48Q, Q50R, and C84Y had significantly higher affinities than WT and were characterized by a significantly greater ΔG (**Table 6-1**). L29Q and A31S also changed the K_d significantly compared to the WT protein with the A8V mutation being the only construct that did not cause a significant elevation in affinity for Ca^{2+}. L48Q, Q50R, and C84Y had lower than WT changes in entropy. The Ca^{2+}-L48Q interacted was exothermic.

Table 6-1 The thermodynamic properties of the titration of Ca^{2+} into apo-state N-cTnC

N-cTnC	n	N	K_A *10^3 (M^{-1})	K_d (μM)	ΔH (kcal*mol^{-1})	T*ΔS (kcal*mol^{-1})	ΔG (kcal*mol^{-1})
WT	9	1.01 ± 0.01	64.48 ± 3.09	15.79 ± 0.74	3.58 ± 0.07	10.14 ± 0.08	-6.56 ± 0.03
A8V	6	1.02 ± 0.01	75.57 ± 1.29	13.25 ± 0.23	3.43 ± 0.04	10.09 ± 0.04	-6.66 ± 0.01
L29Q	5	1.04 ± 0.01	112.10 ± 6.71	9.05 * ± 0.55	3.47 ± 0.08	10.35 ± 0.07	-6.89 * ± 0.03
A31S	6	1.00 ± 0.01	121.30 ± 11.42	8.60 * ± 0.77	2.28 * ± 0.07	9.20 * ± 0.03	-6.93 * ± 0.06
L48Q	7	1.01 ± 0.01	394.71 * ± 7.26	2.54 * ± 0.05	-6.51 * ± 0.04	1.12 * ± 0.03	-7.63 * ± 0.01
Q50R	7	1.01 ± 0.01	232.86 * ± 24.14	4.61 * ± 0.52	1.43 * ± 0.04	8.74 * ± 0.04	-7.31 * ± 0.06
C84Y	7	1.00 ± 0.01	284.29 * ± 59.60	4.47 * ± 0.83	0.64 * ± 0.03	8.01 * ± 0.11	-7.37 * ± 0.12

For each parameter and across the construct type, the difference in mean value was tested using ANOVA followed by Tukey's post-hoc test; constructs differing in their mean $p<0.05$ from the WT are marked by *. Each parameter is displayed as mean ± SEM.

The Gibbs free energy reflects both the ΔH and the ΔS and as such demonstrates that the most favorable interaction occurs in L48Q, then Q50R/C84Y, followed by the other mutants.

Magnesium Binding

It is important to note that the interactions with Mg^{2+} are endothermic and entropically driven for all 6 mutants and the WT protein (**Table 6-2**). The highest affinities were seen in L48Q, Q50R, and C84Y. While the K_d was significantly lower than the WT for all the mutants, the lowest by two orders of magnitude was seen in L48Q. There is a great deal of overlap in the ΔH associated with the interaction of Mg^{2+} and each mutant/WT construct. The exception is L48Q where a significantly greater amount of binding occurs as indicated by the absolute value of ΔH. Every mutant was associated with a higher than WT ΔS, with the highest values associated with L48Q, followed by Q50R, and C84Y.

Competition

1 mM Magnesium Competition

As expected from the affinity for each individual cation, the L48Q construct had the highest affinity for Ca^{2+} in the 1 mM Mg^{2+} pre-incubation condition. The largest

affinities were seen in A31S, Q50R, and C84Y, with A8V and L29Q not distinguishable from the WT (**Table S6-5**).

Table 6-2 Parameters for the titration of Mg^{2+} into apo-state N-cTnC

N-cTnC	n	N	K_A *10^3 (M^{-1})	K_d (μM)	ΔH (kcal*mol^{-1})	T*ΔS (kcal*mol^{-1})	ΔG (kcal*mol^{-1})
WT	7	1.00	1.43 ± 0.07	711.08 ± 32.67	2.50 ± 0.18	6.79 ± 0.17	-4.29 ± 0.03
A8V	6	1.00	2.99 ± 0.08	335.49 * ± 10.11	2.75 ± 0.07	7.48 * ± 0.06	-4.74 ± 0.02
L29Q	6	1.00	2.88 ± 0.23	358.47 * ± 28.10	2.94 ± 0.06	7.65 * ± 0.06	-4.70 ± 0.05
A31S	6	1.00	4.24 ± 0.35	245.69 * ± 24.04	2.72 ± 0.08	7.65 * ± 0.10	-4.93 ± 0.05
L48Q	7	1.00	175.70 * ± 23.50	6.29 * ± 0.84	3.91 * ± 0.23	11.04 * ± 0.19	-10.50 * ± 2.18
Q50R	7	1.00	22.03 ± 0.99	45.97 * ± 2.14	2.27 ± 0.10	8.18 * ± 0.09	-5.92 ± 0.03
C84Y	8	1.00	29.89 ± 3.53	36.52 * ± 3.92	2.29 ± 0.06	8.37 * ± 0.05	-6.08 ± 0.06

The thermodynamic properties of the Mg^{2+} binding interaction with WT N-cTnC and each of the mutants are listed. For each parameter and across the construct type, constructs differing in their mean $p<0.05$ from the WT are marked by *. With the exception of N which that fixed to 1.00, each parameter is displayed as mean ± SEM.

The amount of binding can be tracked through the value of ΔH. The greatest change was seen in the 4 C-terminal most mutations that are also driven by exothermic interactions. The A8V and L29Q, while different from WT, were nonetheless similarly endothermic.

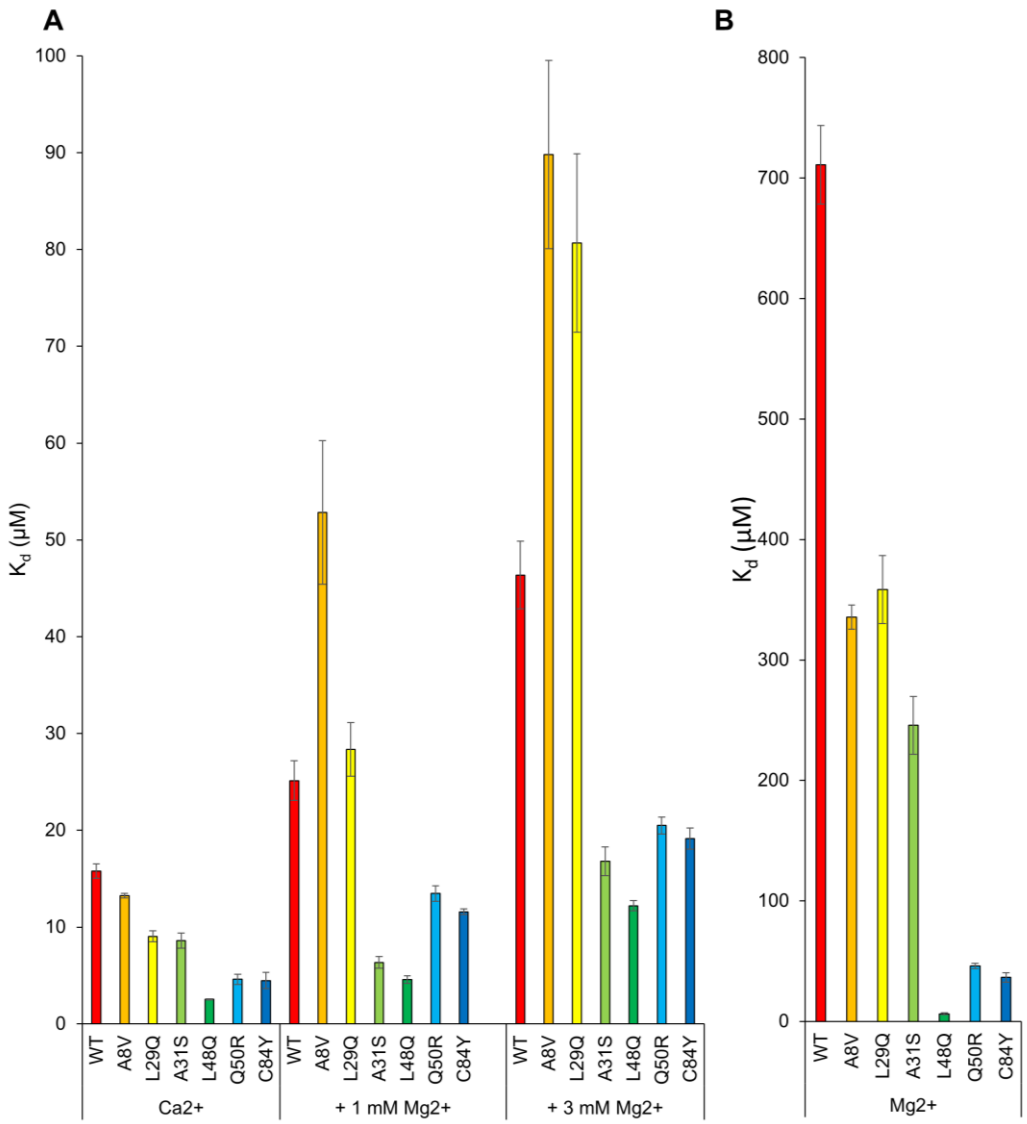

Figure 6-2 Comparing the K_d for Ca^{2+} binding (A) and Mg^{2+} binding (B) in each titration condition between all N-cTnC constructs

SEM error bars are used to depict where significant differences exist in the mean values.

The same four mutations: A31S, L48Q, Q50R, and C84Y showed a less favourable entropy change compared to the WT. Despite this, binding was more spontaneous, this was driven by the change in ΔH associated with each interaction. A8V and L29Q also interact spontaneously due to a favourable change in ΔS.

3 mM Magnesium Competition

The patterns observed in the 1 mM pre-incubation condition were largely maintained and accentuated further in the 3 mM pre-incubation condition. In general, the

highest K_A was seen in the mutants most adjacent to site II, with A8V and L29Q virtually indistinguishable from the WT construct (**Table S6-6**).

L48Q had the highest affinity for Ca^{2+} in this state as expected from its affinity for each individual cation. The ΔH was characteristic of an exothermic interaction in the A31S, L48Q, Q50R, and C84Y constructs and drove these more spontaneous reactions which again had the least favourable ΔS values.

A8V and L29Q are most WT like; they have the most favourable changes in entropy that resulted in spontaneous interactions despite endothermic binding.

6.4.2. Construct Based Comparison

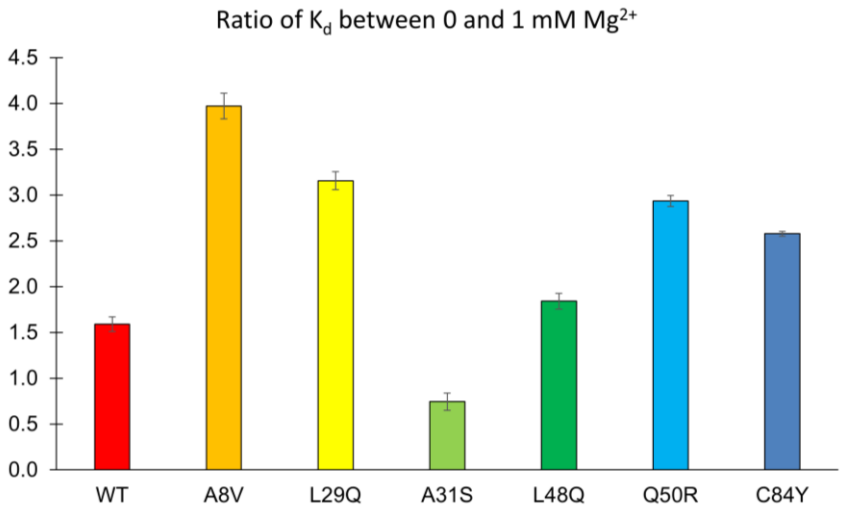

Figure 6-3 Ratio of change in K_d for Ca^{2+} binding between the apo-state titrations and the 1 mM Mg^{2+} pre-incubation experiments

SEM error bars are shown for each construct. ANOVA and Tukey's post-hoc test were used to determine that a significant different exists between each mutant and WT N-cTnC, $p<0.05$.

Figure 6-3 shows the change in K_d for Ca^{2+} as a result of adding 1 mM Mg^{2+} to the N-cTnC construct. A31S had a significantly lower K_d in the presence of 1 mM Mg^{2+}. The other 5 mutants also had a significant response to Mg^{2+} in comparison to WT N-cTnC. In each of these mutants, Ca^{2+} binding to site II occurred with significantly lower affinity in the presence of Mg^{2+}. In the WT N-cTnC and all of the mutants, the presence of Mg^{2+} significantly altered the binding affinity for Ca^{2+}.

WT N-cTnC

The interaction of Ca^{2+} with WT N-cTnC was endothermic and entropically driven. The K_d value associated with the interaction was 15.79 ± 0.74 µM. Mg^{2+} affinity was more than an order of magnitude lower but similarly endothermic and entropically driven. 1 mM Mg^{2+} lowered binding affinity by 35% and reduced the amount of binding (as indicated by lower ΔH) and the entropic favourability of the interaction (**Figure 6-3**). 3 mM Mg^{2+} further accentuated these changes.

A8V N-cTnC

The changes observed in our system should be considered relative rather than absolute. A8V had similar to WT isotherms and parameters with only a moderately higher affinity for both Ca^{2+} and Mg^{2+}. Both interactions were endothermic and entropically driven. The addition of 1 mM Mg^{2+} reduced the Ca^{2+} affinity approximately 3-fold and significantly reduced the amount of binding to site II (ΔH was reduced to less than half) (**Figure 6-3**). The effects of 3 mM Mg^{2+} pre-incubation was similar in that the K_A, ΔH, and ΔS were reduced such that the reactions were less spontaneous and binding occurred with a K_d that was nearly 7-fold higher than the apo-state condition. Therefore, the effect of Mg^{2+} pre-incubation on Ca^{2+} binding was more significant in the A8V mutant compared to the WT protein.

L29Q N-cTnC

The changes observed in L29Q relative to the WT protein was in line with the trends seen in the previous mutant. The affinity was higher than seen in the WT protein and the interaction was again, endothermic and entropically driven. The affinity of the mutant was nearly 2-fold higher than seen in the WT. The addition of 1 and 3 mM Mg^{2+} decreased the affinity such that K_d increased nearly 3- and 9-fold, respectively (**Figure 6-3**). The ΔH, indicative of the amount of binding also decreased in a graded manner with increasing amounts of Mg^{2+} such that a favourable ΔS was nearly the sole factor driving this interaction.

A31S N-cTnC

Ca^{2+} binding to A31S was endothermic and entropically driven and occurred with higher affinity than seen in the WT protein. The affinity of the mutant for Mg^{2+} was 3-fold higher than the WT. Given this, it was not surprising that the addition of 3 mM Mg^{2+}

decreased the affinity for Ca^{2+} to about half of that seen in the apo-state binding condition. However, two surprising findings were seen. Firstly, the addition of Mg^{2+} altered the reaction kinetics such that the interaction became exothermic. Secondly, the 1 mM preincubation condition was characterized by higher than apo-state affinity for Ca^{2+} (**Figure 6-3**). This may be due to the more than 30-fold higher affinity for Ca^{2+} such that 1 mM Mg^{2+} enhanced binding, despite assumed occupation of some percentage of the binding sites. Even still, the affinity for Ca^{2+} was further reduced when Mg^{2+} was elevated to 3 mM.

L48Q N-cTnC

Among the constructs studied, L48Q had the highest affinity for both Ca^{2+} and Mg^{2+} by a significant and substantial margin. It was characterized by an exothermic interaction when binding Ca^{2+} and an endothermic interaction with Mg^{2+}. The addition of 1 mM Mg^{2+} decreased the affinity by less than 2-fold (**Figure 6-3**) and 3 mM Mg^{2+} decreases affinity by nearly 5-fold. In both pre-incubation conditions, the interaction with Ca^{2+} was still exothermic, but the change in entropy was negligibly small such that the reaction was driven almost entirely by the dissipated heat.

Q50R N-cTnC

The affinity of Q50R for both Ca^{2+} and Mg^{2+} was higher than the WT. Binding was similarly endothermic and characterized by a positive ΔS. However, the addition of 1 mM Mg^{2+} had significant effects on the reaction such that binding of Ca^{2+} occurred with one third of the affinity (**Figure 6-3**) and the interaction became exothermically driven as the change in entropy was much less favorable (about one quarter the $T*\Delta S$). The addition of 3 mM Mg^{2+} further reduced the affinity such that it was about 5-fold lower but still exothermic. It should be noted that with greater concentration of pre-incubated Mg^{2+}, the amount of binding was reduced as seen through a lower ΔH.

C84Y N-cTnC

After the engineered L48Q mutation, C84Y caused the largest change in affinity for both Ca^{2+} and Mg^{2+} relative to the WT protein. This was in keeping with the trend of the C-terminal most mutations having a larger effect and enacting more significant changes on the energetics of these titrations. In the apo-state, the interaction with both cations was endothermic (though the absolute value indicated that the amount of binding

was much less than the WT) and entropically driven. The relative contribution of these parameters indicates that entropic favorability played a relatively large role in driving these reactions. Preincubation with 1 mM and 3 mM Mg^{2+} reduced affinity by approximately 3 (**Figure 6-3**) and 5-fold respectively, with the reaction becoming exothermic.

6.5. Discussion

The binding of Ca^{2+} to site II within the N-terminal domain of cTnC is the fundamental molecular precursor to a series of conformational changes that culminate in force production. As such, changes in the sequence of this highly conserved protein often have grave consequences for the force production capabilities of the heart (Gillis, Marshall et al. 2007). The 6 mutations that we have studied all occur outside the EF hand binding region and allosterically alter affinity. Given the location of each mutation of interest and the desire to focus on changes in the binding interaction, we exclusively studied the N-terminal domain of cTnC. The mutations in question have also been studied at various levels of complexity by numerous groups, whose findings agree to a reasonable degree with our conclusions (**Table S6-3**).

ITC directly measures the binding interaction and subsequent conformational change as an alternative to the introduction of naturally occurring fluorophores such as F27W (Gillis, Blumenschein et al. 2003) or bulky fluorophores such as IAANS (Dong, Wang et al. 1997, Li, Stevens et al. 2013). These fluorophores can be used to report on structural changes that proceed the binding interaction and thus, indirectly measure affinity. Fluorescence can also be used to report on the dissociation of Ca^{2+} from cTnC, cTn, or the TF by utilizing chelators such as EDTA and rapid fluid changes through a stopped flow apparatus (Tikunova, Liu et al. 2010).

Equilibrium dialysis studies indicate that Mg^{2+} does not compete with Ca^{2+} for binding to the N-terminal cTnC, and exclusively binds the C-terminal sites (Holroyde, Robertson et al. 1980). This notion has endured for almost 4 decades. However, our studies utilize ITC, that has the capability to detect minute changes in enthalpy (within 0.1 µcal) which accompany these interactions (Freire, Mayorga et al. 1990).

The binding of Ca^{2+} to N-terminal cTnC is governed by the balance between conformational strain resulting from the interaction and the energetics of exposing a hydrophobic cleft to the aqueous environment (Gifford, Walsh et al. 2007). Therefore, we posit that the changes in affinity seen in each mutant result from either the destabilization of the apo-state protein or the stabilization of the solvent exposed state.

In general, we found that the mutants had a more negative ΔG compared to the WT, consistent with the MD Simulations published previously (Stevens, Rayani et al. 2017). Work by Bowman and Lindert corroborates these findings and suggests a unifying theory that increased frequency of opening may result from the lowered energetic cost of exposing the N-terminal domain of cTnC. The placement of more hydrophilic amino acids that destabilize hydrophobic packing in the closed state and stabilize the open, solvent-exposed state that follows, may allow for this mechanism of action (Bowman and Lindert 2018).

A8V was only moderately different from the WT, consistent with previous findings that suggest this mutation alters the interaction of cTnC with other TF proteins rather than altering the Ca^{2+} binding affinity directly (Landstrom, Parvatiyar et al. 2008, Pinto, Parvatiyar et al. 2009). The location of this mutation near the interface with N-cTnI and strengthened interaction with the switch peptide makes this a distinct possibility (Zot, Hasbun et al. 2016, Stevens, Rayani et al. 2017). Nuclear Magnetic Resonance (NMR) data suggest a slight increase in the opening frequency in the apo-state relative to the WT (Cordina, Liew et al. 2013). In our study, the binding affinity of this mutant for Mg^{2+} was higher than the WT and as a result of this, in the pre-incubation conditions, the A8V construct had lower than WT affinity for Ca^{2+} (**Figure 6-6 and Table 6-6**).

L29Q is the next most proximal mutation to the N-helix and caused a statistically significant reduction in the K_d for Ca^{2+} binding compared to the WT. It also had greater than WT Mg^{2+} binding affinity but similar thermodynamic parameters and isotherm characteristics. Fluorescence studies on isolated cTnC containing the L29Q mutations showed increased Ca^{2+} affinity. A complex system containing the entire contractile apparatus with L29Q cTnC had similar to WT Ca^{2+} sensitivity (Dweck, Hus et al. 2008). This mutation changes sensitivity of force generation in a length and phosphorylation-dependent manner (Liang, Chung et al. 2008).

Alteration of a hydrophobic residue to one that is polar underlies sensitization of site II (Pearlstone, Borgford et al. 1992, da Silva, de Araujo et al. 1993). Mechanistically, solvent exposure of an uncharged glutamine may facilitate a greater extent of opening than a hydrophobic leucine (Stevens, Rayani et al. 2017). However, our previous work suggests that this mutant has the highest closed probability amongst the 7 constructs and lowers opening frequency (Stevens, Rayani et al. 2017). In contrast, it has been shown through NMR that this mutation may cause a more open N-domain in the cTnC in both the apo- and holo-states (Potluri, Cordina et al. 2019). L29Q may open in the holo-state with similar frequency as the WT and have similar energetic requirements as the WT for opening in both the apo- and holo-states (Bowman and Lindert 2018). Therefore, it is likely that the effects of this mutation in isolated N-cTnC is minimal and that changes are enacted through modification of the interaction with other cTn complex proteins (Li, Stevens et al. 2013).

A31S is located in the EF hand of the defunct site I and changes a hydrophobic amino acid for an uncharged one. In skeletal tissue, there is a great deal of cooperativity between binding to the two N-terminal sites of TnC (Johnson, Collins et al. 1978). This mutant had a significantly lower K_d for both Ca^{2+} and Mg^{2+} compared to the WT and significantly higher affinity for Ca^{2+} in both pre-incubation conditions. A31S was found through MD simulations to sample a greater number of interhelical angles and to have a lower average angle between helices A and B (Stevens, Rayani et al. 2017). The most interesting finding was that pre-incubation with 1 or 3 mM Mg^{2+} completely changed the reaction isotherm (**Figure S6-3**).

ΔH reflects the strength of hydrogen bonds, van der Waals interactions, and electrostatic forces between the titrant and the target ligand. Optimal placement of hydrogen bond donors and acceptors balances de-solvation of polar groups to contribute to the enthalpy change (Ward and Holdgate 2001). The significant change in enthalpy suggests alteration of the number of bonds formed by the side chains of binding site residues or those exposed to the environment following the conformational change. This mutation may stabilize the binding site I between helices A and B through formation of an additional hydrogen bond causing local changes that minimally alter global structure (Parvatiyar, Landstrom et al. 2012).

L48Q caused by far the largest change in affinity and altered the thermodynamics of each isotherm to the greatest degree. This mutation is located within the BC helical bundle and was strategically engineered to increase the Ca^{2+} sensitivity of force production (Tikunova and Davis 2004). The combination of high Ca^{2+} and Mg^{2+} affinity resulted in the lowest observed K_d in both competition conditions.

Our previously published MD simulations suggest that the absence of a hydrophobic residue disrupts hydrophobic packing in the AB domain. We also found that the L48Q mutant opens more frequently than the other constructs (Stevens, Rayani et al. 2017). Bowman and Lindert's work also suggests that L48Q samples the open state much more frequently than the WT protein (Bowman and Lindert 2018). The changes in ΔH are likely, at least in part, due to the presence of an additional hydrogen bond resulting from the introduction of a polar amino acid in a key domain of cTnC. *In vivo*, this would increase the opportunities for interaction with the TnI_{sw} (Wang, Robertson et al. 2012, Davis, Davis et al. 2016, Shettigar, Zhang et al. 2016).

Tikunova et al. originally suggested that despite a shift towards the Ca^{2+}-bound state, resulting from a reduction in hydrophobic contact between helices NAD and BC, the solvent exposure of the N-domain is minimized by numerous side chain contacts. Their hypothesis regarding the disruption of hydrophobic interactions and minimization of exposure to the surrounding solvent is reconcilable with our findings and explains the much lower ΔS associated with this set of titrations (Tikunova and Davis 2004).

Q50R is a relatively recently identified mutation that has yet to be fully explored. This change replaces a polar side chain with one that is bulky and charged. Given the hypothesized form of action seen in L48Q and the vicinity of these residues, it is conceivable that the packing of helices NAD and BC is also disrupted by this mutant. This mutant had a much higher affinity than WT for both Ca^{2+} and Mg^{2+} which bind endothermically. Similar to L48Q, the interaction with Ca^{2+} was exothermic in the pre-incubation condition. Our previous work suggests that Q50R is more frequently open than the WT cTnC (Stevens, Rayani et al. 2017). The reduced entropic cost of exposing a charged residue to the aqueous environment may explain the decreased ΔS of the system. Further, the energetic cost of opening the hydrophobic patch is increased in this mutant in comparison to the WT protein that has a less stable closed conformation (Bowman and Lindert 2018).

C84Y places a bulky hydrophobic side chain in the region immediately preceding the flexible DE linker that is bound and stabilized in the open state by the TnI_{SW}. This bulky tyrosine may act as a wedge to reduce interaction with the TnI_{SW} and thus increase the Ca^{2+} sensitivity of force development in skinned fibers (Landstrom, Parvatiyar et al. 2008, Pinto, Parvatiyar et al. 2009). This mutation was thermodynamically similar across all titrations with Q50R, which given the location of each does not necessarily suggest a similar mode of action. Interestingly however, our MD Simulations previously showed that a hydrophobic interaction between C84 and Q50 may be disrupted by this mutation. The bulky tyrosine in helix D may reduce the entropic cost of opening associated with the binding interaction, this is consistent with the observed, lower than WT ΔS values in C84Y N-cTnC (Stevens, Rayani et al. 2017).

The results presented in **Figure 6-3** show that WT N-cTnC and each of the mutants responded significantly and variably to the presence of Mg^{2+}. For the mutants, with the exception of A31S, the Ca^{2+} binding affinity of site II was significantly lowered in the presence of 1 mM Mg^{2+}. This desensitization was most pronounced in A8V>L29Q>Q50R>C84Y>L48Q. Given this observations, it is possible that Mg^{2+} binding dampens the presupposed sensitizing effect of HCM-associated mutations (Chang and Potter 2005). The change in pCa_{50} relative to the WT, presented in **Table 7-1** should be interpreted in light of these results; at the very least, the effect of Mg^{2+} in modifying Ca^{2+} sensitivity of force production cannot be ignored.

The abundance of Mg^{2+}, its similarities as a divalent cation and the small difference in atomic radius with Ca^{2+} suggests that this ion is a candidate for binding to site II of cTnC. Despite previous work in this field, the central dogma in the literature is largely dismissive of the possibility that physiologically relevant concentrations of Mg^{2+} bind to site II. A polar serine residue at the 69^{th} position and a negatively charged glutamic acid at the 76^{th} position in the EF hand binding site II of N-cTnC, create a domain that is amicable to Mg^{2+} binding (Reid and Procyshyn 1995, Tikunova, Black et al. 2001). We have explored the hypothesis that binding of both Ca^{2+} and Mg^{2+} occurs in a competitive manner to this site, where affinity for each cation is further modified by single amino acid changes outside the binding domain.

Tikunova and Davis have shown that Mg^{2+} does not cause a structural change upon binding but does significantly alter the affinity of cTnC for Ca^{2+} with 3 mM Mg^{2+}

causing a more than 3-fold reduction in Ca^{2+} binding affinity. Moreover, Mg^{2+} reversed the fluorescence change of Ca^{2+} saturated cTnC. That is to say, 3 mM Mg^{2+} competes for binding to site II (Tikunova and Davis 2004).

The importance of cellular Mg^{2+} is recognized, but the molecular mechanism requires further exploration. We measured a 47-fold difference in the affinity of WT N-cTnC for Ca^{2+} (15.79 ± 0.74 µM) and Mg^{2+} (711.08 ± 32.67 µM). However, Mg^{2+} is at least 1000 times more abundant in the cytosol at systole than Ca^{2+} 1 uM vs. 1 mM (Dai, Friedman et al. 1997, Bers 2002) and may compete for binding to site II in addition to the structural sites III and IV. Mg^{2+} deficiency has been linked to cardiac disease including arrythmias, hypertension, and congestive heart failure (Touyz 2004, Weglicki, Quamme et al. 2005, Mazur, Maier et al. 2007). It is possible that Mg^{2+} modulates the role of Ca^{2+} and alters activation of contractile pathways that are governed by this messenger.

6.6. Conclusions

The interaction of Ca^{2+} with mutant N-cTnC occurred with higher than WT affinities, with the highest affinity seen in the L48Q mutant. In general, A31S, L48Q, Q50R, and C84Y had the highest affinities for both Ca^{2+} and Mg^{2+}. Thermodynamic, structural, and simulation work by our group and multiple others suggests a common mechanism whereby the mutants disrupting stabilizing hydrophobic interactions between helices NAD and BC cause an elevation in binding affinity (Pinto, Parvatiyar et al. 2009, Wang, Robertson et al. 2012, Cordina, Liew et al. 2013, Stevens, Rayani et al. 2017).

We found that the affinity for Mg^{2+} was at least an order of magnitude lower than seen for Ca^{2+}. The change in affinity observed when comparing the Mg^{2+} pre-incubated N-cTnC and apo-state protein was variable in each mutant and significantly different from the WT (**Figure 6-3**). Moreover, 1 mM and 3 mM Mg^{2+} decreased the amount of binding and affinity for Ca^{2+} in a graded manner and may, play a significant role in the cardiomyocyte E-C coupling (Ogawa 1985, Tikunova and Davis 2004).

Less than 15 mins of ischemia can decrease $[ATP]_i$ to increase $[Mg^{2+}]$ three-fold (Murphy, Steenbergen et al. 1989, Hongo, Konishi et al. 1994, Tessman and Romani 1998). This elevated Mg^{2+} may compete with Ca^{2+} for binding to cytosolic buffers. Overall, our study suggests that the effect of cellular Mg^{2+} on the Ca^{2+} binding properties

of site II within N-cTnC is not negligible. This effect is even more pronounced in HCM- and DCM-mutant N-cTnC, where both cytosolic concentrations of free Mg^{2+} (1 mM) and elevated Mg^{2+} that may accompany energy depleted states (3 mM) caused a more than WT reduction in the affinity of the protein for Ca^{2+} and in multiple mutants (especially L48Q, Q50R, and C84Y) changed the energetic landscape of this interaction significantly.

6.7. Supplementary Appendix

```
Binding Site                          |--Site I29-40--|
Helix
  |-N3-9-|      |-----A14-25----|                |----B38-47---|
MDDIYKAAVE10 QLTEEQKNEF20 KAAFDIFVLG30 AEDGCISTKE40 LGKVMRMLGQ50
NPTPEELQEM60 IDEVDEDGSG70 TVDFDEFLVM80 MVRCMKDDSK90
   |----C54-64---|           |-----D74-85----|
Helix
Binding Site    |-Site II65-76-|
```

Supplemental Figure 6-1 Sequence of N-cTnC and key regions within.
The Sequence of the first 89 residues in human cTnC are shown in black, the location of the 6 residues of interest are bolded. The α-helices that determine the secondary structure of the protein are labelled in green. The Binding sites I and II are shown and labelled in blue.

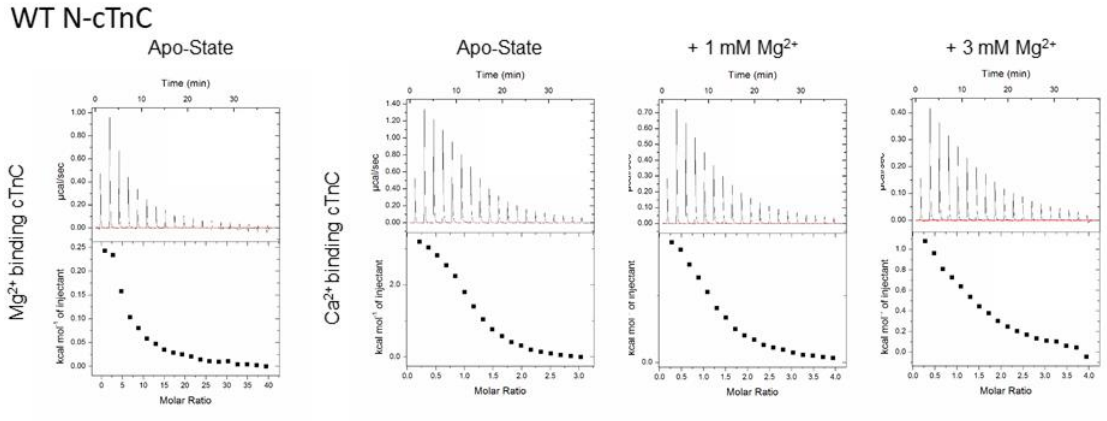

Supplemental Figure 6-2 Representative isotherms for each titration condition in the WT N-cTnC construct
On the left most panel, titration of Mg^{2+} into apo-state protein is shown with the next panels showing the titration of Ca^{2+} into apo-state N-cTnC. The next two panels show the titration of calcium into 1 mM and 3 mM Mg^{2+} incubated WT N-cTnC. All of the titrations are characterized by an endothermic interaction.

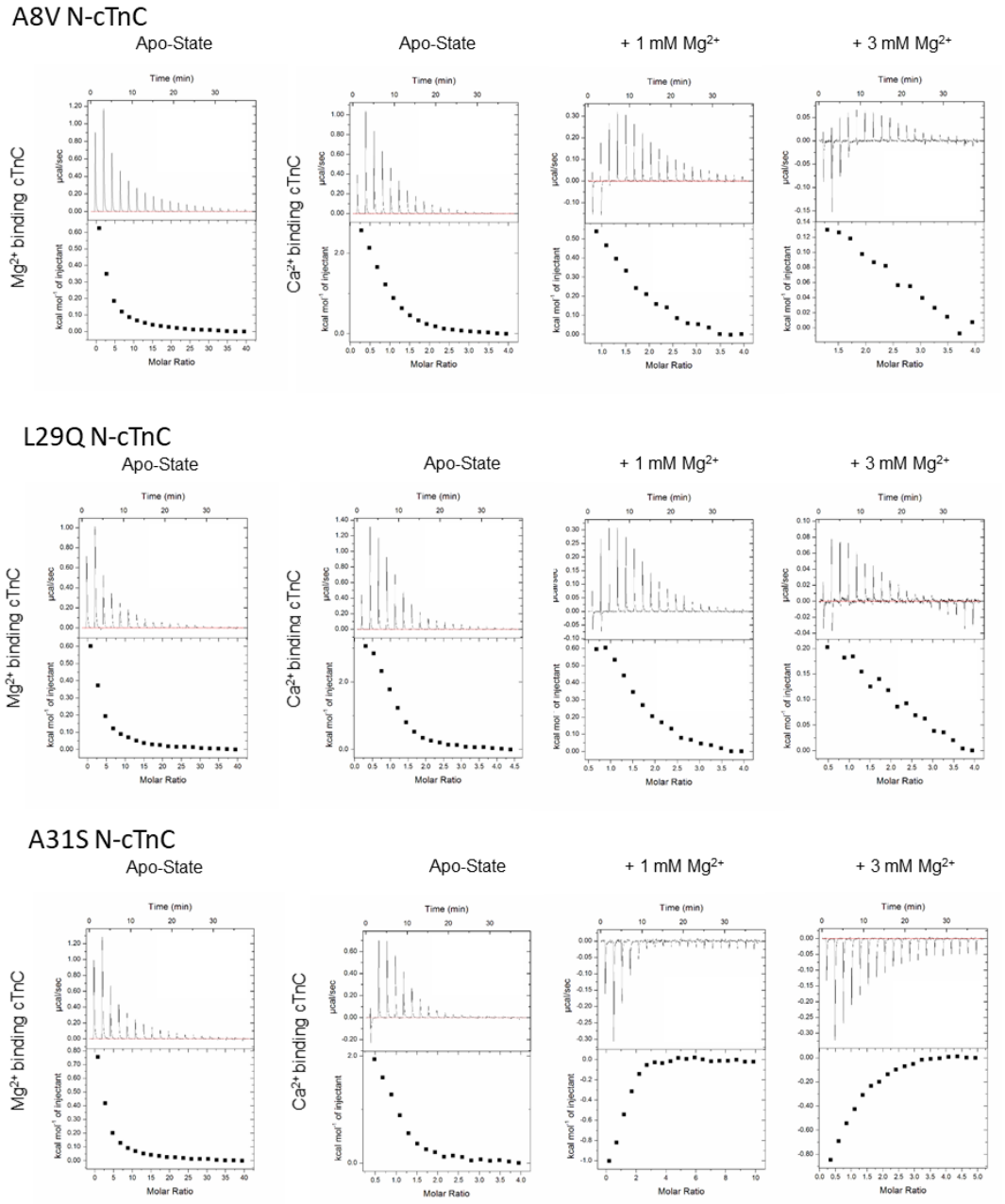

Supplemental Figure 6-3 Representative isotherms for each titration condition into A8V, L29Q, and A31S N-cTnC

The 3 most N-terminal mutations are shown; A8V, L29Q, and A31S from top to bottom. On the left most panel, titration of Mg^{2+} into apo-state protein is shown with the next panels showing the titration of Ca^{2+} into apo-state N-cTnC. The next two panels show the titration of Ca^{2+} into 1 mM and 3 mM Mg^{2+} incubated WT N-cTnC. The majority of titrations are characterized by an endothermic interaction with the exception of A31S, where pre-incubation with Mg^{2+} resulted in an exothermic interaction with Ca^{2+}.

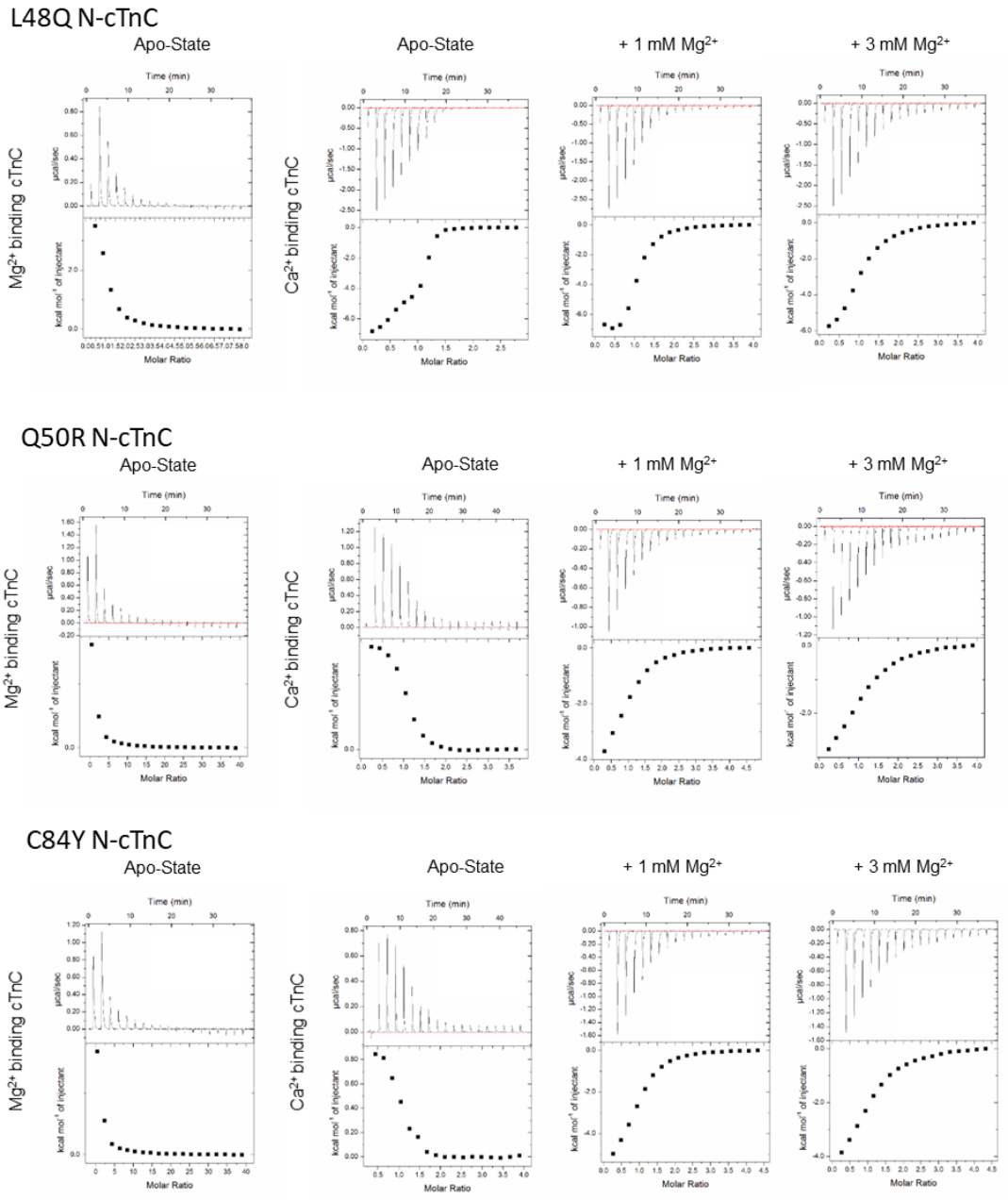

Supplemental Figure 6-4 Representative isotherms for each titration condition for L48Q, Q50R, and, C84Y N-cTnC

In the 3 most N-terminal mutations are shown; L48Q, Q50R, and C84Y from top to bottom. On the left most panel, titration of Mg^{2+} into apo-state protein is shown with the next panels showing the titration of Ca^{2+} into apo-state N-cTnC. The next two panels show the titration of Ca^{2+} into 1 mM and 3 mM Mg^{2+} incubated WT N-cTnC. These three mutants caused the greatest deviation in thermodynamic properties form the WT titration conditions. The Ca^{2+} into apo-protein titration is endothermic for Q50R and C84Y but exothermic for L48Q. The Mg^{2+} into apo-protein titration is endothermic for all 3 mutants. The pre-incubation condition with both 1 mM and 3 mM Mg^{2+} resulted in an exothermic interaction with Ca^{2+}.

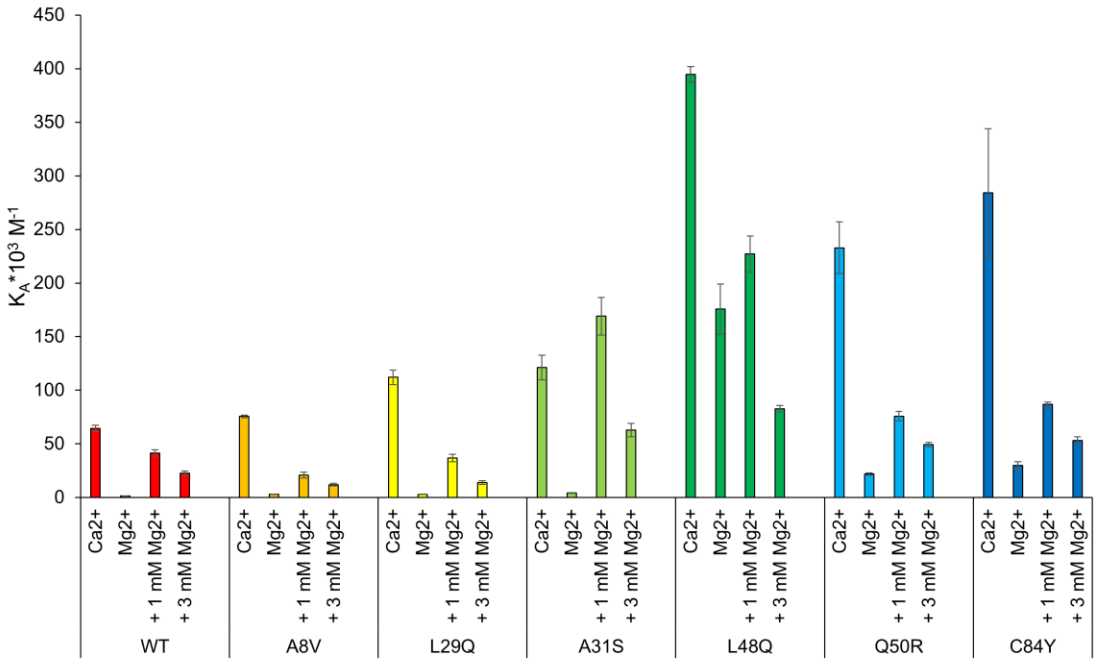

Supplemental Figure 6-5 Comparing the affinity for Ca^{2+}/Mg^{2+} in each titration condition between all N-cTnC constructs

SEM error bars are used to depict where significant differences exist in the mean values. With the exception of L48Q, the highest affinity is seen in the Ca^{2+} titration and the lowest in the Mg^{2+} titrations. L48Q has the highest Mg^{2+} binding affinity by over an order of magnitude. Increasing Mg^{2+} from 0 to 1 to 3 mM lowered Ca^{2+} binding affinity in a graded manner. The more C-terminal mutations cause a greater increase in K_a relative to the WT.

Supplemental Table 6-1 Ca^{2+} into 1 mM Mg^{2+} incubated N-cTnC titration-derived parameters

N-cTnC	n	N	K_A *10^3 (M^{-1})	K_d (μM)	ΔH (kcal*mol^{-1})	T*ΔS (kcal*mol^{-1})	ΔG (kcal*mol^{-1})
WT	8	1.00	41.45 ± 2.98	25.13 ± 2.06	2.36 ± 0.11	8.65 ± 0.09	-6.29 ± 0.05
A8V	6	1.00	20.82 ± 2.75	52.84 * ± 7.43	1.43 * ± 0.05	7.29 * ± 0.04	-5.86 * ± 0.08
L29Q	6	1.00	36.90 ± 3.44	28.37 ± 2.78	1.16 * ± 0.07	7.38 * ± 0.06	-6.22 ± 0.06
A31S	8	1.00	169.00 * ± 17.68	6.36 * ± 0.62	-1.06 * ± 0.10	6.05 * ± 0.14	-7.11 * ± 0.06
L48Q	7	1.00	227.14 * ± 16.85	4.57 * ± 0.39	-7.46 * ± 0.14	-0.16 * ± 0.17	-7.30 * ± 0.05
Q50R	7	1.00	75.77 ± 4.43	13.48 * ± 0.80	-4.67 * ± 0.11	1.98 * ± 0.14	-6.65 * ± 0.04
C84Y	7	1.00	86.69 * ± 2.14	11.58 * ± 0.29	-6.06 * ± 0.22	0.67 * ± 0.22	-6.74 * ± 0.01

The thermodynamic properties of the Ca^{2+} binding interaction with WT N-cTnC and each of the mutants are listed. For each parameter and across the construct type, those differing in their mean $p<0.05$ from the WT are marked by *. With the exception of N which was fixed to 1.00, each parameter is displayed as mean ± SEM.

Supplemental Table 6-2 Ca^{2+} into 3 mM Mg^{2+} incubated N-cTnC titration-derived parameters

N-cTnC	n	N	K_A *10^3 (M^{-1})	K_d (μM)	ΔH (kcal*mol^{-1})	T*ΔS (kcal*mol^{-1})	ΔG (kcal*mol^{-1})
WT	8	1.00	22.6 ± 2.01	46.37 ± 3.40	1.63 ± 0.07	7.55 ± 0.06	-5.92 ± 0.05
A8V	7	1.00	11.95 ± 1.29	89.80 * ± 9.72	0.60 * ± 0.03	6.14 * ± 0.04	-5.55 * ± 0.06
L29Q	9	1.00	13.93 ± 1.76	80.66 * ± 9.20	0.55 * ± 0.04	6.17 * ± 0.04	-5.62 * ± 0.07
A31S	7	1.00	62.84 * ± 6.32	16.80 * ± 1.49	-1.07 * ± 0.05	5.46 * ± 0.09	-6.53 * ± 0.06
L48Q	7	1.00	82.74 * ± 3.18	12.20 * ± 0.52	-6.67 * ± 0.17	0.04 * ± 0.19	-6.71 * ± 0.02
Q50R	7	1.00	49.34 * ± 2.17	20.50 * ± 0.89	-3.65 * ± 0.05	2.75 * ± 0.07	-6.40 * ± 0.02
C84Y	7	1.00	53.30 * ± 3.20	19.15 * ± 1.08	-4.72 * ± 0.09	1.73 * ± 0.12	-6.44 * ± 0.03

The thermodynamic properties of the Ca^{2+} binding interaction with WT N-cTnC and each of the mutants are listed. For each parameter and across the construct type, those differing in their mean $p<0.05$ from the WT are marked by *. With the exception of N which was fixed to 1.00, each parameter is displayed as mean ± SEM.

Supplemental Table 6-3 A comparison of the dissociation constant associated with each of the studied mutations

Construct	Approximate reported K_d (μM)	Publication
WT	11	Liang, Chung et al. 2008
A8V	13	Pinto, Parvatiyar et al. 2009
L29Q	8	Liang, Chung et al. 2008
A31S	12	Parvatiyar, Landstrom et al. 2012
L48Q	2	Tikunova and Davis 2004
Q50R	6	van Spaendonck-Zwarts, van Tintelen et al. 2010
C84Y	4	Pinto, Parvatiyar et al. 2009

6.8. References

Andersson, M., A. Malmendal, S. Linse, I. Ivarsson, S. Forsen and L. A. Svensson (1997). "Structural basis for the negative allostery between Ca(2+)- and Mg(2+)-binding in the intracellular Ca(2+)-receptor calbindin D9k." Protein Sci **6**(6): 1139-1147.

Ashrafian, H. and H. Watkins (2007). "Reviews of translational medicine and genomics in cardiovascular disease: new disease taxonomy and therapeutic implications: Cardiomyopathies: Therapeutics based on molecular phenotype." Journal of the American College of Cardiology **49**(12): 1251-1264.

Bers, D. M. (2000). "Calcium Fluxes Involved in Control of Cardiac Myocyte Contraction." Circulation Research **87**(4): 275-281.

Bers, D. M. (2002). "Cardiac excitation–contraction coupling." Nature **415**(6868): 198-205.

Bowman, J. D. and S. Lindert (2018). "Molecular Dynamics and Umbrella Sampling Simulations Elucidate Differences in Troponin C Isoform and Mutant Hydrophobic Patch Exposure." **122**(32): 7874-7883.

Cordina, N. M., C. K. Liew, D. A. Gell, P. G. Fajer, J. P. Mackay and L. J. Brown (2013). "Effects of Calcium Binding and the Hypertrophic Cardiomyopathy A8V Mutation on the Dynamic Equilibrium between Closed and Open Conformations of the Regulatory N-Domain of Isolated Cardiac Troponin C." Biochemistry **52**(11): 1950-1962.

da Silva, A. C., A. H. de Araujo, O. Herzberg, J. Moult, M. Sorenson and F. C. Reinach (1993). "Troponin-C mutants with increased calcium affinity." Eur J Biochem **213**(1): 599-604.

Dai, L. J., P. A. Friedman and G. A. Quamme (1997). "Cellular mechanisms of chlorothiazide and cellular potassium depletion on Mg2+ uptake in mouse distal convoluted tubule cells." Kidney Int **51**(4): 1008-1017.

Dai, L. J., P. A. Friedman and G. A. Quamme (1997). "Phosphate depletion diminishes Mg2+ uptake in mouse distal convoluted tubule cells." Kidney Int **51**(6): 1710-1718.

Davis, J., L. C. Davis, R. N. Correll, C. A. Makarewich, J. A. Schwanekamp, F. Moussavi-Harami, D. Wang, A. J. York, H. Wu and S. R. Houser (2016). "A tension-based model distinguishes hypertrophic versus dilated cardiomyopathy." Cell **165**(5): 1147-1159.

Davis, J. P., J. A. Rall, P. J. Reiser, L. B. Smillie and S. B. Tikunova (2002). "Engineering competitive magnesium binding into the first EF-hand of skeletal troponin C." J Biol Chem **277**(51): 49716-49726.

Dong, W.-J., C.-K. Wang, A. M. Gordon and H. C. Cheung (1997). "Disparate Fluorescence Properties of 2-[4′-(Iodoacetamido)anilino]-Naphthalene-6-Sulfonic Acid Attached to Cys-84 and Cys-35 of Troponin C in Cardiac Muscle Troponin." Biophysical Journal **72**(2, Part 1): 850-857.

Dweck, D., N. Hus and J. D. Potter (2008). "Challenging current paradigms related to cardiomyopathies Are changes in the Ca2+ sensitivity of myofilaments containing cardiac troponin C mutations (G159D and L29Q) good predictors of the phenotypic outcomes?" Journal of Biological Chemistry **283**(48): 33119-33128.

Elliott, P. and W. J. McKenna (2004). "Hypertrophic cardiomyopathy." Lancet **363**(9424): 1881-1891.

Freire, E., O. L. Mayorga and M. Straume (1990). "Isothermal titration calorimetry." Analytical chemistry **62**(18): 950A-959A.

Gifford, Jessica L., Michael P. Walsh and Hans J. Vogel (2007). "Structures and metal-ion-binding properties of the Ca²⁺-binding helix–loop–helix EF-hand motifs." Biochemical Journal **405**(2): 199-221.

Gillis, T. E., T. M. Blumenschein, B. D. Sykes and G. F. Tibbits (2003). "Effect of temperature and the F27W mutation on the Ca2+ activated structural transition of trout cardiac troponin C." Biochemistry **42**(21): 6418-6426.

Gillis, T. E., C. R. Marshall and G. F. Tibbits (2007). "Functional and evolutionary relationships of troponin C." Physiol Genomics **32**(1): 16-27.

Gomes, A. V. and J. D. Potter (2004). "Molecular and cellular aspects of troponin cardiomyopathies." Ann N Y Acad Sci **1015**: 214-224.

Harada, K. and S. Morimoto (2004). "Inherited cardiomyopathies as a troponin disease." Jpn J Physiol **54**(4): 307-318.

Hoffmann, B., H. Schmidt-Traub, A. Perrot, K. J. Osterziel and R. Gessner (2001). "First mutation in cardiac troponin C, L29Q, in a patient with hypertrophic cardiomyopathy." Hum Mutat **17**(6): 524.

Holroyde, M., S. Robertson, J. Johnson, R. Solaro and J. Potter (1980). "The calcium and magnesium binding sites on cardiac troponin and their role in the regulation of myofibrillar adenosine triphosphatase." Journal of Biological Chemistry **255**(24): 11688-11693.

Johnson, J. D., J. H. Collins and J. D. Potter (1978). "Dansylaziridine-labeled troponin C. A fluorescent probe of Ca2+ binding to the Ca2+-specific regulatory sites." J Biol Chem **253**(18): 6451-6458.

Kalyva, A., F. I. Parthenakis, M. E. Marketou, J. E. Kontaraki and P. E. Vardas (2014). "Biochemical characterisation of Troponin C mutations causing hypertrophic and dilated cardiomyopathies." Journal of muscle research and cell motility **35**(2): 161-178.

Katrukha, I. (2013). "Human cardiac troponin complex. Structure and functions." Biochemistry (Moscow) **78**(13): 1447-1465.

Kirschenlohr, H. L., A. A. Grace, J. I. Vandenberg, J. C. Metcalfe and G. A. Smith (2000). "Estimation of systolic and diastolic free intracellular Ca2+ by titration of Ca2+ buffering in the ferret heart." Biochem J **346 Pt 2**: 385-391.

Landstrom, A. P., M. S. Parvatiyar, J. R. Pinto, M. L. Marquardt, J. M. Bos, D. J. Tester, S. R. Ommen, J. D. Potter and M. J. Ackerman (2008). "Molecular and functional characterization of novel hypertrophic cardiomyopathy susceptibility mutations in TNNC1-encoded troponin C." Journal of molecular and cellular cardiology **45**(2): 281-288.

Li, A. Y., C. M. Stevens, B. Liang, K. Rayani, S. Little, J. Davis and G. F. Tibbits (2013). "Familial hypertrophic cardiomyopathy related cardiac troponin C L29Q mutation alters length-dependent activation and functional effects of phosphomimetic troponin I*."

Liang, B., F. Chung, Y. Qu, D. Pavlov, T. E. Gillis, S. B. Tikunova, J. P. Davis and G. F. Tibbits (2008). "Familial hypertrophic cardiomyopathy-related cardiac troponin C mutation L29Q affects Ca2+ binding and myofilament contractility." Physiological genomics **33**(2): 257-266.

Maguire, M. E. (2006). "Magnesium transporters: properties, regulation and structure." Front Biosci **11**: 3149-3163.

Malmendal, A., J. Evenas, E. Thulin, G. P. Gippert, T. Drakenberg and S. Forsen (1998). "When size is important. Accommodation of magnesium in a calcium binding regulatory domain." J Biol Chem **273**(44): 28994-29001.

Maron, B. J., J. M. Gardin, J. M. Flack, S. S. Gidding, T. T. Kurosaki and D. E. Bild (1995). "Prevalence of hypertrophic cardiomyopathy in a general population of young adults Echocardiographic analysis of 4111 subjects in the CARDIA Study." Circulation **92**(4): 785-789.

Maron, B. J., J. Shirani, L. C. Poliac, R. Mathenge, W. C. Roberts and F. O. Mueller (1996). "Sudden death in young competitive athletes: clinical, demographic, and pathological profiles." JAMA **276**(3): 199-204.

Mazur, A., J. A. Maier, E. Rock, E. Gueux, W. Nowacki and Y. Rayssiguier (2007). "Magnesium and the inflammatory response: potential physiopathological implications." Arch Biochem Biophys **458**(1): 48-56.

Murphy, E., C. Steenbergen, L. A. Levy, B. Raju and R. E. London (1989). "Cytosolic free magnesium levels in ischemic rat heart." J Biol Chem **264**(10): 5622-5627.

Ogawa, Y. (1985). "Calcium binding to troponin C and troponin: effects of Mg2+, ionic strength and pH." The Journal of Biochemistry **97**(4): 1011-1023.

Ohki, S., M. Ikura and M. Zhang (1997). "Identification of Mg2+-binding sites and the role of Mg2+ on target recognition by calmodulin." Biochemistry **36**(14): 4309-4316.

Parvatiyar, M. S., A. P. Landstrom, C. Figueiredo-Freitas, J. D. Potter, M. J. Ackerman and J. R. Pinto (2012). "A mutation in TNNC1-encoded cardiac troponin C, TNNC1-A31S, predisposes to hypertrophic cardiomyopathy and ventricular fibrillation." Journal of Biological Chemistry **287**(38): 31845-31855.

Pearlstone, J. R., T. Borgford, M. Chandra, K. Oikawa, C. M. Kay, O. Herzberg, J. Moult, A. Herklotz, F. C. Reinach and L. B. Smillie (1992). "Construction and characterization of a spectral probe mutant of troponin C: application to analyses of mutants with increased calcium affinity." Biochemistry **31**(28): 6545-6553.

Pinto, J. R., M. S. Parvatiyar, M. A. Jones, J. Liang, M. J. Ackerman and J. D. Potter (2009). "A functional and structural study of troponin C mutations related to hypertrophic cardiomyopathy." J Biol Chem **284**(28): 19090-19100.

Potluri, P. R., N. M. Cordina, E. Kachooei and L. J. Brown (2019). "Characterization of the L29Q Hypertrophic Cardiomyopathy Mutation in Cardiac Troponin C by Paramagnetic Relaxation Enhancement Nuclear Magnetic Resonance." **58**(7): 908-917.

Potter, J. D. and J. Gergely (1975). "The calcium and magnesium binding sites on troponin and their role in the regulation of myofibrillar adenosine triphosphatase." Journal of Biological Chemistry **250**(12): 4628-4633.

Reid, R. E. and R. M. Procyshyn (1995). "Engineering magnesium selectivity in the helix-loop-helix calcium-binding motif." Arch Biochem Biophys **323**(1): 115-119.

Romani, A. and A. Scarpa (1992). "Regulation of cell magnesium." Arch Biochem Biophys **298**(1): 1-12.

Seidman, C. E. and J. G. Seidman (2011). "Identifying sarcomere gene mutations in hypertrophic cardiomyopathy: a personal history." Circ Res **108**(6): 743-750.

Semsarian, C., J. Ingles, M. S. Maron and B. J. Maron (2015). "New perspectives on the prevalence of hypertrophic cardiomyopathy." Journal of the American College of Cardiology **65**(12): 1249-1254.

Shettigar, V., B. Zhang, S. C. Little, H. E. Salhi, B. J. Hansen, N. Li, J. Zhang, S. R. Roof, H. T. Ho, L. Brunello, J. K. Lerch, N. Weisleder, V. V. Fedorov, F. Accornero, J. A. Rafael-Fortney, S. Gyorke, P. M. Janssen, B. J. Biesiadecki, M. T. Ziolo and J. P. Davis (2016). "Rationally engineered Troponin C modulates in vivo cardiac function and performance in health and disease." Nat Commun **7**: 10794.

Sia, S. K., M. X. Li, L. Spyracopoulos, S. M. Gagné, W. Liu, J. A. Putkey and B. D. Sykes (1997). "Structure of cardiac muscle troponin C unexpectedly reveals a closed regulatory domain." Journal of Biological Chemistry **272**(29): 18216-18221.

Stevens, C. M., K. Rayani, C. E. Genge, G. Singh, B. Liang, J. M. Roller, C. Li, A. Y. Li, D. P. Tieleman and F. van Petegem (2016). "Characterization of Zebrafish Cardiac and Slow Skeletal Troponin C Paralogs by MD Simulation and ITC." Biophysical Journal **111**(1): 38-49.

Stevens, C. M., K. Rayani, G. Singh, B. Lotfalisalmasi, D. P. Tieleman and G. F. Tibbits (2017). "Changes in the dynamics of the cardiac troponin C molecule explain the effects of Ca2+-sensitizing mutations." Journal of Biological Chemistry **292**(28): 11915-11926.

Sturtevant, J. M. (1977). "Heat capacity and entropy changes in processes involving proteins." Proc Natl Acad Sci U S A **74**(6): 2236-2240.

Tikunova, S. B., D. J. Black, J. D. Johnson and J. P. Davis (2001). "Modifying Mg2+ binding and exchange with the N-terminal of calmodulin." Biochemistry **40**(11): 3348-3353.

Tikunova, S. B. and J. P. Davis (2004). "Designing calcium-sensitizing mutations in the regulatory domain of cardiac troponin C." Journal of Biological Chemistry **279**(34): 35341-35352.

Tikunova, S. B., B. Liu, N. Swindle, S. C. Little, A. V. Gomes, D. R. Swartz and J. P. Davis (2010). "Effect of calcium-sensitizing mutations on calcium binding and exchange with troponin C in increasingly complex biochemical systems." Biochemistry **49**(9): 1975-1984.

Touyz, R. M. (2004). "Reactive oxygen species, vascular oxidative stress, and redox signaling in hypertension: what is the clinical significance?" Hypertension **44**(3): 248-252.

van Spaendonck-Zwarts, K. Y., J. P. van Tintelen, D. J. van Veldhuisen, R. van der Werf, J. D. Jongbloed, W. J. Paulus, D. Dooijes and M. P. van den Berg (2010). "Peripartum cardiomyopathy as a part of familial dilated cardiomyopathy." Circulation **121**(20): 2169-2175.

Wang, D., I. M. Robertson, M. X. Li, M. E. McCully, M. L. Crane, Z. Luo, A.-Y. Tu, V. Daggett, B. D. Sykes and M. Regnier (2012). "Structural and functional consequences of the cardiac troponin C L48Q Ca2+-sensitizing mutation." Biochemistry **51**(22): 4473-4487.

Ward, W. H. and G. A. Holdgate (2001). 7 Isothermal Titration Calorimetry in Drug Discovery. Progress in medicinal chemistry, Elsevier. **38:** 309-376.

Weglicki, W., G. Quamme, K. Tucker, M. Haigney and L. Resnick (2005). "Potassium, magnesium, and electrolyte imbalance and complications in disease management." Clin Exp Hypertens **27**(1): 95-112.

Willott, R. H., A. V. Gomes, A. N. Chang, M. S. Parvatiyar, J. R. Pinto and J. D. Potter (2010). "Mutations in Troponin that cause HCM, DCM AND RCM: what can we learn about thin filament function?" Journal of molecular and cellular cardiology **48**(5): 882-892.

Zot, H. G., J. E. Hasbun, C. A. Michell, M. Landim-Vieira and J. R. Pinto (2016). "Enhanced troponin I binding explains the functional changes produced by the hypertrophic cardiomyopathy mutation A8V of cardiac troponin C." Arch Biochem Biophys **601**: 97-104.

Chapter 7.

General Discussion

The overarching goal of this thesis is to provide insight into the fundamental interaction of thin filament proteins that underly cardiac contractility. To this end we focused primarily on the binding of Ca^{2+} to site II within the N-terminal domain of cTnC but also explored this interaction at the level of full length cTnC. ITC, the primary technique used in these studies, as any other technique, has inherent advantages and disadvantages. The narrow scope of this study, while providing great sensitivity, is perhaps the largest limitation that needs be considered when interpreting our findings. However, it is hoped that relative changes are transferable, and the perspectives gained in this system can still be used to understand the function of cTnC in general.

This thesis project has explored the effects of a series of cardiomyopathy-associated mutations in the N-terminal domain of cTnC that alter the Ca^{2+} sensitivity of force production in cardiac tissues. The modifying role of cellular Mg^{2+} in the control of contraction has largely been overlooked in the past. Our work suggests that this cation may play a significant role in modulation of contraction at baseline and in the diseased state.

7.1. Ca^{2+} Signaling and hypertrophy

Mutations that alter Ca^{2+} sensitivity disrupt the exquisitely tuned balance needed for optimal force generation. Even small temporal changes in the duration of force production could lead to a significant shift in the energetic balance of the cell. This is to say; prolonged force production would utilize greater energy. Also, SERCA2a which is the second most common sink of myocyte ATP after the myosin ATPase, would be overactive as a result of an elevation in the Ca^{2+} signal (van der Velden and Stienen 2019). These alterations may occur chronically and over many years, potentially lead to structural remodelling of the heart, possibly through expression of the so-called fetal gene expression program.

The hypertrophic phenotype is highly dependent on the animal model in which they are observed. This means that systems with inherently higher than human rates of

contraction, such as murine models, when incorporated with human mutations may not develop overt hypertrophy. For example, in work by Davis et al., treatment with the β-receptor antagonist Metoprolol unmasked the effects of L48Q cTnC, causing a significant increase in: the left ventricular wall thickness, septal wall thickness, and cardiac mass (Davis, Davis et al. 2016). Similarly, treatment of the mice with Ivabradine (an HCN antagonist) caused hypertrophy of hearts infected with L48Q cTnC despite only ~15% incorporation of the mutant cTnC (Davis, Davis et al. 2016).

In general, it is posited that HCM-causing mutations increase and DCM-associated mutations decrease the Ca^{2+} sensitivity of force production. In fact, HCM mutants are often associated with diastolic dysfunction and DCM mutants with systolic dysfunction; though it is clear that this is highly system dependent and even still not consistently applicable to all HCM and DCM-associated mutants (Robinson, Griffiths et al. 2007). A recently developed unifying mechanism may be more predictive of the HCM and DCM phenotype and utilizes an index of force production (Davis, Davis et al. 2016). This study found that mutations that induce Ca^{2+} retention lead to greater duration of force production and cause concentric hypertrophy consistent with HCM. In contrast, mutations that cause a lower sensitivity towards Ca^{2+} and therefore interaction with the cation for a shorter period of time (and produce force for an attenuated period) induce dilation consistent with DCM (Davis, Davis et al. 2016).

While considering these points, it also seems appropriate to conclude this thesis by discussing, albeit briefly the complex mechanisms that underly the hypertrophic phenotype which is commonly a hallmark of HCM. To this end, a few key and interrelated pathways will be discussed. These pathways seem to be activated by the main culprit within this disease, that is mishandled Ca^{2+}. While hypertrophy is likely adaptive, when prolonged it leads to increased risk of heart failure and sudden cardiac death (Vakili, Okin et al. 2001).

Altered Ca^{2+} handling is undoubtedly an area of interest in HCM pathophysiology. Downregulation of SERCA2a that has been observed in HCM patients (Somura, Izawa et al. 2001) would lead to elevation of diastolic Ca^{2+} and delayed decay of the Ca^{2+} signal. In fact, the Ca^{2+}-sensitive dye Fluoforte was used in isolated single cells from mouse models of HCM to establish elevated diastolic concentrations of cytosolic Ca^{2+}. While this dye provides a relative measure of Ca^{2+}, it cannot be used to determine

absolute levels (Coppini, Ferrantini et al. 2013). Adenoviral delivery of SERCA2a in HCM mutant mice is protective against hypertrophy (Pena, Szkudlarek et al. 2010).

Ca^{2+} can affect a variety of targets such as CaMKII which in turn alters PLN phosphorylation to indirectly affect SERCA2a (Guinto, Haim et al. 2009). Moreover, the CaMKII regulated transcription factor MEF2 directly associates with histone deacetylases that promote chromosomal condensation and gene repression (McKinsey, Zhang et al. 2002). Interestingly, transgenic overexpression of the Ca^{2+} buffer, parvalbumin is also protective against impaired relaxation in mice carrying a tropomyosin mutation known to cause HCM (Coutu, Bennett et al. 2004).

7.2. Altered force requirements

In HCM, the duration of interaction with Ca^{2+} (Davis, Davis et al. 2016), possibly modified by the amount of cTnI that cTnC “sees” (Siddiqui, Tikunova et al. 2016) alters the duration of force production, increases crossbridge turnover, and thus the amount of energy utilized in this ATP dependent process (Abozguia, Clarke et al. 2006, Belus, Piroddi et al. 2008). HCM causing mutations that increase the energetic cost of force production, cause bioenergetic alterations that may be causative for remodeling and the hypertrophic phenotype (Timmer, Germans et al. 2011).

7.2.1. Energetic balance

An increase in ATP turnover and metabolic imbalance has been seen in models of HCM (Ashrafian, Redwood et al. 2003). In patients carrying specific HCM-causing mutations, phosphocreatine (PCr) which is used by creatine kinase to phosphorylate ADP, is depleted (Abraham, Bottomley et al. 2013). In general, it is thought that in the hypertrophic heart, fatty acid utilization is decreased and glucose use is increased (Depre, Shipley et al. 1998). Decreased PCr/ATP ratio in HCM patients, prior to the manifestation of hypertrophy indicates an increase in carbohydrate utilization in response to greater energetic demands (Jung, Sieverding et al. 1998). Similarly, transgenic mice with a specific HCM-causing myosin mutation have decreased PCr/ATP ratio and mitochondrial abnormalities (Spindler, Saupe et al. 1998).

7.2.2. Energetic distribution as predictive of HCM

Greater amounts of ATP are used per unit of force produced in HCM mutant mouse models (Ferrantini, Coppini et al. 2017) and human hearts (Witjas-Paalberends, Ferrara et al. 2014). Interestingly, inefficient energy utilization seems to precede hypertrophy in HCM (Timmer, Germans et al. 2011, Witjas-Paalberends, Ferrara et al. 2014). Numerous studies show that HCM-causing mutations impair cellular energetic balance prior to cardiac remodeling (Spindler, Saupe et al. 1998, Frey, Brixius et al. 2006, Luedde, Flogel et al. 2009).

Force production and energy generation are co-regulated in the myocyte. CICR activates the thin filaments but also allows for Ca^{2+} entry into the mitochondria to regulate the carboxylic acid cycle and energy production (Maack and O'Rourke 2007). Numerous studies have pointed to altered energetics in HCM leading to the reasonable conclusion that this imbalance would further exacerbate Ca^{2+} mishandling by affecting key ATPases such as: myosin, Na^{+}/K^{+} ATPase, and SERCA2a (Javadpour, Tardiff et al. 2003, Critoph, Patel et al. 2014).

7.2.3. Energy unbalancing mutations cause HCM-like phenotype

AMP-activated protein kinase (AMPK) is activated during energy-depleted states to restore cellular ATP stores. AMPK mutants have an HCM-like phenotype of asymmetrical septal hypertrophy (Blair, Redwood et al. 2001). Moreover, mutations in mitochondrial DNA also have the potential to cause an HCM-resembling phenotype (Elliott and McKenna 2004).

The inability of the heart to provide sufficient ATP, especially during times of increased demand (such as during exercise) may underly sudden cardiac death events (Ashrafian, McKenna et al. 2011). Further, the effects of altered Ca^{2+} sequestration in the mitochondria may be mediated through reactive oxygen species (ROS) that cause direct damage or alter signaling pathways (Terentyev, Gyorke et al. 2008). In general, it has been suggested that reduced availability of energetic substrates leads to elevated Ca^{2+} in the cytosol and imbalance in other ionic gradients, which in turn can activate pathogenic signaling and possibly lead to arrhythmic events (Ashrafian, Redwood et al. 2003). In support of this, when the adenine nucleotide translocator-1, that exports ATP

from the mitochondria is knocked out, the HCM phenotype is seen in mice (Graham, Waymire et al. 1997).

7.3. Hypertrophic signaling pathways

7.3.1. Calcineurin/NFAT pathway

There is evidence that the nucleus functions as a Ca^{2+} microdomain, where the phosphatase calcineurin senses the presence of this signal and modifies transcription of nuclear factor of activator T-cells (NFAT) DNA (Olivares-Florez, Czolbe et al. 2018). Calcineurin expression and activity is increased by pressure overload in the heart (Lim, De Windt et al. 2000). Elevated contractile Ca^{2+} has also been shown to activate cytosolic calcineurin leading to the dephosphorylation of NFAT. This in turn unmasks nuclear localization signals, NFAT is translocated to the nucleus, and activates numerous gene targets leading to pathological hypertrophy (Molkentin, Lu et al. 1998, Houser and Molkentin 2008, Makarewich, Correll et al. 2012). Stressors such as catecholamines and Ca^{2+} transient frequency may act through caveolin microdomains to activate the calcineurin-NFAT pathway and induce a pathological hypertrophic response (Tavi, Pikkarainen et al. 2004, Colella, Grisan et al. 2008).

A distinction has been made between pathological and “physiological” hypertrophy with the latter being attributed to exercise-induced hypertrophy and linked with specific microdomain signaling (Houser and Molkentin 2008). G-protein coupled receptors (GPCRs) including α- and β-adrenergic receptors can be activated to turn on phosphoinositide 3 kinases (PI3Ks) in which the primary target is Akt (a serine/threonine protein kinase). The Akt-GSK3 (Glycogen synthase kinase 3)-mTOR (mammalian target of rapamycin) pathway is a distinct signaling cascade that has been purported to modulate the physiological hypertrophy resulting from exercise (Knollmann, Kirchhof et al. 2003, Heineke and Molkentin 2006, Backs, Backs et al. 2009). During moderate exercise, the Akt-GSK3-mTOR pathway suppresses the effects of imbalanced Ca^{2+} signaling (Wilkins, Dai et al. 2004).

Kinases such as GSK3, p38, and c-Jun N-terminal kinases (JNK) phosphorylate the N-terminal region of NFAT to decrease cardiac hypertrophy (Haq, Choukroun et al. 2000). Similarly, mTOR is a large kinase, which when activated reduces protein

synthesis and limits increase in cell size by inhibiting p70S6 and other kinases (Fingar, Salama et al. 2002). Akt (also known as protein kinase B) phosphorylates GSK3, which in turn phosphorylates and masks nuclear translocation signals in the N-terminal domain of NFAT (Zhou, Sun et al. 1998). It is important to note then that NFAT signaling may be a link between pathological and physiological hypertrophy. In addition to NFAT, GSK3 regulates numerous transcription factors such as Myc, GATA4, Jun, and STAT, all of which have been implicated in development of cardiac hypertrophy (Frey and Olson 2003).

7.3.2. Pak1 signaling

There is also some level of interplay between the NFAT and p21 activated kinase 1 (Pak1) pathways. Pak1 is part of the angiotensin II (Ang II) signaling cascade and controls expression of genes that alter control of the Ca^{2+} transient, including expression of: T-tubules, LTCC, SERCA2a, and NCX (Wang, Tsui et al. 2015). Ang II signaling also increases translocation of Ca^{2+} into the nucleus through inositol 3 phosphate receptors (IP3Rs), where it is sensed by nuclear calcineurin and alters NFAT DNA expression (Olivares-Florez, Czolbe et al. 2018).

Exercise training has been shown, under certain conditions to increase myofilament sensitivity towards Ca^{2+} (Wisloff, Loennechen et al. 2002). The type of exercise is thought to determine the remodeling that occurs ie. resistance training causes pressure overload and leads to concentric hypertrophy. Conversely, aerobic training causes volume overload leading to eccentric training. Remodeling in response to regular aerobic exercise seems to be mediated in part by Pak1, which has been shown to have anti-hypertrophic effects in pathologically-stressed hearts (Ke, Wang et al. 2004). Pak1 is needed for normal phosphorylation of TnT, Tm, MyBP-C, Ser 16 in PLN, as well as elevation of calcineurin which accompanies exercise training. Knock-out of the gene for this kinase is significantly maladaptive in mice (Davis, Simon et al. 2015).

7.3.3. MEK/ERK1/2 pathway

MEK1 is a mitogen-activated protein kinase (MAPK) that activates extracellular signal-regulated kinase (ERK) (Bueno, De Windt et al. 2000). The MAPK/ERK pathway is involved in pressure overload-induced cardiac hypertrophy. Ras is a small G-protein

that is involved in hypertrophic gene expression in the heart and is linked to downstream effectors such as Raf, PI3K, and the MAPK/ERK1/2 pathway (Fuller, Gillespie-Brown et al. 1998). Ras is involved in the calcineurin pathway and causes nuclear translocation of NFAT3 (Ichida and Finkel 2001).

This pathway involves extracellular signaling and activates intermediate players such as the proto-oncogene Raf, ultimately activating transcription factors such as Myc and altering hypertrophic gene targets (Nicol, Frey et al. 2001, Bernardo, Weeks et al. 2010). The MEK-ERK pathway is closely related to hypertrophic signaling through calcineurin and implicated in the HCM phenotype leading to increased myocyte width. In contrast, DCM mutations also increase signaling through calcineurin but reduced activation of the MEK-ERK pathway resulting in cardiomyocyte elongation (Davis, Davis et al. 2016).

These pathways are understandably complex, still under investigation, and largely beyond the scope of this dissertation. However, by discussing them in brief here, we explore the complex nature of numerous signaling pathways that mediate the manifestation of hypertrophy. Understanding of these pathways is essential to our studies given that the link between HCM-causing mutations and hypertrophy in the disease is yet to be determined.

7.4. Effect of N-terminal mutations on Ca^{2+} binding affinity

In the early stages of our study, we established a workflow that incorporated the use of melting point analysis to explore global stability. We relied to a greater extent on MD Simulations and ITC experiments to explore the energetic landscape of the Ca^{2+}-N-cTnC interaction. The advantages of ITC (as laid out in chapter 2 of this thesis) are numerous, with the most significant being the absence of any changes in the protein backbone, including the incorporation of bulky fluorophores that are also highly system dependent. Moreover, ITC allows for exact control of the experimental conditions and certainty is the obtained results through minimization of potentially confounding factors (Davis, Norman et al. 2007, Johnson, Fulcher et al. 2019).

7.4.1. The mutations investigated in this dissertation

Table 7-1 Summary of information regarding studied cTnC mutants

TnC Mutation	Clinical Report (if any)	Distinguishing Phenotype in Probands	Ca^{2+} Sensitivity of Force Production (Change in pCa Units Relative to WT)	Ca^{2+} Affinity (Change in K_d Relative to WT)	X-ray or NMR Structure (if any)
A8V	→Landstrom AP, Parvatiyar MS, et al. 2008[1]	→Proband with 18 mm of LV wall thickness	→Actomyosin ATPase (+0.51)[6] →Reconstituted porcine fibers (+0.36)[6]	→IAANS fluorescence in cTnC, cTn, TF (-0.5, -0.06, +0.2 μM respectively)[6]	N/A
L29Q	→Hoffmann B, Schmidt-Traub H et al. 2001[2]	→60 year old proband with 15 mm of LV wall thickness	Variable data from different labs: →Actomyosin ATPase & invitro motility assays (-0.13)[7] →Reconstituted mouse cardiomyocytes (-0.45)[8] →Reconstituted mouse fibers (+0.25)[9]	→IAANS fluorescence in Tn and TF (+0.06 μM and +0.46 μM respectively)[8] →F27W fluorescence in cTnC (-3.3 μM)[9]	PDB:2N79 (Ca^{2+}-bound) PDB:4GJF (Cd^{2+}-bound)
A31S	→Parvatiyar MS, Landstrom AP, et al. 2012[3]	→5 year old with asymmetrical hypertrophy, 20 mm of LV wall thickness, and presenting with episodic VF	→Actomyosin ATPase assay (+0.38)[3] →Reconstituted porcine fibers (+0.17)[3]	→IAANS fluorescence in isolated TnC, Tn complex, thin filaments, and thin filament with S1 heads (+3.6, +0.1, +0.5, and +0.01 respectively)[3]	N/A
L48Q	→Tikunova SB, Davis J 2004[5]	→Engineered mutation	→Actomyosin ATPase assay (+0.3)[10] →Reconstituted rabbit cardiomyocytes (+0.5)[11]	→F27W fluorescence in cTnC (-6.44 μM)[5] →IAANS fluorescence in Tn complex, thin filament, and thin filament with S1 myosin heads (-0.37, -4.9, and -0.76 μM respectively)[10]	N/A
Q50R	→van Spaendonck-Zwarts, van Tintelen et al. 2010[4]	→16 month old with peripartum cardiomyopathy and family history of DCM	No data available	→ITC binding data N-cTnC (-9.05 μM)[12]	N/A
C84Y	→Landstrom AP, Parvatiyar MS, et al. 2008[1]	→17 year old with 19 mm LV wall thickness and exertion induced syncope	→Actomyosin ATPase assay (+0.56)[6] →Reconstituted porcine fibers (+0.27)[6]	→IAANS fluorescence in cTnC and cTn (-24.9 and -0.03 μM respectively)[6]	N/A

Normal LV wall thickness is approximately 8 mm. In the absence of family history 15 mm is the upper limit of normal LV wall thickness. The upper limit of normal is 13 mm for those with family history of heart disease. Numbered citations are as follows: Landstrom, Parvatiyar et al. 2008[1]; Hoffmann, Schmidt-Traub et al. 2001[2]; Parvatiyar, Landstrom et al. 2012[3]; van Spaendonck-Zwarts, van Tintelen et al. 2010[4]; Tikunova and Davis 2004[5]; Pinto, Parvatiyar et al. 2009[6]; Schmidtmann, Lindow et al. 2005[7]; Li, Stevens et al. 2013[8]; Liang, Chung et al. 2008[9]; Tikunova, Liu et al. 2010[10]; Shettigar, Zhang et al. 2016[11], Stevens, Rayani et al. 2017[12].

We have selected several mutations localized to the N-terminal domain of cTnC. All of these mutations are adjacent to regulatory site II of cTnC and have been associated with HCM (A8V, L29Q, A31S, and C84Y), DCM (Q50R), and a “synthetic” increase in Ca^{2+} binding affinity (L48Q) (Tikunova and Davis 2004, Liang, Chung et al. 2008, Pinto, Parvatiyar et al. 2009, van Spaendonck-Zwarts, van Tintelen et al. 2010, Parvatiyar, Landstrom et al. 2012).

A8V was first identified in a patient with increased left ventricular wall thickness. (Landstrom, Parvatiyar et al. 2008). The left ventricular wall is normally ~8 ± 1 mm and thus 18 mm of thickness that was observed represents significant hypertrophy by clinical standards (Kawel, Turkbey et al. 2012). Other probands have also been identified, therefore this may not be a de novo mutation (Jaafar, Girolami et al. 2015). Large structural deviations were observed in this variant, which appears to have significantly more open apo and holo-states compared to the WT cTnC (Pinto, Parvatiyar et al. 2009,

Cordina, Liew et al. 2013). However, when tested in isolation, A8V cTnC had similar to WT Ca^{2+} sensitivity, a finding that we also corroborated. In contrast, IAANS fluorescence-based studies in reconstituted TF, showed higher than WT sensitivity (Pinto, Parvatiyar et al. 2009).

TnI phosphorylation caused a greater degree of desensitization of the actomyosin ATPase when in complex with the A8V mutant compared to WT cTnC (Albury, Swindle et al. 2012). Stopped-flow analysis suggested a slower dissociation rate from both the non-phosphorylated and phosphorylated TnI (Albury, Swindle et al. 2012). This may be mitigated in part by the greater affinity of A8V cTnC for binding by the regulatory region of cTnI (Swindle and Tikunova 2010). In general, the reduced dissociation rate of Ca^{2+} from A8V cTnC offsets the unchanged affinity of site II in isolation to cause elevated sensitivity of the mutant in systems of greater complexity.

L29Q was the first HCM-associated variant identified in cTnC. It presented clinically for the only time in a 60 year-old patient with mild ventricular hypertrophy (15 mm) (Hoffmann, Schmidt-Traub et al. 2001). Reconstituted filaments had unchanged sensitivity of force production compared to the WT (Neulen, Stehle et al. 2009). Others however, showed a small but significant increase in the mutant for both peak force and sensitivity of force production in reconstituted rat papillary fibers (Gollapudi and Chandra 2012). Skinned and reconstituted mouse cardiac fibers had increased sensitivity of force production with reduced LDA (Liang, Chung et al. 2008) and abolished effect of TnI phosphorylation (Li, Stevens et al. 2013) compared to the WT. Stopped-flow spectro-fluorometry also showed that dissociation of Ca^{2+} from cTnC is greater in phosphorylated cTn complex with WT cTnC compared to the mutant (Dong et al. 2008). Actomyosin ATPase assays were used to determine that the interaction of the mutant cTnC is weakened with the N-terminus of cTnI (Schmidtmann, Lindow et al. 2005) thus explaining the reduced effect of TnI phosphorylation observed through NMR spectroscopy (Baryshnikova, Li et al. 2008).

A similar overall NMR-derived structure was seen when comparing L29Q cTnC to the WT (Baryshnikova, Li et al. 2008, Robertson, Sevrieva et al. 2015). Recent ITC and MD Simulations on the N-terminus of cTnC indicates a similar affinity by site II for Ca^{2+} in the WT and the L29Q mutant (chapter 4). Studies utilizing IAANS fluorescence suggest that systems of greater complexity result in lesser degrees of difference

between the L29Q mutant and WT cTnC (Dweck, Hus et al. 2008). This mutation may destabilize the A-helix, thus leading to disruptions in Ca^{2+} binding properties of site II (Liang, Chung et al. 2008). In general, this relatively mild mutation seems not to alter cTnC structure but may affect moderate changes in affinity of the Ca^{2+}-sensor for cTnI and thus modulation through phosphorylation of this protein.

A31S was identified in a 5-year-old with 20 mm of left ventricular wall thickness and presenting with episodes of ventricular fibrillation. Isolated cTnC carrying the A31S mutation was found to have similar to WT structure in both the apo and Ca^{2+}-bound states. However, both actomyosin ATPase and reconstituted porcine fibers had higher than WT Ca^{2+} sensitivity when incorporated with A31S cTnC (Parvatiyar, Landstrom et al. 2012).

IAANS-based fluorescence change was used to follow affinity for Ca^{2+} in systems of: isolated cTnC, cTn, TF, and TF with myosin S1; A31S cTnC containing systems had higher than WT affinity in each case (Parvatiyar, Landstrom et al. 2012). These changes in sensitivity are inconsistent with our ITC studies on affinity of site II, where we found similar to WT affinity in a system including only the N-terminal domain of cTnC (chapter 4). Our simulations suggest that the A31S mutation stabilizes the loop between helices A and B with a hydrogen bond not present in the WT cTnC. However, this mutant also samples the open-state with greater frequency. Moreover, significant changes in hydrophobicity of the exposed surface area and potentially reduced interaction energy with the TnI_{SW} also merit mention (Stevens, Rayani et al. 2017). The lack of data on this mutant necessitates further structural and functional exploration of its mode of action.

L48Q is an “engineered” mutation that was conceived to increase Ca^{2+} sensitivity by replacing a hydrophobic residue with polar glutamine in the interface between helices BC and NAD (Tikunova and Davis 2004). Using the F27W fluorescent reporter, this mutant was shown to increase the affinity of isolated cTnC. Moreover, Quin-2 fluorescence was used to show faster association rates and similar to WT dissociation rates in this mutant (Tikunova and Davis 2004). In a later publication, the same group used IAANS fluorescence to explore the sensitivity of L48Q at increasing levels of complexity; from the isolated cTnC to the TF + myosin S1 and found an increase in sensitivity for Ca^{2+} at all levels. This mutant also significantly reduced the dissociation

rate from the cTn complex as seen through stopped flow studies (Tikunova, Liu et al. 2010).

Incorporation of the L48Q mutant into cardiomyocytes by adeno-viral transduction was used to deliver cDNA (only ~20% exchange); this enhanced sensitivity and force production, seemingly without alterations in relaxation (Feest, Steven Korte et al. 2014). These findings were also shown in skinned myofibrils and cardiac tissue where enhanced sensitivity was accompanied by only slight delays in relaxation due to more complete exchange of the native protein (Kreutziger, Piroddi et al. 2011, Korte, Feest et al. 2012). The most recent work on this mutant involves *in vivo* incorporation of the L48Q cTnC into mice resulting in normal baseline heart characteristics and function with enhanced cardiac function during exercise (with the caveat that only ~15% of native cTnC was replaced). The researchers suggest a therapeutic use for this mutant (Shettigar, Zhang et al. 2016).

The design of such a mutant, based on an understanding of the dynamics that govern cTnC is heartening; such an understanding opens the the path to a potentially unifying mechanism of disease-causing mutations in cTnC. We found corroborating evidence through our ITC and MD Simulations (chapter 4), whereby the openness of the apo-state cTnC initially and the propensity to opening in the holo-state (once site II is bound by Ca^{2+}) plays a significant role in modulating affinity for Ca^{2+} (Stevens, Rayani et al. 2017).

Q50R was identified in a 16 month-old patient demonstrating peripartum cardiomyopathy and with a family history of the disease (van Spaendonck-Zwarts, van Tintelen et al. 2010). This DCM-associated mutation was explored to add a point of comparison with the HCM mutants. In general, DCM mutants are thought to decrease the sensitivity of force production with a major effect of potentially uncoupling the cTnI-cTnC interaction (Vikhorev, Song et al. 2014).

It has been suggested that the Q50R variant has similar to WT interhelical angles and higher free energy of opening as it stabilizes the closed regulatory domain (Bowman and Lindert 2018). To our knowledge, the work presented herein (chapter 4) and published by our group was the first biophysical characterization of this mutant (Stevens,

Rayani et al. 2017). Our determination of a higher than WT binding affinity for Ca^{2+} at site II necessitates exploration of this mutant in systems of higher complexity.

C84Y was identified in a 17 year-old patient with a left ventricular wall thickness of 19 mm (indicating significant hypertrophy) and exertion-induced syncope (Landstrom, Parvatiyar et al. 2008). There is a limited amount of *in vitro* work on the functional consequences of this mutation. Circular dichroism showed lower than WT α-helical content in the mutant in the apo-state that was normalized in the holo-state (Pinto, Parvatiyar et al. 2009). Moreover, IAANS fluorescence in isolated C84Y cTnC indicated lower than WT affinities at the C-terminal sites and similar to WT affinity at site II (Pinto, Parvatiyar et al. 2009). Our studies (presented in chapters 4 and 6) are closest to this system and suggest greater openness of the N-domain of cTnC and increased affinity at site II for Ca^{2+}. Moreover, actomyosin ATPase activity has also shown increased Ca^{2+} sensitivity. Work on experimental systems of greater complexity has included porcine fibers, which when reconstituted with the mutant had higher than WT Ca^{2+}-sensitivities (Landstrom, Parvatiyar et al. 2008).

Based on previous studies, we posit that mutations that alter the stability of cTnC in the closed form, alter the interaction with the TnI_{SW}, or alter the hydrophobicity of the patch that is exposed upon Ca^{2+} binding have an affect on the Ca^{2+}-affinity of site II (Johnson, Collins et al. 1980, Pinto, Parvatiyar et al. 2009, Lindert, Kekenes-Huskey et al. 2012, Schlecht, Li et al. 2016).

In chapter 4, we probed the effect of the above cTnC point mutations on their Ca^{2+} binding affinity. The interactions were entropically driven and endothermic in nature, with the exception of L48Q. The global stability of most constructs was similar with only A8V and L48Q having a lower than WT melting temperature; which may explain our finding that these two constructs spend the least time in the closed state. Moreover, among the mutants only L48Q, Q50R, and C84Y had a higher than WT affinity for Ca^{2+}. These true measurements of site II affinity differ with the majority of studies relying on a pseudo-measure of affinity, namely the sensitivity (Gillis, Blumenschein et al. 2003, Tikunova, Liu et al. 2010). This true measure is associated with caveats however, as previous results (Katrukha 2013, Li, Stevens et al. 2013) and current findings make clear that Ca^{2+} binding is highly system dependent.

A unifying method for analyzing the affinity of these mutants that we propose may also be applied to cTnC in general is the openness of the N-terminal domain that seems to play a determining role in controlling affinity. The mutations that increased binding affinity (L48Q, Q50R, C84Y) all introduce a polar residue into the hydrophobic region between helices NAD and BC and create at least one additional stabilizing hydrogen bond (Stevens, Rayani et al. 2017).

7.5. Systemic complexity and the distinction of affinity and sensitivity

Of paramount importance is the often-ignored effect of inter-protein interactions that give rise to the difference between sensitivity (which can be measured at any level of complexity) and affinity which is the direct measure of Ca^{2+} binding to site II (achieved at the level of cTnC). Significant differences in molecular etiology despite similarities in clinical manifestation of the disease phenotype lead us to believe that understanding the molecular underpinnings is essential to the interpretation of phenotypic manifestation. We hope that this understanding will pave the path, in the future to appropriate treatments through rational drug design.

The mutations discussed in this project are HCM associated and thus generally expected to increase the Ca^{2+}-sensitivity of force production (Chang and Potter 2005). We tested the hypothesis that changes in force production (visualized as altered pCa_{50}) would result from underlying changes in Ca^{2+} binding affinity of site II. The work presented in chapter 4 shows that this is not the case. Despite this, reductionist studies that focus on isolated cTnC or the N-cTnC are valuable in that they provide information about the mechanism of action of a given mutation.

Indeed, as shown above in section 7.4.1, these mutations are highly system dependent. This further corroborates our previously published work, which showed that mutations need to be tested at higher levels of complexity such as in single cardiomyocytes or reconstituted myofibrils to better understand their functional impact (Li, Stevens et al. 2013). Studies carried out at the level of the TF or in a system of lower complexity that utilizes fluorescence can be quantified through K_d values. In contrast, experiements at higher levels of complexity are quantified through pCa_{50} values. **Table 7.1** represents an attempt to summarize the findings regarding each mutation of interest

through both these parameters. A brief glance will make clear that there is often a lack of consensus regarding changes induced by the mutations. Even with the same technique, numerous fineries such as the phosphorylation state of cTnI can cause significant changes (Li, Stevens et al. 2013). When conflicts arise regarding the directional change in K_d or pCa_{50} relative to the WT, systems of study will likely be to blame. Presumably, higher complexity systems that best maintain intermolecular interactions will be most physiological and should be deferred to.

In regards to each HCM mutation, the existing body of work shows that reconstituted fibers generally cause a left shift in the force-pCa relationship. Increases in units of pCa relative to the WT are seen for each of: A8V (+0.36) (Pinto, Parvatiyar et al. 2009), L29Q (-0.45→+0.25) (Li, Stevens et al. 2013, Liang, Chung et al. 2008), A31S (+0.17) (Parvatiyar, Landstrom et al. 2012), L48Q (+0.5) (Shettigar, Zhang et al. 2016), and C84Y (+0.27) (Pinto, Parvatiyar et al. 2009). A few points to note are that Q50R (van Spaendonck-Zwarts, van Tintelen et al. 2010) has not yet been characterized in reconstituted fibers, L48Q is an "engineered" mutation (Tikunova and Davis 2004), and L29Q is highly variable and system dependent (Li, Stevens et al. 2013, Liang, Chung et al. 2008). In general, however, the direction of change in pCa_{50} is consistent across the studied mutants.

As mentioned previously, alterations in K_d are even more system dependent than pCa_{50} and thus differ significantly based on the prepartion (**Table 7.1**). Generally, K_d would be expected to decrease (corresponding to an increase in affinity) in HCM associated mutation containing systems (Chang and Potter 2005). The thin filament is the highest level of complexity at which K_d was measured for the majority of the mutants (some systems also included S1 myosin heads). The change in K_d units, relative to the WT is as follows: A8V (+0.2 µM) (Pinto, Parvatiyar et al. 2009), L29Q (+0.46 µM) (Li, Stevens et al. 2013), A31S (+0.5 µM) (Parvatiyar, Landstrom et al. 2012), and L48Q (-4.9 µM) (Tikunova, Liu et al. 2010). The highest level of complexity available for Q50R is the N-cTnC where K_d changed -9.05 µM units relative to WT (Stevens, Rayani et al. 2017) and the highest available level of complexity for C84Y is the cTn complex where K_d changed -0.03 µM units relative to the WT (Pinto, Parvatiyar et al. 2009). With these results, it is clear that there are inconsistencies, which point to the pitfalls of using structural changes (as reported by change in fluoresence) to quantify alteration of force production capability. Given the observed changes in pCa_{50} (**Table 7.1**), we hypothesize

that unaltered or elevated K_d observed in some of these mutants may be informative about the mechanism. The mutations which elevate K_d, may be dependent on other interacting partners in the thin filament to bring about their effects.

7.6. The role of cytosolic Mg^{2+} in modifying the binding of Ca^{2+} to cTnC

Mishandling of Ca^{2+} is a common hallmark of HCM that seems to lead, through multiple complex and interacting signaling pathways to the disease phenotype. To make matters worse, the signaling pathways, presumably in place to offset minimal disturbances are unable to alleviate the effects of extensive changes imposed on the tissue and thus become maladaptive, such that the function of the heart is further affected. These pathways have been discussed previously and will not be covered further here. However, it is clear from our most recent studies (presented in chapters 5 and 6) that altered Ca^{2+} handling may be affected by Mg^{2+} binding. That is to say that competition between these two cations for binding to the contractile apparatus may have previously ignored implications on the force production capabilities of the heart, even under normal conditions. This competition may become even more significant if cytosolic free Mg^{2+} is elevated. Regardless, the major goal of the later sections of this thesis is to advocate for the inclusion of cellular Mg^{2+} in the conversation regarding cardiac contractility. It is clear from our work and that of others that this cation interacts with the regulatory site of cTnC at physiologically relevant affinities.

Mg^{2+} is more than 3 orders of magnitude more abundant than Ca^{2+} in the cytosol and these cations are similar in ionic radius, charge, and many other properties. Despite this, the current paradigm states that both cations bind the structural sites (III and IV) of cTnC with high affinity to tether this protein to the rest of the cTn complex. However, Mg^{2+} binding to site II is thought to be non-existent or non-significant. Our studies cast reasonable doubt on this theory. Moreover, work by Davis' group suggests that Mg^{2+} binding to site II may indeed be significant at physiological concentrations of the ion (Davis, Rall et al. 2002, Tikunova and Davis 2004).

Details of this work (presented in chapter 5) will not be covered here once again. However, in brief, we found that Mg^{2+} binding would occur significantly to site II of cTnC and at the measured affinities compete with Ca^{2+} for binding to this site. Given that ~90%

of Mg^{2+} is buffered to cellular ATP, energy depletion may liberate Mg^{2+} and thus lower sensitivity of force production, possibly in a protective mechanism.

7.7. Cellular Mg^{2+} interaction with cTnC N-terminal mutants

In chapter 4, we showed that mutations that are associated with an increase in sensitivity of force production do not necessarily increase Ca^{2+} binding affinity (A8V, L29Q, A31S). Chapter 5 established that Mg^{2+} may compete with and limit the binding of Ca^{2+} to site II of cTnC. However, it was not clear if the observed changes in Ca^{2+} sensitivity of force production in the subset of mutations studied in chapter 4 was in any way modulated by Mg^{2+}. Therefore, in chapter 6 we sought to explore role of Mg^{2+} binding to cTnC harboring the previously discussed mutations in modulating their interaction with Ca^{2+}.

The implications of these findings can only be guessed at, as the role of Mg^{2+} in diseases that alter sensitivity of the contractile apparatus is not yet widely acknowledged. The findings communicated in chapter 5 of this thesis build on previous work by the Davis and Tikunova laboratories (Davis, Rall et al. 2002, Tikunova and Davis 2004). Despite this, the contributions of these well-established labs to this domain of the field of research appear to be largely overlooked based on citations. It is clear that Mg^{2+} could play a key role in the regulation of contraction and given both the abundance of the cation in the cell, as well as the similarities with Ca^{2+}, this possibility is not at all far fetched.

We have established a solid workflow that allows for the exploration of molecular interactions governing cardiac contractility. However, the work presented in this thesis gives rise to numerous questions. Our findings are in good agreement with other work in the field that uses systems of greater physiological complexity. Numerous labs have previously explored the role of Mg^{2+} at the level of the thin filament and muscle fibers. The role of the mutations explored herein merits exploration in fluorescence-based systems containing all TF proteins. Further, systems such as the skinned myofibril and single myocyte reconstituted with recombinant Tn provide great strength in further testing our hypotheses and allow for the study of length-dependent force production capabilities. Such studies are the logical continuation of this project and would have been explored as such if not for technical and temporal limitations. Therefore, we

propose that the work contained in this thesis provides valuable insight into the mechanisms that underlie the action of disease-causing mutations in cTnC and points to a potential modifying role by Mg^{2+}.

7.8. References

Abozguia, K., K. Clarke, L. Lee and M. Frenneaux (2006). "Modification of myocardial substrate use as a therapy for heart failure." Nat Clin Pract Cardiovasc Med **3**(9): 490-498.

Abraham, M. R., P. A. Bottomley, V. L. Dimaano, A. Pinheiro, A. Steinberg, T. A. Traill, T. P. Abraham and R. G. Weiss (2013). "Creatine kinase adenosine triphosphate and phosphocreatine energy supply in a single kindred of patients with hypertrophic cardiomyopathy." Am J Cardiol **112**(6): 861-866.

Albury, A. N. J., N. Swindle, D. R. Swartz and S. B. Tikunova (2012). "Effect of hypertrophic cardiomyopathy-linked troponin C mutations on the response of reconstituted thin filaments to calcium upon troponin I phosphorylation." Biochemistry **51**(17): 3614-3621.

Ashrafian, H., W. J. McKenna and H. Watkins (2011). "Disease pathways and novel therapeutic targets in hypertrophic cardiomyopathy." Circ Res **109**(1): 86-96.

Ashrafian, H., C. Redwood, E. Blair and H. Watkins (2003). "Hypertrophic cardiomyopathy:a paradigm for myocardial energy depletion." Trends Genet **19**(5): 263-268.

Backs, J., T. Backs, S. Neef, M. M. Kreusser, L. H. Lehmann, D. M. Patrick, C. E. Grueter, X. Qi, J. A. Richardson, J. A. Hill, H. A. Katus, R. Bassel-Duby, L. S. Maier and E. N. Olson (2009). "The delta isoform of CaM kinase II is required for pathological cardiac hypertrophy and remodeling after pressure overload." Proc Natl Acad Sci U S A **106**(7): 2342-2347.

Baryshnikova, O. K., M. X. Li and B. D. Sykes (2008). "Modulation of Cardiac Troponin C Function by the Cardiac-Specific N-Terminus of Troponin I: Influence of PKA Phosphorylation and Involvement in Cardiomyopathies." Journal of Molecular Biology **375**(3): 735-751.

Belus, A., N. Piroddi, B. Scellini, C. Tesi, G. D'Amati, F. Girolami, M. Yacoub, F. Cecchi, I. Olivotto and C. Poggesi (2008). "The familial hypertrophic cardiomyopathy-associated myosin mutation R403Q accelerates tension generation and relaxation of human cardiac myofibrils." J Physiol **586**(15): 3639-3644.

Bernardo, B. C., K. L. Weeks, L. Pretorius and J. R. McMullen (2010). "Molecular distinction between physiological and pathological cardiac hypertrophy: experimental findings and therapeutic strategies." Pharmacol Ther **128**(1): 191-227.

Blair, E., C. Redwood, H. Ashrafian, M. Oliveira, J. Broxholme, B. Kerr, A. Salmon, I. Ostman-Smith and H. Watkins (2001). "Mutations in the gamma(2) subunit of AMP-activated protein kinase cause familial hypertrophic cardiomyopathy: evidence for the central role of energy compromise in disease pathogenesis." Hum Mol Genet **10**(11): 1215-1220.

Bowman, J. D. and S. Lindert (2018). "Molecular Dynamics and Umbrella Sampling Simulations Elucidate Differences in Troponin C Isoform and Mutant Hydrophobic Patch Exposure." **122**(32): 7874-7883.

Bueno, O. F., L. J. De Windt, K. M. Tymitz, S. A. Witt, T. R. Kimball, R. Klevitsky, T. E. Hewett, S. P. Jones, D. J. Lefer, C. F. Peng, R. N. Kitsis and J. D. Molkentin (2000). "The MEK1-ERK1/2 signaling pathway promotes compensated cardiac hypertrophy in transgenic mice." Embo j **19**(23): 6341-6350.

Colella, M., F. Grisan, V. Robert, J. D. Turner, A. P. Thomas and T. Pozzan (2008). "Ca²⁺ oscillation frequency decoding in cardiac cell hypertrophy: Role of calcineurin/NFAT as Ca²⁺ signal integrators." Proceedings of the National Academy of Sciences **105**(8): 2859-2864.

Coppini, R., C. Ferrantini, L. Yao, P. Fan, M. Del Lungo, F. Stillitano, L. Sartiani, B. Tosi, S. Suffredini, C. Tesi, M. Yacoub, I. Olivotto, L. Belardinelli, C. Poggesi, E. Cerbai and A. Mugelli (2013). "Late sodium current inhibition reverses electromechanical dysfunction in human hypertrophic cardiomyopathy." Circulation **127**(5): 575-584.

Cordina, N. M., C. K. Liew, D. A. Gell, P. G. Fajer, J. P. Mackay and L. J. Brown (2013). "Effects of Calcium Binding and the Hypertrophic Cardiomyopathy A8V Mutation on the Dynamic Equilibrium between Closed and Open Conformations of the Regulatory N-Domain of Isolated Cardiac Troponin C." Biochemistry **52**(11): 1950-1962.

Coutu, P., C. N. Bennett, E. G. Favre, S. M. Day and J. M. Metzger (2004). "Parvalbumin corrects slowed relaxation in adult cardiac myocytes expressing hypertrophic cardiomyopathy-linked alpha-tropomyosin mutations." Circ Res **94**(9): 1235-1241.

Critoph, C. H., V. Patel, B. Mist and P. M. Elliott (2014). "Cardiac output response and peripheral oxygen extraction during exercise among symptomatic hypertrophic cardiomyopathy patients with and without left ventricular outflow tract obstruction." Heart **100**(8): 639-646.

Davis, J., L. C. Davis, R. N. Correll, C. A. Makarewich, J. A. Schwanekamp, F. Moussavi-Harami, D. Wang, A. J. York, H. Wu and S. R. Houser (2016). "A tension-based model distinguishes hypertrophic versus dilated cardiomyopathy." Cell **165**(5): 1147-1159.

Davis, J. P., C. Norman, T. Kobayashi, R. J. Solaro, D. R. Swartz and S. B. Tikunova (2007). "Effects of thin and thick filament proteins on calcium binding and exchange with cardiac troponin C." Biophysical journal **92**(9): 3195-3206.

Davis, J. P., J. A. Rall, P. J. Reiser, L. B. Smillie and S. B. Tikunova (2002). "Engineering competitive magnesium binding into the first EF-hand of skeletal troponin C." J Biol Chem **277**(51): 49716-49726.

Davis, R. T., 3rd, J. N. Simon, M. Utter, P. Mungai, M. G. Alvarez, S. A. Chowdhury, A. Heydemann, Y. Ke, B. M. Wolska and R. J. Solaro (2015). "Knockout of p21-activated kinase-1 attenuates exercise-induced cardiac remodelling through altered calcineurin signalling." Cardiovasc Res **108**(3): 335-347.

Depre, C., G. L. Shipley, W. Chen, Q. Han, T. Doenst, M. L. Moore, S. Stepkowski, P. J. Davies and H. Taegtmeyer (1998). "Unloaded heart in vivo replicates fetal gene expression of cardiac hypertrophy." Nat Med **4**(11): 1269-1275.

Dweck, D., N. Hus and J. D. Potter (2008). "Challenging current paradigms related to cardiomyopathies Are changes in the Ca2+ sensitivity of myofilaments containing cardiac troponin C mutations (G159D and L29Q) good predictors of the phenotypic outcomes?" Journal of Biological Chemistry **283**(48): 33119-33128.

Elliott, P. and W. J. McKenna (2004). "Hypertrophic cardiomyopathy." Lancet **363**(9424): 1881-1891.

Feest, E. R., F. Steven Korte, A. Y. Tu, J. Dai, M. V. Razumova, C. E. Murry and M. Regnier (2014). "Thin filament incorporation of an engineered cardiac troponin C variant (L48Q) enhances contractility in intact cardiomyocytes from healthy and infarcted hearts." J Mol Cell Cardiol **72**: 219-227.

Ferrantini, C., R. Coppini, J. M. Pioner, F. Gentile, B. Tosi, L. Mazzoni, B. Scellini, N. Piroddi, A. Laurino, L. Santini, V. Spinelli, L. Sacconi, P. De Tombe, R. Moore, J. Tardiff, A. Mugelli, I. Olivotto, E. Cerbai, C. Tesi and C. Poggesi (2017). "Pathogenesis of Hypertrophic Cardiomyopathy is Mutation Rather Than Disease Specific: A Comparison of the Cardiac Troponin T E163R and R92Q Mouse Models." J Am Heart Assoc **6**(7).

Fingar, D. C., S. Salama, C. Tsou, E. Harlow and J. Blenis (2002). "Mammalian cell size is controlled by mTOR and its downstream targets S6K1 and 4EBP1/eIF4E." Genes Dev **16**(12): 1472-1487.

Frey, N., K. Brixius, R. H. Schwinger, T. Benis, A. Karpowski, H. P. Lorenzen, M. Luedde, H. A. Katus and W. M. Franz (2006). "Alterations of tension-dependent ATP utilization in a transgenic rat model of hypertrophic cardiomyopathy." J Biol Chem **281**(40): 29575-29582.

Frey, N. and E. Olson (2003). Cardiac Hypertrophy: The Good, the Bad, and the Ugly.

Fuller, S. J., J. Gillespie-Brown and P. H. Sugden (1998). "Oncogenic src, raf, and ras stimulate a hypertrophic pattern of gene expression and increase cell size in neonatal rat ventricular myocytes." J Biol Chem **273**(29): 18146-18152.

Gillis, T. E., T. M. Blumenschein, B. D. Sykes and G. F. Tibbits (2003). "Effect of temperature and the F27W mutation on the Ca2+ activated structural transition of trout cardiac troponin C." Biochemistry **42**(21): 6418-6426.

Gollapudi, S. K. and M. Chandra (2012). "Cardiomyopathy-Related Mutations in Cardiac Troponin C, L29Q and G159D, Have Divergent Effects on Rat Cardiac Myofiber Contractile Dynamics." Biochemistry research international **2012**: 824068-824068.

Graham, B. H., K. G. Waymire, B. Cottrell, I. A. Trounce, G. R. MacGregor and D. C. Wallace (1997). "A mouse model for mitochondrial myopathy and cardiomyopathy resulting from a deficiency in the heart/muscle isoform of the adenine nucleotide translocator." Nat Genet **16**(3): 226-234.

Guinto, P. J., T. E. Haim, C. C. Dowell-Martino, N. Sibinga and J. C. Tardiff (2009). "Temporal and mutation-specific alterations in Ca2+ homeostasis differentially determine the progression of cTnT-related cardiomyopathies in murine models." Am J Physiol Heart Circ Physiol **297**(2): H614-626.

Haq, S., G. Choukroun, Z. B. Kang, H. Ranu, T. Matsui, A. Rosenzweig, J. D. Molkentin, A. Alessandrini, J. Woodgett, R. Hajjar, A. Michael and T. Force (2000). "Glycogen synthase kinase-3beta is a negative regulator of cardiomyocyte hypertrophy." J Cell Biol **151**(1): 117-130.

Heineke, J. and J. D. Molkentin (2006). "Regulation of cardiac hypertrophy by intracellular signalling pathways." Nat Rev Mol Cell Biol **7**(8): 589-600.

Hoffmann, B., H. Schmidt-Traub, A. Perrot, K. J. Osterziel and R. Gessner (2001). "First mutation in cardiac troponin C, L29Q, in a patient with hypertrophic cardiomyopathy." Hum Mutat **17**(6): 524.

Houser, S. R. and J. D. Molkentin (2008). "Does contractile Ca2+ control calcineurin-NFAT signaling and pathological hypertrophy in cardiac myocytes?" Science signaling **1**(25): pe31-pe31.

Ichida, M. and T. Finkel (2001). "Ras regulates NFAT3 activity in cardiac myocytes." J Biol Chem **276**(5): 3524-3530.

Jaafar, N., F. Girolami, I. Zairi, S. Kraiem, M. Hammami and I. Olivotto (2015). "Genetic profile of hypertrophic cardiomyopathy in Tunisia: Is it different?" Glob Cardiol Sci Pract **2015**: 16.

Javadpour, M. M., J. C. Tardiff, I. Pinz and J. S. Ingwall (2003). "Decreased energetics in murine hearts bearing the R92Q mutation in cardiac troponin T." J Clin Invest **112**(5): 768-775.

Johnson, J. D., J. H. Collins, S. P. Robertson and J. D. Potter (1980). "A fluorescent probe study of Ca2+ binding to the Ca2+-specific sites of cardiac troponin and troponin C." Journal of Biological Chemistry **255**(20): 9635-9640.

Johnson, R. A., L. M. Fulcher, K. Vang, C. D. Palmer, N. E. Grossoehme and A. M. Spuches (2019). "In depth, thermodynamic analysis of Ca(2+) binding to human cardiac troponin C: Extracting buffer-independent binding parameters." Biochim Biophys Acta Proteins Proteom **1867**(4): 359-366.

Jung, W. I., L. Sieverding, J. Breuer, T. Hoess, S. Widmaier, O. Schmidt, M. Bunse, F. van Erckelens, J. Apitz, O. Lutz and G. J. Dietze (1998). "31P NMR spectroscopy detects metabolic abnormalities in asymptomatic patients with hypertrophic cardiomyopathy." Circulation **97**(25): 2536-2542.

Katrukha, I. (2013). "Human cardiac troponin complex. Structure and functions." Biochemistry (Moscow) **78**(13): 1447-1465.

Kawel, N., E. B. Turkbey, J. J. Carr, J. Eng, A. S. Gomes, W. G. Hundley, C. Johnson, S. C. Masri, M. R. Prince, R. J. van der Geest, J. A. C. Lima and D. A. Bluemke (2012). "Normal left ventricular myocardial thickness for middle-aged and older subjects with steady-state free precession cardiac magnetic resonance: the multi-ethnic study of atherosclerosis." Circulation. Cardiovascular imaging **5**(4): 500-508.

Ke, Y., L. Wang, W. G. Pyle, P. P. d. Tombe and R. J. Solaro (2004). "Intracellular Localization and Functional Effects of P²¹-Activated Kinase-1 (Pak1) in Cardiac Myocytes." Circulation Research **94**(2): 194-200.

Knollmann, B. C., P. Kirchhof, S. G. Sirenko, H. Degen, A. E. Greene, T. Schober, J. C. Mackow, L. Fabritz, J. D. Potter and M. Morad (2003). "Familial hypertrophic cardiomyopathy-linked mutant troponin T causes stress-induced ventricular tachycardia and Ca2+-dependent action potential remodeling." Circ Res **92**(4): 428-436.

Korte, F. S., E. R. Feest, M. V. Razumova, A.-Y. Tu and M. Regnier (2012). "Enhanced Ca2+ binding of cardiac troponin reduces sarcomere length dependence of contractile activation independently of strong crossbridges." American journal of physiology. Heart and circulatory physiology **303**(7): H863-H870.

Kreutziger, K. L., N. Piroddi, J. T. McMichael, C. Tesi, C. Poggesi and M. Regnier (2011). "Calcium binding kinetics of troponin C strongly modulate cooperative activation and tension kinetics in cardiac muscle." Journal of molecular and cellular cardiology **50**(1): 165-174.

Landstrom, A. P., M. S. Parvatiyar, J. R. Pinto, M. L. Marquardt, J. M. Bos, D. J. Tester, S. R. Ommen, J. D. Potter and M. J. Ackerman (2008). "Molecular and functional characterization of novel hypertrophic cardiomyopathy susceptibility mutations in TNNC1-encoded troponin C." Journal of molecular and cellular cardiology **45**(2): 281-288.

Li, A. Y., C. M. Stevens, B. Liang, K. Rayani, S. Little, J. Davis and G. F. Tibbits (2013). "Familial hypertrophic cardiomyopathy related cardiac troponin C L29Q mutation alters length-dependent activation and functional effects of phosphomimetic troponin I*."

Liang, B., F. Chung, Y. Qu, D. Pavlov, T. E. Gillis, S. B. Tikunova, J. P. Davis and G. F. Tibbits (2008). "Familial hypertrophic cardiomyopathy-related cardiac troponin C mutation L29Q affects Ca2+ binding and myofilament contractility." Physiological genomics **33**(2): 257-266.

Lim, H. W., L. J. De Windt, L. Steinberg, T. Taigen, S. A. Witt, T. R. Kimball and J. D. Molkentin (2000). "Calcineurin expression, activation, and function in cardiac pressure-overload hypertrophy." Circulation **101**(20): 2431-2437.

Lindert, S., P. M. Kekenes-Huskey, G. Huber, L. Pierce and J. A. McCammon (2012). "Dynamics and calcium association to the N-terminal regulatory domain of human cardiac troponin C: a multiscale computational study." The Journal of Physical Chemistry B **116**(29): 8449-8459.

Luedde, M., U. Flogel, M. Knorr, C. Grundt, H. J. Hippe, B. Brors, D. Frank, U. Haselmann, C. Antony, M. Voelkers, J. Schrader, P. Most, B. Lemmer, H. A. Katus and N. Frey (2009). "Decreased contractility due to energy deprivation in a transgenic rat model of hypertrophic cardiomyopathy." J Mol Med (Berl) **87**(4): 411-422.

Maack, C. and B. O'Rourke (2007). "Excitation-contraction coupling and mitochondrial energetics." Basic Res Cardiol **102**(5): 369-392.

Makarewich, C. A., R. N. Correll, H. Gao, H. Zhang, B. Yang, R. M. Berretta, V. Rizzo, J. D. Molkentin and S. R. Houser (2012). "A caveolae-targeted L-type Ca2+ channel antagonist inhibits hypertrophic signaling without reducing cardiac contractility." Circulation research **110**(5): 669-674.

McKinsey, T. A., C. L. Zhang and E. N. Olson (2002). "MEF2: a calcium-dependent regulator of cell division, differentiation and death." Trends Biochem Sci **27**(1): 40-47.

Molkentin, J. D., J. R. Lu, C. L. Antos, B. Markham, J. Richardson, J. Robbins, S. R. Grant and E. N. Olson (1998). "A calcineurin-dependent transcriptional pathway for cardiac hypertrophy." Cell **93**(2): 215-228.

Neulen, A., R. Stehle and G. Pfitzer (2009). "The cardiac troponin C mutation Leu29Gln found in a patient with hypertrophic cardiomyopathy does not alter contractile parameters in skinned murine myocardium." Basic research in cardiology **104**(6): 751-760.

Nicol, R. L., N. Frey, G. Pearson, M. Cobb, J. Richardson and E. N. Olson (2001). "Activated MEK5 induces serial assembly of sarcomeres and eccentric cardiac hypertrophy." Embo j **20**(11): 2757-2767.

Olivares-Florez, S., M. Czolbe and F. Riediger (2018). "Nuclear calcineurin is a sensor for detecting Ca(2+) release from the nuclear envelope via IP3R." **96**(11): 1239-1249.

Parvatiyar, M. S., A. P. Landstrom, C. Figueiredo-Freitas, J. D. Potter, M. J. Ackerman and J. R. Pinto (2012). "A mutation in TNNC1-encoded cardiac troponin C, TNNC1-A31S, predisposes to hypertrophic cardiomyopathy and ventricular fibrillation." Journal of Biological Chemistry **287**(38): 31845-31855.

Pena, J. R., A. C. Szkudlarek, C. M. Warren, L. S. Heinrich, R. D. Gaffin, G. Jagatheesan, F. del Monte, R. J. Hajjar, P. H. Goldspink, R. J. Solaro, D. F. Wieczorek and B. M. Wolska (2010). "Neonatal gene transfer of Serca2a delays onset of hypertrophic remodeling and improves function in familial hypertrophic cardiomyopathy." J Mol Cell Cardiol **49**(6): 993-1002.

Pinto, J. R., M. S. Parvatiyar, M. A. Jones, J. Liang, M. J. Ackerman and J. D. Potter (2009). "A functional and structural study of troponin C mutations related to hypertrophic cardiomyopathy." J Biol Chem **284**(28): 19090-19100.

Robertson, I. M., I. Sevrieva, M. X. Li, M. Irving, Y. B. Sun and B. D. Sykes (2015). "The structural and functional effects of the familial hypertrophic cardiomyopathy-linked cardiac troponin C mutation, L29Q." J Mol Cell Cardiol **87**: 257-269.

Robinson, P., P. J. Griffiths, H. Watkins and C. S. Redwood (2007). "Dilated and hypertrophic cardiomyopathy mutations in troponin and α-tropomyosin have opposing effects on the calcium affinity of cardiac thin filaments." Circulation research **101**(12): 1266-1273.

Schlecht, W., K. L. Li, D. Hu and W. Dong (2016). "Fluorescence Based Characterization of Calcium Sensitizer Action on the Troponin Complex." Chem Biol Drug Des **87**(2): 171-181.

Schmidtmann, A., C. Lindow, S. Villard, A. Heuser, A. Mügge, R. Geßner, C. Granier and K. Jaquet (2005). "Cardiac troponin C-L29Q, related to hypertrophic cardiomyopathy, hinders the transduction of the protein kinase A dependent phosphorylation signal from cardiac troponin I to C." FEBS Journal **272**(23): 6087-6097.

Shettigar, V., B. Zhang, S. C. Little, H. E. Salhi, B. J. Hansen, N. Li, J. Zhang, S. R. Roof, H. T. Ho, L. Brunello, J. K. Lerch, N. Weisleder, V. V. Fedorov, F. Accornero, J. A. Rafael-Fortney, S. Gyorke, P. M. Janssen, B. J. Biesiadecki, M. T. Ziolo and J. P. Davis (2016). "Rationally engineered Troponin C modulates in vivo cardiac function and performance in health and disease." Nat Commun **7**: 10794.

Siddiqui, J. K., S. B. Tikunova, S. D. Walton, B. Liu, M. Meyer, P. P. de Tombe, N. Neilson, P. M. Kekenes-Huskey, H. E. Salhi, P. M. Janssen, B. J. Biesiadecki and J. P. Davis (2016). "Myofilament Calcium Sensitivity: Consequences of the Effective Concentration of Troponin I." Front Physiol **7**: 632.

Somura, F., H. Izawa, M. Iwase, Y. Takeichi, R. Ishiki, T. Nishizawa, A. Noda, K. Nagata, Y. Yamada and M. Yokota (2001). "Reduced myocardial sarcoplasmic reticulum Ca(2+)-ATPase mRNA expression and biphasic force-frequency relations in patients with hypertrophic cardiomyopathy." Circulation **104**(6): 658-663.

Spindler, M., K. W. Saupe, M. E. Christe, H. L. Sweeney, C. E. Seidman, J. G. Seidman and J. S. Ingwall (1998). "Diastolic dysfunction and altered energetics in the alphaMHC403/+ mouse model of familial hypertrophic cardiomyopathy." J Clin Invest **101**(8): 1775-1783.

Stevens, C. M., K. Rayani, G. Singh, B. Lotfalisalmasi, D. P. Tieleman and G. F. Tibbits (2017). "Changes in the dynamics of the cardiac troponin C molecule explain the effects of Ca2+-sensitizing mutations." Journal of Biological Chemistry **292**(28): 11915-11926.

Swindle, N. and S. B. Tikunova (2010). "Hypertrophic cardiomyopathy-linked mutation D145E drastically alters calcium binding by the C-domain of cardiac troponin C." Biochemistry **49**(23): 4813-4820.

Tavi, P., S. Pikkarainen, J. Ronkainen, P. Niemelä, M. Ilves, M. Weckström, O. Vuolteenaho, J. Bruton, H. Westerblad and H. Ruskoaho (2004). "Pacing-induced calcineurin activation controls cardiac Ca2+ signalling and gene expression." The Journal of physiology **554**(Pt 2): 309-320.

Terentyev, D., I. Gyorke, A. E. Belevych, R. Terentyeva, A. Sridhar, Y. Nishijima, E. C. de Blanco, S. Khanna, C. K. Sen, A. J. Cardounel, C. A. Carnes and S. Gyorke (2008). "Redox modification of ryanodine receptors contributes to sarcoplasmic reticulum Ca2+ leak in chronic heart failure." Circ Res **103**(12): 1466-1472.

Tikunova, S. B. and J. P. Davis (2004). "Designing calcium-sensitizing mutations in the regulatory domain of cardiac troponin C." Journal of Biological Chemistry **279**(34): 35341-35352.

Tikunova, S. B., B. Liu, N. Swindle, S. C. Little, A. V. Gomes, D. R. Swartz and J. P. Davis (2010). "Effect of calcium-sensitizing mutations on calcium binding and exchange with troponin C in increasingly complex biochemical systems." Biochemistry **49**(9): 1975-1984.

Timmer, S. A. J., T. Germans, W. P. Brouwer, M. Lubberink, J. van der Velden, A. A. M. Wilde, I. Christiaans, A. A. Lammertsma, P. Knaapen and A. C. van Rossum (2011). "Carriers of the hypertrophic cardiomyopathy MYBPC3 mutation are characterized by reduced myocardial efficiency in the absence of hypertrophy and microvascular dysfunction." European Journal of Heart Failure **13**(12): 1283-1289.

Vakili, B. A., P. M. Okin and R. B. Devereux (2001). "Prognostic implications of left ventricular hypertrophy." Am Heart J **141**(3): 334-341.

van der Velden, J. and G. J. M. Stienen (2019). "Cardiac Disorders and Pathophysiology of Sarcomeric Proteins." Physiol Rev **99**(1): 381-426.

van Spaendonck-Zwarts, K. Y., J. P. van Tintelen, D. J. van Veldhuisen, R. van der Werf, J. D. Jongbloed, W. J. Paulus, D. Dooijes and M. P. van den Berg (2010). "Peripartum cardiomyopathy as a part of familial dilated cardiomyopathy." Circulation **121**(20): 2169-2175.

Vikhorev, P. G., W. Song, R. Wilkinson, O. N. Copeland, A. E. Messer, M. A. Ferenczi and S. B. Marston (2014). "The dilated cardiomyopathy-causing mutation ACTC E361G in cardiac muscle myofibrils specifically abolishes modulation of Ca(2+) regulation by phosphorylation of troponin I." Biophysical journal **107**(10): 2369-2380.

Wang, Y., H. Tsui, E. L. Bolton, X. Wang, C. L.-H. Huang, R. J. Solaro, Y. Ke and M. Lei (2015). "Novel insights into mechanisms for Pak1-mediated regulation of cardiac Ca2+ homeostasis." Frontiers in Physiology **6**(76).

Wilkins, B. J., Y. S. Dai, O. F. Bueno, S. A. Parsons, J. Xu, D. M. Plank, F. Jones, T. R. Kimball and J. D. Molkentin (2004). "Calcineurin/NFAT coupling participates in pathological, but not physiological, cardiac hypertrophy." Circ Res **94**(1): 110-118.

Wisloff, U., J. P. Loennechen, S. Currie, G. L. Smith and O. Ellingsen (2002). "Aerobic exercise reduces cardiomyocyte hypertrophy and increases contractility, Ca2+ sensitivity and SERCA-2 in rat after myocardial infarction." Cardiovasc Res **54**(1): 162-174.

Witjas-Paalberends, E. R., C. Ferrara, B. Scellini, N. Piroddi, J. Montag, C. Tesi, G. J. Stienen, M. Michels, C. Y. Ho, T. Kraft, C. Poggesi and J. van der Velden (2014). "Faster cross-bridge detachment and increased tension cost in human hypertrophic cardiomyopathy with the R403Q MYH7 mutation." J Physiol **592**(15): 3257-3272.

Zhou, P., L. J. Sun, V. Dotsch, G. Wagner and G. L. Verdine (1998). "Solution structure of the core NFATC1/DNA complex." Cell **92**(5): 687-696.